



POWERING INNOVATION THAT DRIVES HUMAN ADVANCEMENT

© 2024 ANSYS, Inc. or its affiliated companies  
Unauthorized use, distribution, or duplication is prohibited.

## Aqwa Theory Manual

---



ANSYS, Inc.  
Southpointe  
2600 Ansys Drive  
Canonsburg, PA 15317  
[ansysinfo@ansys.com](mailto:ansysinfo@ansys.com)  
<http://www.ansys.com>  
(T) 724-746-3304  
(F) 724-514-9494

Release 2024 R1  
January 2024

ANSYS, Inc. and  
ANSYS Europe,  
Ltd. are UL  
registered ISO  
9001:2015  
companies.

---

## **Copyright and Trademark Information**

© 2024 ANSYS, Inc. Unauthorized use, distribution or duplication is prohibited.

ANSYS, Ansys Workbench, AUTODYN, CFX, FLUENT and any and all ANSYS, Inc. brand, product, service and feature names, logos and slogans are registered trademarks or trademarks of ANSYS, Inc. or its subsidiaries located in the United States or other countries. ICEM CFD is a trademark used by ANSYS, Inc. under license. CFX is a trademark of Sony Corporation in Japan. All other brand, product, service and feature names or trademarks are the property of their respective owners. FLEXIm and FLEXnet are trademarks of Flexera Software LLC.

## **Disclaimer Notice**

THIS ANSYS SOFTWARE PRODUCT AND PROGRAM DOCUMENTATION INCLUDE TRADE SECRETS AND ARE CONFIDENTIAL AND PROPRIETARY PRODUCTS OF ANSYS, INC., ITS SUBSIDIARIES, OR LICENSORS. The software products and documentation are furnished by ANSYS, Inc., its subsidiaries, or affiliates under a software license agreement that contains provisions concerning non-disclosure, copying, length and nature of use, compliance with exporting laws, warranties, disclaimers, limitations of liability, and remedies, and other provisions. The software products and documentation may be used, disclosed, transferred, or copied only in accordance with the terms and conditions of that software license agreement.

ANSYS, Inc. and ANSYS Europe, Ltd. are UL registered ISO 9001: 2015 companies.

## **U.S. Government Rights**

For U.S. Government users, except as specifically granted by the ANSYS, Inc. software license agreement, the use, duplication, or disclosure by the United States Government is subject to restrictions stated in the ANSYS, Inc. software license agreement and FAR 12.212 (for non-DOD licenses).

## **Third-Party Software**

See the [legal information](#) in the product help files for the complete Legal Notice for ANSYS proprietary software and third-party software. If you are unable to access the Legal Notice, contact ANSYS, Inc.

Published in the U.S.A.

---

# Table of Contents

|  |    |
|--|----|
| <b>1. Introduction to Aqwa Solver Theory .....</b>                   | 11 |
| 1.1. Aqwa General Capabilities .....                                 | 11 |
| 1.2. Axes Conventions .....  | 11 |
| 1.2.1. Fixed Reference Axes .....                                    | 12 |
| 1.2.2. Local Structure Axes .....                                    | 12 |
| 1.2.3. Local Articulation Axes .....                                 | 12 |
| 1.2.4. Axis Transformation and Euler Rotations .....                 | 14 |
| 1.3. Direction and Phase Angle Conventions .....                     | 16 |
| <b>2. Ocean Environmental Conditions .....</b>                       | 19 |
| 2.1. Ocean Waves .....   | 19 |
| 2.1.1. Regular Wave .....  | 19 |
| 2.1.1.1. Linear Regular Wave .....                                   | 19 |
| 2.1.1.2. Second Order Stokes Wave .....                              | 21 |
| 2.1.1.3. Fifth Order Stokes Wave .....                               | 23 |
| 2.1.2. Irregular Waves .....   | 26 |
| 2.1.2.1. Formulated Wave Spectra .....                               | 27 |
| 2.1.2.1.1. JONSWAP Spectrum .....                                    | 27 |
| 2.1.2.1.2. Pierson-Moskowitz Spectrum .....                          | 28 |
| 2.1.2.1.3. Gaussian Spectrum .....                                   | 29 |
| 2.1.2.1.4. Ochi-Hubble Spectrum .....                                | 29 |
| 2.1.2.1.5. Bretschneider Spectrum .....                              | 30 |
| 2.1.2.1.6. TMA Spectrum .....  | 30 |
| 2.1.2.2. User Defined Wave-Spectrum .....                            | 30 |
| 2.1.2.3. Import Time History of Wave Elevation .....                 | 31 |
| 2.1.2.4. Cross-Swell Waves .....                                     | 32 |
| 2.1.2.5. Spreading Sea .....   | 33 |
| 2.1.2.6. User-Defined Carpet Spectra .....                           | 35 |
| 2.1.2.7. Wave Spectral Group .....                                   | 35 |
| 2.2. Wind .....  | 35 |
| 2.2.1. Uniform Wind .....  | 36 |
| 2.2.2. Wind Velocity Profile and Fluctuation .....                   | 36 |
| 2.2.2.1. Ochi and Shin Wind Spectrum .....                           | 36 |
| 2.2.2.2. API Wind Spectrum .....                                     | 37 |
| 2.2.2.3. NPD Wind Spectrum .....                                     | 38 |
| 2.2.2.4. ISO Wind Spectrum .....                                     | 39 |
| 2.2.2.5. User Defined Wind Spectrum .....                            | 39 |
| 2.2.2.6. Import of a Time History of Wind Speed and Direction .....  | 40 |
| 2.3. Current .....   | 40 |
| 2.3.1. Uniform and Profiled Current .....                            | 40 |
| 2.3.2. Wave and Current Interaction .....                            | 41 |
| <b>3. Hydrostatics of Free-Floating Structures .....</b>             | 43 |
| 3.1. Hydrostatic Forces and Moments .....                            | 43 |
| 3.2. Hydrostatic Equilibrium .....                                   | 44 |
| 3.2.1. Free-Floating Hydrostatic Stability .....                     | 45 |
| 3.2.2. Small Angle Stability .....                                   | 45 |
| 3.2.3. Large Angle Stability .....                                   | 47 |
| 3.3. Hydrostatic Stiffness Matrix .....                              | 48 |
| 3.4. Hydrostatic Property of Floating Body with Internal Tanks ..... | 49 |
| 3.4.1. Local Internal Tank Axes and Combined COG .....               | 49 |

|   |     |
|---|-----|
| 3.4.2. Internal Tank Basic Motions .....  | 51  |
| 3.4.3. Hydrostatic Force and Moment Due to Internal Tanks .....   | 51  |
| 3.4.4. Hydrostatic Stiffness Due to Internal Tanks .....  | 52  |
| 3.4.5. Small Angle Stability of Freely Floating Structure with Internal Tanks .....                                   | 54  |
| 3.4.6. Large Angle Stability of Freely Floating Structure with Internal Tanks .....                                   | 55  |
| 3.5. Free Trim Large Angle Stability .....  | 56  |
| <b>4. Hydrodynamic Radiation and Diffraction Analysis by Source Distribution Method</b> .....                         | 59  |
| 4.1. Radiation and Diffraction Wave Forces .....  | 59  |
| 4.1.1. General Formula in Zero Forward Speed Case .....   | 60  |
| 4.1.2. Source Distribution Method .....   | 62  |
| 4.1.3. Removal of Irregular Frequencies .....   | 64  |
| 4.1.4. Mesh Quality Check .....   | 65  |
| 4.2. Hydrodynamic Interaction .....   | 67  |
| 4.2.1. Extended Hydrodynamic Coefficient Matrices .....   | 67  |
| 4.2.2. Suspending Standing Waves .....  | 68  |
| 4.3. Corrections for Small Forward Speed .....  | 69  |
| 4.4. Response Amplitude Operators .....   | 70  |
| 4.5. Response Amplitude Operators with Additional Input .....   | 71  |
| 4.6. Disturbed Wave Elevation and Air Gap .....   | 72  |
| 4.7. Composite Source Distribution Method for Symmetric Structures .....  | 73  |
| 4.8. Generalized Hydrodynamic Damping .....   | 75  |
| 4.9. Radiation Wave Properties at Negative Encounter Frequency .....  | 76  |
| 4.10. Fictitious Damping at Small Magnitude of Encounter Frequency .....  | 80  |
| 4.11. Hydrodynamic Properties of Internal Tanks .....   | 80  |
| 4.12. Hydrodynamic Analysis with Moonpool Effects .....   | 83  |
| 4.12.1. Resonant Frequency of Water Motion within Moonpools .....   | 84  |
| 4.12.2. Prescribed Oscillatory Pressure Distribution Approach .....   | 84  |
| 4.12.3. Multi-region Matching Approach for Simulation of Moonpool Effects .....                                       | 88  |
| 4.12.4. Artificial Damping for Suspending Resonant Water Motion within Moonpools .....                                | 89  |
| 4.12.5. Composite Source Distribution Method for Symmetric Moonpool Configuration .....                               | 89  |
| 4.12.6. Extended Hydrodynamic Coefficient Matrices of a Hydrodynamic Interaction Structure Group with Moonpools ..... | 95  |
| <b>5. Second Order Wave Excitation Forces</b> .....   | 97  |
| 5.1. Second Order Motion and Force .....  | 97  |
| 5.2. Unidirectional Mean Wave Drift Forces (Far Field Solution) .....   | 99  |
| 5.3. General QTF Coefficient Matrix in Multiple Directional Waves .....   | 101 |
| 5.4. Mean Wave Drift Forces (Near Field Solution) .....   | 104 |
| 5.5. Extended Newman's Approximation .....  | 105 |
| 5.6. Second Order Wave Potential and Its Simplification .....   | 106 |
| <b>6. Morison Element Forces</b> .....  | 109 |
| 6.1. Morison Equation .....   | 109 |
| 6.2. Scale Factor for Model Test Simulation .....   | 111 |
| 6.3. Morison Elements in Frequency Domain Dynamic Response Analysis .....   | 112 |
| 6.4. Morison Drag Linearization .....   | 112 |
| 6.5. Effects of Morison Elements in Equilibrium and Static Stability Analysis .....                                   | 116 |
| 6.6. Effects of Morison Elements in a Time Domain Dynamic Response Analysis .....                                     | 117 |
| 6.7. Properties of Typical Morison Elements .....   | 117 |
| <b>7. Hull Drag and Damping</b> .....   | 121 |
| 7.1. Current and Wind Hull Drag .....   | 121 |
| 7.2. Nonlinear Roll Damping .....   | 122 |
| 7.2.1. Nonlinear Bilge Vortex Shedding Damping .....  | 123 |

|  |            |
|--|------------|
| 7.2.2. Bilge Keel Damping .....  | 124        |
| 7.2.3. User-Defined Quadratic Roll Damping .....                                   | 126        |
| 7.3. Yaw Rate Drag Force .....   | 126        |
| 7.4. Morison Hull Drag Force .....   | 126        |
| 7.5. Wave Drift Damping .....  | 127        |
| <b>8. Articulation and Constraint .....</b>  | <b>131</b> |
| 8.1. Articulations Between Structures .....  | 131        |
| 8.1.1. Motion Restriction due to Articulation .....                                | 131        |
| 8.1.2. Effect of Articulation Stiffness, Damping and Friction .....                | 133        |
| 8.2. Elimination of Freedoms at the Center of Gravity .....                        | 134        |
| <b>9. Moorings and Fenders .....</b>   | <b>137</b> |
| 9.1. Linear Elastic Cable .....  | 137        |
| 9.2. Pulley .....  | 138        |
| 9.2.1. Pulley with Sliding Friction .....  | 138        |
| 9.2.2. Pulley with Bearing Friction .....  | 139        |
| 9.3. Linear Drum Winch .....   | 140        |
| 9.4. Winch Line and Force Line .....   | 142        |
| 9.5. Weightless Nonlinear Mooring Line .....                                       | 143        |
| 9.5.1. Steel Wire .....  | 143        |
| 9.5.2. Polynomial Nonlinear Mooring Line .....                                     | 143        |
| 9.5.3. Nonlinear Mooring with 2-Dimensional Load Extension Database .....          | 144        |
| 9.6. Quasi-Static Composite Catenary Mooring Line .....                            | 145        |
| 9.6.1. Catenary Segment with Influence of Axial Linear Elasticity .....            | 145        |
| 9.6.2. Catenary Segment with Influence of Axial Nonlinear Elasticity .....         | 147        |
| 9.6.3. Cable on Global Sloped Seabed .....   | 148        |
| 9.7. Dynamic Composite Catenary Mooring Line .....                                 | 150        |
| 9.8. Fender .....  | 159        |
| 9.8.1. Fixed Fender .....  | 159        |
| 9.8.2. Floating Fender .....   | 160        |
| 9.8.3. Fender Friction and Damping .....   | 162        |
| <b>10. Tethers .....</b>   | <b>163</b> |
| 10.1. Mass and Stiffness Matrices .....  | 164        |
| 10.2. Boundary Conditions and Constraints .....                                    | 166        |
| 10.3. Total Applied Forces .....   | 166        |
| 10.4. Integration in Time of Motion Equation .....                                 | 168        |
| 10.5. Fatigue/Extreme Value Statistical Post-Processing for Towed Tethers .....    | 169        |
| <b>11. Equilibrium Estimation and Stability Analysis of Structure System .....</b> | <b>171</b> |
| 11.1. External Static Forces .....   | 171        |
| 11.2. Equilibrium Analysis .....   | 173        |
| 11.2.1. The Stiffness Matrix .....   | 173        |
| 11.2.2. Iteration Towards Equilibrium .....  | 175        |
| 11.3. Static Stability Analysis .....  | 176        |
| 11.4. Dynamic Stability Analysis .....   | 176        |
| <b>12. Frequency Domain Dynamic Simulation .....</b>                               | <b>179</b> |
| 12.1. Linearization .....  | 179        |
| 12.1.1. Wind Drag Linearization .....  | 179        |
| 12.1.2. Dynamic Cable Drag Linearization .....                                     | 180        |
| 12.1.3. Morison Element Drag Linearization .....                                   | 181        |
| 12.1.4. Current Hull Drag Linearization .....                                      | 181        |
| 12.1.5. Nonlinear Roll Damping Linearization .....                                 | 183        |
| 12.2. Response Spectral Density .....  | 183        |

|   |            |
|---|------------|
| 12.3. Significant Value Calculation .....                                 | 184        |
| <b>13. Time Domain Dynamic Simulation .....</b>                           | <b>187</b> |
| 13.1. Radiation Force by Convolution Integration .....                    | 188        |
| 13.2. Sloshing Forces by Convolution Integration .....                    | 190        |
| 13.3. Optional Additional External Forces .....                           | 191        |
| 13.4. Inertia Forces in Time Domain Analysis .....                        | 192        |
| 13.5. Irregular Wave Responses with Slow Drift (Aqwa-Drift) .....         | 194        |
| 13.5.1. Wave Excitation Forces and Motion Equation .....                  | 194        |
| 13.5.2. Motions at Drift Frequency .....                                  | 195        |
| 13.5.3. Motions at Drift and Wave Frequency .....                         | 196        |
| 13.5.4. Initial Position and Transients .....                             | 197        |
| 13.6. Motion Response in Severe Sea State (Aqwa-Naut) .....               | 197        |
| 13.6.1. Extended Wheeler Stretching Method .....                          | 198        |
| 13.6.1.1. Wheeler Stretching for Regular Linear Airy Waves .....          | 198        |
| 13.6.1.2. Wheeler Stretching for Irregular Airy Waves .....               | 200        |
| 13.6.1.3. Extended Wheeler Stretching for Second Order Stokes Waves ..... | 201        |
| 13.6.2. Second Order Correction of Linear Irregular Waves .....           | 203        |
| 13.6.3. Wave Ramp .....   | 204        |
| 13.6.4. Hydrodynamic pressure and disturbed wave elevation .....          | 204        |
| 13.6.7. Nodal Motion Response .....                                       | 205        |
| 13.8. Morison Tube Element and Nodal Loads .....                          | 206        |
| 13.8.1. Nodal Loads of Tube Elements in Space Frames .....                | 206        |
| 13.8.2. Nodal Loads of Tube Elements in Riser-Type Structures .....       | 208        |
| 13.9. Integration in Time of Motion Equation .....                        | 209        |
| 13.10. Low Frequency Maneuvering Loads .....                              | 210        |
| <b>14. Extended Functionalities .....</b>                                 | <b>213</b> |
| 14.1. Effective Nodal Acceleration RAOs .....                             | 213        |
| 14.2. Shear Force and Bending Moment along Axes .....                     | 214        |
| 14.3. Splitting Force and Moment .....                                    | 216        |
| 14.4. Evaluation of Percentage of Critical Damping from Twang Test .....  | 217        |
| 14.5. Aqwa Parallel Processing Calculation .....                          | 219        |
| <b>15. References .....</b>   | <b>223</b> |

---

# List of Figures

|   |     |
|---|-----|
| 1.1. Definition of Axis Systems .....   | 12  |
| 1.2. Local Articulation Axes .....  | 13  |
| 1.3. Axis Transformation .....  | 14  |
| 1.4. Floating Rigid Motions .....   | 15  |
| 1.5. Direction Definition .....   | 17  |
| 1.6. Phase Definition .....   | 17  |
| 2.1. Fifth Order Stokes Wave .....  | 23  |
| 2.2. Extension of Wave Elevation Record .....   | 32  |
| 3.1. Metacenter of a Free-Floating Body .....   | 46  |
| 3.2. Large Angle Stability .....  | 48  |
| 3.3. Local Internal Tank Axes and Basic Motions .....   | 49  |
| 4.1. Discrete Wetted Hull Surface and Internal LID Panels .....                               | 65  |
| 4.2. Encounter Frequencies vs. Incident Wave Frequencies in Different Relative Headings ..... | 77  |
| 4.3. Fluid Regions of Floating Structures with Moonpools .....                                | 85  |
| 4.4. Symmetric Types of Moonpool Geometry .....   | 90  |
| 4.5. Port-Starboard Symmetric Types of Moonpool Geometry .....                                | 92  |
| 4.6. Fore-aft Symmetric Types of Moonpool Geometry .....                                      | 93  |
| 4.7. Coefficient Locations in Added Mass and Hydrodynamic Damping Matrices .....              | 96  |
| 5.1. Floating Body and Vertical Control Surface at Infinity .....                             | 100 |
| 6.1. Local Tube Axis System .....   | 110 |
| 6.2. Drag Coefficients Versus Reynolds Numbers for Circular Cylinder .....                    | 111 |
| 6.3. Slender Tube Definition .....  | 118 |
| 7.1. Relative Directional Angle Between Current/Wind and Structure .....                      | 121 |
| 7.2. Ship-Like Cross Section with Bilge .....   | 123 |
| 9.1. Pulley with Sheave Surface Sliding Friction .....  | 139 |
| 9.2. Pulley with Axle Surface Bearing Friction .....  | 140 |
| 9.3. Winding in Drum Winch .....  | 141 |
| 9.4. 2-D Load Extension Database .....  | 144 |
| 9.5. Composite Catenary Mooring Line .....  | 145 |
| 9.6. Catenary Solution .....  | 146 |
| 9.7. Global Sloped Seabed Definition .....  | 149 |
| 9.8. Modeling of a Dynamic Cable .....  | 151 |
| 9.9. Forces on a Cable Element .....  | 152 |
| 9.10. Double Quadratic Transition Function .....  | 156 |
| 9.11. Fixed Fender .....  | 159 |
| 9.12. Floating Fender .....   | 161 |
| 10.1. Tether Element Axes and Nodal Displacement .....  | 164 |
| 13.1. Added Mass and its Extrapolation for Impulse Function Estimation .....                  | 191 |
| 13.2. Loads at Riser Nodes .....  | 209 |
| 14.1. Effective Surge Acceleration in LSA .....   | 213 |
| 14.2. Bending Moment and Shear Force Distribution Along a Neutral Axis .....                  | 215 |
| 14.3. Structure Partition and Reference Point for Splitting Force Calculation .....           | 217 |
| 14.4. Freely-Decaying Record .....  | 218 |



---

## List of Tables

|  |     |
|--|-----|
| 2.1. Weighting Function Values .....   | 28  |
| 2.2. Weighting Factors with Respect to the Power Number of Spreading Function .....      | 34  |
| 4.1. Numbers of Pressure Modes due to Geometric Symmetry .....                           | 94  |
| 7.1. Database of Non-Dimensional Roll Damping Coefficient $C_{db}(R_{BD}, R_{RD})$ ..... | 124 |
| 8.1. Constraint Types .....  | 131 |
| 9.1. Summary of Force Components on Dynamic Cable .....                                  | 158 |
| 14.1. Speed-Up of Hydrodynamic Diffraction Analysis ( $S_N$ ) .....                      | 220 |
| 14.2. Summary of Cores Used in Parallel Calculation .....                                | 221 |
| 14.3. Speed-Up of Hydrodynamic Time Domain Analysis with Tethers ( $S_N$ ) .....         | 222 |



---

# **Chapter 1: Introduction to Aqwa Solver Theory**

---

Ansys® Aqwa™ provides a toolset for investigating the effects of environmental loads on floating and fixed offshore and marine structures. This includes, but is not limited to, floating production and offloading systems, spars, semi-submersibles, renewable energy systems, and ships.

This document provides a description of the theoretical basis of this product.

## **1.1. Aqwa General Capabilities**

---

Aqwa can simulate linearized hydrodynamic fluid wave loading on floating or fixed rigid bodies. This is accomplished by employing three-dimensional radiation/diffraction theory and/or Morison's equation in regular waves in the frequency domain. Unidirectional or multiple directional second order drift forces are evaluated by the far-field, or near field solution, or full quadratic transfer function (QTF) matrix. Free-floating hydrostatic and hydrodynamic analyses in the frequency domain can also be performed.

Aqwa can estimate the equilibrium characteristics and static and dynamic stability of coupled (by moorings and/or connectors) bodies under steady state environmental loads (e.g. wind, wave drift and current).

Aqwa can perform frequency domain statistical analysis of the coupled or uncoupled responses of floating bodies while operating in irregular waves. The linearized drag due to Morison elements (tube, disc), wind and dynamic cables can also be simulated in Aqwa.

The real-time motion of a floating body or bodies while operating in regular or irregular waves can be simulated, in which nonlinear Froude-Krylov and hydrostatic forces are estimated under instantaneous incident wave surface. Additionally, the real-time motion of a floating body or bodies while operating in multi-directional or unidirectional irregular waves can be simulated under first- and second-order wave excitations. Wind and current loading can also be applied to the bodies, as well as external forces at each time step imported or defined by a user-written dynamic-link library. If more than one body is being studied, coupling effects between bodies can be simulated. The convolution approach is used to account for the memory effect of the radiation force.

Wave loads on fixed or floating structures calculated during radiation/diffraction simulation in Aqwa can be mapped to a finite element structural analysis package. Specific details of this procedure are not included in this document.

## **1.2. Axes Conventions**

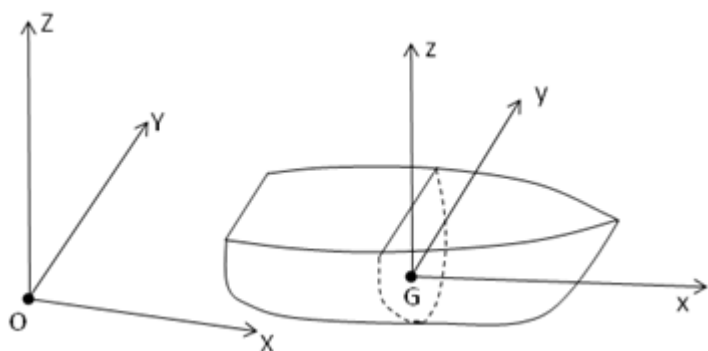
---

Various coordinate systems are employed in Aqwa for representing motions, loads, and other vector values. The general transformation matrix between different coordinate systems and the Euler transformation matrix as a special case are described in this section. The fixed reference axes (FRA), local structure axes (LSA) and local articulation axes are also described in this section. Other Aqwa-used axis frames, such as local axis systems for tether elements and tube elements, will be described in more detail in subsequent chapters.

### 1.2.1. Fixed Reference Axes

In hydrodynamic problems that include a fluid free-surface boundary, it is common practice to define a system of axes with the origin in the mean free surface of the fluid, as shown in [Figure 1.1: Definition of Axis Systems \(p. 12\)](#). In Aqwa this is referred to as the fixed reference axes (FRA), global axes, or OXYZ, which is a fixed right handed axis system with the origin in the mean free surface and Z-axis pointing vertically upwards.

**Figure 1.1: Definition of Axis Systems**

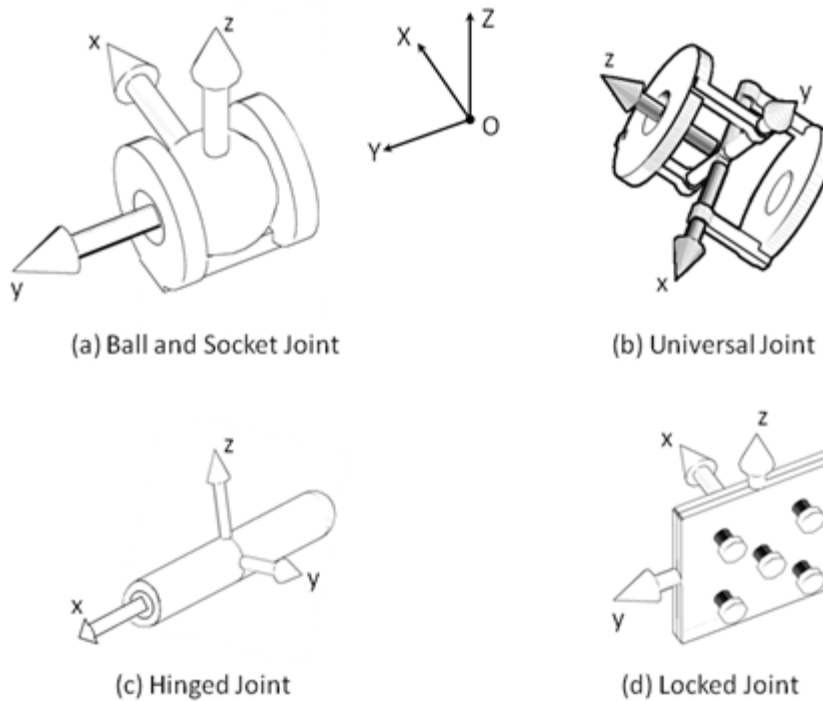


### 1.2.2. Local Structure Axes

For the description of rigid body motions, it is more convenient to use the center of gravity of the body, or the combined COG of mass of the structure and the liquid in the internal tanks, as a dynamic reference point. The local structure axes (LSA), body fixed axes, or Gxyz, is defined for each individual structure. As shown in [Figure 1.1: Definition of Axis Systems \(p. 12\)](#), the origin of the local structure axes is at this dynamic reference point. The local structure axes through the origin will initially be parallel to the fixed reference axes.

### 1.2.3. Local Articulation Axes

Aqwa allows structures to be connected by articulated joints. These joints do not permit relative translation of the two structures but allow relative rotational movement in a number of ways that can be defined by the user. The local articulation axes (LAA) or Axyz is shown in [Figure 1.2: Local Articulation Axes \(p. 13\)](#).

**Figure 1.2: Local Articulation Axes**

The local articulation axes are a local right handed coordinate system based on the following constraint types:

#### **Ball and Socket Joint:**

The origin is located at the connecting point, with the local x-, y-, and z-axes parallel to the X-, Y-, and Z-axes of the FRA at the initial position.

#### **Universal Joint:**

The origin is located at the connecting point, with the local x- and y-axes parallel to the two freely rotational freedoms. The local z-axis is at right angles to the local x- and y-axes.

#### **Hinged Joint:**

The origin is located at the connecting point, with the local x-axis parallel to the hinge axis. The local y-axis is at right angle to the local x-axis and in the OXY plane of the FRA at the initial position. In cases where the hinge axis is parallel to the Z-axis of the FRA in the initial position, the local y-axis will be parallel to the Y-axis of FRA.

#### **Locked Joint:**

The origin is located at the connecting point, with the local x-, y- and z-axes parallel to the X-, Y- and Z-axes of the FRA at the initial position.

## 1.2.4. Axis Transformation and Euler Rotations

Position, velocity, acceleration and force are represented in Aqwa by vectors with both magnitude and direction. These vectors can be described in the different coordinate systems by means of an axis transformation.

**Figure 1.3: Axis Transformation**

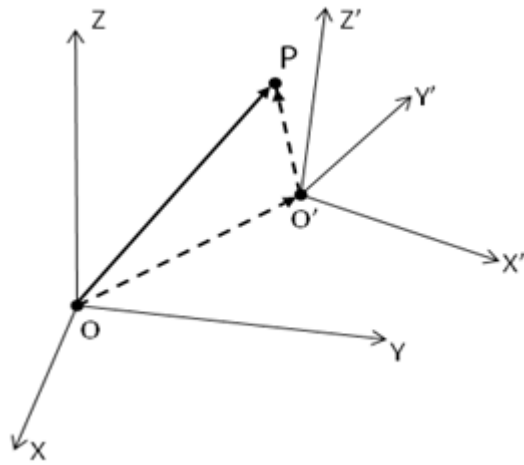


Figure 1.3: Axis Transformation (p. 14) shows two coordinate systems, the origin of the O'X'Y'Z' frame is at  $[X_0 \ Y_0 \ Z_0]^T$  in the OXYZ frame, where the superscript  $T$  denotes a matrix transpose. The directional cosines of the O'X'Y'Z' axes relative to the OXYZ axes are written as

$$\mathbf{e}_j = \begin{bmatrix} e_{1j} \\ e_{2j} \\ e_{3j} \end{bmatrix} \quad (j=1, 3) \quad (1.1)$$

If the coordinate of a point is represented as  $[X \ Y \ Z]^T$  in OXYZ and  $[x \ y \ z]^T$  in O'X'Y'Z', then we have

$$\begin{aligned} \begin{bmatrix} X \\ Y \\ Z \end{bmatrix} &= \begin{bmatrix} X_0 \\ Y_0 \\ Z_0 \end{bmatrix} + \begin{bmatrix} e_{11} & e_{12} & e_{13} \\ e_{21} & e_{22} & e_{23} \\ e_{31} & e_{32} & e_{33} \end{bmatrix} \begin{bmatrix} x \\ y \\ z \end{bmatrix} \\ &= \begin{bmatrix} X_0 \\ Y_0 \\ Z_0 \end{bmatrix} + \mathbf{E} \begin{bmatrix} x \\ y \\ z \end{bmatrix} \end{aligned} \quad (1.2)$$

where  $\mathbf{E}$  is the transformation matrix.

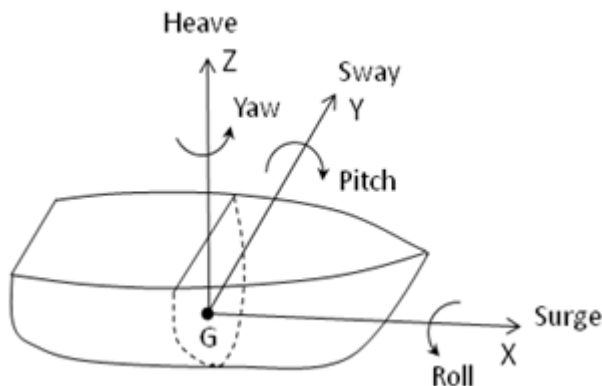
To transfer  $[X \ Y \ Z]^T$  in OXYZ into a coordinate in the O'X'Y'Z' frame, we have

$$\begin{bmatrix} x \\ y \\ z \end{bmatrix} = \mathbf{E}^T \left\{ \begin{bmatrix} X \\ Y \\ Z \end{bmatrix} - \begin{bmatrix} X_0 \\ Y_0 \\ Z_0 \end{bmatrix} \right\} \quad (1.3)$$

Employing the conventional seakeeping notation of a floating rigid body (see [40]), motions of that body are defined as the translational movements of the center of gravity and rotations about a set

of orthogonal axes through the origin of GXYZ, as illustrated in [Figure 1.4: Floating Rigid Motions \(p. 15\)](#). This intermediate coordinate system moves with the mean forward speed of the vessel but its X-, Y-, and Z-axes remain constantly parallel to the corresponding X-, Y-, and Z-axes of the fixed reference axes.

**Figure 1.4: Floating Rigid Motions**



### Translations

$$u_1 = \text{surge (along } X\text{)}$$

$$u_2 = \text{sway (along } Y\text{)}$$

$$u_3 = \text{heave (along } Z\text{)}$$

### Rotations

$$\theta_1 = \text{roll (about } X\text{)}$$

$$\theta_2 = \text{pitch (about } Y\text{)}$$

$$\theta_3 = \text{yaw (about } Z\text{)}$$

The naming of the various motions assumes that the body is described such that the forward and aft direction is parallel to the X-axis. If the body lies parallel to the Y-axis, then the rolling of the body will be termed 'pitch' and the pitching termed 'roll'.

For large amplitude rotational motion analysis, determination of Euler angles is a necessary step in kinematics and model graphic presentation. Aqwa defines the orientation of a structure using Euler angles. These are the rotation angles about the three axes of GXYZ:

A rotation of  $\theta_1$  about the X-axis:

$$E_x = \begin{bmatrix} 1 & 0 & 0 \\ 0 & \cos\theta_1 & -\sin\theta_1 \\ 0 & \sin\theta_1 & \cos\theta_1 \end{bmatrix} \quad (1.4)$$

A rotation of  $\theta_2$  about the Y-axis:

$$\mathbf{E}_y = \begin{bmatrix} \cos\theta_2 & 0 & \sin\theta_2 \\ 0 & 1 & 0 \\ -\sin\theta_2 & 0 & \cos\theta_2 \end{bmatrix} \quad (1.5)$$

A rotation of  $\theta_3$  about the Z-axis:

$$\mathbf{E}_z = \begin{bmatrix} \cos\theta_3 & -\sin\theta_3 & 0 \\ \sin\theta_3 & \cos\theta_3 & 0 \\ 0 & 0 & 1 \end{bmatrix} \quad (1.6)$$

The Euler rotation matrix is defined as a sequence of three rotations, in the order of the rotation first about the X-axis of GXYZ, then the Y-axis, and finally the Z-axis of GXYZ. It can be represented as the matrix product:

$$\begin{aligned} \mathbf{E} &= \mathbf{E}_z \mathbf{E}_y \mathbf{E}_x \\ &= \begin{bmatrix} \cos\theta_2\cos\theta_3 & \sin\theta_1\sin\theta_2\cos\theta_3 - \cos\theta_1\sin\theta_3 & \cos\theta_1\sin\theta_2\cos\theta_3 + \sin\theta_1\sin\theta_3 \\ \cos\theta_2\sin\theta_3 & \sin\theta_1\sin\theta_2\sin\theta_3 + \cos\theta_1\cos\theta_3 & \cos\theta_1\sin\theta_2\sin\theta_3 - \sin\theta_1\cos\theta_3 \\ -\sin\theta_2 & \sin\theta_1\cos\theta_2 & \cos\theta_1\cos\theta_2 \end{bmatrix} \end{aligned} \quad (1.7)$$

With this Euler rotation matrix, similar to [Equation 1.2 \(p. 14\)](#), the position of a point in the fixed reference axes can be expressed as

$$\begin{bmatrix} X \\ Y \\ Z \end{bmatrix} = \begin{bmatrix} X_g \\ Y_g \\ Z_g \end{bmatrix} + \mathbf{E} \begin{bmatrix} x \\ y \\ z \end{bmatrix} \quad (1.8)$$

where  $(X_g, Y_g, Z_g)^T$  is the coordinate of the center of gravity in the fixed reference axes and  $(x, y, z)^T$  is the coordinate of this point in the local structure axes (LSA).

As a special case when all the rotational angles are small, for instance  $\theta_j=O(\varepsilon)$  ( $j=1,3$ ), the Euler rotation matrix can be simplified to:

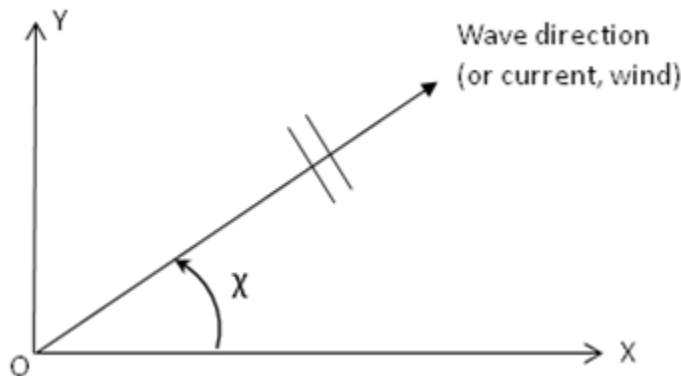
$$\mathbf{E} = \mathbf{I} + \boldsymbol{\Xi} \quad (1.9)$$

where

$$\begin{aligned} \mathbf{I} &= \begin{bmatrix} 1 & 0 & 0 \\ 0 & 1 & 0 \\ 0 & 0 & 1 \end{bmatrix} \\ \boldsymbol{\Xi} &= \begin{bmatrix} 0 & -\theta_3 & \theta_2 \\ \theta_3 & 0 & -\theta_1 \\ -\theta_2 & \theta_1 & 0 \end{bmatrix} \end{aligned}$$

### 1.3. Direction and Phase Angle Conventions

The wave, current and wind directions are defined in the OXY plane of the fixed reference axes (FRA). The direction is defined as the angle between the wave, current, or wind propagating direction and the positive X-axis measured anti-clockwise, as shown in [Figure 1.5: Direction Definition \(p. 17\)](#). For example, the heading angle is 0 when the wave propagation is along the positive X-axis of the global axes (following wave) and 90 when along the positive Y-axis of the global axes (beam wave).

**Figure 1.5: Direction Definition**

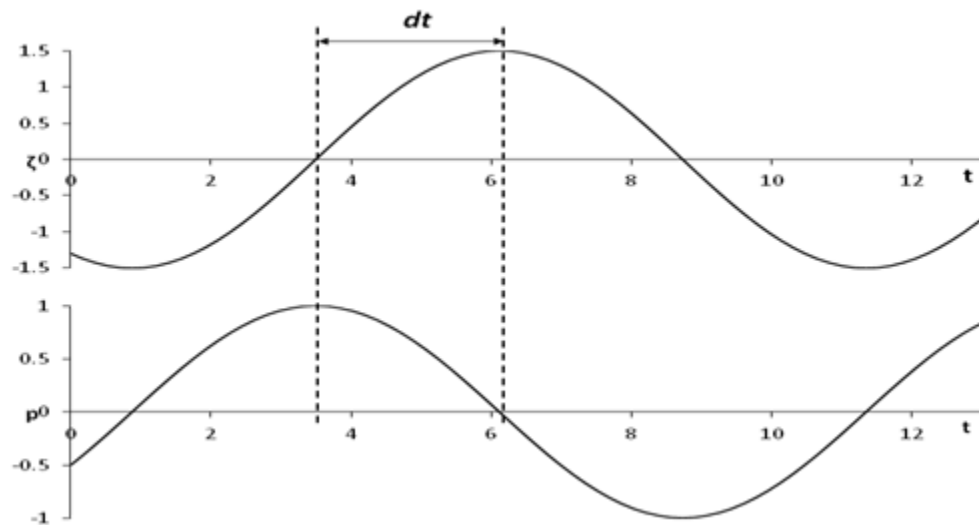
The phase angle of a parameter, such as the surge response amplitude operator (RAO) or wave exciting force, is defined according to the difference from the time when the regular wave crest is at the origin of GXYZ of a structure to the time when this parameter reaches its peak value. In other words, the time histories of an incident wave elevation and a corresponding force or response parameter are represented in the fixed reference axes as

$$\begin{aligned}\zeta &= a_w \cos(-\omega t + \alpha), \\ p &= a_p \cos(-\omega t + \alpha + \vartheta)\end{aligned}\quad (1.10)$$

where  $a_w$  is the regular wave amplitude,  $\omega$  is the wave frequency (in rad/s),  $\alpha$  is the wave phase angle (in radians) relative to the origin of the fixed reference axes,  $a_p$  is the amplitude of the parameter, and  $\vartheta$  is the phase angle of the parameter (in rad/s). The phase angle in degrees is given by:

$$\vartheta = \frac{360^\circ}{2\pi} \vartheta = \frac{360^\circ}{2\pi} \omega dt \quad (1.11)$$

As shown in [Figure 1.6: Phase Definition \(p. 17\)](#), a positive phase angle indicates that the parameter lags behind the wave.

**Figure 1.6: Phase Definition**



# Chapter 2: Ocean Environmental Conditions

---

Information on ocean environmental conditions, such as winds, waves and current, is critical for the design of all types of marine structures, and is especially important for floating offshore structures for which hydrodynamic behavior in open sea is more complicated than fixed structures. Waves apply exciting forces at wave frequency and nonlinear wave forces (for example, low frequency drift force and sum frequency second order forces), or alternatively nonlinear wave forces due to variation of the instantaneous wetted hull surface. Winds and current cause forces on the exposed members of the structure above and below the water surface respectively, and the forces are generally evaluated in Aqwa by a nonlinear drag force term.

This chapter describes the numerical models of waves, wind, and current available in Aqwa.

## 2.1. Ocean Waves

---

Ocean waves are composed of waves with different frequencies and directions. The waves from different directions interact and cause wave conditions to be very difficult to model mathematically. Various simplified theories and wave spectral models of ocean waves are introduced in the literature, such as small amplitude linear Airy wave, higher order Stokes wave, and irregular waves represented by wave spectra.

Aqwa can simulate first order (Airy wave) and second order (2nd order Stokes wave) regular waves in deep and finite depth water. Additionally, unidirectional or multi-directional irregular waves can be modeled by using the linear superposition approach.

### 2.1.1. Regular Wave

This section provides a brief description of the linear regular wave (Airy wave) and the second order Stokes wave in either deep water or finite depth water.

#### 2.1.1.1. Linear Regular Wave

Linear wave (Airy wave) is considered as the simplest ocean wave, and is based on the assumption of homogeneous, incompressible, inviscid fluid and irrotational flow. In addition, the wave amplitude is assumed to be small compared to the wave length and water depth; hence the linear free surface condition is used.

In the fixed reference axes (FRA), the water surface elevation at position X and Y can be expressed in complex value form as

$$\zeta = a_w e^{i[-\omega t + k(X \cos \chi + Y \sin \chi) + \alpha]} \quad (2.1)$$

where  $a_w$  is the wave amplitude,  $\omega$  is the wave frequency (in rad/s),  $k$  is the wave number,  $\chi$  is the wave propagating direction, and  $\alpha$  is the wave phase.

Assuming ideal, irrotational fluid, the flow can be represented by a velocity potential satisfying the Laplace equation in the whole fluid domain, the linear free surface condition, and horizontal impermeable bottom condition.

In finite depth water, the velocity potential at the location of  $\vec{X}=(X, Y, Z)$  is

$$\begin{aligned}\Phi_l(\vec{X}, t) &= \varphi_l(\vec{X}) e^{-i\omega t} \\ &= -\frac{iga_w \cosh[k(Z+d)]}{\omega \cosh(kd)} e^{[-\omega t + k(X \cos \chi + Y \sin \chi) + \alpha]}\end{aligned}\quad (2.2)$$

where  $d$  is water depth and  $g$  is gravitational acceleration.

Employing the linear free surface condition, the relationship between the wave frequency and the wave number (the linear dispersion relationship) is represented by

$$\nu = \frac{\omega^2}{g} = k \tanh(kd) \quad (2.3)$$

The wave length and wave period are

$$\begin{aligned}\lambda &= \frac{2\pi}{k} \\ T &= \frac{2\pi}{\omega}\end{aligned}\quad (2.4)$$

Using the Bernoulli equation and only taking account the linear term, the fluid pressure is

$$p(\vec{X}, t) = \frac{\rho g a_w \cosh[k(Z+d)]}{\cosh(kd)} e^{i[-\omega t + k(X \cos \chi + Y \sin \chi) + \alpha]} - \rho g Z \quad (2.5)$$

where  $\rho$  is the water density.

The wave celerity is

$$\begin{aligned}C &= \frac{\lambda}{T} \\ &= \frac{gT}{2\pi} \tanh\left(\frac{2\pi d}{\lambda}\right)\end{aligned}\quad (2.6)$$

Taking the partial derivative of the velocity potential, the fluid particle velocity is

$$\begin{aligned}\vec{v} &= (u, v, w) \\ &= \frac{a_w \omega \cosh[k(Z+d)]}{\sinh(kd)} e^{[-\omega t + k(X \cos \chi + Y \sin \chi) + \alpha]} (\cos \chi, \sin \chi, -i \tanh\{k[Z+d]\})\end{aligned}\quad (2.7)$$

When the wave particle velocity at the crest equals the wave celerity, the wave becomes unstable and begins to break (see [39]). The limiting condition for wave breaking in any water depth is given by:

$$\left(\frac{2a_w}{\lambda}\right)_{\max} = \frac{1}{7} \tanh(kd) \quad (2.8)$$

In infinite depth water ( $d \rightarrow \infty$ ), the wave elevation keeps the same form as Equation 2.1 (p. 19), but velocity potential is further simplified as

$$\begin{aligned}\Phi_l(\vec{X}, t) &= \varphi_l(\vec{X}) e^{-i\omega t} \\ &= -\frac{iga_w}{\omega} e^{[-\omega t + k(X \cos \chi + Y \sin \chi) + \alpha] + kZ}\end{aligned}\quad (2.9)$$

the linear dispersion relation is expressed as

$$\omega^2 = gk \quad (2.10)$$

and the fluid pressure is

$$p(\vec{X}, t) = -\rho g a_w e^{i[-\omega t + k(X \cos \chi + Y \sin \chi) + \alpha] + kZ} - \rho g Z \quad (2.11)$$

the wave celerity and fluid particle velocity are expressed as

$$\begin{aligned} C &= \frac{gT}{2\pi}, \\ \vec{v} &= a_w \omega e^{i[-\omega t + k(X \cos \chi + Y \sin \chi) + \alpha] + kZ} (\cos \chi, \sin \chi, -i) \end{aligned} \quad (2.12)$$

From [Equation 2.8 \(p. 20\)](#), for deep water wave, the wave breaks when the wave height ( $2a_w$ ) is  $1/7^{\text{th}}$  of the wave length.

### 2.1.1.2. Second Order Stokes Wave

Advanced wave theories may be necessary in some cases when the nonlinearities are important (see [4] and [8]). Aqwa allows application of the second order Stokes wave theory for moderate or severe regular wave conditions when the nonlinear Froude-Krylov force over the instantaneous wetted surface is estimated.

Choosing the ratio of the wave amplitude to wave length as the smallness parameter  $\varepsilon$ , Taylor expansions for the velocity potential and wave surface elevation in  $\varepsilon$  can be written as

$$\begin{aligned} \Phi &= \Phi^{(0)} + \Phi^{(1)} + \Phi^{(2)} + O(\varepsilon^3) \\ \zeta &= \zeta^{(0)} + \zeta^{(1)} + \zeta^{(2)} + O(\varepsilon^3) \end{aligned} \quad (2.13)$$

For water of finite depth, the second order Stokes wave is expressed as

$$\begin{aligned} \Phi(\vec{X}, t) &= \Phi^{(1)}(\vec{X}, t) + \Phi^{(2)}(\vec{X}, t) \\ &= -\frac{iga_w}{\omega} \frac{\cosh[k(Z+d)]}{\cosh(kd)} e^{i(-\omega t + kX' + \alpha)} \\ &\quad - i \frac{3}{8} \omega a_w^2 \frac{\cosh[2k(Z+d)]}{\sinh^4(kd)} e^{i(-2\omega t + 2kX' + 2\alpha)} \\ \zeta(X, Y; t) &= \zeta^{(1)}(X, Y; t) + \zeta^{(2)}(X, Y; t) \\ &= a_w e^{i(-\omega t + kX' + \alpha)} \\ &\quad + \frac{1}{4} k a_w^2 \frac{\cosh(kd)}{\sinh^3(kd)} [2 + \cosh(2kd)] e^{i(-2\omega t + 2kX' + 2\alpha)} \end{aligned} \quad (2.14)$$

where  $X' = X \cos \chi + Y \sin \chi$ .

When the set-down in the second-order Stokes waves is included, the potential and wave elevation are written as

$$\begin{aligned}
 \Phi(\vec{X}, t) &= \Phi^{(1)}(\vec{X}, t) + \Phi^{(2)}(\vec{X}, t) \\
 &= -\frac{ig a_w}{\omega} \frac{\cosh[k(Z+d)]}{\cosh(kd)} e^{i(-\omega t+kX'+\alpha)} \\
 &\quad - i \frac{3}{8} \omega a_w^2 \frac{\cosh[2k(Z+d)]}{\sinh^4(kd)} e^{i(-2\omega t+2kX'+2\alpha)} - Cgt \\
 \zeta(X, Y; t) &= \zeta^{(1)}(X, Y; t) + \zeta^{(2)}(X, Y; t) \\
 &= a_w e^{i(-\omega t+kX'+\alpha)} \\
 &\quad + \frac{1}{4} k a_w^2 \frac{\cosh(kd)}{\sinh^3(kd)} [2 + \cosh(2kd)] e^{i(-2\omega t+2kX'+2\alpha)} + (D+C)
 \end{aligned} \tag{2.15}$$

where

$$\begin{aligned}
 D &= -\frac{ka_w^2}{2\sinh(2kd)} \\
 C &= -\frac{ka_w^2}{4} \left[ \frac{4S+1-\tanh^2(kd)}{4S^2kd-\tanh(kd)} \right] \\
 S &= \frac{\sinh(2kd)}{2kd+\sinh(2kd)}
 \end{aligned}$$

The above new terms are negative constants called set-down, which represent the mean level in regular Stokes waves.

The velocity of a fluid particle at coordinates  $(X, Y, Z)$  is

$$\begin{aligned}
 \vec{v}(\vec{X}, t) &= \vec{v}^{(1)}(\vec{X}, t) + \vec{v}^{(2)}(\vec{X}, t) \\
 &= k\Phi^{(1)}(\vec{X}, t) (i\cos\chi, i\sin\chi, \tanh[k(Z+d)]) \\
 &\quad + 2k\Phi^{(2)}(\vec{X}, t) (i\cos\chi, i\sin\chi, \tanh[2k(Z+d)])
 \end{aligned} \tag{2.16}$$

The fluid pressure up to the second order is

$$\begin{aligned}
 p &= -\rho \frac{\partial \Phi(\vec{X}, t)}{\partial t} - \frac{1}{2} \rho \left\{ \operatorname{Re}(\vec{v}) \cdot \operatorname{Re}(\vec{v}) + i \operatorname{Im}(\vec{v}) \cdot \operatorname{Im}(\vec{v}) \right\} - \rho g Z \\
 &= -\rho \frac{\partial \Phi^{(1)}(\vec{X}, t)}{\partial t} - \rho \frac{\partial \Phi^{(2)}(\vec{X}, t)}{\partial t} - \rho g Z \\
 &\quad - \frac{1}{2} \rho \left\{ \operatorname{Re}(\vec{v}^{(1)}) \cdot \operatorname{Re}(\vec{v}^{(1)}) + i \operatorname{Im}(\vec{v}^{(1)}) \cdot \operatorname{Im}(\vec{v}^{(1)}) \right\} + O(\varepsilon^3)
 \end{aligned} \tag{2.17}$$

Comparing with the linear Airy wave, the second order Stokes wave profile shows higher peaked crests and shallower, flatter troughs.

For deep water cases ( $d \rightarrow \infty$ ), the second order Stokes wave given in [Equation 2.15 \(p. 22\)](#) becomes

$$\begin{aligned}
 \Phi(\vec{X}, t) &= \Phi^{(1)}(\vec{X}, t) + \Phi^{(2)}(\vec{X}, t) \\
 &= -\frac{ig \zeta_a}{\omega} e^{i(-\omega t+kX'+\alpha)+kZ} \\
 \zeta(X, Y; t) &= \zeta^{(1)}(X, Y; t) + \zeta^{(2)}(X, Y; t) \\
 &= a_w e^{-i\omega t+ikX} + \frac{1}{2} k a_w^2 e^{i(-2\omega t+2kX'+2\alpha)}
 \end{aligned} \tag{2.18}$$

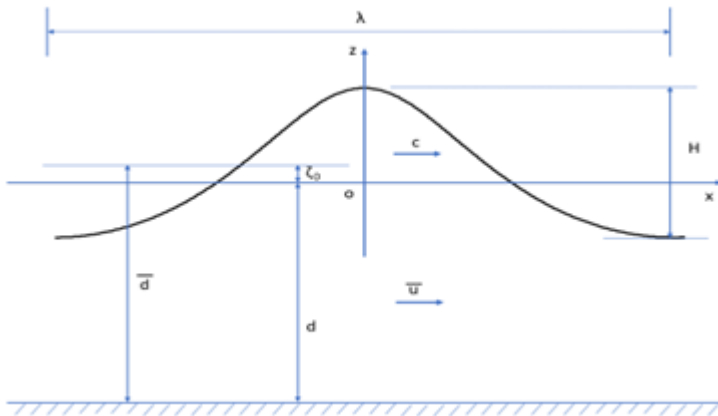
Note that in deep water, the second order Stokes wave potential only consists of the first order components, and there is no set-down term.

### 2.1.1.3. Fifth Order Stokes Wave

Aqwa allows the application of the fifth order Stokes wave theory for moderate or severe regular wave conditions when the nonlinear Froude-Krylov force over the instantaneous wetted surface is estimated.

The fifth order Stokes wave solution developed by Zhao, et al. [44] is employed. The solution is represented in the wave fixed reference coordinate system, of which the origin is on the undisturbed water surface, the x-axis is along the wave propagation direction, and the z-axis is upwards. The time equals zero when the wave crest passes through the origin of this coordinate system. [Figure 2.1: Fifth Order Stokes Wave \(p. 23\)](#) shows one cycle wave sketch and some important quantities, i.e.  $c$  as the wave celerity,  $\bar{u}$  as the uniform current along the wave propagation direction,  $d$  as the still water depth,  $\bar{d}$  as the mean water depth that is wave dependent, and  $H$  as the crest-to-trough wave height.

**Figure 2.1: Fifth Order Stokes Wave**



Denoting  $\chi$  as the wave direction in the fixed reference axes of OXYZ, the relationship between the wave fixed reference axes and the fixed reference axes of OXYZ (see [Figure 1.1: Definition of Axis Systems \(p. 12\)](#)) is

$$\begin{aligned} X &= x \cos \chi \\ Y &= x \sin \chi \\ Z &= z \end{aligned} \tag{2.19}$$

Choosing the wave steepness as the smallness parameter, i.e.  $\varepsilon = kH/2$ , where  $k$  is the wave number, the velocity potential and wave surface elevation in  $\varepsilon$  are written as (see [44])

$$\begin{aligned}
\phi(x, z; t) = & \bar{u}x + \frac{c - \bar{u}}{k} \left\{ \begin{array}{l} \varepsilon(\phi_{11} + \varepsilon^2\phi_{13} + \varepsilon^4\phi_{15})\cosh[k(d+z)]\sin\theta \\ + \varepsilon^2(\phi_{22} + \varepsilon^2\phi_{24})\cosh[2k(d+z)]\sin2\theta \\ + \varepsilon^3(\phi_{33} + \varepsilon^2\phi_{35})\cosh[3k(d+z)]\sin3\theta \\ + \varepsilon^4\phi_{44}\cosh[4k(d+z)]\sin4\theta \\ + \varepsilon^5\phi_{55}\cosh[5k(d+z)]\sin5\theta \end{array} \right\} \\
\zeta(x, z; t) = & \zeta_0 + \varepsilon(\zeta_{11} + \varepsilon^2\zeta_{13} + \varepsilon^4\zeta_{15})\cos\theta \\
& + \varepsilon^2(\zeta_{22} + \varepsilon^2\zeta_{24})\cos2\theta \\
& + \varepsilon^3(\zeta_{33} + \varepsilon^2\zeta_{35})\cos3\theta \\
& + \varepsilon^4\zeta_{44}\cos4\theta \\
& + \varepsilon^5\zeta_{55}\cos5\theta
\end{aligned} \tag{2.20}$$

where  $\theta = kx - \omega t$  and  $\omega$  is the wave frequency,

$$\begin{aligned}
\phi_{11} = & \frac{1}{s_1} \\
\phi_{13} = & -\frac{1}{s_1} \left( \frac{3}{2} + \frac{3}{s_1^2} + \frac{15}{8s_1^4} + \frac{27}{64s_1^6} \right) \\
\phi_{15} = & \frac{1}{s_1(6s_1^2+5)(8s_1^2+5)} \left( -2s_1^4 + 155s_1^2 + \frac{6819}{8} + \frac{7673}{4s_1^2} + \frac{149567}{64s_1^4} + \frac{198169}{128s_1^6} \right. \\
& \left. + \frac{320031}{512s_1^8} + \frac{328185}{2048s_1^{10}} + \frac{62775}{4096s_1^{12}} \right) \\
\phi_{22} = & \frac{3}{8s_1^4} \\
\phi_{24} = & \frac{1}{4s_1^2} - \frac{7}{12s_1^4} - \frac{69}{32s_1^6} - \frac{27}{16s_1^8} - \frac{27}{64s_1^{10}} \\
\phi_{33} = & -\frac{1}{16s_1^5} + \frac{9}{64s_1^7} \\
\phi_{35} = & \frac{1}{8s_1^3(6s_1^2+5)} \left( s_1^2 + \frac{201}{8} + \frac{615}{16s_1^2} - \frac{93}{4s_1^4} - \frac{4725}{64s_1^6} - \frac{5913}{128s_1^8} - \frac{1215}{128s_1^{10}} \right) \\
\phi_{44} = & \frac{1}{6s_1^2+5} \left( \frac{5}{96s_1^4} - \frac{3}{8s_1^6} - \frac{9}{256s_1^8} + \frac{135}{512s_1^{10}} \right) \\
\phi_{55} = & \frac{1}{8s_1^3(6s_1^2+5)(8s_1^2+5)} \left( -\frac{3}{8} + \frac{121}{16s_1^2} - \frac{131}{16s_1^4} - \frac{279}{16s_1^6} + \frac{135}{256s_1^8} + \frac{2025}{512s_1^{10}} \right)
\end{aligned} \tag{2.21}$$

the wave setup is

$$\zeta_0 = \frac{1}{k} \frac{c_1}{s_1} \left[ \frac{1}{2} \varepsilon^2 + \varepsilon^4 \left( -\frac{1}{2} - \frac{9}{8s_1^2} - \frac{75}{64s_1^4} + \frac{9}{32s_1^6} \right) \right] \tag{2.22}$$

and

$$\begin{aligned}
\zeta_{11} &= \frac{1}{k} \\
\zeta_{13} &= -\zeta_{33} \\
\zeta_{15} &= -\frac{1}{k(6s_1^2+5)(8s_1^2+5)} \left( \frac{211}{4}s_1^4 + \frac{19249}{96}s_1^2 + \frac{10645}{64} - \frac{5871}{16s_1^2} - \frac{374909}{384s_1^4} - \frac{219815}{256s_1^6} \right. \\
&\quad \left. - \frac{224091}{512s_1^8} - \frac{284985}{2048s_1^{10}} - \frac{62775}{4096s_1^{12}} \right) \\
\zeta_{22} &= \frac{1}{2k} \frac{c_1}{s_1} \left( 1 + \frac{3}{2s_1^2} \right) \\
\zeta_{24} &= \frac{1}{k} \frac{c_1}{s_1} \left( \frac{1}{3} - \frac{7}{6s_1^2} - \frac{33}{8s_1^4} - \frac{27}{8s_1^6} - \frac{27}{32s_1^8} \right) \\
\zeta_{33} &= \frac{1}{k} \left( \frac{3}{8} + \frac{9}{8s_1^2} + \frac{9}{8s_1^4} + \frac{27}{64s_1^6} \right) \\
\zeta_{35} &= \frac{1}{k} \frac{1}{6s_1^2+5} \left( \frac{297}{64}s_1^2 + \frac{1179}{128} - \frac{1396}{64s_1^2} - \frac{23247}{256s_1^4} - \frac{62559}{512s_1^6} - \frac{33615}{512s_1^8} - \frac{27495}{1024s_1^{10}} - \frac{3645}{1024s_1^{12}} \right) \\
\zeta_{44} &= \frac{1}{k} \frac{c_1}{s_1} \frac{1}{6s_1^2+5} \left( 2s_1^2 + \frac{53}{6} + \frac{365}{24s_1^2} + \frac{51}{4s_1^4} + \frac{351}{64s_1^6} + \frac{135}{128s_1^8} \right) \\
\zeta_{55} &= -(\zeta_{15} + \zeta_{35})
\end{aligned} \tag{2.23}$$

where  $s_1 = \sinh(kd)$  and  $c_1 = \cosh(kd)$ .

The wave dispersion relation is given by

$$(c - \bar{u})^2 = c_{(0)}^2 + \varepsilon^2 c_{(2)}^2 + \varepsilon^4 c_{(4)}^2 \tag{2.24}$$

where

$$\begin{aligned}
c_{(0)}^2 &= \frac{g}{k} \frac{s_1}{c_1} \\
c_{(2)}^2 &= \frac{g}{k} \frac{s_1}{c_1} \left( 1 + \frac{3}{2s_1^2} + \frac{9}{8s_1^4} \right) \\
c_{(4)}^2 &= \frac{g}{k} \frac{s_1}{c_1} \left( \frac{1}{2} + \frac{7}{8s_1^2} - \frac{99}{32s_1^4} - \frac{405}{64s_1^6} - \frac{945}{256s_1^8} + \frac{81}{512s_1^{10}} \right)
\end{aligned}$$

and  $c = \omega/k$ .

The volume flux underneath the wave per unit span is defined as  $Q = \overline{\int_{-d}^{\zeta} u(x, z) dz}$ . It is further expressed as

$$Q = \bar{u}d + c\zeta_0 \tag{2.25}$$

The mean water level, which is wave dependent, can be written as

$$\bar{d} = d + \zeta_0 \tag{2.26}$$

One of five sets of the wave parameters are selected to uniquely determine the fifth order Stokes wave in the wave fixed reference axes:

- Wave height ( $H$ ), wavelength ( $\lambda$ ), still water depth ( $d$ ), and uniform current ( $\bar{u}$ ) are known.

The wave number ( $k$ ) is obtained from [Equation 2.4 \(p. 20\)](#) and the wave celerity (and wave frequency) may be estimated from [Equation 2.24 \(p. 25\)](#).

- Wave height ( $H$ ), wave period ( $T$ ), still water depth ( $d$ ), and uniform current ( $\bar{u}$ ) are known.

The wave frequency is determined by [Equation 2.4 \(p. 20\)](#) and the wave celerity (and wave number) may be estimated from [Equation 2.24 \(p. 25\)](#).

- Wave height ( $H$ ), wavelength ( $\lambda$ ), mean water depth ( $\bar{d}$ ), and uniform current ( $\bar{u}$ ) are known.

The wave number ( $k$ ) is obtained from [Equation 2.4 \(p. 20\)](#), the still water depth is determined by [Equation 2.26 \(p. 25\)](#), then the wave celerity (and wave frequency) may be estimated from [Equation 2.24 \(p. 25\)](#).

- Wave height ( $H$ ), wavelength ( $\lambda$ ), still water depth ( $d$ ), and volume flux ( $Q$ ) are known.
- Wave height ( $H$ ), wave period ( $T$ ), still water depth ( $d$ ), and volume flux ( $Q$ ) are known.

This is notably the case in laboratory experiments, in which the mass flux under waves is known or assumed. The wave number ( $k$ ) is obtained from [Equation 2.4 \(p. 20\)](#), the uniform current may be determined by [Equation 2.25 \(p. 25\)](#), then the wave celerity (and wave frequency) may be estimated from [Equation 2.24 \(p. 25\)](#).

The Ursell number ( $Ur$ ) is introduced to simply check the applicable range of the fifth order Stokes wave solution (see [44]), which satisfies

$$Ur = \frac{H\lambda^2}{d^3} < 46.7 \quad (2.27)$$

## 2.1.2. Irregular Waves

Most energy at the ocean surface is contributed by wind generated waves, which usually result from the wind blowing over a vast expanse of fluid surface. A wind sea is the wind induced wave system which is directly being generated and affected by the local winds, while a swell consists of wind generated waves that are hardly affected by the local wind at that time but have been generated elsewhere or some time ago. Full-development sea waves are in a state where the largest of the waves in the sea cannot grow any larger and its wave height and wavelength have reached the full potential.

In practice, the linear theory is used to express the multi-directional sea waves (short crested waves) as the summation of a large number of wave components, for instance:

$$\zeta(X, Y, t) = \sum_{m=1}^{N_d} \sum_{j=1}^{N_m} a_{jm} e^{i(k_{jm} X \cos \chi_m + k_{jm} Y \sin \chi_m - \omega_{jm} t + \alpha_{jm})} \quad (2.28)$$

where  $N_d$  and  $N_m$  are the number of wave directions and number of wave components along each wave direction  $\chi_m$  ( $m=1, N_d$ ),  $a_{jm}$  is the wave amplitude,  $\omega_{jm}$  is the wave frequency,  $k_{jm}$  is the wave number, and  $\alpha_{jm}$  is the random phase angle of a wave component  $jm$  ( $j=1, N_m$ ).

The wave representation for irregular seas can be achieved by specification of wave spectra. Mathematically speaking, the wave spectrum spreads from zero to infinite frequencies. However, examination of the spectrum shows that the wave energy is often concentrated in a relatively narrow band, which determines the actual wave pattern. Employing characteristic, the summation given in [Equation 2.28 \(p. 26\)](#) could numerically consist of a limited number of wave components, starting from a non-zero lower bounded frequency and finishing at a finite-value upper bounded frequency. The selection of these starting and finishing frequencies should ensure that this truncated frequency range covers at least 99% of overall wave energy.

If a wave spectrum,  $S_m(\omega)$ , is introduced for the  $m$ -th sub-directional waves, the wave amplitude  $a_{jm}$  can be expressed as

$$a_{jm} = \sqrt{2S_m(\omega_j)\Delta\omega_j} \quad (2.29)$$

Uni-directional waves ( $N_d=1$ ) are also called long-crested waves, which propagate along one specified direction only.

Aqwa can accept formulated wave spectrum, user-defined wave spectrum or import time history of wave elevation, and any combination thereof to describe an irregular sea.

The following wave spectral parameters may be useful:

Significant wave height:  $H_s = 4\sqrt{m_0}$

Mean wave period:  $T_1 = 2\pi m_0 / m_1$

Mean zero crossing period:  $T_2 = 2\pi\sqrt{m_0/m_2} = T_z$

Peak period:  $T_0 = 2\pi/\omega_p$

where  $m_k = \int_0^{\infty} \omega^k S(\omega) d\omega$  and  $\omega_p$  is the peak frequency (in rad/s) at which the maximum wave energy occurs.

In Aqwa time domain analysis, the irregular waves in the  $m$ -th sub-direction are represented by the wavelets (in other words, wave components) with constant wave amplitude. Denoting the significant wave height in this sub-direction as  $H_s^m$ , from [Equation 2.29 \(p. 27\)](#) the constant wavelet amplitude is

$$a_{jm} = \frac{H_s^m}{\sqrt{8N_m}} , (j=1, N_m) \quad (2.30)$$

where  $N_m$  is the number of wavelets introduced in [Equation 2.28 \(p. 26\)](#).

### 2.1.2.1. Formulated Wave Spectra

There are several pre-configured wave spectra that only require knowledge of a couple of statistical parameters to fully define the sea state. These are explained below.

#### 2.1.2.1.1. JONSWAP Spectrum

The JONSWAP (Joint North Sea Wave Project) spectrum can take into account the imbalance of energy flow in the wave system (for instance, when seas are not fully developed). Energy imbalance is nearly always the case when there is a high wind speed. Parameterization of the classic form of the JONSWAP spectrum (using fetch and wind speed) was undertaken by Houmb and Overvik [17]. The peak frequency as well as empirical parameters  $\gamma$  and  $\alpha$  are used in this formulation.

The spectral ordinate at a frequency is given by

$$S(\omega) = \frac{\alpha g^2 \gamma^a}{\omega^5} \exp\left(-\frac{5\omega_p^4}{4\omega^4}\right) \quad (2.31)$$

where

$\omega_p$  is the peak frequency in rad/s,  $\gamma$  is the peak enhancement factor,  $\alpha$  is a constant that relates to the wind speed and the peak frequency of wave spectrum, and

$$\alpha = \exp\left[-\frac{(\omega - \omega_p)^2}{2\sigma^2\omega_p^2}\right]$$

$$\sigma = \begin{cases} 0.07 & \text{where } \omega \leq \omega_p \\ 0.09 & \text{where } \omega > \omega_p \end{cases}$$

Because  $\alpha$  is a constant, the integration of this spectrum can be expressed as

$$m_0 = \int_0^\infty S(\omega) d\omega = \alpha \int_0^\infty \frac{g^2 \gamma^a}{\omega^5} \exp\left(-\frac{5\omega_p^4}{4\omega^4}\right) d\omega = \left(\frac{H_s}{4}\right)^2 \quad (2.32)$$

Therefore if  $\gamma$ ,  $\omega_p$ , and  $H_s$  are known, then the variable  $\alpha$  can be determined by

$$\alpha = \left(\frac{H_s}{4}\right)^2 \left| \int_0^\infty \frac{g^2 \gamma^a}{\omega^5} \exp\left(-\frac{5\omega_p^4}{4\omega^4}\right) d\omega \right| \quad (2.33)$$

You can define the starting and finishing frequencies of the JONSWAP spectrum used in [Equation 2.31 \(p. 27\)](#). By default, Aqwa gives the definitions as:

Starting frequency (in rad/s):

$$\omega_s = \omega_p \left(0.58 + 0.05 \frac{\gamma-1}{19}\right) \quad (2.34)$$

Finishing frequency (in rad/s):

$$\omega_f = \omega_p \cdot F(\gamma) \quad (2.35)$$

where the weighting function values against  $\gamma \in [1.0, 20.0]$  are listed in [Table 2.1: Weighting Function Values \(p. 28\)](#).

**Table 2.1: Weighting Function Values**

| $\gamma$ | $F(\gamma)$ | $\gamma$ | $F(\gamma)$ | $\gamma$ | $F(\gamma)$ |
|----------|-------------|----------|-------------|----------|-------------|
| 1.0      | 5.1101      | 8.0      | 3.3700      | 15.0     | 2.9650      |
| 2.0      | 4.4501      | 9.0      | 3.2900      | 16.0     | 2.9300      |
| 3.0      | 4.1000      | 10.0     | 3.2200      | 17.0     | 2.8950      |
| 4.0      | 3.8700      | 11.0     | 3.1600      | 18.0     | 2.8600      |
| 5.0      | 3.7000      | 12.0     | 3.1050      | 19.0     | 2.8300      |
| 6.0      | 3.5700      | 13.0     | 3.0550      | 20.0     | 2.8000      |
| 7.0      | 3.4600      | 14.0     | 3.0100      |          |             |

### 2.1.2.1.2. Pierson-Moskowitz Spectrum

The Pierson-Moskowitz spectrum is a special case for a fully developed long crested sea. In Aqwa, the Pierson-Moskowitz spectrum is formulated in terms of two parameters of the significant wave height and the average (mean zero-crossing) wave period. The form used in Aqwa is considered

of more direct use than the classic form (in terms of the single parameter wind speed), and the form involving the peak frequency (where the spectral energy is a maximum). For more information, see [15]. The spectral ordinate at a frequency (in rad/s) is given by

$$S(\omega) = 4\pi^3 \frac{H_s^2}{T_z^4} \frac{1}{\omega^5} \exp\left(-\frac{16\pi^3}{T_z^4} \frac{1}{\omega^4}\right) \quad (2.36)$$

The following relationship exists between  $T_z$ ,  $T_1$ , and  $T_0$ :

$$\begin{aligned} T_0 &= 1.408 \cdot T_z \\ T_1 &= 1.086 \cdot T_z \end{aligned} \quad (2.37)$$

where  $T_1$  is the mean wave period and  $T_0$  is the peak period.

You can define the starting and finishing frequencies of the Pierson-Moskowitz spectrum used in [Equation 2.36 \(p. 29\)](#). By default, Aqwa gives the definitions as:

Starting frequency (in rad/s):

$$\omega_s = 0.58 \frac{2\pi}{T_z} \quad (2.38)$$

Finishing frequency (in rad/s):

$$\omega_f = 5.1101 \frac{2\pi}{T_z} \quad (2.39)$$

### 2.1.2.1.3. Gaussian Spectrum

The standard Gaussian spectrum is:

$$S(\omega) = \frac{H_s^2}{16\sqrt{2\pi}\sigma} \exp\left(-\frac{(\omega-\omega_p)^2}{2\sigma^2}\right) \quad (2.40)$$

where  $\omega_p$  is the peak frequency (in rad/s),  $\sigma$  is the standard deviation and  $\sigma \geq 0.08 \cdot \omega_p$ .

You can define the starting and finishing frequencies of the Gaussian spectrum used in [Equation 2.40 \(p. 29\)](#). By default, Aqwa gives the definitions as:

Starting frequency (in rad/s):

$$\omega_s = \min\{100.0, \max[(\omega_p - 3\sigma), 0.001]\} \quad (2.41)$$

Finishing frequency (in rad/s):

$$\omega_f = \min\{100.0, \max[(\omega_p + 3\sigma), 0.001]\} \quad (2.42)$$

If  $\omega_f - \omega_s < 0.001$ , they are alternatively defined as

$$\begin{aligned} \omega_s &= 0.1 \\ \omega_f &= 6.0 \end{aligned} \quad (2.43)$$

### 2.1.2.1.4. Ochi-Hubble Spectrum

Ochi-Hubble bimodal spectrum represents almost all stages of the sea condition associated with storm (Ochi and Hubble, 1976 [33]). The spectrum is expressed by the sum of two sets of three-

parameter spectra, to cover the lower frequency and high components of the wave energy respectively.

$$S(\omega) = \frac{1}{4} \sum_{j=1}^2 \frac{\left(\frac{4\lambda_j+1}{4}\omega_m^4\right)^{\lambda_j}}{\Gamma(\lambda_j)} \frac{H_{sj}^2}{\omega^{4\lambda_j+1}} \exp\left[-\left(\frac{4\lambda_j+1}{4}\right)\left(\frac{\omega_m}{\omega}\right)^4\right] \quad (2.44)$$

where  $H_{sj}$  is the significant wave height,  $\lambda_j$  is the spectral shape parameter and  $\omega_m$  is the modal frequency in rad/s of the j-th sub-spectrum, and  $\Gamma$  is the Gamma function.

The total significant wave height of the Ochi-Hubble spectrum is

$$H_s = \sqrt{H_{s1}^2 + H_{s2}^2} \quad (2.45)$$

#### 2.1.2.1.5. Bretschneider Spectrum

Bretschneider spectrum is the special case of the Ochi-Hubble spectrum when  $\lambda=1$  and  $j=1$ . It is expressed by two parameters of significant wave height and modal frequency,

$$S(\omega) = \frac{1.25}{4} \frac{H_s^2 \omega_m^4}{\omega^5} \exp\left[-1.25\left(\frac{\omega_m}{\omega}\right)^4\right] \quad (2.46)$$

The zero-crossing frequency (ITTC, 2002 [20]) is

$$\omega_z = 1.331 \times (1.25 \omega_m^4)^{\frac{1}{4}} = 1.407 \omega_m \quad (2.47)$$

#### 2.1.2.1.6. TMA Spectrum

Finite water depth TMA spectrum for non-breaking waves is given as the JONSAWP spectrum multiplying a water depth function (ITTC, 2002 [20]),

$$S(\omega) = \frac{\alpha g^2 \gamma^a}{\omega^5} \exp\left(-\frac{5\omega_p^4}{4\omega^4}\right) \phi(\omega) \quad (2.48)$$

where the depth function  $\phi(\omega) = \frac{\omega^5 \partial k}{2g^2 k^3}$ ,  $k$  is the wave number derived from the linear dispersion relationship of Equation 2.3 (p. 20); the approximately expression (ITTC, 2002 [20]) of  $\phi(\omega)$  is

$$\phi(\omega) = 1 - \frac{1}{2} \frac{B\omega_h^3 + 3A\omega_h^2 + 2}{(A\omega_h^2 + 1)^2} \quad (2.49)$$

where  $\omega_h = \omega \sqrt{\frac{d}{g}}$ ,  $d$  is the water depth and

$$A = 1.0 + 0.6522\omega_h^2 + 0.4622\omega_h^4 + 0.0864\omega_h^8 + 0.0675\omega_h^{10}$$

$$B = 0.6522\omega_h + 0.9244\omega_h^3 + 0.3456\omega_h^7 + 0.3375\omega_h^9$$

#### 2.1.2.2. User Defined Wave-Spectrum

You can input any other spectrum into Aqwa. User-defined wave spectra are normally employed for input of non-deterministic spectra such as tank spectra, recorded full-scale spectra, or simply where the formulated spectrum is not yet available in Aqwa.

The values of frequencies (in rad/s by default) and the values of the spectral ordinates can also be defined.

### 2.1.2.3. Import Time History of Wave Elevation

Aqwa can import a time history series of wave elevation in order to reproduce model test wave conditions.

In an Aqwa time domain analysis (Aqwa-Drift or Aqwa-Naut analysis), the wave elevation time-history will be reproduced exactly, within the frequency range of the fitted spectrum and subject to the limitations of round-off error. This is achieved by multiplying each of the spectral wave components (as in standard Aqwa) by a different low frequency perturbation (LFP) function:

$$\zeta(t) = \sum_{j=1}^N a_j \cos(-\omega_j t + k_j X' + \alpha_j) F_j(t) \quad (2.50)$$

where  $N$  is the number of wave components,  $a_j$  is the wave amplitude,  $\omega_j$  is the frequency,  $k_j$  is the wave number,  $\alpha_j$  is the phase angle of wave component  $j$  ( $j=1,N$ ),  $X' = X \cos \chi + Y \sin \chi$  where  $\chi$  is the wave direction, and  $F_j(t)$  is the low frequency perturbation (LFP) function automatically estimated by Aqwa based on the imported time history record. The starting and finishing wave frequencies are defined by [Equation 2.34 \(p. 28\)](#) and [Equation 2.35 \(p. 28\)](#), and the amplitude of a wave component is defined as  $a_j = \sqrt{2S_w(\omega_j)\Delta\omega_j}$  where  $S_w(\omega_j)$  is the fitted JONSWAP wave spectral ordinate and  $\Delta\omega_j$  is the frequency band of the  $j$ -th wave component.

No spurious low frequency waves are generated by the above method. For any wave component, the minimum frequency present in the wave elevation is  $\omega_j - d\omega$ , where  $d\omega$  is the highest frequency present in the LFP function. Note also that there is no frequency overlap for each wave component. Each LFP function can be considered as a frequency spreading function over a limited set of contiguous frequency bands.

The minimum duration of the time history required by the program is 7200s (2 hours). This duration is necessary in order to give sufficient resolution of low frequency resonant responses. You may encounter situations where model tests cannot be performed to cover the 2-hour duration. In such cases, Aqwa will extend the imported wave elevation time history record to 7200 seconds by the following approach.

As shown in [Figure 2.2: Extension of Wave Elevation Record \(p. 32\)](#), if the original length of time history of wave elevation is assumed to be  $T_{N_0} < 7200$ , it will be first extended to

$T_{N_1} = \min(2T_{N_0}, 7200)$  by

$$\begin{aligned} t_{N_0+j} &= 2t_{N_0} - t_{N_0-j} \leq T_{N_1} \\ \zeta(t_{N_0+j}) &= \zeta(t_{N_0-j}) \text{ where } j=1, N_0-1 \end{aligned} \quad (2.51)$$

where  $N_0$  is the number of time steps of the original imported time history records.

If  $T_{N_1} < 7200$  after the extension treatment by [Equation 2.51 \(p. 31\)](#), further extension of  $N_1 = 2N_0 - 1$  wave elevation points will be done by using [Equation 2.51 \(p. 31\)](#) again but replacing the parameters  $N_0$  and  $T_{N_1}$  by  $N_1$  and  $T_{N_2} = \min(2T_{N_1}, 7200)$  respectively. The described extension procedure will be iterated until the last time step reaches 7200 seconds with  $N_k$  wave elevation points in total.

An end-correction treatment will be carried out to enable the Fourier transform to be more accurate. Denoting  $N_T$  as the total number of wave elevation points such that

$$N_T = \begin{cases} N_0 & \text{if } T_{N_0} \geq 7200 \\ N_k & \text{if } T_{N_0} < 7200 \end{cases} \quad (2.52)$$

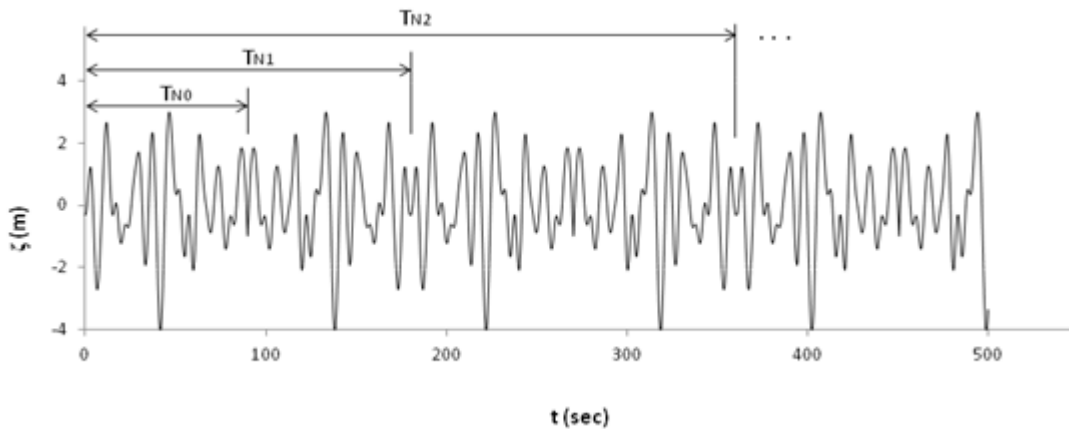
the wave elevation values at the starting and finishing ends of the record are corrected as

$$\begin{aligned} \zeta(1) &= 0 \\ \zeta(j) &= (1 - \cos^2 \varphi_j) \zeta(j) \\ \zeta(N_T - j + 2) &= (1 - \cos^2 \varphi_j) \zeta(N_T - j + 2) \text{ where } j = 2, N_c \end{aligned} \quad (2.53)$$

where  $N_c = \frac{N_0}{180}$  and  $\varphi_j = \frac{\pi}{2} \cdot \frac{j-1}{N_c}$ .

This end-corrected time series of wave elevations can also be employed to generate a user-defined spectrum by using a Fast Fourier Transform. The frequency range is based on a JONSWAP fit of the wave elevation spectral density. This fitted wave spectrum is used in the same way as a normal user-defined spectrum, and is employed by Aqwa in equilibrium prediction, frequency domain dynamic statistic analysis, and time domain analysis of severe waves. As the phases of the spectral wave components are allocated randomly, the imported wave elevation time history cannot be reproduced exactly in these types of Aqwa analyses.

**Figure 2.2: Extension of Wave Elevation Record**



#### 2.1.2.4. Cross-Swell Waves

Aqwa can simulate the effects of cross swell in most types of analyses, with the exception of time history response of severe waves. It can be defined by a JONSWAP, Pierson-Moskowitz, or Gaussian wave spectrum. The default starting and finishing frequencies of the cross swell wave spectrum will be used automatically, which are defined in [Equation 2.34 \(p. 28\)](#) and [Equation 2.35 \(p. 28\)](#) for JONSWAP spectra, [Equation 2.38 \(p. 29\)](#) and [Equation 2.39 \(p. 29\)](#) for Pierson-Moskowitz spectra, and [Equation 2.42 \(p. 29\)](#) and [Equation 2.43 \(p. 29\)](#) for Gaussian spectra.

### 2.1.2.5. Spreading Sea

As the wind over sea surface is turbulent, the induced wave spectrum is often expressed as two-dimensional, of which one dimension corresponds to frequency and the other to wave direction.

For design/analysis purposes representative spectra  $S(\omega, \chi)$  should be in the form of:

- An ordinary spectrum  $S(\omega)$ , for example a JONSWAP wave spectrum
- A mean direction for each frequency  $\bar{\chi}(\omega)$
- A formula giving the spreading function about the mean wave direction,  $G(\omega, \chi)$

$$S(\omega, \chi) = G(\omega, \chi)S(\omega) \quad (2.54)$$

For more information, see [4].

The mean direction is assumed to be constant for all wave frequencies and the spreading function is of the form

$$G(\omega, \chi) = C \cos^n \left[ \frac{\pi}{\Delta\chi} (\chi - \bar{\chi}) \right] \text{ for } -\frac{\Delta\chi}{2} \leq \chi - \bar{\chi} \leq \frac{\Delta\chi}{2} \quad (2.55)$$

Where  $n$  is the power of the wave spreading function and  $C$  is selected to ensure that at each frequency, it is satisfied that

$$\int_{-\frac{\Delta\chi}{2} + \bar{\chi}}^{\frac{\Delta\chi}{2} + \bar{\chi}} S(\omega, \chi) d\chi = S(\omega) \quad (2.56)$$

Based on this definition, the above equation becomes

$$\int_{-\frac{\Delta\chi}{2}}^{\frac{\Delta\chi}{2}} G(\omega, \chi) d\chi = 1 \quad (2.57)$$

which leads to

$$C \int_{-\frac{\Delta\chi}{2}}^{\frac{\Delta\chi}{2}} \cos^n \left[ \frac{\pi}{\Delta\chi} \chi \right] d\chi = 1 \quad (2.58)$$

For the case of  $n=2$ ,

$$C = \frac{2}{\Delta\chi} \quad (2.59)$$

When the spreading angle is set to 180 degrees ( $\Delta\chi=\pi$ ), Equation 2.58 (p. 33) becomes

$$C \int_{-\frac{\pi}{2}}^{\frac{\pi}{2}} \cos^n \chi d\chi = 1 \text{ where } n \geq 2 \quad (2.60)$$

Selections of the constant factor  $C$  are listed in Table 2.2: Weighting Factors with Respect to the Power Number of Spreading Function (p. 34).

**Table 2.2: Weighting Factors with Respect to the Power Number of Spreading Function**

| n   | 2       | 3     | 4          | 5       | 6           | 7       | 8             | 9         | 10            |
|-----|---------|-------|------------|---------|-------------|---------|---------------|-----------|---------------|
| $C$ | $2/\pi$ | $3/4$ | $8/(3\pi)$ | $15/16$ | $16/(5\pi)$ | $35/32$ | $128/(35\pi)$ | $315/256$ | $256/(63\pi)$ |

Aqwa employs a Gaussian integral to numerically represent spreading seas. When an  $N_w$ -point Gaussian integration scheme is used to represent a spreading sea, the following equations are used:

$$\begin{aligned} S_m(\omega) &= W_m S(\omega) \\ \sum_{m=1}^{N_w} S_m(\omega) &= S(\omega) \end{aligned} \quad (2.61)$$

where  $S_m(\omega)$  is the wave energy spectrum in the  $m$ -th sub-direction.

$$\begin{aligned} W_m &= \frac{w_m \cos^n(\chi_m - \bar{\chi})}{d_1} \\ d_1 &= \frac{2}{\Delta\chi} \int_{-\frac{\Delta\chi}{2}}^{\frac{\Delta\chi}{2}} \cos^n \chi d\chi \end{aligned} \quad (2.62)$$

where  $w_m$  is the Gaussian integration weighting factor between the standard integration range of  $[-1, 1]$  and  $\chi_m$  is the sub-direction corresponding to the  $m$ -th standard Gaussian integration point.

For spreading wave functions with a higher power ( $n > 4$ ), the wave energy is mainly distributed over a narrower direction range centered in the mean direction  $\bar{\chi}$ . To increase the numerical accuracy of the spreading wave representation, an effective wave direction range,  $\Delta\chi_e < \Delta\chi$ , is introduced.

Outside this range, the spreading wave energy is negligible:

$$\frac{E_e}{E} < \varepsilon, (\varepsilon \ll 1) \quad (2.63)$$

where:

$$E_e = \int_{-\frac{\Delta\chi_e}{2}}^{-\frac{\Delta\chi_e}{2}} \cos^n \chi d\chi + \int_{\frac{\Delta\chi_e}{2}}^{\frac{\Delta\chi_e}{2}} \cos^n \chi d\chi$$

$$E = \int_{-\frac{\Delta\chi}{2}}^{\frac{\Delta\chi}{2}} \cos^n \chi d\chi$$

The Gaussian integration is over the effective wave range  $\Delta\chi_e$  instead of the wave spreading direction range of  $\Delta\chi$ . As an example, the effective range is about  $\frac{2}{15}\pi$  when  $n = 250$  and  $\Delta\chi = \pi$ .

### 2.1.2.6. User-Defined Carpet Spectra

You may also define spreading seas with user-defined carpet spectra. You can input each of these carpet spectra with each wave spectrum as a series of directions. It is assumed that the directions are in ascending order, as well as the frequencies at which the value of the spectral ordinates are given. Optionally the specification of individual weighting factors for each direction can be defined.

If you do not define weighting factors, the contribution of each directional spectrum is calculated by a simple trapezoidal integral and will add up to unity. The weighting factors are calculated using the following equation:

$$W_m = \frac{1}{2} \frac{\chi_{m+1} - \chi_{m-1}}{\Delta\chi} \text{ where } m=2, N_d-1 \quad (2.64)$$

where  $m$  is the direction sequence number in a carpet spectral definition and  $\Delta\chi$  is the total direction range.

In the case of the first or the last direction, the weighting functions are

$$\begin{aligned} W_1 &= \frac{1}{2} \frac{\chi_2 - \chi_1}{\Delta\chi} \\ W_{N_d} &= \frac{1}{2} \frac{\chi_{N_d} - \chi_{N_d-1}}{\Delta\chi} \end{aligned} \quad (2.65)$$

### 2.1.2.7. Wave Spectral Group

It is possible to employ a spectral group to define a specified environmental condition by introducing any combination of the above described wave spectra and/or imported wave elevation time history records.

In Aqwa, each cross swell will be considered as one sub-directional wave spectrum, a spreading sea is represented by  $N_W$  sub-directional spectra (by using an  $N_W$ -point Gaussian integration scheme). The overall maximum total number of sub-directional spectra in each spectral group is specified by the program. Among each wave spectra group, a limited number of imported wave elevation time history files may be included. These sub-directional spectral numbers may vary with different Aqwa versions. For more information, see the [Aqwa User's Manual](#).

A spectral group may contain only one definition of wind and/or current.

## 2.2. Wind

Winds not only creates wind induced waves, but also directly generates loads on marine structures when the superstructure (portion above the mean water surface) is significant.

Winds have three main features:

- A mean velocity: An average wind speed over a given period of time (mostly 1 hour) at a standard height above water surface (usually 10m);
- A mean speed profile: The velocity of the mean wind variation with height from water surface;
- Turbulence or gusts: The time-varying wind speed about the mean speed.

For more information, see [4].

It is assumed that there is no vertical component of the wind velocity in the fixed reference axes (FRA): the wind speed is always in the OXY (horizontal) plane of the FRA.

In Aqwa, the wind drag force is calculated using the wind speed at 10m above mean water surface. If some other reference height is input, Aqwa will firstly calculate the corresponding wind speed at 10m.

## 2.2.1. Uniform Wind

You can define a uniform wind in Aqwa. Aqwa takes the mean wind velocity, including speed, amplitude, and direction, at 10m above water surface and assumes that the wind is unidirectional and uniform with height. This uniform wind is typically used to calculate the steady wind load on a marine structure.

## 2.2.2. Wind Velocity Profile and Fluctuation

For a wind with a constant direction over time, the frequency distribution of the wind speed fluctuations can be described by means of a wind spectrum. Aqwa is also capable of importing a time history of wind speed amplitude and direction.

The wind profile is the variation of the mean wind speed with height. The mean wind speed  $\bar{V}_Z$  at the height of interest  $Z$  is in the form of

$$\bar{V}_Z = F(\bar{V}_{10}, Z) \quad (2.66)$$

where  $\bar{V}_{10}$  is the mean wind velocity at 10m above the mean water surface.

The time dependent wind speed at this height is expressed as

$$V(t, Z) = \bar{V}_Z + v(t, Z) \quad (2.67)$$

where  $v(t, Z)$  is the time-varying wind speed about the mean speed.

Given the wind spectral model and reference height, the mean speed profile and wind speed spectrum can be determined. Together with information about wind direction and wind drag coefficients, Aqwa can calculate the effect of the fluctuation of wind about the mean speed on the dynamic load on a marine structure. These dynamic loads generate low frequency motions on floating offshore structures.

The following wind velocity models are available in Aqwa.

[2.2.2.1. Ochi and Shin Wind Spectrum](#)

[2.2.2.2. API Wind Spectrum](#)

[2.2.2.3. NPD Wind Spectrum](#)

[2.2.2.4. ISO Wind Spectrum](#)

[2.2.2.5. User Defined Wind Spectrum](#)

[2.2.2.6. Import of a Time History of Wind Speed and Direction](#)

### 2.2.2.1. Ochi and Shin Wind Spectrum

Ochi and Shin [34] suggested a wind spectral formulation based on wind speed measurements at sea.

At the height  $Z$ , the mean wind velocity is written as

$$\bar{V}_Z = \bar{V}_{10} + 2.5v\ln\left(\frac{Z}{10}\right) \text{ where } Z > 0 \quad (2.68)$$

where  $\bar{V}_Z$  is the mean wind speed (in m/s) at height  $Z$  (in m) above the mean water surface,  $\bar{V}_{10}$  is the mean wind speed (in m/s) at 10m above mean water surface, and  $v$  is the shear velocity (in m/s) defined as

$$v = \bar{V}_{10}\sqrt{C_{10}}$$

$$C_{10} = 0.000794 + 0.00006658\bar{V}_{10}$$

The Ochi and Shin non-dimensional wind spectrum is given by:

$$S(\tilde{f}) = \begin{cases} 583\tilde{f} & \text{for } 0 \leq \tilde{f} \leq 0.003 \\ \frac{420\tilde{f}^{0.70}}{\left[1+\tilde{f}^{0.35}\right]^{11.5}} & \text{for } 0.003 \leq \tilde{f} \leq 0.1 \\ \frac{838\tilde{f}}{\left[1+\tilde{f}^{0.35}\right]^{11.5}} & \text{for } \tilde{f} \geq 0.1 \end{cases} \quad (2.69)$$

where  $\tilde{f}$  is non-dimensional frequency,  $\tilde{f} = \frac{fZ}{\bar{V}_Z}$ ,  $f$  is frequency (in Hz),  $\bar{V}_Z$  is mean wind speed (in m/s) at height  $Z$  (in m).

The dimensional wind speed spectral density (in  $\text{m}^2/\text{s}$ ) is defined as

$$S(f) = \frac{v^2}{f} S(\tilde{f}) \quad (2.70)$$

The time dependent wind speed is obtained by the sum of wind speed spectral wave components with random phases

$$V(t, Z) = \bar{V}_Z + \sum_{j=1}^N \sqrt{2S(f_j)\Delta f_j} \cos(-2\pi f_j t + \alpha_j) \quad (2.71)$$

### 2.2.2.2. API Wind Spectrum

The mean one hour wind speed (in m/s) profile at height  $Z$  (in m) is defined by API [1].

$$\bar{V}_Z = \bar{V}_{10} \left( \frac{Z}{10} \right)^{0.125} \quad (2.72)$$

The gust factor is used to calculate the mean speed of a given duration of gust from the 1 hour mean wind speed and can be defined as

$$G(t, Z) = \frac{\bar{V}(t, Z)}{\bar{V}_Z}$$

$$= 1 + g(t) I(Z) \quad (2.73)$$

Where  $\bar{V}(t, Z)$  is the mean speed duration  $t$  seconds at height  $Z$ ,  $\bar{V}_Z$  is the mean speed duration 1 hour at the height  $Z$ , and  $I(Z)$  is the turbulence intensity. The factor  $g(t)$  is given by

$$g(t) = 3 + \ln \left[ \left( \frac{3}{t} \right)^{0.6} \right] \text{ for } t \leq 60\text{s} \quad (2.74)$$

Turbulence intensity is the standard deviation of wind speed normalized by the mean wind speed over 1 hour and can be expressed as

$$I(Z) = \frac{\sigma(Z)}{\bar{V}_Z} \quad (2.75)$$

and the recommended API values are

$$I(Z) = \begin{cases} 0.15\left(\frac{Z}{Z_s}\right)^{-0.125} & \text{for } Z \leq Z_s \\ 0.15\left(\frac{Z}{Z_s}\right)^{-0.275} & \text{for } Z > Z_s \end{cases} \quad (2.76)$$

where  $Z_s$  is the thickness of the surface layer (20m).

The non-dimensional API wind spectrum is given by

$$S(\tilde{f}) = \frac{\tilde{f}}{(1+1.5\tilde{f})^{5/3}} \quad (2.77)$$

where  $\tilde{f}$  is non-dimensional frequency defined by

$$\begin{aligned} \tilde{f} &= \frac{f}{f_p} \\ f_p &= 0.025 \frac{\bar{V}_Z}{Z} \end{aligned}$$

in which frequencies  $f$  and  $f_p$  are in Hz.

Based on the above definitions, the dimensional API wind speed spectral energy density in (in  $\text{m}^2/\text{s}$ ) is given by

$$S(f) = \frac{\sigma(z)^2}{f} S(\tilde{f}) \quad (2.78)$$

### 2.2.2.3. NPD Wind Spectrum

The API [2] recommends the use of the Norwegian Petroleum Directorate (NPD) wind profiles, gust factors, and spectra (Appendix B).

The mean one hour wind speed (in m/s) profile at height  $Z$  is

$$\bar{V}_Z = \bar{V}_{10} [1 + C \ln(\frac{Z}{10})] \quad (2.79)$$

where  $C = 0.0573 \sqrt{1 + 0.15 \bar{V}_{10}}$ .

The dimensional NPD wind energy density spectrum (in  $\text{m}^2/\text{s}$ ) of the longitudinal wind speed fluctuations at the height  $Z$  is given by

$$S(f) = \frac{320 \left( \frac{\bar{V}_{10}}{10} \right)^2 \left( \frac{Z}{10} \right)^{0.45}}{\left( 1 + \tilde{f}^{0.468} \right)^{3.561}} \quad (2.80)$$

where

$$\tilde{f} = \frac{172f \left(\frac{Z}{10}\right)^{2/3}}{\left(\frac{V}{10}\right)^{3/4}}$$

#### 2.2.2.4. ISO Wind Spectrum

The ISO spectrum is defined in ISO 19901-1 [18]. It is the same as the NPD spectrum shown in [Equation 2.79 \(p. 38\)](#) and [Equation 2.80 \(p. 38\)](#), except that the frequency range is limited to  $0.00167 \leq f \leq 0.5$  (in Hz).

#### 2.2.2.5. User Defined Wind Spectrum

The user-defined wind spectral energy density (in  $\text{m}^2/\text{s}$ ) at a frequency  $f$  (in Hz) is expressed in the form of

$$S(f) = \frac{\sigma(Z)^2}{f} c_s S(\tilde{f}) \quad (2.81)$$

where  $\tilde{f}$  is non-dimensional frequency expressed by

$$\tilde{f} = c_f f \frac{Z}{\bar{V}_Z}$$

where  $c_f$  is the frequency coefficient,  $\sigma(Z) = I(Z) \bar{V}_Z$  is the standard deviation of the wind speed at the height  $Z$ ,  $c_s$  is the spectrum coefficient, and  $S(\tilde{f})$  is the non-dimensional wind spectrum.

$c_f$  is associated with the length scale in some formulations, but it may not be used in others. By default  $c_f=1$ . The frequency coefficient  $c_s$  is associated with the spectral weighting factor; by default it is unity.

To define a user-defined wind spectrum, some frequency independent parameters must be defined:

- reference height  $Z$
- turbulence intensity  $I(Z)$
- mean wind speed  $\bar{V}_Z$  at height  $Z$
- frequency coefficient  $c_f$  (optional, default value 1)
- spectrum coefficient  $c_s$  (optional, default value 1)

Then a series of non-dimensional frequency  $\tilde{f}$  in ascending order and the corresponding non-dimensional wind spectral ordinate  $S(\tilde{f})$  may be created.

### 2.2.2.6. Import of a Time History of Wind Speed and Direction

Wind spectrum models discussed in [Wind Velocity Profile and Fluctuation \(p. 36\)](#) are for constant wind direction with respect to time. Fluctuations of wind speed and direction with respect to time can be handled in Aqwa time domain analyses by importing a time history record of wind speed amplitude and direction.

The time defined in the imported time history record does not need to match the time step used for motion equation simulation. Aqwa will interpolate the wind speed and direction when necessary, using a cubic spline interpolation technique. There is no limit on the length of the record, but when modeling periods of constant wind velocity, adequate data points must be provided to satisfy the interpolation method.

## 2.3. Current

Currents create significant loads on marine structures, particularly on moored vessels and offshore structures.

### 2.3.1. Uniform and Profiled Current

It is usually assumed that the current moves in a horizontal direction but may vary depending on the depth of the water.

There are several different currents, such as oceanic current, thermohaline currents, tidal currents and currents due to the internal waves at the boundary between two different density water layers. The change in tidal current speed with depth normally has a 1/7 power law decay. The current associated with storm surge may have a logarithmic form near the surface layer [4]. The Ekman current results from a balance between Coriolis and surface wind frictional drag forces, and has a decaying spiral with increasing depth (see [39]). As mentioned by Barltrop [4], despite the fact that at larger water depths tides and storm surge currents become less important, the total current may be very significant.

Aqwa allows defining a uniform current velocity and/or a current profile with depth:

- Uniform current is defined by a positive scalar quantity  $U_0$  and a direction angle  $\theta_0$  (in degrees) in the fixed reference axes (FRA). Uniform current is constant from the seabed to the water surface.
- Current profile is defined by a series of current velocity (amplitude  $U_z$  and direction  $\theta_z$  (in degrees)) with the  $Z$  position defined in the FRA whose origin is at the water surface. These  $Z$  values will therefore always be negative and must also appear in ascending order, from the seabed up to the water surface. Velocity and direction values at positions between those defined are computed by linear interpolation of adjacent defined values. The current profile remains constant below the lowest  $Z$  position or above the highest, it does not drop to zero outside the defined range.

The total current velocity  $\vec{U}_c(z)$  at a specified  $Z$  position in water is the sum of the uniform current velocity and the profiled current velocity, such that

$$\vec{U}_c(z) = (U_0 \cos \theta_0, U_0 \sin \theta_0, 0) + (U_z \cos \theta_z, U_z \sin \theta_z, 0) \quad (2.82)$$

### 2.3.2. Wave and Current Interaction

The interaction between currents and waves is particularly relevant in the simulation of offshore structures.

The combined fluid particle velocity of currents and waves may increase the fluid drag force on the smaller components, for example, risers of a floating structure. The diffraction and radiation forces on the floating structure are also affected by the current.

This section deals with wave phase shifting or an apparent Doppler shift to wave period.

Barltrop [4] described that under the assumptions of constant steady current with depth and constant water depth, a regular wave travelling on the current can be modeled by the established wave theory, but the wave period relative to a stationary observer (or encounter period due to current) should be shifted as

$$\frac{\lambda}{T_e} = \frac{\lambda}{T} + U_c \cos \theta' \quad (2.83)$$

where  $T_e$  is the wave period relative to stationary observer,  $\lambda$  is the wavelength,  $\lambda$  is the wave period relative to current (predicted by zero current theory),  $U_c$  is the current speed amplitude, and  $\theta'$  is angle between the current and waves.

[Equation 2.83 \(p. 41\)](#) can be written in the alternate form

$$\omega_e = \omega + U_c k \cos \theta' \quad (2.84)$$

where  $\omega_e$  is the wave frequency relative to a stationary observer (encounter frequency due to current),  $\omega$  is the wave frequency relative to current, and  $k$  is the wave number. From this equation, it is understood that at a time  $t$ , the incident wave phase will be shifted  $U_c k \cos \theta' t$  relative to the incident wave with zero current speed expressed by [Equation 2.1 \(p. 19\)](#) and [Equation 2.2 \(p. 20\)](#).

For a profiled current case, Aqwa uses the current velocity at the mean water surface in [Equation 2.83 \(p. 41\)](#) and [Equation 2.84 \(p. 41\)](#).



# Chapter 3: Hydrostatics of Free-Floating Structures

This chapter discusses the hydrostatic properties of a free-floating structure in still water.

The equilibrium and stability behaviors of a multi-structural system connected by moorings and/or articulations in realistic environmental condition consisting of wind, current and waves is discussed in [Equilibrium Estimation and Stability Analysis of Structure System \(p. 171\)](#).

## 3.1. Hydrostatic Forces and Moments

When a body is partially or totally immersed in water, the volume of displacement of water can be determined by integrating over its submerged surface:

$$\nabla = \int_{S_0} Z n_3 dS \quad (3.1)$$

where  $S_0$  is the wetted surface of the body in still water,  $\vec{n} = (n_1, n_2, n_3)$  is the unit normal vector of the body surface pointing outwards and  $Z$  is the vertical coordinate of a wetted surface point with reference to the fixed reference axes (FRA).

The buoyancy of a submerged body is the vertical upthrust due to displacement of water:

$$F_B = \rho g \nabla \quad (3.2)$$

where  $\rho$  is the water density and  $g$  is gravitational acceleration.

and the center of buoyancy  $\vec{X}_B = (X_B, Y_B, Z_B)$  can be calculated by

$$\vec{X}_B = \frac{\rho g \int_{S_0} (X, Y, \frac{Z}{2}) Z n_3 dS}{F_B} \quad (3.3)$$

where  $\vec{X} = (X, Y, Z)$  is the location of a point on the submerged body surface in the FRA.

More generally, the hydrostatic force and moment are referred to as the fluid loads acting on a body when placed in still water. The hydrostatic force can be calculated by integrating the hydrostatic pressure over the wetted surface of the body, up to the still water level. The hydrostatic moments are taken about the center of gravity of the body. The expressions for hydrostatic force and moment are:

$$\begin{aligned} \vec{F}_{hys} &= - \int_{S_0} p_s \vec{n} dS \\ \vec{M}_{hys} &= - \int_{S_0} p_s (\vec{r} \times \vec{n}) dS \end{aligned} \quad (3.4)$$

where  $p_s = -\rho g Z$  and represents the hydrostatic pressure and  $\vec{r} = \vec{X} - \vec{X}_g$  and represents the position vector of a point on the hull surface with respect to the center of gravity in the FRA. The vertical component of the hydrostatic force vector in [Equation 3.4 \(p. 43\)](#) is the buoyancy of submerged body, which is defined by [Equation 3.2 \(p. 43\)](#).

## 3.2. Hydrostatic Equilibrium

When dealing with problems in the frequency domain, we are concerned with small-amplitude motions about an equilibrium floating position. Thus, the wetted surface of the body becomes time-independent and the hydrostatic forces and moments about the mean position of the body must be computed. This is done using the above equations. Obviously, the prescribed position must be one which allows the body to take up an equilibrium position in the still fluid. The equilibrium position will be dependent on the mass and mass distribution of the body combined with the distribution of hydrostatic pressure. The distribution of hydrostatic pressure may be described in terms of the total upward buoyant force and the position of the center of buoyancy. For an equilibrium state to exist, the following static conditions must be true:

- The weight of the body must be equal to the total upward force produced by buoyancy. Lateral force components must also sum to zero. If the only forces acting on the body are gravity and hydrostatic pressure (as the free-floating body is here), then the weight of the body must equal the upward buoyant force:

$$\vec{F}_{hys} + M_s g(0, 0, -1) = 0 \quad (3.5)$$

where  $M_s = \sum_j m_s(\vec{X}_j)$  is the total structural mass of the floating body and  $m_s(\vec{X}_j)$  is the structural mass distributed at the location of  $\vec{X}_j$ .

- The moments acting on the body must sum to zero. If the moments are taken about the center of gravity, then the buoyancy moment and the moment of all external static forces must be zero:

$$\vec{M}_{hys} + \sum_j (\vec{X}_j - \vec{X}_g) \times m_s(\vec{X}_j) g(0, 0, -1) = 0 \quad (3.6)$$

where the center of gravity  $\vec{X}_g = (X_g, Y_g, Z_g)$  is estimated with the mass distribution

$$\vec{X}_g = \frac{\sum_j \vec{X}_j m_s(\vec{X}_j)}{M_s} \quad (3.7)$$

Again, if the only forces acting on the body are gravity and hydrostatic pressure, then the center of gravity and the center of buoyancy must be in the same vertical line when the free-floating body is at equilibrium position in still water; in other words,

$$\begin{aligned} X_g &= X_B \\ Y_g &= Y_B \end{aligned} \quad (3.8)$$

Otherwise, if the prescribed body position is not at the equilibrium location, the out-of-balance force and moment are output in the forms of

$$\begin{aligned}\frac{\nabla \vec{F}}{M_s g} &= \frac{\vec{F}_{hys}}{M_s g} + (0, 0, -1) \\ \frac{\nabla \vec{M}}{M_s g} &= \frac{\vec{M}_{hys}}{M_s g}\end{aligned}\quad (3.9)$$

in which the out-of-balance force and moment are divided by the weight of the body and are with respect to the intermediate coordinate frame GXYZ introduced in [Axis Transformation and Euler Rotations \(p. 14\)](#) for Euler rotations.

### 3.2.1. Free-Floating Hydrostatic Stability

When the prescribed body position is one of equilibrium, we may ascertain if it is a stable position, an unstable position or a neutrally stable position. The stable position occurs when a body subjected to a small disturbance from an equilibrium state tends to return to that state. The neutrally stable position occurs when the body reaches and remains in its new position following the disturbance. The unstable position occurs when, following the disturbance, the body tends to increase its shift away from equilibrium.

According to the above definitions, the horizontal disturbance force or moment may cause the free-floating body to translate or rotate horizontally and remain in a new equilibrium position, so that the surge, sway, and yaw motion modes are in the neutral equilibrium states. The equilibrium condition for heave motion of a free-floating body which pierces the water surface is always stable. However, the equilibrium conditions of roll and pitch for the same body may be stable, neutral or unstable, and are required for further investigation. These conditions are referred to as the transverse and longitudinal stabilities for ship-like structures.

### 3.2.2. Small Angle Stability

The stability criterion used for a free-floating body is the metacentric height. When the body's weight equals the weight of fluid displaced and the center of gravity and center of buoyancy are in the same vertical line, you must check the metacentric heights so that the sign of the hydrostatic restoration can be assessed.

The cut water-plane properties of a body in the equilibrium position can be used to estimate the body's metacenter. The cut water-plane area can be calculated by

$$A = - \int_{S_0} n_3 dS \quad (3.10)$$

and the center of the cut water-plane area (center of flotation) in the fixed reference axes (FRA) is

$$(X_F, Y_F, 0) = \frac{\int_A (X, Y, 0) dA}{A} = \frac{- \int_{S_0} (X, Y, 0) n_3 dS}{A} \quad (3.11)$$

The second moments of the cut water-plane area about the center of flotation are

$$\begin{aligned}
 I_{XX} &= \int_A (Y - Y_F)^2 dA = - \int_{S_0} (Y - Y_F)^2 n_3 dS \\
 I_{YY} &= \int_A (X - X_F)^2 dA = - \int_{S_0} (X - X_F)^2 n_3 dS \\
 I_{XY} &= \int_A (X - X_F)(Y - Y_F) Y dA = - \int_{S_0} (X - X_F)(Y - Y_F) n_3 dS
 \end{aligned} \tag{3.12}$$

The angle between the principal X'-axis and the positive X-axis measured counterclockwise is

$$\theta_p = \frac{1}{2} \cot^{-1} \left( \frac{I_{YY} - I_{XX}}{2I_{XY}} \right) \tag{3.13}$$

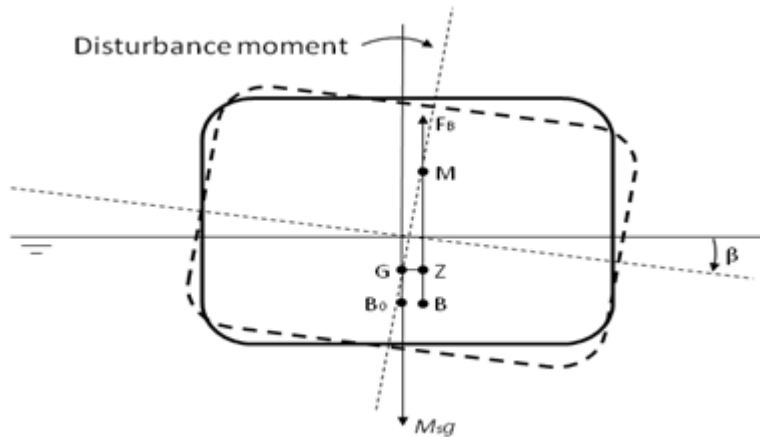
with respect to the principal X'- and Y'-axes,

$$\begin{aligned}
 I_{XX'} &= \int_A Y'^2 dA = I_{XX} \cos^2 \theta_p + I_{YY} \sin^2 \theta_p - 2I_{XY} \sin \theta_p \cos \theta_p \\
 I_{YY'} &= \int_A X'^2 dA = I_{XX} \sin^2 \theta_p + I_{YY} \cos^2 \theta_p + 2I_{XY} \sin \theta_p \cos \theta_p \\
 I_{X'Y'} &= 0
 \end{aligned} \tag{3.14}$$

As shown in [Figure 3.1: Metacenter of a Free-Floating Body \(p. 46\)](#), a free-floating body is in the initial equilibrium position, the center of gravity and center of buoyancy are at the locations of G and B<sub>0</sub> respectively and on the same vertical line. By turning the body through a small angle with respect to the center of flotation, the total buoyant force remains constant, but the center of buoyancy moves to a new position, B. The metacenter, M, is defined as the intersection of the body's upward buoyant force with the centerline of the body after the body has been subjected a rotational disturbance and rotated by a small angle. The distance  $\overline{GM}$ , is the metacentric height.

The righting moment,  $\rho g \nabla \overline{GM} \sin \beta$  balances the disturbance moment and to restores the body to its original position if the rotational mode is stable. If  $\overline{GM} > 0$ , it represents a stable equilibrium. If  $\overline{GM} = 0$ , the equilibrium is in the neutral state. If  $\overline{GM} < 0$ , the equilibrium is unstable.

**Figure 3.1: Metacenter of a Free-Floating Body**



The longitudinal and transverse metacentric heights are defined as

$$\begin{aligned}\overline{GM}_L &= \frac{I_{YY}}{\nabla} \\ \overline{GM}_T &= \frac{I_{XX}}{\nabla}\end{aligned}\quad (3.15)$$

### 3.2.3. Large Angle Stability

The stability at a large angle of inclination is similar to the concept applied for small angle stability. We assume that a free-floating body rotates a specified angle about a prescribed horizontal hinge axis and shifts upwards or downwards from its initial equilibrium position to ensure that the total displacement remains constant. The righting moments about this hinge axis and its perpendicular axis on the water plane are calculated and output in Aqwa.

At a known inclination angle rotated about a given horizontal hinge axis from the original equilibrium state of a free-floating body, Aqwa first calculates the vertical shifting position of the center of gravity to keep the displacement unchanged. Then, at the body's new orientation and position state, the wetted body surface can be determined numerically. Denoting the directional angle between the horizontal hinge axis and the global X-axis as  $\theta_H$  and the inclination angle about the hinge axis from the initial equilibrium position as  $\beta_H$ , the new position of the center of gravity ( $X'_g, Y'_g, Z'_g$ ) and the corresponding wetted body surface as  $S(\theta_H, \beta_H)$ , the righting moments about the horizontal axes of GXYZ are

$$\begin{aligned}M_{RX} &= - \int_{S(\theta_H, \beta_H)} p_s [(Y - Y'_g)n_3 - (Z - Z'_g)n_2] dS \\ M_{RY} &= - \int_{S(\theta_H, \beta_H)} p_s [(Z - Z'_g)n_1 - (X - X'_g)n_3] dS\end{aligned}\quad (3.16)$$

where  $p$  is the hydrostatic pressure.

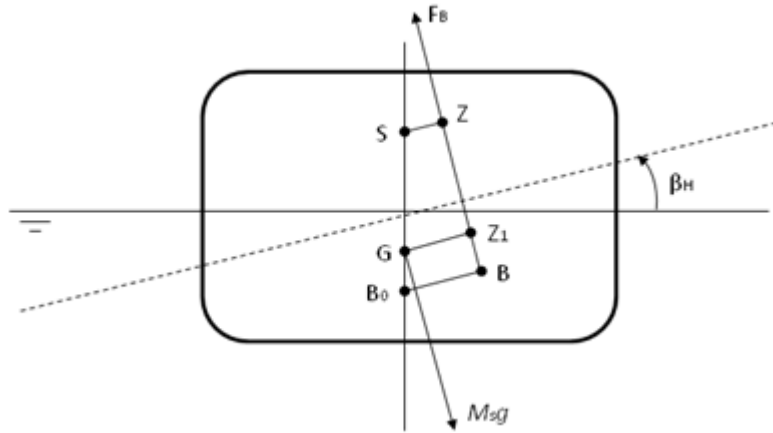
The righting moments about the hinge axis and its perpendicular axis on the water plane are

$$\begin{bmatrix} M_{RH} \\ M_{RP} \end{bmatrix} = \begin{bmatrix} \cos\theta_H & \sin\theta_H \\ -\sin\theta_H & \cos\theta_H \end{bmatrix} \begin{bmatrix} M_{RX} \\ M_{RY} \end{bmatrix} \quad (3.17)$$

This can be further interpreted into the conventional  $\overline{SZ}$  value used in the cross curves of stability for a free-floating ship (see [40])

$$\begin{aligned}\overline{SZ} &= \overline{GZ}_1 - \overline{SG} \sin\beta_H \\ \overline{GZ}_1 &= \frac{M_{RH}}{\rho g \nabla}\end{aligned}\quad (3.18)$$

where  $S$  represents an arbitrary but fixed pole above the center of gravity and parallel to the hinge axis, as shown in [Figure 3.2: Large Angle Stability \(p. 48\)](#).

**Figure 3.2: Large Angle Stability**

### 3.3. Hydrostatic Stiffness Matrix

For an analysis of rigid body motion about a mean equilibrium position, Aqwa requires a hydrostatic stiffness matrix for each body. If the stiffness matrix is expressed in terms of motions about the center of gravity, and only the hydrostatic pressure is considered, the matrix will take the form:

$$\mathbf{K}_{hys} = \begin{bmatrix} 0 & 0 & 0 & 0 & 0 & 0 \\ 0 & 0 & 0 & 0 & 0 & 0 \\ 0 & 0 & K_{33} & K_{34} & K_{35} & 0 \\ 0 & 0 & K_{43} & K_{44} & K_{45} & K_{46} \\ 0 & 0 & K_{53} & K_{54} & K_{55} & K_{56} \\ 0 & 0 & 0 & 0 & 0 & 0 \end{bmatrix} \quad (3.19)$$

where the various terms in the stiffness matrix are:

$$K_{33} = -\rho g \int_{S_0} n_3 dS = \rho g A$$

$$K_{34} = K_{43} = -\rho g \int_{S_0} (Y - Y_g) n_3 dS$$

$$K_{35} = K_{53} = \rho g \int_{S_0} (X - X_g) n_3 dS$$

$$K_{44} = -\rho g \int_{S_0} (Y - Y_g)^2 n_3 dS + \rho g (Z_B - Z_g) \nabla$$

$$K_{45} = K_{54} = -\rho g \int_{S_0} (X - X_g)(Y - Y_g) n_3 dS$$

$$K_{55} = -\rho g \int_{S_0} (X - X_g)^2 n_3 dS + \rho g (Z_B - Z_g) \nabla$$

$$K_{46} = -\rho g (X_B - X_g) \nabla$$

$$K_{56} = -\rho g (Y_B - Y_g) \nabla$$

where  $A$  is the cut water-plane area from [Equation 3.10 \(p. 45\)](#) and  $\nabla$  is the displacement calculated from [Equation 3.1 \(p. 43\)](#).

If the body is in a free-floating equilibrium state with no external forces acting on it, from [Equation 3.8 \(p. 44\)](#) the center of buoyancy and the center of gravity will be in the same vertical line, so that the terms  $K_{46}$  and  $K_{56}$  in the equation above will be zero and the stiffness matrix will be symmetric. The metacentric heights in both the longitudinal and transverse directions may be used to generate the X and Y rotational stiffness terms in the overall hydrostatic stiffness matrix, such that

$$\begin{aligned} K_{44} &= \rho g [\nabla \overline{GM}_T + (Y_F - Y_B)^2 A] \\ K_{55} &= \rho g [\nabla \overline{GM}_L + (X_F - X_B)^2 A] \end{aligned} \quad (3.20)$$

## 3.4. Hydrostatic Property of Floating Body with Internal Tanks

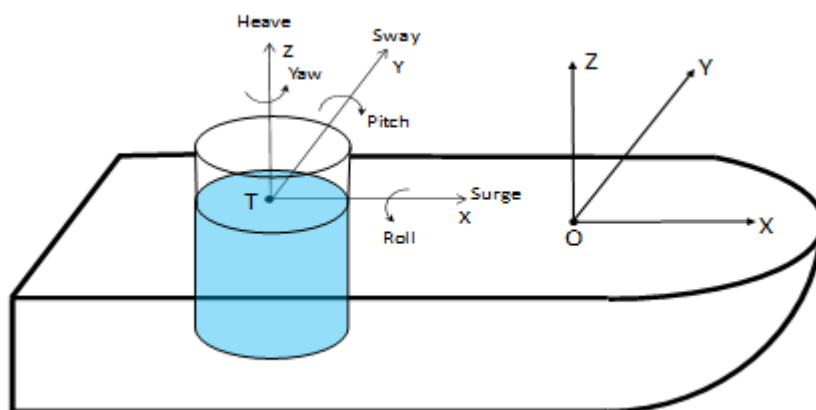
Liquids and their movements in the partially filled internal tanks have important coupling effects on the hydrostatic and hydrodynamic properties of the attached marine structures, such as LNG tankers and FPSO vessels.

### 3.4.1. Local Internal Tank Axes and Combined COG

It is numerically convenient to represent the liquid hydrostatic and hydrodynamic properties using the local internal tank axes, then to transfer them into the global reference axes where the values are with respect to the combined center of gravity of mass of the structure and the liquid in the internal tanks. There may be several internal tanks on a marine structure; therefore multiple local internal tank axes could be introduced to refer to the individual tanks respectively.

[Figure 3.3: Local Internal Tank Axes and Basic Motions \(p. 49\)](#) shows the local internal tank axes (LTA) for an internal tank. The LTA origin is at the center of the internal tank liquid plane (the center of flotation), and the LTA x-, y-, and z-axes are parallel to the X-, Y- and Z- axes of the global reference axes (FRA) respectively. In the LTA, six basic motions of the internal tank are three translational motions in the LTA axis directions and three rotational motions about the LTA axes.

**Figure 3.3: Local Internal Tank Axes and Basic Motions**



The internal tank structure would contain items such as stiffeners, web frame, etc., which reduces the total volume occupied by the liquid. Permeability is the percentage of the empty volume in that

space and could be represented by a coefficient,  $\mu$ , in the range of  $0 < \mu \leq 1$ . The typical value for internal tanks is 0.95 or higher.

The area of the liquid plane inside a tank at the structure equilibrium position in still water is determined by

$$A_t = \mu \int_{S_t} n_3 dS \quad (3.21)$$

where  $S_t$  is the wetted surface of the tank, and  $\vec{n} = (n_1, n_2, n_3)$  is the unit normal vector of the tank hull surface pointing inwards. A zero value for the liquid surface area indicates the fully filled tank condition.

The LTA origin of a partially filled internal tank,  $\vec{X}_t = (X_t, Y_t, Z_t)$ , is set to be at the center of floatation, with the horizontal location in the FRA determined by

$$(X_t, Y_t) = \frac{\mu \int_{S_t} (X, Y) n_3 dS}{A_t} \quad (3.22)$$

For a fully filled tank case, the horizontal location of the LTA origin could be above the tank and along the vertical line across the center of the internal tank liquid volume.

The volume of the liquid in an internal tank can be determined by the integration over its wetted surface in the LTA,

$$\nabla_t = -\mu \int_{S_t} z_t n_3 dS \quad (3.23)$$

where  $\vec{x}_t = (x_t, y_t, z_t)$  is the coordinate of the wetted surface point in the LTA.

The center of the liquid volume in the tank in LTA,  $\vec{x}_B^t = (x_B^t, y_B^t, z_B^t)$ , is determined by

$$\vec{x}_B^t = \frac{-\mu \int_{S_t} (x_t, y_t, \frac{z_t}{2}) z_t n_3 dS}{\nabla_t} \quad (3.24)$$

The center of the liquid volume in the tank in FRA is given by  $\vec{X}_B^t = (X_B^t, Y_B^t, Z_B^t) = \vec{x}_B^t + \vec{X}_t$ .

The combined center of gravity of the mass of the structure and the liquid in tanks at the equilibrium position in still water with respect to the FRA is defined by

$$\vec{X}_g = (X_g, Y_g, Z_g) = \frac{m \vec{X}_g^s + \sum \rho_t \nabla_t \vec{X}_B^t}{m + \sum \rho_t \nabla_t} \quad (3.25)$$

where  $m$  is the structure mass,  $\vec{X}_g^s = (X_g^s, Y_g^s, Z_g^s)$  is the structural COG in the FRA,  $\rho_t$  is the liquid density in a tank associated with this structure, and  $\Sigma$  indicates the summation of all the internal tanks associated with the structure.

### 3.4.2. Internal Tank Basic Motions

Under the small amplitude motion assumption, the basic movements of the internal tank at the LTA origin is expressed in the 6x1 matrix form of  $\mathbf{u}_t = (u_{t1}, u_{t2}, u_{t3}, \theta_{t1}, \theta_{t2}, \theta_{t3})^T$ , and can be determined by

$$\mathbf{u}_t = \begin{bmatrix} \mathbf{I} & \mathbf{R} \\ 0 & \mathbf{I} \end{bmatrix} \mathbf{u}_g \quad (3.26)$$

where  $\mathbf{u}_g = (u_1, u_2, u_3, \theta_1, \theta_2, \theta_3)^T$  is a matrix form of the rigid motions with respect to the combined COG at equilibrium, which is illustrated in [Figure 1.4: Floating Rigid Motions \(p. 15\)](#), and

$$\mathbf{I} = \begin{bmatrix} 1 & 0 & 0 \\ 0 & 1 & 0 \\ 0 & 0 & 1 \end{bmatrix}, \quad \mathbf{R} = \begin{bmatrix} 0 & Z_t - Z_g & -(Y_t - Y_g) \\ -(Z_t - Z_g) & 0 & X_t - X_g \\ Y_t - Y_g & -(X_t - X_g) & 0 \end{bmatrix}$$

From [Equation 3.26 \(p. 51\)](#), it is found that:

$$\vec{\theta}_t = (\theta_{t1}, \theta_{t2}, \theta_{t3}) = (\theta_1, \theta_2, \theta_3).$$

$\vec{X}_G$  is the position of the combined COG acquired by [Equation 3.26 \(p. 51\)](#) while  $\vec{\theta}_t = 0$ , which means it is also the position of the LSA origin in the FRA.

The force and the moment with respect to the LTA origin is expressed as a 6x1 matrix in the form of  $\mathbf{F}_t = (F_{t1}, F_{t2}, F_{t3}, M_{t1}, M_{t2}, M_{t3})^T$ , which can be transferred as the force and moment with respect to the LSA origin in the FRA,

$$\mathbf{F}_g = \begin{bmatrix} \mathbf{I} & 0 \\ -\mathbf{R} & \mathbf{I} \end{bmatrix} \mathbf{F}_t \quad (3.27)$$

where  $\mathbf{F}_g = (F_1, F_2, F_3, M_1, M_2, M_3)^T$  is the 6x1 matrix form of the force and moment with respect to the LSA origin.

### 3.4.3. Hydrostatic Force and Moment Due to Internal Tanks

The hydrostatic force acting on a tank is

$$\vec{F}_{hyst} = \mu \rho_t g \int_{S_t} z_t \vec{n} dS \quad (3.28)$$

where  $\rho_t$  is the liquid density and  $g$  is the gravitational acceleration.

The hydrostatic moment acting on the tank about the LTA origin is

$$\vec{M}_{hyst} = \mu \rho_t g \int_S z_t (\vec{x}_t \times \vec{n}) dS \quad (3.29)$$

Employing [Equation 3.27 \(p. 51\)](#) the general form of the hydrostatic force and moment with respect to the LSA origin is

$$\mathbf{F}_{hysg} = \begin{bmatrix} \mathbf{I} & 0 \\ -\mathbf{R} & \mathbf{I} \end{bmatrix} \mathbf{F}_{hyst} \quad (3.30)$$

where  $\mathbf{F}_{hyst}$  is of the  $6 \times 1$  matrix form containing the force and moment components given by [Equation 3.28 \(p. 51\)](#) and [Equation 3.29 \(p. 51\)](#).

When a structure with internal tanks freely floats in still water, at its equilibrium position the following conditions are satisfied:

$$\begin{aligned} m &= \rho \nabla - \sum \rho_t \nabla_t \\ m(X_g^s, Y_g^s) &= \rho \nabla(X_B, Y_B) - \sum \rho_t \nabla_t(X_B^t, Y_B^t) \end{aligned} \quad (3.31)$$

where  $\rho$  is the water density,  $\nabla$  is the volume of the displacement of external water (see [Equation 3.1 \(p. 43\)](#)), and  $\vec{X}_B = (X_B, Y_B, Z_B)$  is the center of buoyancy in FRA.

### 3.4.4. Hydrostatic Stiffness Due to Internal Tanks

The hydrostatic stiffness matrix is used to calculate the hydrostatic varying force and moment due to the small movement away from the equilibrium position.

The translational motions of the internal tank center of floatation do not generate any linear restoring force and moment with respect to the LTA origin. The linear hydrostatic restoring force on the internal tank with respect to the LTA origin induced by the rotational movement of the tank is given by:

$$\begin{aligned} \vec{F}_t(\mathbf{u}_t) &= \mu \rho_t g \int_{S_t} \left\{ (\theta_{t1} y_t - \theta_{t2} x_t) \vec{n} + z_t \vec{\theta}_t \times \vec{n} \right\} dS \\ &= 0 \end{aligned} \quad (3.32)$$

The linear hydrodynamic restoring moment on the internal tank with respect to the LTA origin is

$$\vec{M}_t(\mathbf{u}_t) = \mu \rho_t g \int_{S_t} \left\{ z_t [(\vec{\theta}_t \cdot \vec{n}) \vec{x}_t - (\vec{\theta}_t \cdot \vec{x}_t) \vec{n}] + (\theta_{t1} y_t - \theta_{t2} x_t) \vec{x}_t \times \vec{n} \right\} dS \quad (3.33)$$

From the above equation,

$$\begin{aligned} M_{t4} &= \left\{ \rho_t g \left[ \mu \int_{S_t} (y_t)^2 n_3 dS + \nabla_t z_B^t \right] \right\} \theta_{t1} - \left\{ \mu \rho_t g \int_{S_t} x_t^0 y_t^0 n_3^0 dS \right\} \theta_{t2} - \left\{ \rho_t g \nabla_t x_B^t \right\} \theta_{t3} \\ M_{t5} &= \left\{ \rho_t g \left[ \mu \int_{S_t} (x_t)^2 n_3 dS + \nabla_t z_B^t \right] \right\} \theta_{t2} - \left\{ \mu \rho_t g \int_{S_t} x_t^0 y_t^0 n_3^0 dS \right\} \theta_{t1} - \left\{ \rho_t g \nabla_t y_B^t \right\} \theta_{t3} \\ M_{t6} &= 0 \end{aligned} \quad (3.34)$$

By using the general matrix form, the hydrostatic restoring force and moment with respect to the LTA origin is

$$\mathbf{F}_t = -\mathbf{K}_t \mathbf{u}_t \quad (3.35)$$

which is of the  $6 \times 6$  matrix form,

$$\mathbf{K}_t = \begin{bmatrix} 0 & 0 & 0 & 0 & 0 & 0 \\ 0 & 0 & 0 & 0 & 0 & 0 \\ 0 & 0 & 0 & 0 & 0 & 0 \\ 0 & 0 & 0 & k_{44}^t & k_{45}^t & k_{46}^t \\ 0 & 0 & 0 & k_{54}^t & k_{55}^t & k_{56}^t \\ 0 & 0 & 0 & 0 & 0 & 0 \end{bmatrix} \quad (3.36)$$

where

$$k_{44}^t = -\rho_t g [\mu \int_{S_t} (y_t)^2 n_3 dS + \nabla_t z_B^t] = -\rho_t g [I_{11}^t + \nabla_t z_B^t]$$

$$k_{45}^t = \mu \rho_t g \int_{S_t} x_t y_t n_3 dS = \rho_t g I_{12}^t$$

$$k_{54}^t = \mu \rho_t g \int_{S_t} y_t x_t n_3 dS = k_{45}^t$$

$$k_{55}^t = -\rho_t g [\mu \int_{S_t} (x_t)^2 n_3 dS + \nabla_t z_B^t] = -\rho_t g [I_{22}^t + \nabla_t z_B^t]$$

$$k_{46}^t = \rho_t g \nabla_t x_B^t$$

$$k_{56}^t = \rho_t g \nabla_t y_B^t$$

$$I_{11}^t = \mu \int_{S_t} (y_t)^2 n_3 dS$$

$$I_{12}^t = \mu \int_{S_t} x_t y_t n_3 dS$$

$$I_{22}^t = \mu \int_{S_t} (x_t)^2 n_3 dS$$

To calculate the hydrostatic stiffness with respect to the combined COG in equilibrium, the liquid in each of the tanks is considered as a rigid part of the whole structure. The fictitious rigid body motion of the liquid in each tank must be taken into account, which gives

$$\vec{M}_B = [\vec{\theta} \times (-\vec{x}_G^t)] \times (0, 0, -\rho_t g \nabla_t) \quad (3.37)$$

$\vec{x}_G^t$  is the position of center of gravity of the liquid in the single tank, which is the same as the tank buoyancy center in the LTA. Converting [Equation 3.37 \(p. 53\)](#) into the matrix form,

$$\begin{bmatrix} M_{B1} \\ M_{B2} \\ M_{B3} \end{bmatrix} = \rho_t g \nabla_t \mathbf{H} \begin{bmatrix} \theta_1 \\ \theta_2 \\ \theta_3 \end{bmatrix} \quad (3.38)$$

where  $\mathbf{H} = \begin{bmatrix} -z_B^t & 0 & x_B^t \\ 0 & -z_B^t & y_B^t \\ 0 & 0 & 0 \end{bmatrix}$ .

Combining [Equation 3.35 \(p. 52\)](#) and [Equation 3.38 \(p. 53\)](#), the total force and moment with respect to the LTA origin is

$$\mathbf{F}_{tt} = \rho_t g \begin{bmatrix} 0 & 0 & 0 & 0 & 0 & 0 \\ 0 & 0 & 0 & 0 & 0 & 0 \\ 0 & 0 & 0 & 0 & 0 & 0 \\ 0 & 0 & 0 & I_{11}^t & -I_{12}^t & 0 \\ 0 & 0 & 0 & -I_{12}^t & I_{22}^t & 0 \\ 0 & 0 & 0 & 0 & 0 & 0 \end{bmatrix} \mathbf{u}_t \\ = -\mathbf{K}_{tt} \mathbf{u}_t \quad (3.39)$$

where

$$\mathbf{K}_{tt} = -\rho_t g \begin{bmatrix} 0 & 0 & 0 & 0 & 0 & 0 \\ 0 & 0 & 0 & 0 & 0 & 0 \\ 0 & 0 & 0 & 0 & 0 & 0 \\ 0 & 0 & 0 & I_{11}^t & -I_{12}^t & 0 \\ 0 & 0 & 0 & -I_{12}^t & I_{22}^t & 0 \\ 0 & 0 & 0 & 0 & 0 & 0 \end{bmatrix}$$

Employing [Equation 3.26 \(p. 51\)](#), [Equation 3.27 \(p. 51\)](#), and [Equation 3.39 \(p. 54\)](#), the hydrostatic stiffness of the fluid in the tank with respect to the LSA origin can be derived:

$$\begin{aligned} \mathbf{F}_g &= -\mathbf{K}_g^t \mathbf{u}_g \\ &= \begin{bmatrix} \mathbf{I} & 0 \\ -\mathbf{R} & \mathbf{I} \end{bmatrix} \mathbf{F}_{tt} \\ &= -\mathbf{K}_{tt} \mathbf{u}_g \end{aligned} \quad (3.40)$$

From [Equation 3.40 \(p. 54\)](#), it is found that the hydrostatic stiffness matrix with respect to the LSA origin is

$$\mathbf{K}_g^t = \mathbf{K}_{tt} \quad (3.41)$$

Together with the hydrostatic stiffness due to external fluid buoyant force and moment variation given by [Equation 3.19 \(p. 48\)](#), the total hydrostatic stiffness with respect to the LSA origin is

$$\mathbf{K} = \mathbf{K}_{hys} + \sum \mathbf{K}_g^t \quad (3.42)$$

Note that when there is any internal tank, the structure center of gravity in [Equation 3.19 \(p. 48\)](#) should be replaced by the LSA origin defined in the internal tank section.

### 3.4.5. Small Angle Stability of Freely Floating Structure with Internal Tanks

The motion of the liquid in partially filled internal tanks reduces the hydrostatic stability of the floating structure.

As the liquid densities in the internal tanks may differ from the external water density, the definition of the metacentric height for a free-floating body with internal tanks is slightly different from that discussed in [Small Angle Stability \(p. 45\)](#). The coefficients of the hydrostatic stiffness matrix are employed instead.

The principal axes are defined by

$$\begin{aligned}\theta_p &= \frac{1}{2} \cot^{-1} \left( \frac{K_{55} - K_{44}}{2K_{45}} \right), \\ K'_{44} &= K_{44} \cos^2 \theta_p + K_{55} \sin^2 \theta_p - 2K_{45} \sin \theta_p \cos \theta_p \\ K'_{55} &= K_{44} \sin^2 \theta_p + K_{55} \cos^2 \theta_p + 2K_{45} \sin \theta_p \cos \theta_p \\ K'_{54} &= K'_{45} = 0\end{aligned}\quad (3.43)$$

where  $\theta_p$  is the angle between the principal X'-axis and the positive X-axis measured counterclockwise in the X-Y plane of the FRA.

The longitudinal and transverse metacentric heights are defined as

$$\begin{aligned}\bar{GM}_L &= \frac{K_{55}}{\rho g \nabla} \\ \bar{GM}_T &= \frac{K_{44}}{\rho g \nabla}\end{aligned}\quad (3.44)$$

where  $\rho$  is the water density, and  $\nabla$  is the buoyant volume due to the displacement of external water (see [Equation 3.1 \(p. 43\)](#)). The righting moment is defined by  $\rho g \nabla \bar{GM} \sin \beta$  where the small angle  $\beta$  is indicated in [Figure 3.1: Metacenter of a Free-Floating Body \(p. 46\)](#).

From [Equation 3.44 \(p. 55\)](#) and [Equation 3.39 \(p. 54\)](#), the reduction in the stability of the structure with internal tanks is proportional to the liquid surface area moment about the center of floatation of each tank. The large fuel and fresh water tanks of a ship may be distributed into the port, center and starboard compartments to reduce the liquid surface effect on the transverse stability. Each watertight compartment should be treated as a separate internal tank in the analysis.

### 3.4.6. Large Angle Stability of Freely Floating Structure with Internal Tanks

The calculation approach on the stability at a large angle of inclination of a freely floating structure with internal tanks is similar to the concept discussed in [Large Angle Stability \(p. 47\)](#). We assume that a free-floating body rotates a specified angle about a prescribed horizontal hinge axis and shifts upwards or downwards from its initial equilibrium position to ensure that the total external fluid displacement remains constant.

It is assumed that the combined COG defined in [Equation 3.25 \(p. 50\)](#) is "frozen" on the structure and will rigidly move with the structure.

At a known inclination angle rotated about a given horizontal hinge axis from the original equilibrium state of a free-floating body with internal tanks, Aqwa first calculates the vertical shifting position of the combined COG to keep the external fluid displacement unchanged. Then, at the body's new orientation and position state, the external wetted body surface and the wetted internal tank surfaces can be determined numerically. Denoting the directional angle between the horizontal hinge axis and the global X-axis as  $\theta_H$ , the inclination angle about the hinge axis from the initial equilibrium position as  $\beta_{H'}$ , the combined COG (LSA origin) as  $(X_g, Y_g, Z_g)$  and the corresponding wetted body surface and wetted internal tank surfaces as  $S(\theta_H, \beta_{H'})$ , the righting moments about the horizontal axes of the FRA are similar to those defined in [Equation 3.16 \(p. 47\)](#) but with the additional moments due to the structure gravity force to the combined COG,

$$\begin{aligned} M_{RX} &= - \int_{S(\theta_H, \beta_H)} p_s [(Y - Y_g)n_3 - (Z - Z_g)n_2] dS - mg(Y_g^s - Y_g), \\ M_{RY} &= - \int_{S(\theta_H, \beta_H)} p_s [(Z - Z_g)n_1 - (X - X_g)n_3] dS + mg(X_g^s - X_g) \end{aligned} \quad (3.45)$$

The righting moment about the hinge direction and its perpendicular direction are given in the same form of [Equation 3.17 \(p. 47\)](#).

The conventional  $\overline{SZ}$  value, which is indicated in [Figure 3.2: Large Angle Stability \(p. 48\)](#) for a free-floating structure with internal tanks, is given in [Equation 3.18 \(p. 47\)](#).

### 3.5. Free Trim Large Angle Stability

The free trim large angle stability is similar to the concept discussed in [Large Angle Stability \(p. 47\)](#). It is assumed that a free-floating body rotates at a specified angle about a prescribed horizontal hinge axis, and the body's righting moments about this hinge axis are calculated under a free trim large angle position when:

- The total displacement remains constant. This means forces are balanced in the vertical axis of the fixed reference axes (FRA).
- The moments on the hinge axis' horizontal perpendicular direction are balanced by allowing a trim rotation.
- No horizontal force/moment and displacement/rotation are present and considered.

The buoyance and gravity centers stay on the rotation plane, which is perpendicular to the hinge axis. This renders the least work to be performed in order to heel the body up to the prescribed rotation angle, and the direction of the righting moment is always parallel to the hinge axis [36].

The free trim large angle position is defined in the hinge axis local coordinate system, which has the hinge axis as the X-axis, the FRA's Z axis as the Z-axis, and the Y-axis following the right-hand rule. The trim, heel, and heave discussed in this section all refer to the hinge axis local coordinate system.

The iterative approach discussed in [Iteration Towards Equilibrium \(p. 175\)](#) calculates the free trim large angle heave and trim positions. The righting moment is formed by the hydrostatic and gravity forces in the rotation plane. The hydrostatic force is calculated by [Equation 3.4 \(p. 43\)](#) and [Equation 3.29 \(p. 51\)](#) through [Equation 3.30 \(p. 51\)](#) under the free trim large angle position (including internal tanks, moon-pools, and tubes). Furthermore, the additional hydrostatic stiffness-related forces and point buoyancy force are included. The righting moment,  $M_R$ , is positive when its direction is opposite to the heeling moment, which rotates the body about the hinge axis to the prescribed angle.

$$M_R = -M_{hys} + K_{heel\_heel}\beta + K_{heel\_heave}Z + K_{heel\_trim}\theta - \sum_i (y_i - y_g)F_{bi} + \sum_j (y_j - y_g)m_{jg} \quad (3.46)$$

where  $M_{hys}$  is the hydrostatic moment about the hinge axis calculated by [Equation 3.4 \(p. 43\)](#) and [Equation 3.29 \(p. 51\)](#) through [Equation 3.30 \(p. 51\)](#);

$K_{heel\_heel}$ ,  $K_{heel\_heave}$ , and  $K_{heel\_trim}$  are with respect to the hinge axis local coordinate system;

$K_{\text{heel\_heel}}$  is the heeling term of the additional hydrostatic stiffness matrix;

$K_{\text{heel\_heave}}$  is the heel and heave coupled term of the additional hydrostatic stiffness matrix;

$K_{\text{heel\_trim}}$  is the heel and trim coupled term of the additional hydrostatic stiffness matrix;

$Z$  is the displacement of the combined gravity center in the Z-axis direction of the hinge axis local coordinate system;

$\beta$  is the heeling angle in the hinge axis local coordinate system;

$\theta$  is the trim angle in the hinge axis local coordinate system;

$F_{bi}$  is the  $i$ -th point buoyancy with the Y-axis coordinate value of  $y_i$  in the hinge axis local coordinate system;

$m_j$  is the  $j$ -th point mass with the Y-axis coordinate value of  $y_j$  in the hinge axis local coordinate system;

and  $y_g$  is the combined gravity center's Y-axis coordinate value in the hinge axis local coordinate system.

After the right moment is obtained, the conventional GZ value is calculated by

$$\overline{GZ} = \frac{M_R}{\Delta} \quad (3.47)$$

where  $\Delta$  is the total gravity force of the body including the internal tank fluid, i.e., the total buoyancy force.

The area  $A_{GZ}$  under the GZ curve at the rotation angle  $\beta_i$  is calculated by

$$A_{GZ} = \int_{\beta_0}^{\beta_i} \overline{GZ} d\beta \quad (3.48)$$

where  $\beta_0$  is the smallest prescribed heeling angle where the GZ curve starts.



---

# Chapter 4: Hydrodynamic Radiation and Diffraction Analysis by Source Distribution Method

---

Hydrodynamic loading on a marine structure is mainly caused by the kinematics of water particles in waves, motions of the structure, and interactions between waves and the structure.

Offshore structure designers and engineers are normally concerned with three categories of hydrodynamic loading on marine structures: drag load, wave exciting load, and inertia load ([4]).

Drag loads are induced by viscosity and are proportional to the square of relative velocity between fluid particle and structure surface. They are important when structural members are slender and wave amplitude is large.

In small amplitude waves, the wave exciting load consists of the first order incident wave force (Froude-Krylov force) and the diffraction force which is induced by the disturbance wave due to the existence of a body. In larger seas, both the first order forces and the second order forces are important. In severe seas, bottom and flare slamming transient forces may also be included.

Wave inertia load or radiation load is caused by the disturbed waves induced by the body motions. Fluid potential theories are commonly used for solving the wave inertia load and wave exciting load.

Three dimensional panel methods are the most common numerical tools to analyze the hydrodynamic behavior of a large-volume structure in waves. These methods are based on the fluid potential theory and represent the structure surface by a series of diffraction panels. The Morison's equation approach is widely used for slender body components. Aqwa employs a hybrid method to model the large-volume components of a structure by diffracting panels and the small cross sectional components by Morison elements.

In this chapter, the numerical approach (the source distribution method) is described for estimation of the first order wave load. Methods for calculating the second order force are described in [Second Order Wave Excitation Forces \(p. 97\)](#). The formula for slender body force in waves is presented in [Morison Element Forces \(p. 109\)](#).

## 4.1. Radiation and Diffraction Wave Forces

---

The main theoretical assumptions and limitations of linear potential theory employed in Aqwa are listed below:

- The body or bodies have zero or very small forward speed.
- The fluid is inviscid and incompressible, and the fluid flow is irrotational.
- The incident regular wave train is of small amplitude compared to its length (small slope).

- The motions are to the first order and hence must be of small amplitude. All body motions are harmonic. The linearized drag damping on the Morison elements (see [Morison Drag Linearization \(p. 112\)](#)) or any additional user-defined viscous damping can be optionally included in the equation of motion.

### 4.1.1. General Formula in Zero Forward Speed Case

This section deals with the hydrodynamic fluid loading of a diffracting body in regular harmonic waves. The theory may be used to calculate the wave excitation on a fixed body or the wave exciting forces and radiation forces on a floating body.

Since the first order potential theory of diffraction and radiation waves is used here for radiation and diffraction analysis, the linear superposition theorem may be used to formulate the velocity potential within the fluid domain.

The fluid flow field surrounding a floating body by a velocity potential is defined by

$$\Phi(\vec{X}, t) = a_w \varphi(\vec{X}) e^{-i\omega t} \quad (4.1)$$

where  $a_w$  is the incident wave amplitude and  $\omega$  is the wave frequency.

In [Equation 4.1 \(p. 60\)](#), the isolated space dependent term  $\varphi(\vec{X})$  may be separated into contributions from the radiation waves due to six basic modes of body motion, the incident wave and the diffracted or scattered wave. The potential functions are complex but the resultant physical quantities such as fluid pressure and body motions in time domain analysis will be obtained by considering the real part only.

Adopting the conventional notation of the six rigid body motions in seakeeping theory, as demonstrated in [Figure 1.4: Floating Rigid Motions \(p. 15\)](#), three translational and three rotational motions of the body's center of gravity are excited by an incident regular wave with unit amplitude:

$$\begin{aligned} x_j &= u_j, \quad (j=1, 3) \\ x_j &= \theta_{j-3}, \quad (j=4, 6) \end{aligned} \quad (4.2)$$

The potential due to incident, diffraction, and radiation waves may therefore be written as:

$$\varphi(\vec{X}) e^{-i\omega t} = \left[ (\varphi_1 + \varphi_d) + \sum_6^{j=1} \varphi_{rj} x_j \right] e^{-i\omega t} \quad (4.3)$$

where  $\varphi_1$  is the first order incident wave potential with unit wave amplitude,  $\varphi_d$  is the corresponding diffraction wave potential,  $\varphi_{rj}$  is the radiation wave potential due to the  $j$ -th motion with unit motion amplitude.

In finite depth water, the linear incident wave potential  $\varphi_1$  at a point  $\vec{X}=(X, Y, Z)$  in [Equation 4.3 \(p. 60\)](#) has been given in [Equation 2.2 \(p. 20\)](#), but as a special case of unit amplitude  $a_w=1$ .

When the wave velocity potentials are known, the first order hydrodynamic pressure distribution may be calculated by using the linearized Bernoulli's equation,

$$p^{(1)} = -\rho \frac{\partial \Phi(\vec{X}, t)}{\partial t} = i\omega \rho \varphi(\vec{X}) e^{-i\omega t} \quad (4.4)$$

From the pressure distribution, the various fluid forces may be calculated by integrating the pressure over the wetted surface of the body. To have a general form for the forces and moments acting on the body, we extend the notation of unit normal vector of hull surface previously introduced through [Equation 3.1 \(p. 43\)](#) into 6 components corresponding to the six basic rigid body motions, such as

$$\begin{aligned}(n_1, n_2, n_3) &= \vec{n} \\ (n_4, n_5, n_6) &= \vec{r} \times \vec{n}\end{aligned}\quad (4.5)$$

where  $\vec{r} = \vec{X} - \vec{X}_g$  is the position vector of a point on the hull surface with respect to the center of gravity in the fixed reference axes (FRA). Employing this notation, the first order hydrodynamic force and moment components can be expressed in a generalized form:

$$F_j e^{-i\omega t} = - \int_{S_0} p^{(1)} n_j dS = [-i\omega\rho \int_{S_0} \varphi(\vec{X}) n_j dS] e^{-i\omega t} \quad (4.6)$$

where  $S_0$  is the mean wetted surface of body.

From [Equation 4.3 \(p. 60\)](#), the total first order hydrodynamic force can be written as

$$F_j = [(F_{Ij} + F_{dj}) + \sum_{k=1}^6 F_{rjk} x_k] \quad \text{where } j=1, 6 \quad (4.7)$$

of which the  $j$ -th Froude-Krylov force due to incident wave is

$$F_{Ij} = -i\omega\rho \int_{S_0} \varphi_i(\vec{X}) n_j dS \quad (4.8)$$

the  $j$ -th diffracting force due to diffraction wave is

$$F_{dj} = -i\omega\rho \int_{S_0} \varphi_d(\vec{X}) n_j dS \quad (4.9)$$

the  $j$ -th radiation force due to the radiation wave induced by the  $k$ -th unit amplitude body rigid motion is

$$F_{rjk} = -i\omega\rho \int_{S_0} \varphi_{rk}(\vec{X}) n_j dS \quad (4.10)$$

Fluid forces can be further described in terms of reactive and active components. The active force, or the wave exciting force, is made up of the Froude-Krylov force and the diffraction force. The reactive force is the radiation force due to the radiation waves induced by body motions.

The radiation wave potential,  $\varphi_{rk}$ , may be expressed in real and imaginary parts and substituted into [Equation 4.10 \(p. 61\)](#) to produce the added mass and wave damping coefficients

$$\begin{aligned}F_{rjk} &= -i\omega\rho \int_{S_0} \left\{ \operatorname{Re}[\varphi_{rk}(\vec{X})] + i\operatorname{Im}[\varphi_{rk}(\vec{X})] \right\} n_j dS \\ &= \omega\rho \int_{S_0} \operatorname{Im}[\varphi_{rk}(\vec{X})] n_j dS - i\omega\rho \int_{S_0} \operatorname{Re}[\varphi_{rk}(\vec{X})] n_j dS \\ &= \omega^2 A_{jk} + i\omega B_{jk}\end{aligned}\quad (4.11)$$

where the added mass and damping are

$$A_{jk} = \frac{\rho}{\omega} \int_{S_0} \text{Im}[\varphi_{rk}(\vec{X})] n_j dS \quad (4.12)$$

$$B_{jk} = -\rho \int_{S_0} \text{Re}[\varphi_{rk}(\vec{X})] n_j dS$$

If a problem requires the wave loading on a fixed body, then only the active wave forces are of interest. When the body is floating, both the active and reactive fluid forces must be considered. It is also worth noting that all fluid forces calculated above are a function of the wetted body surface geometry only and are independent of the structural mass characteristics of the body.

#### 4.1.2. Source Distribution Method

By assuming the fluid ideal such that there exists a velocity potential function  $\Phi(\vec{X}, t)$  with isolated space dependent term  $\varphi(\vec{X})$  and employing linear hydrodynamic theory (for example, see [30]), accounting for wave radiation and diffraction, the fluid-structure interaction behavior is described by the following set of equations in the fixed reference axes (FRA):

- Laplace equation:

$$\Delta\varphi = \frac{\partial^2\varphi}{\partial X^2} + \frac{\partial^2\varphi}{\partial Y^2} + \frac{\partial^2\varphi}{\partial Z^2} = 0 \quad (4.13)$$

applicable everywhere in the fluid domain,  $\Omega$ .

- Linear free surface equation of zero forward speed case:

$$-\omega^2\varphi + g \frac{\partial\varphi}{\partial Z} = 0 \text{ on } Z=0 \quad (4.14)$$

- Body surface conditions:

$$\frac{\partial\varphi}{\partial n} = \begin{cases} -i\omega n_j & \text{for radiation potential} \\ -\frac{\partial\varphi_I}{\partial n} & \text{for diffraction potential} \end{cases} \quad (4.15)$$

on the mean wetted body surface  $S_0$ . Here,  $\varphi_I$  represents the velocity potential function describing the initial incoming sinusoidal wave system.

- Seabed surface condition at depth of  $d$ :

$$\frac{\partial\varphi}{\partial Z} = 0 \text{ on } Z=-d \quad (4.16)$$

- A suitable radiation condition must be added to these equations so that as  $\sqrt{(x^2+y^2)} \rightarrow \infty$  the generalized wave disturbance dies away.

A boundary integration approach is employed in Aqwa to solve the fluid velocity potential governed by the above control conditions. In this approach the frequency domain pulsating Green's function in finite depth water is introduced, which obeys the same linear free surface boundary condition, seabed condition, and far field radiation conditions as those given in [Equation 4.14 \(p. 62\)](#) and [Equation 4.16 \(p. 62\)](#), and the following condition in the fluid field is satisfied:

$$\Delta G(\vec{X}, \vec{\xi}, \omega) = \frac{\partial^2 G}{\partial X^2} + \frac{\partial^2 G}{\partial Y^2} + \frac{\partial^2 G}{\partial Z^2} = \delta(\vec{X} - \vec{\xi}) \text{ where } X \in \Omega \text{ and } \xi \in \Omega \quad (4.17)$$

where  $\vec{\xi} = (\xi, \eta, \zeta)$  denotes the position of a source, and the Dirac delta function is

$$\delta(\vec{X} - \vec{\xi}) = \begin{cases} 0 & \text{where } \vec{X} - \vec{\xi} \neq 0 \\ \infty & \text{where } \vec{X} - \vec{\xi} = 0 \end{cases}$$

The Green's function is expressed as

$$G(\vec{X}, \vec{\xi}, \omega) = \frac{1}{r} + \frac{1}{r_2} + \int_0^\infty \frac{2(k+\nu) e^{-kd} \cosh[k(Z+d)] \cosh[k(\zeta+d)]}{ksinh(kd) - v \cosh(kd)} J_0(kR) dk + i 2\pi \frac{(k_0+\nu) e^{-k_0 d} \cosh[k_0(Z+d)] \cosh[k_0(\zeta+d)]}{\sinh(k_0 d) + k_0 d \cosh(k_0 d) - v d \sinh(k_0 d)} J_0(k_0 R) \quad (4.18)$$

where  $J_0$  is the Bessel function of the first kind, and

$$\begin{aligned} R &= [(X-\xi)^2 + (Y-\eta)^2]^{1/2} \\ r &= [R^2 + (Z-\zeta)^2]^{1/2} \\ r_2 &= [R^2 + (Z+\zeta+2d)^2]^{1/2} \\ v &= \frac{\omega^2}{g} \\ k_0 \tanh(k_0 d) &= v \end{aligned}$$

Using Green's theorem, the velocity potential of diffraction and radiation waves can be expressed as a Fredholm integral equation of the second kind:

$$c\varphi(\vec{X}) = \int_{S_0} \left\{ \varphi(\vec{\xi}) \frac{\partial G(\vec{X}, \vec{\xi}, \omega)}{\partial n(\vec{\xi})} - G(\vec{X}, \vec{\xi}, \omega) \frac{\partial \varphi(\vec{\xi})}{\partial n(\vec{\xi})} \right\} dS \quad (4.19)$$

where

$$c = \begin{cases} 0 & \vec{X} \notin \Omega \cup S_0 \\ 2\pi & \vec{X} \in S_0 \\ 4\pi & \vec{X} \in \Omega \end{cases}$$

Further introducing the source distribution over the mean wetted surface, the fluid potential is expressed as

$$\varphi(\vec{X}) = \frac{1}{4\pi} \int_{S_0} \sigma(\vec{\xi}) G(\vec{X}, \vec{\xi}, \omega) dS \text{ where } \vec{X} \in \Omega \cup S_0 \quad (4.20)$$

in which the source strength over the mean wetted hull surface can be determined by the hull surface boundary condition given by [Equation 4.15 \(p. 62\)](#), such as

$$\frac{\partial \varphi(\vec{X})}{\partial n(\vec{X})} = -\frac{1}{2}\sigma(\vec{X}) + \frac{1}{4\pi} \int_{S_0} \sigma(\vec{\xi}) \frac{\partial G(\vec{X}, \vec{\xi}, \omega)}{\partial n(\vec{X})} dS \quad \text{where } \vec{X} \in S_0 \quad (4.21)$$

The Hess-Smith constant panel method is employed in Aqwa to solve the above equation, in which the mean wetted surface of a floating body is divided into quadrilateral or triangular panels. It is assumed that the potential and the source strength within each panel are constant and taken as the corresponding average values over that panel surface. The discrete integral form of [Equation 4.20 \(p. 63\)](#) and [Equation 4.21 \(p. 64\)](#) are therefore expressed as

$$\begin{aligned} \varphi(\vec{X}) &= \frac{1}{4\pi} \sum_{N_p}^{m=1} \sigma_m G(\vec{X}, \vec{\xi}_m, \omega) \Delta S_m \quad \text{where } \vec{X} \in \Omega \cup S_0 \\ &- \frac{1}{2} \sigma_k + \frac{1}{4\pi} \sum_{N_p}^{m=1} \sigma_m \frac{\partial G(\vec{X}_k, \vec{\xi}_m, \omega)}{\partial n(\vec{X}_k)} \Delta S_m = \frac{\partial \varphi(\vec{X}_k)}{\partial n(\vec{X}_k)} \quad \text{where } \vec{X}_k \in S_0, k=1, N_p \end{aligned} \quad (4.22)$$

where  $N_p$  is the total number of the panels over the mean wetted body surface,  $\Delta S_m$  is the area of the  $m$ -th panel, and  $\vec{\xi}_m$ ,  $\vec{X}_k$  are the coordinates of panel geometric center over the  $m$ -th and  $k$ -th panels respectively.

Directly evaluating the frequency domain by the pulsating Green's function in finite depth is time-consuming. Aqwa uses a Green's function database to efficiently calculate the Green's function and its first order derivatives. The low frequency limit (in rad/s) of this database is

$$\omega_{\min} = 0.001 \sqrt{\frac{g}{d}} \quad (4.23)$$

where  $d$  is the water depth and  $g$  is the acceleration due to gravity.

### 4.1.3. Removal of Irregular Frequencies

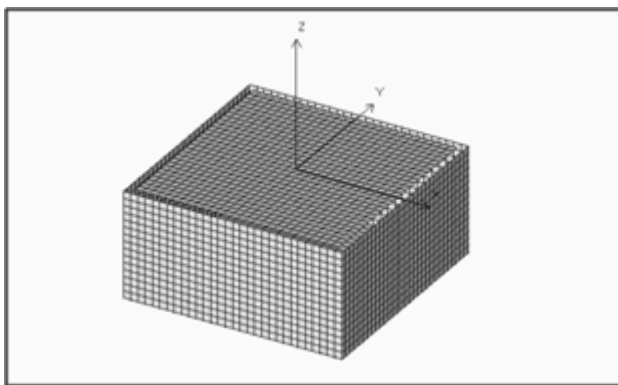
The occurrence of irregular frequencies in unsteady hydrodynamic analyses of floating structures using a boundary-integral formulation causes large errors in the solution over a substantial frequency band around these frequencies. These errors cause abrupt variations in the calculated hydrodynamic coefficients (as shown by Du et al [14]). This is the case in all forms of surface piercing hulls but especially when multi-hull structures and/or the hydrodynamic interaction between multiple structures are considered. In such cases, there exists the real physical phenomenon of resonant wave frequencies due to standing waves formed between the hulls, and this occurs in a similar manner to irregular frequencies. Distinguishing between these two phenomena occurring at closely spaced frequencies is difficult.

The irregular frequencies of the source distribution approach coincide with the eigenvalues of the interior Dirichlet problem, and are of purely numerical problem with no physical explanation. Hence, they must be removed. In Aqwa, the internal lid method is employed for the source distribution approach. In this method, it is assumed that a fluid field exists interior to the mean wetted body surface  $S_0$ , satisfying the same free-surface boundary condition experienced by the floating body. The vertical component of this interior fluid velocity is forced to be zero. In Aqwa, this interior mean free surface is represented by a series of panels (internal LID panels). As shown in [Figure 4.1: Discrete Wetted Hull Surface and Internal LID Panels \(p. 65\)](#), the discrete wetted hull surface and a series of LID elements are created. The original source distribution integration, [Equation 4.22 \(p. 64\)](#), is extended to cover both the mean wetted hull surface and the interior imaginary mean free surface:

$$\begin{aligned}
 \varphi(\vec{X}) = & \frac{1}{4\pi} \sum_{m=1}^{N_p+N_{Lid}} \sigma_m G(\vec{X}, \vec{\xi}_m, \omega) \Delta S_m && \text{where } \vec{X} \in \Omega \cup S_0 \\
 & -\frac{1}{2} \sigma_k + \frac{1}{4\pi} \sum_{m=1}^{N_p+N_{Lid}} \sigma_m \frac{\partial G(\vec{X}_k, \vec{\xi}_m, \omega)}{\partial n(\vec{X}_k)} \Delta S_m = \frac{\partial \varphi(\vec{X}_k)}{\partial n(\vec{X}_k)} && \text{where } \vec{X}_k \in S_0, k=1, N_p \\
 & -\frac{1}{2} \sigma_k + \frac{1}{4\pi} \sum_{m=1}^{N_p+N_{Lid}} \sigma_m \frac{\partial G(\vec{X}_k, \vec{\xi}_m, \omega)}{\partial n(\vec{X}_k)} \Delta S_m = 0 && \text{where } \vec{X}_k \in S_F^i, k=N_p+1, N_p+N_{Lid}
 \end{aligned} \tag{4.24}$$

where  $N_{Lid}$  is the total number of the interior LID panels over the interior imaginary mean free surface  $S_F^i$ . All the panels involved in [Equation 4.24 \(p. 65\)](#) are referred to as the diffraction panels.

**Figure 4.1: Discrete Wetted Hull Surface and Internal LID Panels**



#### 4.1.4. Mesh Quality Check

The quality of the hull surface mesh affects the accuracy of the hydrodynamic properties of analyzed structures.

Aqwa requires that

- The hull surface must be represented by a sufficient number of quadrilateral and/or triangular panels.
- The panel normals must point towards the surrounding fluid field, as discussed in [Equation 3.1 \(p. 43\)](#).
- The hull surface, especially the mean wetted hull surface part, must be fully covered by panels without gaps or overlap between panels.
- The mean wetted hull surface is required when the source distribution approach is used in a frequency domain analysis. The hull surface above the mean water level may be needed when doing a nonlinear time domain analysis. For such cases, both the mean wetted hull surface and the hull surface above mean water level may be modelled by panels. These panels must not cut the mean water surface. All the panels not involved in [Equation 4.24 \(p. 65\)](#) are referred to as non-diffracting panels.

Each individual panel must satisfy the following requirements:

- The panel area should be nearly the same as those of adjacent panels:

$$\frac{1}{3} \leq \frac{\Delta S_m}{\Delta S_k} \leq 3 \text{ where } m=1, N_p + N_{Lid} \quad (4.25)$$

where  $\Delta S_k$  is any adjacent panel area.

- The panel aspect ratio should not be too small:

$$C \frac{\Delta S_m}{L_{\max}^2} \geq \frac{1}{3} \text{ where } m=1, N_p + N_{Lid} \quad (4.26)$$

where  $L_{\max}$  is the length of the longest side of the  $m$ -th panel, and

$$C = \begin{cases} 1.0 & \text{for quadrilateral panels} \\ 2.3 & \text{for triangular panels} \end{cases}$$

- The panel center must not be too close to the adjacent panel centers:

$$d_{mk} \geq r_{fm} \text{ where } m=1, N_p + N_{Lid} \quad (4.27)$$

where  $d_{mk}$  is the distance between the center of the  $m$ -th panel to the center of the adjacent panel and  $r_{fm}$  is the radius of the  $m$ -th panel which is defined as  $r_{fm} = \sqrt{\frac{\Delta S_m}{\pi}}$

If  $d_{mk} < 0.1r_{fm}$  a fatal error is issued.

- The panel shape must be regular. To quantitatively check this requirement, a shape factor for the panel is introduced:

$$f_{Sm} = \frac{n_s}{2\Delta S_m} \sqrt{B} \text{ where } m=1, N_p + N_{Lid} \quad (4.28)$$

where  $n_s$  is the number of panel sides (4 for quadrilateral panels and 3 for triangular panels) and

$$B = \min \left\{ [(\vec{X}_i - \vec{X}_m) \times (\vec{X}_{i+1} - \vec{X}_m)] \cdot [(\vec{X}_{i+1} - \vec{X}_m) \times (\vec{X}_{i+2} - \vec{X}_m)] \right\}$$

where  $\vec{X}_i, \vec{X}_{i+1}, \vec{X}_{i+2}$  are the nodal coordinates of any 3 nodes of the  $m$ -th panel in order and  $\vec{X}_m$  is the coordinates of this panel center.

With this definition, it is required that

$$f_{Sm} \geq \begin{cases} 0.2 & \text{otherwise an error is issued} \\ 0.02 & \text{otherwise a fatal error is issued} \end{cases} \quad (4.29)$$

- The panel size should be small relative to the wave length:

$$L_{\max} \leq \frac{1}{7} \lambda \quad (4.30)$$

- The centers of the diffracting panels must be above the seabed to avoid any singularity of the Green's function (given by [Equation 4.18 \(p. 63\)](#)):

$$Z_m + d \geq \frac{1}{2} r_{fm} \text{ where } m=1, N_p \quad (4.31)$$

where  $Z_m$  is the Z-coordinate of the center of the  $m$ -th panel in the fixed reference axes (FRA) and  $r_{fm}$  is the panel radius defined in [Equation 4.27 \(p. 66\)](#).

## 4.2. Hydrodynamic Interaction

Multi-body hydrodynamic interaction analysis is a complex task relevant to many offshore activities and navy operations. Approaches based on three-dimensional potential theory are employed in Aqwa for hydrodynamic analyses of complex multiple-body systems.

### 4.2.1. Extended Hydrodynamic Coefficient Matrices

Hydrodynamic interaction concerns the influence of one body's flow field on another's. The importance of interaction will depend on both the body separation distances and the relative sizes of the bodies. The hydrodynamic interaction includes not only the radiation coupling but also the shielding effects as well.

Two points regarding hydrodynamic interaction should be emphasized:

First, the response amplitude operators (RAOs) for each of the hydrodynamic interacting structures will be different from those that would have resulted if each of these structures were on its own. The RAOs are not a physical property of a structure but, as can be seen from the equations of motion, depend on the radiation and diffraction forces. The radiation as well as the diffraction forces change in the case of hydrodynamic interaction and therefore the RAOs of the structures in the equation of motion will also change.

Second, when hydrodynamic interaction is employed, special attention is needed when you move the structures relative to each other. In Aqwa, the RAOs of hydrodynamic interaction structures are always evaluated relative to the fixed reference axes (FRA). Therefore, if different positions of one or more hydrodynamic interacting structures are defined in two consecutive Aqwa radiation and diffraction analyses, the results between these two runs will not be comparable.

In the multiple structure hydrodynamic interaction case, the total degrees of rigid body motions are  $6 \times M$  where  $M$  is the number of structures; the total unsteady potential is usually expressed as a superposition,

$$\varphi(\vec{X})e^{-i\omega t} = [(\varphi_I + \varphi_d) + \sum_{m=1}^M \sum_{j=1}^6 \varphi_{rjm} x_{jm}] e^{-i\omega t} \quad (4.32)$$

where  $\varphi_I$  is the isolated space dependent incident,  $\varphi_d$  is the diffraction wave potential, and  $x_{jm}$  is the amplitude of motion of the  $j$ -th degree of freedom of the  $m$ -th structure.  $\varphi_{rjm}$  is the radiation potential due to the unit  $j$ -th motion of the  $m$ -th structure while other structures remain stationary, mathematically it is defined by the boundary condition on the wetted hull surface:

$$\frac{\partial \varphi_{rjm}(\vec{X})}{\partial n} = \begin{cases} n_{jm} & \text{where } \vec{X} \in S_{0m} \\ 0 & \text{where } \vec{X} \in S_{0n} (n \neq m) \end{cases} \quad (4.33)$$

where, similar to the definitions in [Equation 4.5 \(p. 61\)](#),

$$\begin{aligned} (n_{1m}, n_{2m}, n_{3m}) &= \vec{n} \\ (n_{4m}, n_{5m}, n_{6m}) &= (\vec{X} - \vec{X}_{gm}) \times \vec{n} \quad \text{where } \vec{X} \in S_{0m} \end{aligned} \quad (4.34)$$

in which  $S_{0m}$  is the mean wetted hull surface of the  $m$ -th structure with its center of gravity at  $\vec{X}_{gm}$  in the FRA.

By employing [Equation 4.32 \(p. 67\)](#), [Equation 4.33 \(p. 67\)](#), and [Equation 4.34 \(p. 67\)](#), the source distribution approach discussed in [Radiation and Diffraction Wave Forces \(p. 59\)](#) can be used directly. Once the unsteady potential is calculated, the wave exciting forces and radiation force related added mass and damping coefficients are expressed as

$$\begin{aligned} F_{jm} = & F_{Ijm} + F_{djm} = -i\omega\rho \int_{S_{0m}} [\varphi_I + \varphi_d] n_{jm} dS \\ A_{jm,kn} + \frac{i}{\omega} B_{jm,kn} = & -\frac{i\rho}{\omega} \int_{S_{0m}} \varphi_{rkn} n_{jm} dS \end{aligned} \quad (4.35)$$

where the subscripts  $m, n$  correspond to the  $m$ -th and  $n$ -th structures, and the subscripts  $j, k$  refer to the motion modes.

#### 4.2.2. Suspending Standing Waves

One of the difficulties of solving the hydrodynamic interaction problem is related to the fluid resonance phenomenon taking place in the gap between the adjacent bodies. Due to the absence of viscous flow effects in the potential flow diffraction and radiation calculation, unrealistic resonant wave oscillation may occur. It is necessary to simulate the additional damping due to viscous and separation effects to suppress these unrealistic wave phenomena by the ordinary potential theory.

In Aqwa, a new damped free-surface boundary is implemented by extending the widely used wave-absorbing beach method used in fully nonlinear time domain hydrodynamic analysis and applied on the free-surface between adjacent structures. This condition is expressed as

$$\frac{\omega^2}{g} (\alpha_d^2 f_1^2 - 1) \varphi - 2i \frac{\omega^2}{g} \alpha_d f_1 \varphi + \frac{\partial \varphi}{\partial Z} = 0 \quad \text{where } Z=0 \quad (4.36)$$

where  $\alpha_d$  is a damping factor which should be mainly determined by model tests or trial measurements,  $f_1$  is a function which relates to the gap size,  $d_{gap}$ , between adjacent structures:

$$\begin{aligned} f_1 = & \begin{cases} \sin^2\left(\frac{\pi}{2}\delta\right) & \text{where } \delta < 1 \\ \delta^{-2} & \text{where } \delta \geq 1 \end{cases} \\ \omega_0 = & \sqrt{\frac{\pi g}{d_{gap}}} \\ \delta = & \begin{cases} \frac{\omega}{\omega_0} & \text{where } \omega_0 < 0.1 \\ 0.1 & \text{where } \omega_0 \geq 0.1 \end{cases} \end{aligned}$$

It is recommended that damping factor  $\alpha_d$  be set between 0.0 and 0.2. The value of 0 will give no effect, while 0.2 may result in heavy damping of surface elevation at the external LID panels (Cheetham, et al, [9]).

The range of external LID panels on the mean free surface between adjacent structures or within a moon-pool should be defined manually. The modified free surface boundary condition given by [Equation 4.36 \(p. 68\)](#) will be applied on those panels.

## 4.3. Corrections for Small Forward Speed

Using a reference frame moving with the forward speed of a structure, the coordinate of a point in this reference frame satisfies

$$\vec{X} = \vec{U}t + \vec{x} \quad (4.37)$$

where  $\vec{U} = (U_1, U_2, 0)$  is the forward speed of structure with respect to the fixed reference axes (FRA),  $\vec{X}$  is the coordinate of the point with respect to the FRA, and  $\vec{x}$  is the coordinate of the point with respect to the moving reference frame.

The total unsteady fluid potential varies with the encounter frequency:

$$\phi(\vec{X}, t) = a_w \varphi(\vec{x}) e^{-i\omega_e t} \quad (4.38)$$

where the encounter frequency can be given as

$$\omega_e = \omega - kU \cos \beta \quad (4.39)$$

where  $k$  is the incident wave number,  $U = |\vec{U}|$ , and  $\beta$  is the heading angle between the vessel forward speed and the wave propagation direction.

In this moving reference frame, if the disturbed steady flow is neglected, the linear free surface equation is satisfied, such that

$$(-i\omega_e + \vec{U} \cdot \nabla)^2 \varphi + g \frac{\partial \varphi}{\partial z} = 0 \quad \text{where } z=0 \quad (4.40)$$

and the body surface conditions

$$\frac{\partial \varphi}{\partial n} = \begin{cases} -i\omega_e n_j + Um_j & \text{for radiation} \\ -\frac{\partial \varphi_i}{\partial n} & \text{for diffraction} \end{cases} \quad (4.41)$$

are satisfied on the mean wetted body surface  $S_0$ , where

$$\begin{aligned} (m_1, m_2, m_3) &= (0, 0, 0) \\ (m_4, m_5, m_6) &= -\frac{1}{U} \vec{U} \times \vec{n} \end{aligned} \quad (4.42)$$

Based on the Bernoulli equation, the first order hydrodynamic pressure is:

$$p^{(1)} = \rho [i\omega_e \varphi(\vec{x}) + \vec{U} \cdot \nabla \varphi(\vec{x})] e^{-i\omega_e t} \quad (4.43)$$

Similar to [Equation 4.7 \(p. 61\)](#) through [Equation 4.11 \(p. 61\)](#), we have the  $j$ -th Froude-Krylov force due to incident wave

$$F_{Ij} = -\rho \int_{S_0} \left\{ (i\omega_e + \vec{U} \cdot \nabla) \varphi_i(\vec{x}) \right\} n_j dS \quad (4.44)$$

the  $j$ -th diffracting force due to diffraction wave

$$F_{dj} = -\rho \int_{S_0} \left\{ (i\omega_e + \vec{U} \cdot \nabla) \varphi_d(\vec{x}) \right\} n_j dS \quad (4.45)$$

and the  $j$ -th radiation force due to the radiation wave induced by the  $k$ -th unit amplitude body rigid motion

$$\begin{aligned}
 F_{rjk} &= \omega_e^2 A_{jk} + i\omega_e B_{jk} \\
 &= -\rho \int_{S_0} \left\{ (i\omega_e + \vec{U} \cdot \nabla) \varphi_{rk}(\vec{x}) \right\} n_j dS \\
 &= -i\omega_e \rho \int_{S_0} \left( n_j + \frac{i}{\omega_e} \vec{U} \cdot \nabla n_j \right) \varphi_{rk}(\vec{x}) dS
 \end{aligned} \tag{4.46}$$

Note that the frequency domain pulsating Green's function source distribution method, as described in [Source Distribution Method \(p. 62\)](#), does not account for forward speed in its formulation. The translating-pulsating source method, contrary to the pulsating source method, explicitly accounts for forward speed in its formulation and should be used for the hydrodynamic analysis for cases where forward speed is simulated. The numerical evaluation of the translating-pulsating Green's function is very time-consuming. When the forward speed is small in amplitude, an approximate free surface boundary condition can be used, for example

$$-\omega_e^2 \varphi + g \frac{\partial \varphi}{\partial z} = 0 \quad \text{where } z=0 \tag{4.47}$$

Under this situation, the frequency domain pulsating Green's function can be employed together with the new body boundary condition given in [Equation 4.41 \(p. 69\)](#) and [Equation 4.42 \(p. 69\)](#) to numerically solve the diffraction and radiation potential components. The wave exciting forces, added mass, and damping can be estimated from [Equation 4.44 \(p. 69\)](#) , [Equation 4.45 \(p. 69\)](#), [Equation 4.46 \(p. 70\)](#) afterwards.

This approximate pulsating source method has been extensively tested against the translating-pulsating Green's function method. It was found that, although the translating-pulsating source gives benefits in the calculation of individual hydrodynamic coefficients and wave action, the differences in the response calculations are quite small in cases where low to moderate speeds are considered (i.e.  $Fn = \frac{U}{\sqrt{gL}} < 0.3$ ).

It should be noted that the computational effort required for the translating-pulsating source far exceeds that for the pulsating source methods ([Inglis & Price \[19\]](#)).

This approximate method can also be applied for hydrodynamic analysis of multiple structures travelling side by side with same constant forward speed. Similar to [Equation 4.35 \(p. 68\)](#), the wave exciting force and the added mass and damping coefficients are written as

$$\begin{aligned}
 F_{jm} &= F_{Ijm} + F_{dm} \\
 &= -i\omega \rho \int_{S_0} \varphi_I n_{jm} dS - i\omega_e \rho \int_{S_0} \left( n_{jm} + \frac{i}{\omega_e} \vec{U} \cdot \nabla n_{jm} \right) \varphi_{dm} dS \\
 A_{jm,kn} + \frac{i}{\omega_e} B_{jm,kn} &= -i \frac{\rho}{\omega_e} \int_{S_0} \left( n_{jm} + \frac{i}{\omega_e} \vec{U} \cdot \nabla n_{jm} \right) \varphi_{rkn}(\vec{x}) dS
 \end{aligned} \tag{4.48}$$

## 4.4. Response Amplitude Operators

Aqwa solves a set of linear algebraic equations to obtain the harmonic response of the body to regular waves. These response characteristics are commonly referred to as response amplitude operators (RAOs) and are proportional to wave amplitude.

The set of linear motion equations of  $M$  hydrodynamic interaction structures with frequency dependent coefficients are obtained as:

$$[-\omega_e^2 (\mathbf{M}_s + \mathbf{M}_a) - i\omega_e \mathbf{C} + \mathbf{K}_{hys}] [\mathbf{x}_{jm}] = [\mathbf{F}_{jm}] \tag{4.49}$$

where  $\mathbf{M}_s$  is a  $6M \times 6M$  structural mass matrix,  $\mathbf{M}_a = [A_{jm,kn}]$  and  $\mathbf{C} = [B_{jm,kn}]$  are the  $6M \times 6M$  hydrodynamic added mass and damping matrices including the hydrodynamic interaction coupling terms between different structures,  $\mathbf{K}_{hys}$  is the assembled hydrostatic stiffness matrix of which each diagonal  $6 \times 6$  hydrostatic stiffness sub-matrix corresponding to individual structure is defined by [Equation 3.19 \(p. 48\)](#), and all off-diagonal  $6 \times 6$  sub-matrices are null as there is no hydrostatic interaction between different structures.

[Equation 4.49 \(p. 70\)](#) can alternatively expressed as

$$[x_{jm}] = \mathbf{H} [F_{jm}] \quad (4.50)$$

where

$$\mathbf{H} = \left\{ -\omega_e^2 (\mathbf{M}_s + \mathbf{M}_a) - i\omega_e \mathbf{C} + \mathbf{K}_{hys} \right\}^{-1}$$

is termed the transfer function or modal receptance which relates input forces to output response.

In addition, Aqwa can calculate the RAOs at any point of the structure given the RAOs at the structure's center of gravity and the vector from the center of gravity to the position of interest. The RAOs of a point P of  $(X_{pm}, Y_{pm}, Z_{pm})^T$  on the m-th structure may be found using the following relationship

$$(x_{pm}, y_{pm}, z_{pm})^T = \mathbf{T} [x_{jm}] \quad (4.51)$$

where the translation matrix between the center of gravity  $(X_{gm}, Y_{gm}, Z_{gm})^T$  and the point P is

$$\mathbf{T} = \begin{bmatrix} 1 & 0 & 0 & 0 & (Z_{pm}-Z_{gm}) & -(Y_{pm}-Y_{gm}) \\ 0 & 1 & 0 & -(Z_{pm}-Z_{gm}) & 0 & (X_{pm}-X_{gm}) \\ 0 & 0 & 1 & (Y_{pm}-Y_{gm}) & -(X_{pm}-X_{gm}) & 0 \end{bmatrix}$$

## 4.5. Response Amplitude Operators with Additional Input

In the previous section, it is assumed that each structure in a hydrodynamic interaction structure system is purely modeled by panel elements. The response amplitude operators (RAOs) of a free-floating hydrodynamic interaction structure system are determined by [Equation 4.49 \(p. 70\)](#).

In Aqwa, it is also possible to model each structure by a mixture of panels and Morison elements (discussed in [Morison Element Forces \(p. 109\)](#)). The following parameters of Morison elements are added in the equation of motion in the frequency domain:

- Tube and slender tube structural mass and moment of inertia with respect to the center of gravity of structure
- Hydrostatic stiffness matrix due to tube and slender tube elements
- Added mass matrix of tube and slender tube elements and flooded fluid mass inside the opened tube elements
- Froude-Krylov and wave inertia force and moment on tube and slender tube elements

In addition, the wave frequency dependent hydrodynamic parameters and the linear hydrostatic stiffness matrix of one or more structures can be changed or appended. The additional structural stiffness matrix can also be defined.

The equation of motion given by [Equation 4.49 \(p. 70\)](#) may be extended as

$$[-\omega_e^2(\mathbf{M}_s + \mathbf{M}'_a + \Delta\mathbf{M}_a) - i\omega_e(\mathbf{C} + \Delta\mathbf{C}) + \mathbf{K}'_{hys} + \Delta\mathbf{K}_{hys} + \mathbf{K}_a][x_{jm}] = [F'_{jm}] \quad (4.52)$$

where  $\mathbf{M}_s$  is the total structural mass matrix,  $\mathbf{M}'_a$  is the total added mass matrix due to diffracting panels and Morison elements (or the amended added mass matrix input),  $\Delta\mathbf{M}_a$  is the user-defined additional added mass matrix,  $\mathbf{C}$  is the hydrodynamic damping matrix by the diffracting panel elements (or the amended hydrodynamic damping matrix input),  $\Delta\mathbf{C}$  is the user-defined additional linear hydrodynamic damping (which could be the equivalent linear damping values to compensate for the viscous and eddy drag effects),  $\mathbf{K}'_{hys}$  is the assembled hydrostatic stiffness matrix (calculated or user-defined),  $\Delta\mathbf{K}_{hys}$  is the user-defined additional hydrostatic stiffness matrix,  $\mathbf{K}_a$  is the additional structural stiffness matrix, and  $[F'_{jm}]$  are the total Froude-Krylov and diffracting force and moments (calculated or user-defined).

## 4.6. Disturbed Wave Elevation and Air Gap

In a moving reference frame with the same forward speed as the structure, the fluid particle velocity is expressed as

$$\vec{V} = -\vec{U} + \nabla \Phi(\vec{X}, t) = -\vec{U} + a_w \nabla \varphi(\vec{x}) e^{-i\omega_e t} \quad (4.53)$$

where the unsteady fluid potential  $\Phi(\vec{X}, t)$  is defined in [Equation 4.37 \(p. 69\)](#) and [Equation 4.38 \(p. 69\)](#) and includes the incident, diffraction and radiation potential components.

Based on the first order wave potential, the fluid pressure (up to the second order) at a position  $\vec{x} = (x, y, \zeta)$  on the instantaneous wave surface is

$$\begin{aligned} p(\vec{x}, t) \approx & -\rho \operatorname{Re} \left\{ \frac{\partial a_w \varphi(\vec{x}) e^{-i\omega_e t}}{\partial t} \right\} - \rho g \zeta - \\ & \frac{1}{2} \rho \operatorname{Re} \{ \nabla \Phi(\vec{X}, t) \} \cdot \operatorname{Re} \{ \nabla \Phi(\vec{X}, t) \} + \rho \vec{U} \cdot \operatorname{Re} \{ \nabla \Phi(\vec{X}, t) \} \end{aligned} \quad (4.54)$$

Taking the perturbation to the second order with respect to the corresponding location on the mean wave surface,  $\vec{x}_0 = (x, y, 0)$ , we have

$$\begin{aligned} \frac{p(\vec{x}, t)}{\rho} \approx & -\operatorname{Re} \left\{ \frac{\partial a_w \varphi(\vec{x}) e^{-i\omega_e t}}{\partial t} \right\} - \operatorname{Re} \left\{ \frac{\partial^2 \Phi(\vec{x}_0, t)}{\partial t \partial Z} \right\} \zeta + \\ & \frac{1}{2} \operatorname{Re} \{ \nabla \Phi(\vec{X}_0, t) \} \cdot \operatorname{Re} \{ \nabla \Phi(\vec{X}_0, t) \} + \vec{U} \cdot \operatorname{Re} \{ \nabla \Phi(\vec{X}_0, t) \} - g \zeta \end{aligned} \quad (4.55)$$

Note that the second order term of  $\vec{U} \cdot \operatorname{Re} \left\{ \frac{\partial}{\partial Z} \nabla \Phi(\vec{X}_0, t) \right\} \zeta$  is ignored to avoid calculating the second order derivatives of the unsteady wave potential.

From [Equation 4.38 \(p. 69\)](#), it is found that

$$\operatorname{Re} \left\{ \frac{\partial a_w \varphi(\vec{x}) e^{-i\omega_e t}}{\partial t} \right\} = \omega_e \operatorname{Im} \{ \Phi(\vec{X}_0, t) \} \quad (4.56)$$

as the fluid pressure on the actual disturbed wave surface must be zero, from [Equation 4.55 \(p. 72\)](#) and [Equation 4.56 \(p. 72\)](#) the disturbed wave elevation with the second order correction can be derived as

$$\begin{aligned}\zeta(x,y,t) &= \frac{-\omega_e \operatorname{Im}\{\phi(\vec{X}_0 t)\} + \frac{1}{2} \operatorname{Re}\{\nabla \phi(\vec{X}_0 t)\} \operatorname{Re}\{\nabla \phi(\vec{X}_0 t)\} + \vec{U} \cdot \operatorname{Re}\{\nabla \phi(\vec{X}_0 t)\}}{g + \omega_e \operatorname{Im}\left\{\frac{\partial \phi(\vec{X}_0 t)}{\partial Z}\right\}} \\ &= \frac{1}{g} \left[ -\omega_e \operatorname{Im}\phi(\vec{X}_0, t) + \vec{U} \cdot \operatorname{Re}\{\nabla \phi(\vec{X}_0, t)\} \right] \left( 1 - \frac{\omega_e}{g} \operatorname{Im}\left\{\frac{\partial \phi(\vec{X}_0 t)}{\partial Z}\right\} \right) \\ &\quad + \frac{1}{2g} \operatorname{Re}\{\nabla \phi(\vec{X}_0, t)\} \cdot \operatorname{Re}\{\nabla \phi(\vec{X}_0, t)\}\end{aligned}\quad (4.57)$$

If only the first order disturbed wave elevation is required, [Equation 4.57 \(p. 73\)](#) is simplified as

$$\zeta^{(1)}(X, Y, t) = \frac{1}{g} \left[ -\omega_e \operatorname{Im}\{\phi(\vec{X}_0, t)\} + \vec{U} \cdot \operatorname{Re}\{\nabla \phi(\vec{X}_0, t)\} \right] \quad (4.58)$$

If only the linear incident wave elevation is required, [Equation 4.58 \(p. 73\)](#) is further simplified as

$$\begin{aligned}\zeta_I^{(1)}(X, Y, t) &= \frac{1}{g} \left[ -\omega_e \operatorname{Im}\{\phi_I(\vec{X}_0, t)\} + \vec{U} \cdot \operatorname{Re}\{\nabla \phi_I(\vec{X}_0, t)\} \right] \\ &= -\frac{\omega_e}{g} \operatorname{Im}\{\phi_I(\vec{X}_0, t)\}\end{aligned}\quad (4.59)$$

[Equation 4.57 \(p. 73\)](#), [Equation 4.58 \(p. 73\)](#), and [Equation 4.59 \(p. 73\)](#) are applicable for both single structure and multi-body hydrodynamic interaction cases with or without forward speed. For a case without forward speed,  $\omega_e = \omega$ .

From [Equation 4.51 \(p. 71\)](#) and [Equation 4.57 \(p. 73\)](#), the air gap at a point P of  $(X_{pm}, Y_{pm}, Z_{pm})^T$  on the  $m$ -th structure is:

$$Z_{\text{gap}} = Z_{pm} + \operatorname{Re}\{a_w z_{pme} e^{-i\omega_e t}\} - \zeta(X_{pm}, Y_{pm}, t) \quad (4.60)$$

## 4.7. Composite Source Distribution Method for Symmetric Structures

The composite source distribution method can be used to increase calculation efficiency when a model is symmetric.

For a structure with port-starboard and fore-aft symmetry,  $\vec{X}^{(1)} = (X, Y, Z)$  and  $\vec{\xi}^{(1)} = (\xi, \eta, \zeta)$  are a pair of field and source points on the first quadrant of the hull surface. There are three pairs of corresponding points in the other quadrants:

$$\begin{aligned}\vec{X}^{(2)} &= (-X, Y, Z) & \vec{\xi}^{(2)} &= (-\xi, \eta, \zeta) \\ \vec{X}^{(3)} &= (X, -Y, Z) & \vec{\xi}^{(3)} &= (\xi, -\eta, \zeta) \\ \vec{X}^{(4)} &= (-X, -Y, Z) & \vec{\xi}^{(4)} &= (-\xi, -\eta, \zeta)\end{aligned}\quad (4.61)$$

The source strengths and potentials on these points are denoted as:

$$\begin{aligned}\sigma^{(i)} &= \sigma(\vec{\xi}^{(i)}) \\ \varphi^{(i)} &= \varphi(\vec{X}^{(i)})\end{aligned} \quad \text{where } i=1,4 \quad (4.62)$$

The composite source strengths and composite potentials are defined as:

$$\begin{aligned}
 \text{Type \#1} & \quad \begin{cases} \sigma^{(+,+)} = \sigma^{(1)} + \sigma^{(2)} + \sigma^{(3)} + \sigma^{(4)} \\ \varphi^{(+,+)} = \varphi^{(1)} + \varphi^{(2)} + \varphi^{(3)} + \varphi^{(4)} \end{cases} \\
 \text{Type \#2} & \quad \begin{cases} \sigma^{(+,-)} = \sigma^{(1)} - \sigma^{(2)} + \sigma^{(3)} - \sigma^{(4)} \\ \varphi^{(+,-)} = \varphi^{(1)} - \varphi^{(2)} + \varphi^{(3)} - \varphi^{(4)} \end{cases} \\
 \text{Type \#3} & \quad \begin{cases} \sigma^{(-,+)} = \sigma^{(1)} + \sigma^{(2)} - \sigma^{(3)} - \sigma^{(4)} \\ \varphi^{(-,+)} = \varphi^{(1)} + \varphi^{(2)} - \varphi^{(3)} - \varphi^{(4)} \end{cases} \\
 \text{Type \#4} & \quad \begin{cases} \sigma^{(-,-)} = \sigma^{(1)} - \sigma^{(2)} - \sigma^{(3)} + \sigma^{(4)} \\ \varphi^{(-,-)} = \varphi^{(1)} - \varphi^{(2)} - \varphi^{(3)} + \varphi^{(4)} \end{cases}
 \end{aligned} \tag{4.63}$$

The composite source strengths can be estimated by integrating over the first quadrant of the hull surface,  $S_0^{(1)}$ :

$$\frac{\partial}{\partial n} \varphi^{(\pm\pm)}(\vec{X}^{(1)}) = -\frac{1}{2} \sigma^{(\pm\pm)}(\vec{X}^{(1)}) + \frac{1}{4\pi} \int_{S_0^{(1)}} \sigma^{(\pm\pm)}(\vec{\xi}) \frac{\partial G^{(\pm\pm)}}{\partial n(\vec{X}^{(1)})} dS \text{ where } \vec{X}^{(1)} \in S_0^{(1)} \tag{4.64}$$

where the composite Green functions are defined as:

$$\begin{aligned}
 G^{(+,+)} &= G(\vec{X}^{(1)}, \vec{\xi}^{(1)}) + G(\vec{X}^{(1)}, \vec{\xi}^{(2)}) + G(\vec{X}^{(1)}, \vec{\xi}^{(3)}) + G(\vec{X}^{(1)}, \vec{\xi}^{(4)}) \\
 G^{(+,-)} &= G(\vec{X}^{(1)}, \vec{\xi}^{(1)}) - G(\vec{X}^{(1)}, \vec{\xi}^{(2)}) + G(\vec{X}^{(1)}, \vec{\xi}^{(3)}) - G(\vec{X}^{(1)}, \vec{\xi}^{(4)}) \\
 G^{(-,+)} &= G(\vec{X}^{(1)}, \vec{\xi}^{(1)}) + G(\vec{X}^{(1)}, \vec{\xi}^{(2)}) - G(\vec{X}^{(1)}, \vec{\xi}^{(3)}) - G(\vec{X}^{(1)}, \vec{\xi}^{(4)}) \\
 G^{(-,-)} &= G(\vec{X}^{(1)}, \vec{\xi}^{(1)}) - G(\vec{X}^{(1)}, \vec{\xi}^{(2)}) - G(\vec{X}^{(1)}, \vec{\xi}^{(3)}) + G(\vec{X}^{(1)}, \vec{\xi}^{(4)})
 \end{aligned} \tag{4.65}$$

The composite potential is expressed as:

$$\varphi^{(\pm\pm)}(\vec{X}^{(1)}) = \frac{1}{4\pi} \int_{S_0^{(1)}} \sigma^{(\pm\pm)}(\vec{\xi}) G^{(\pm\pm)} dS \text{ where } \vec{X}^{(1)} \in S_0^{(1)} \tag{4.66}$$

Once the composite source strength and composite potential are derived, the source strength and the potential at all four pairs of source and field points on the four quadrants of the hull surface can be determined from [Equation 4.63 \(p. 74\)](#):

$$\begin{aligned}
 \sigma^{(1)} &= \frac{1}{4} [\sigma^{(+,+)} + \sigma^{(+,-)} + \sigma^{(-,+)} + \sigma^{(-,-)}] & \varphi^{(1)} &= \frac{1}{4} [\varphi^{(+,+)} + \varphi^{(+,-)} + \varphi^{(-,+)} + \varphi^{(-,-)}] \\
 \sigma^{(2)} &= \frac{1}{4} [\sigma^{(+,+)} - \sigma^{(+,-)} + \sigma^{(-,+)} - \sigma^{(-,-)}] & \varphi^{(2)} &= \frac{1}{4} [\varphi^{(+,+)} - \varphi^{(+,-)} + \varphi^{(-,+)} - \varphi^{(-,-)}] \\
 \sigma^{(3)} &= \frac{1}{4} [\sigma^{(+,+)} + \sigma^{(+,-)} - \sigma^{(-,+)} - \sigma^{(-,-)}] & \varphi^{(3)} &= \frac{1}{4} [\varphi^{(+,+)} + \varphi^{(+,-)} - \varphi^{(-,+)} - \varphi^{(-,-)}] \\
 \sigma^{(4)} &= \frac{1}{4} [\sigma^{(+,+)} - \sigma^{(+,-)} - \sigma^{(-,+)} + \sigma^{(-,-)}] & \varphi^{(4)} &= \frac{1}{4} [\varphi^{(+,+)} - \varphi^{(+,-)} - \varphi^{(-,+)} + \varphi^{(-,-)}]
 \end{aligned} \tag{4.67}$$

For a single symmetric structure (a structure with either port-starboard or fore-aft symmetry),

$\vec{X}^{(1)} = (X, Y, Z)$  and  $\vec{\xi}^{(1)} = (\xi, \eta, \zeta)$  are a pair of field and source points on the first half of the hull surface, and there is a pair of corresponding points on the other half:

$$\begin{aligned}
 \vec{X}^{(2)} &= \begin{cases} (X, -Y, Z) & \text{for port-starboard symmetry} \\ (-X, Y, Z) & \text{for fore-aft symmetry} \end{cases} \\
 \vec{\xi}^{(2)} &= \begin{cases} (\xi, -\eta, \zeta) & \text{for port-starboard symmetry} \\ (-\xi, \eta, \zeta) & \text{for fore-aft symmetry} \end{cases}
 \end{aligned} \tag{4.68}$$

The source strengths and potential on these points are:

$$\begin{aligned}\sigma^{(i)} &= \sigma(\vec{\xi}^{(i)}) \\ \varphi^{(i)} &= \varphi(\vec{X}^{(i)})\end{aligned} \quad \text{where } i=1,2 \quad (4.69)$$

The composite source strengths and composite potentials are defined as:

$$\begin{aligned}\text{Type #1} \quad &\begin{cases} \sigma^{(+)} = \sigma^{(1)} + \sigma^{(2)} \\ \varphi^{(+)} = \varphi^{(1)} + \varphi^{(2)} \end{cases} \\ \text{Type #2} \quad &\begin{cases} \sigma^{(-)} = \sigma^{(1)} - \sigma^{(2)} \\ \varphi^{(-)} = \varphi^{(1)} - \varphi^{(2)} \end{cases}\end{aligned} \quad (4.70)$$

Employing the same concept discussed for the double symmetric case, the composite source strengths and composite potentials can be estimated by integrating over the half part of the hull surface. Once these variables are calculated, the source strengths and potentials are obtained by:

$$\begin{aligned}\sigma^{(1)} &= \frac{1}{2} [\sigma^{(+)} + \sigma^{(-)}] & \varphi^{(1)} &= \frac{1}{2} [\varphi^{(+)} + \varphi^{(-)}] \\ \sigma^{(2)} &= \frac{1}{2} [\sigma^{(+)} - \sigma^{(-)}] & \varphi^{(2)} &= \frac{1}{2} [\varphi^{(+)} - \varphi^{(-)}]\end{aligned} \quad (4.71)$$

## 4.8. Generalized Hydrodynamic Damping

Generalized damping is calculated for a quality check of the hydrodynamic damping coefficients.

The structural mass eigen space  $\mathbf{E}_M$  is introduced, such that

$$\mathbf{E}_M^T \mathbf{M}_S \mathbf{E}_M = \begin{bmatrix} \lambda_1^2 & 0 & 0 & 0 & 0 \\ \dots & & & & \\ 0 & \lambda_i^2 & & & 0 \\ & & \dots & & \\ 0 & 0 & 0 & 0 & \lambda_n^2 \end{bmatrix} \quad (4.72)$$

where  $\mathbf{M}_S$  is the structural mass matrix,  $i=1,\dots,n$ ,  $n = 6 \times m$  (where  $m$  is the number of hydrodynamic interaction structures), and  $\lambda_i > 0$ .

The eigenvector satisfies

$$\mathbf{E}_M^T \mathbf{E}_M = \mathbf{I} \quad (4.73)$$

Defining a new diagonal matrix:

$$\mathbf{A}_{1/2} = \begin{bmatrix} \lambda_1 & 0 & 0 & 0 & 0 \\ \dots & & & & \\ 0 & \lambda_i & & & 0 \\ & & \dots & & \\ 0 & 0 & 0 & 0 & \lambda_n \end{bmatrix} \quad (4.74)$$

the square root mass matrix is written as:

$$\mathbf{M}_{1/2} = \mathbf{E}_M^T \mathbf{A}_{1/2} \mathbf{E}_M \quad (4.75)$$

Denoting  $\mathbf{C}$  as the hydrodynamic damping matrix at the frequency  $\omega$ , the normalized damping matrix is given as:

$$\mathbf{C}_N = \mathbf{M}_{1/2}^{-1} \mathbf{C} \mathbf{M}_{1/2}^{-1} \quad (4.76)$$

**Note:**

The hydrodynamic damping matrix  $\mathbf{C}$  consists of the diffraction panel induced damping and the frequency-independent damping.

The damping eigensolution is:

$$\mathbf{D}^T \mathbf{C}_N \mathbf{D} = \begin{bmatrix} \gamma_1 & 0 & 0 & 0 & 0 \\ \dots & & & & \\ 0 & \gamma_i & & & 0 \\ & & \dots & & \\ 0 & 0 & 0 & 0 & \gamma_n \end{bmatrix} \quad (4.77)$$

where  $\mathbf{D}^T \mathbf{D} = \mathbf{I}$  and  $\gamma_i$  ( $i=1,\dots,n$ ) is considered the generalized damping at the motion mode  $i$ , which should generally be positive.

The generalized damping is checked when the radiation force is evaluated by the convolution integration approach in a time domain analysis (see [Radiation Force by Convolution Integration \(p. 188\)](#)).

If  $\gamma_i$  is negative, denoting the  $i$ -th eigenvector in the matrix  $\mathbf{D}$  as

$$D_i^T = \{d_{jk}\}_i \quad (j=1,6; k=1, m) \quad (4.78)$$

it is recommended that you add the frequency-independent diagonal damping coefficients for some dominant motions in this eigenvector. The value is suggested to not be less than

$$c_{jjk} = M_{S_{jjk}} |d_{jk} \gamma_i| \quad (4.79)$$

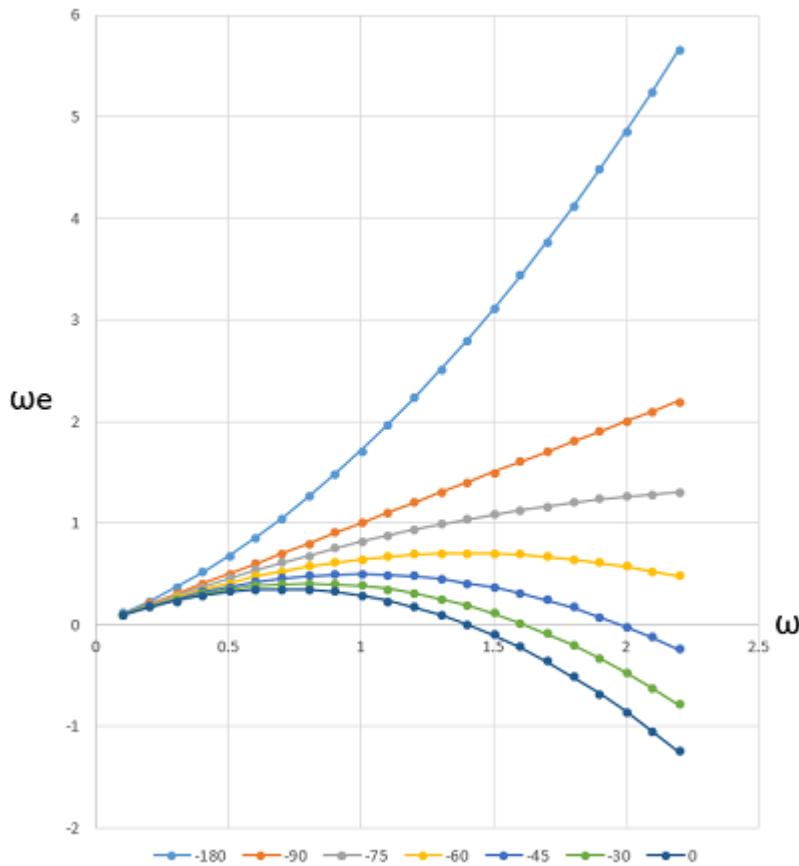
where  $M_{S_{jjk}}$  is the structural mass or moment of inertia of the  $j$ -th motion of the  $k$ -th structure.

## 4.9. Radiation Wave Properties at Negative Encounter Frequency

For vessels traveling with a constant speed, [Equation 4.39 \(p. 69\)](#) shows that the encounter frequency associated to an incident wave frequency varies with the relative heading angle between the forward speed and the wave propagation direction. When the magnitude of the relative heading angle is less than  $90^\circ$  ( $0 \leq |\beta| < 90^\circ$ ), the peak encounter frequency,  $\omega_{e\_peak}(\beta)$ , is determined by:

$$\frac{d\omega_e}{d\omega} = 1 - \frac{dk}{d\omega} U \cos \beta = 0 \quad (4.80)$$

and negative encounter frequency may occur when the incident wave frequency is high enough, as shown in the following figure:

**Figure 4.2: Encounter Frequencies vs. Incident Wave Frequencies in Different Relative Headings**

Only a single structure traveling with a constant speed is discussed in this section. Considering the body boundary condition given in [Equation 4.41 \(p. 69\)](#), the radiation potential  $\varphi_{rj}(\omega_e)$  due to the  $j^{\text{th}}$  motion with unit amplitude is split into two components: the encounter frequency related component  $\varphi_{rj}^0$  and the forward speed related component  $\varphi_{rj}^U$ :

$$\varphi_{rj}(\omega_e) = \varphi_{rj}^0(\omega_e) + \varphi_{rj}^U(\omega_e) \quad (4.81)$$

In addition, to satisfying the Laplace equation ([Equation 4.13 \(p. 62\)](#)), the seabed boundary condition ([Equation 4.16 \(p. 62\)](#)), and the simplified free surface equation ([Equation 4.47 \(p. 70\)](#)),  $\varphi_{rj}^0$ ,  $\varphi_{rj}^U$  satisfy the wetted surface boundary conditions:

$$\begin{aligned} \frac{\partial \varphi_{rj}^0}{\partial n} &= -i\omega_e n_j \\ \frac{\partial \varphi_{rj}^U}{\partial n} &= Um_j \quad (j=1,6) \end{aligned} \quad (4.82)$$

The definition of the forward speed related component  $\varphi_{rj}^U$  can be simply derived as:

$$\begin{aligned}
 \varphi_{rj}^U &= 0 \quad (j=1,3) \\
 \varphi_{r4}^U &= \frac{U_2}{i\omega_e} \varphi_{r3}^0 \\
 \varphi_{r5}^U &= -\frac{U_1}{i\omega_e} \varphi_{r3}^0 \\
 \varphi_{r6}^U &= \frac{U_1}{i\omega_e} \varphi_{r2}^0 - \frac{U_2}{i\omega_e} \varphi_{r1}^0
 \end{aligned} \tag{4.83}$$

The total radiation potential due to the  $j^{\text{th}}$  unit motion is rewritten as:

$$\begin{aligned}
 \varphi_{rj} &= \varphi_{rj}^0 \quad (j=1,3) \\
 \varphi_{r4} &= \varphi_{r4}^0 + \frac{U_2}{i\omega_e} \varphi_{r3}^0 \\
 \varphi_{r5} &= \varphi_{r5}^0 - \frac{U_1}{i\omega_e} \varphi_{r3}^0 \\
 \varphi_{r6} &= \varphi_{r6}^0 + \frac{U_1}{i\omega_e} \varphi_{r2}^0 - \frac{U_2}{i\omega_e} \varphi_{r1}^0
 \end{aligned} \tag{4.84}$$

Based on all the boundary conditions of the encounter frequency related potential component  $\varphi_{rj}^0$ , it is found that:

$$\varphi_{rj}^0(-\omega_e) = -\varphi_{rj}^0(\omega_e) \quad (\omega_e > 0, j=1,6) \tag{4.85}$$

Combining the relationships given in [Equation 4.80 \(p. 76\)](#) through [Equation 4.85 \(p. 78\)](#), the radiation potentials at a negative encounter frequency can be expressed by the radiation potentials at the corresponding positive encounter frequency:

$$\begin{aligned}
 \varphi_{rj}(-\omega_e) &= -\varphi_{rj}(\omega_e) \quad (j=1,3) \\
 \varphi_{r4}(-\omega_e) &= -\varphi_{r4}(\omega_e) + 2\frac{U_2}{i\omega_e} \varphi_{r3}(\omega_e) \\
 \varphi_{r5}(-\omega_e) &= -\varphi_{r5}(\omega_e) - 2\frac{U_1}{i\omega_e} \varphi_{r3}(\omega_e) \\
 \varphi_{r6}(-\omega_e) &= -\varphi_{r6}(\omega_e) + 2\frac{U_1}{i\omega_e} \varphi_{r2}(\omega_e) - 2\frac{U_2}{i\omega_e} \varphi_{r1}(\omega_e)
 \end{aligned} \tag{4.86}$$

Introducing a new function:

$$F_{rjk}^0 = \omega_e^2 A_{jk}^0 + i\omega_e B_{jk}^0 = -i\omega_e \rho \int_{S_0} n_j \varphi_{rk}^0 dS \tag{4.87}$$

and substituting [Equation 4.84 \(p. 78\)](#) into [Equation 4.46 \(p. 70\)](#), the added mass and damping of a structure with forward speed can be represented as:

$$\begin{aligned}
 F_{rjk} &= F_{rjk}^0 \quad (j \leq 3, k \leq 3) \\
 F_{rj4} &= F_{rj4}^0 + \frac{U_2}{i\omega_e} F_{rj3}^0 \quad (j \leq 3) \\
 F_{rj5} &= F_{rj5}^0 - \frac{U_1}{i\omega_e} F_{rj3}^0 \quad (j \leq 3) \\
 F_{rj6} &= F_{rj6}^0 + \frac{U_1}{i\omega_e} F_{rj2}^0 - \frac{U_2}{i\omega_e} F_{rj1}^0 \quad (j \leq 3) \\
 F_{r4j} &= F_{r4j}^0 - \frac{U_2}{i\omega_e} F_{r3j}^0 \quad (j \leq 3) \\
 F_{r5j} &= F_{r5j}^0 + \frac{U_1}{i\omega_e} F_{r3j}^0 \quad (j \leq 3) \\
 F_{r6j} &= F_{r6j}^0 - \frac{U_1}{i\omega_e} F_{r2j}^0 + \frac{U_2}{i\omega_e} F_{r1j}^0 \quad (j \leq 3) \\
 F_{r44} &= F_{r44}^0 + \left( \frac{U_2}{\omega_e} \right)^2 F_{r33}^0 \\
 F_{r45} &= F_{r45}^0 - \frac{U_1}{i\omega_e} F_{r43}^0 - \frac{U_2}{i\omega_e} F_{r35}^0 - \frac{U_1 U_2}{\omega_e^2} F_{r33}^0 \\
 F_{r46} &= F_{r46}^0 + \frac{U_1}{i\omega_e} F_{r42}^0 - \frac{U_2}{i\omega_e} F_{r41}^0 - \frac{U_2}{i\omega_e} F_{r36}^0 + \frac{U_1 U_2}{\omega_e^2} F_{r32}^0 - \left( \frac{U_2}{\omega_e} \right)^2 F_{r31}^0 \\
 F_{r54} &= F_{r54}^0 + \frac{U_2}{i\omega_e} F_{r53}^0 + \frac{U_1}{i\omega_e} F_{r34}^0 - \frac{U_1 U_2}{\omega_e^2} F_{r33}^0 \\
 F_{r55} &= F_{r55}^0 + \left( \frac{U_1}{\omega_e} \right)^2 F_{r33}^0 \\
 F_{r56} &= F_{r56}^0 + \frac{U_1}{i\omega_e} F_{r52}^0 - \frac{U_2}{i\omega_e} F_{r51}^0 + \frac{U_1}{i\omega_e} F_{r36}^0 - \left( \frac{U_1}{\omega_e} \right)^2 F_{r32}^0 + \frac{U_1 U_2}{\omega_e^2} F_{r31}^0 \\
 F_{r64} &= F_{r64}^0 + \frac{U_2}{i\omega_e} F_{r63}^0 - \frac{U_1}{i\omega_e} F_{r24}^0 + \frac{U_1 U_2}{\omega_e^2} F_{r23}^0 + \frac{U_2}{i\omega_e} F_{r14}^0 - \frac{U_2^2}{\omega_e^2} F_{r13}^0 \\
 F_{r65} &= F_{r65}^0 - \frac{U_1}{i\omega_e} F_{r63}^0 - \frac{U_1}{i\omega_e} F_{r25}^0 - \left( \frac{U_1}{\omega_e} \right)^2 F_{r23}^0 + \frac{U_2}{i\omega_e} F_{r15}^0 + \frac{U_1 U_2}{\omega_e^2} F_{r13}^0 \\
 F_{r66} &= F_{r66}^0 + \left( \frac{U_1}{\omega_e} \right)^2 F_{r22}^0 + \left( \frac{U_2}{\omega_e} \right)^2 F_{r11}^0 - \frac{U_1 U_2}{\omega_e^2} \left( F_{r12}^0 + F_{r21}^0 \right)
 \end{aligned} \tag{4.88}$$

Employing the definition given by [Equation 4.87 \(p. 78\)](#) and the property of the encounter frequency related potential component  $\varphi_{rj}^0$  from [Equation 4.85 \(p. 78\)](#), it is found that:

$$\begin{aligned}
 F_{rjk}^0(-\omega_e) &= (-\omega_e)^2 A_{jk}^0(-\omega_e) + i(-\omega_e) B_{jk}^0(-\omega_e) \\
 &= \omega_e^2 A_{jk}^0(\omega_e) + i\omega_e B_{jk}^0(\omega_e) \\
 &= F_{rjk}^0(\omega_e)
 \end{aligned} \tag{4.89}$$

Substituting this relationship into [Equation 4.88 \(p. 79\)](#), the added mass and damping coefficients at the negative frequency can be uniquely determined through the hydrodynamic properties at the corresponding positive encounter frequency.

Based on the above discussions, a set of positive encounter frequencies are necessarily selected to create the hydrodynamic database when the frequency domain simulation of the vessel traveling in multi-directional waves is carried out. The radiation wave properties, such as radiation wave pressure, added mass, and damping coefficients, at the negative encounter frequencies can be derived from the hydrodynamic database at the corresponding positive encounter frequencies.

## 4.10. Fictitious Damping at Small Magnitude of Encounter Frequency

If there are no additional restoring coefficients for surge, sway, and yaw motions, the equation of motion of a structure traveling in waves may become singular at a small enough magnitude of encounter frequency while its associated incident wave frequency is relatively high.

In Aqwa frequency domain simulation, the fictitious damping coefficients are introduced when the incident wave frequency is greater than 0.1 rad/s but the magnitude of the associated encounter frequency is less than or equal to 0.1 rad/s:

$$B_{kk}^F(\omega_e) = \text{sign}(\omega_e) \times M_{kk} \times (10^{-30.3|\omega_e|+0.0303} - 10^{-2.9997}) \quad k=1,2,6 \quad (4.90)$$

where  $M_{kk}$  ( $k=1,2,6$ ) are the structure mass and moment of inertia of yaw motion.

From the above equation, it is observed that if  $\omega > 0.1$  rad/s:

$$\begin{aligned} B_{kk}^F &= 0 && \text{if } |\omega_e| = 0.1 \text{ rad/s} \\ B_{kk}^F &\approx \text{sign}(\omega_e) \times M_{kk} && \text{if } |\omega_e| = 0.001 \text{ rad/s} \end{aligned} \quad (4.91)$$

## 4.11. Hydrodynamic Properties of Internal Tanks

The liquid motion (sloshing) in the internal tanks has strong coupling effects with the structure rigid body motions in waves. The sloshing problem is modelled under the assumption of the linear potential theory similar to the seakeeping analysis of a floating structure in waves, which assumes that the liquid is inviscid and incompressible, the liquid flow is irrotational, and the amplitudes of motions are small.

There is no incident and diffraction wave potential components of the internal tank liquid. In the frequency domain, the total potential of the liquid in the internal tank in the LTA consists of the sloshing motion components due to six rigid body basic motions of the internal tank,

$$\Phi(\vec{x}_t, t) = \phi(\vec{x}_t, \omega) e^{-i\omega t} = \sum_{j=1}^6 x_{tj} \phi_j(\vec{x}_t, \omega) e^{-i\omega t} \quad (4.92)$$

where  $\omega$  is the harmonic motion frequency of the floating body,  $\phi_j(\vec{x}_t, \omega)$  is the isolated space dependent term due to the  $j$ -th basic internal tank motion with unit amplitude, which is defined in [Figure 3.3: Local Internal Tank Axes and Basic Motions \(p. 49\)](#),  $x_{tj}$  is the response amplitude operator (RAO) of the internal tank  $j$ -th basic motion,

$$x_{tj} = \begin{cases} u_{tj}, & (j=1,3) \\ \theta_{tj-3}, & (j=4,6) \end{cases} \quad (4.93)$$

The potential of the liquid in the internal tank is governed by the following equations.

In the fluid domain,  $\vec{x}_t \in \Omega_t$ ,

$$\Delta \phi_j = \left( \frac{\partial^2}{\partial x^2} + \frac{\partial^2}{\partial y^2} + \frac{\partial^2}{\partial z^2} \right) \phi_j = 0 \quad (4.94)$$

On the mean liquid free surface in the LTA,  $z_t = 0$ ,

$$-\nu\phi_j + \frac{\partial\phi_j}{\partial z} = \begin{cases} 0, & (j \neq 3) \\ -i\omega, & (j = 3) \end{cases} \quad (4.95)$$

where  $\nu = \frac{\omega^2}{g}$ .

In Equation 4.95 (p. 81) the mean liquid free surface moves rigidly in the vertical direction with the internal tank heave motion. Note that in the LTA the basic internal tank motions (except for the heave motion) do not cause any vertical displacement of the center of flotation of the internal tank liquid.

On the internal tank hull surface,  $\vec{x}_t \in S_t$ , the rigid body boundary condition is

$$\frac{\partial\phi_j}{\partial n} = -i\omega n_j \quad (4.96)$$

where

$$\begin{aligned} (n_1, n_2, n_3) &= \vec{n} \\ (n_4, n_5, n_6) &= \vec{x}_{tj} \times \vec{n} \quad (j=4,6) \end{aligned}$$

From Equation 4.94 (p. 80) through Equation 4.96 (p. 81), the sloshing motion potential due to the internal tank heave motion with unit amplitude is

$$\phi_3 = -i\omega z_t \quad (4.97)$$

The internal tank heave motion does not cause any liquid free surface deformation; instead, the free surface moves rigidly with the tank.

The CFD model may be required for the detailed analysis of the sloshing problem. When the linear potential theory is applied for the coupling hydrodynamic responses analysis, the overestimated resonant liquid motion in an internal tank may occur without taking account of any viscous effect. To overcome this problem, a simplified damping treatment is introduced by Malenica et al [27], which can be easily defined and calibrated by the experimental results. Adopting this concept, the body boundary condition on the tank surface expressed in Equation 4.96 (p. 81) is amended,

$$\frac{\partial\phi_j}{\partial n} + i\alpha_t f_t(\nu, k_0) \phi_j = -i\omega n_j, \quad (j \neq 3) \quad (4.98)$$

where  $\alpha_t$  is the positive non-dimensional damping factor,  $k_0$  is the approximate value of the lowest sloshing resonant wavenumber of the internal tank, and

$$f_t(\nu, k_0) = \begin{cases} k_0 \sin^2\left(\frac{\pi\nu}{2k_0}\right) & \text{where } \nu < k_0 \\ k_0 & \text{where } \nu \geq k_0 \end{cases}$$

For a rectangular box with the dimension (L, B, T) where L and B are the length and breadth of the box, T is the draft of the liquid in the tank, the lowest sloshing resonant wavenumber of the internal tank liquid is approximately given by

$$k_0 = \frac{\pi}{\max(L, B)} \tanh\left[\frac{\pi T}{\max(L, B)}\right] \quad (4.99)$$

The dissipation mainly exists in the boundary layer when this modification is employed, which is not physically true. However it is reported that the global floating structure seakeeping behaviour is less sensitive to the internal tank liquid damping factor introduced in Equation 4.98 (p. 81), the rough es-

timation of this factor may be good enough for the numerical simulation of the dynamic coupling between liquid motions and rigid body motions of the structure (Malenica et al [27]). The selection range of the internal tank liquid damping factor is about [0, 0.1].

The boundary integration approach discussed in [Source Distribution Method \(p. 62\)](#) is used for the internal tank liquid potential calculation. The deep water pulsating source Green function is employed, the potential  $\phi_j$  is represented as

$$\phi_j(\vec{x}_t, \omega) = \frac{1}{4\pi} \int_{S_t} \sigma_j(\vec{\xi}_t, \omega) G(\vec{x}_t, \vec{\xi}_t, \omega) dS \quad (4.100)$$

where  $\vec{x}_t \in S_t \cup \Omega_t$ ,  $\vec{\xi}_t \in S_t$  and  $j \neq 3$ .

The source strength  $\sigma_j(\vec{\xi}_t, \omega)$  over the wetted internal tank surface is determined by the modified boundary condition given by [Equation 4.98 \(p. 81\)](#), such as

$$-\frac{1}{2}\sigma_j(\vec{x}_t, \omega) + \frac{1}{4\pi} \int_{S_t} \sigma_j(\vec{\xi}_t, \omega) \left[ \frac{\partial G}{\partial n(\vec{x}_t)} + i\alpha_t f_t G \right] dS = -i\omega n_j(\vec{x}_t) \quad (4.101)$$

where  $\vec{x}_t \in S_t$ ,  $\vec{\xi}_t \in S_t$ .

The composite source distribution method discussed in [Composite Source Distribution Method for Symmetric Structures \(p. 73\)](#) can be applied for the geometric symmetric internal tank with respect to the  $T_{xz}$  plane and/or  $T_{yz}$  plane of the LTA.

The first order hydrodynamic pressure is calculated by using the linearized Bernoulli's equation

$$p^{(1)}(\vec{x}_t, t) = p^{(1)}(\vec{x}_t, \omega) e^{-i\omega t} = -\rho_t \frac{\partial [\phi(\vec{x}_t, \omega) e^{-i\omega t}]}{\partial t} = i\omega \rho_t \phi(\vec{x}_t, \omega) e^{-i\omega t} \quad (4.102)$$

where  $p^{(1)}(\vec{x}_t, \omega) = i\omega \rho_t \phi(\vec{x}_t, \omega)$ .

The j-th force due to the sloshing wave induced by the k-th unit amplitude internal tank motion with respect to the LTA origin is

$$F_{tjk} = -i\omega \mu \rho_t \int_{S_t} \phi_k n_j dS \quad (4.103)$$

where  $\mu$  is the permeability of the internal tank.

The added mass and damping coefficients are derived from [Equation 4.103 \(p. 82\)](#),

$$\begin{aligned} F_{tjk} &= -i\omega \mu \rho_t \int_{S_t} \left\{ \operatorname{Re}(\phi_k) + i\operatorname{Im}(\phi_k) \right\} n_j dS \\ &= \omega \mu \rho_t \int_{S_t} \operatorname{Im}(\phi_k) n_j dS - i\omega \mu \rho_t \int_{S_t} \operatorname{Re}(\phi_k) n_j dS \\ &= \omega^2 A_{tjk} + i\omega B_{tjk} \end{aligned} \quad (4.104)$$

where the added mass and damping coefficients are

$$\begin{aligned} A_{tjk} &= \frac{\mu \rho_t}{\omega} \int_{S_t} \text{Im}(\phi_k) n_j dS \\ B_{tjk} &= -\mu \rho_t \int_{S_t} \text{Re}(\phi_k) n_j dS \end{aligned} \quad (4.105)$$

For the heave-heave added mass and damping coefficients, substituting [Equation 4.97 \(p. 81\)](#) into [Equation 4.105 \(p. 83\)](#) gives

$$\begin{aligned} A_{t33} &= \frac{\mu \rho_t}{\omega} \int_{S_t} \text{Im}(\phi_3) n_3 dS = \rho_t \nabla_t \\ B_{t33} &= 0 \end{aligned} \quad (4.106)$$

in which  $\nabla_t$  is the volume of the liquid in the internal tank [Equation 3.23 \(p. 50\)](#).

Applying the same concept of the global hydrostatic stiffness matrix calculation in [Equation 3.40 \(p. 54\)](#), the added mass and damping matrices with respect to the LSA origin motions in the FRA are

$$\begin{aligned} \mathbf{A}_g^t &= \begin{bmatrix} \mathbf{I} & 0 \\ -\mathbf{R} & \mathbf{I} \end{bmatrix} \mathbf{A}_t \begin{bmatrix} \mathbf{I} & \mathbf{R} \\ 0 & \mathbf{I} \end{bmatrix} \\ \mathbf{C}_g^t &= \begin{bmatrix} \mathbf{I} & 0 \\ -\mathbf{R} & \mathbf{I} \end{bmatrix} \mathbf{C}_t \begin{bmatrix} \mathbf{I} & \mathbf{R} \\ 0 & \mathbf{I} \end{bmatrix} \end{aligned} \quad (4.107)$$

where  $\mathbf{A}_t = [A_{tjk}]$  and  $\mathbf{C}_t = [B_{tjk}]$  are the matrices of added mass and damping coefficients respectively due to the basic internal tank motion in the LTA.

To estimate the coupling motions of the structure and the internal tanks, [Equation 4.49 \(p. 70\)](#) for the motion equations of multiple hydrodynamic interaction structures can be used with the assembled added mass and damping matrices including the submatrices given by [Equation 4.107 \(p. 83\)](#).

For a ship traveling with a constant forward speed in waves, the excitation frequency, i.e. the encounter frequency, may be negative. Based on [Equation 4.94 \(p. 80\)](#) through [Equation 4.98 \(p. 81\)](#), the internal tank liquid potential at a negative frequency,  $-\omega$  ( $\omega > 0$ ), can be determined by

$$\phi_j(\vec{x}_t, -\omega) = -\phi_j(\vec{x}_t, \omega) \quad (4.108)$$

Substituting this relationship into [Equation 4.102 \(p. 82\)](#), the first order hydrodynamic pressure in internal tank at a negative frequency is

$$p^{(1)}(\vec{x}_t, -\omega) = p^{(1)}(\vec{x}_t, \omega) \quad (4.109)$$

The added mass and damping at negative frequency have the relationships of

$$\begin{aligned} A_{tjk}(-\omega) &= A_{tjk}(\omega) \\ B_{tjk}(-\omega) &= -B_{tjk}(\omega) \end{aligned} \quad (4.110)$$

## 4.12. Hydrodynamic Analysis with Moonpool Effects

Moonpools are the openings through the hull of ships and offshore structures from deck to keel for safe and easy access to water. The large water column oscillation inside the moonpool affects the structure's motion and impacts workers' safety and the condition of equipment. DNV-recommended

practice (2010) suggests that the fluid motion in the moonpool can be calculated by a radiation or diffraction panel program, but the viscous damping should be introduced.

- 4.12.1. Resonant Frequency of Water Motion within Moonpools
- 4.12.2. Prescribed Oscillatory Pressure Distribution Approach
- 4.12.3. Multi-region Matching Approach for Simulation of Moonpool Effects
- 4.12.4. Artificial Damping for Suspending Resonant Water Motion within Moonpools
- 4.12.5. Composite Source Distribution Method for Symmetric Moonpool Configuration
- 4.12.6. Extended Hydrodynamic Coefficient Matrices of a Hydrodynamic Interaction Structure Group with Moonpools

## 4.12.1. Resonant Frequency of Water Motion within Moonpools

The major types of water motion inside the moonpool are piston and sloshing motions. Fukula's formula of the piston motion resonant period (Vijith, 2014) is

$$\omega_0 = \sqrt{\frac{g}{h+\kappa\sqrt{A}}} \quad (4.111)$$

where  $A$  is the cross-sectional area of the moonpool,  $h$  is the draft and  $\kappa=0.479$  for a circular area, 0.460 for a rectangular area ( $b/l=0.5$ ) and 0.473 for a square area. The coefficient of  $\kappa$  could be related to the added mass at the lower surface of the moonpool.

A simple approximation for the natural frequencies of the sloshing modes inside the rectangular moonpool is given by

$$\omega_n = \sqrt{\pi n g / l} = \sqrt{g k_n} \quad (4.112)$$

where  $n = (1, 2, 3, \dots)$ ,  $l$  is the moonpool length and  $k_n = \pi n / l$  (Newman, 2018).

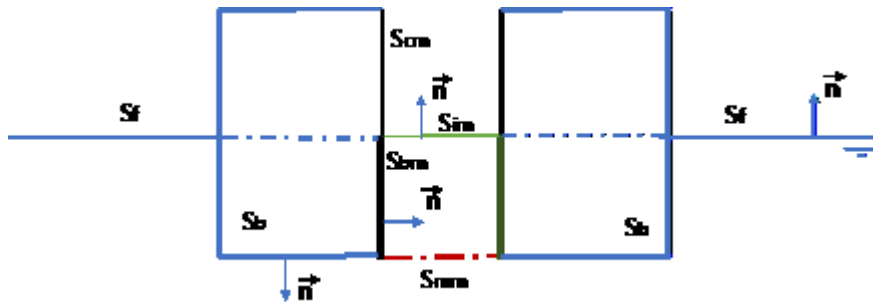
## 4.12.2. Prescribed Oscillatory Pressure Distribution Approach

It is assumed that there is a group of  $N_m$  moonpools in a structure. As shown in [Figure 4.3: Fluid Regions of Floating Structures with Moonpools \(p. 85\)](#), the air chamber surface boundary of the  $m$ -th moonpool is  $S_{am}=S_{cm}+S_{im}$ , where  $S_{cm}$  is the moonpool hull surface above the mean free surface  $S_{im}$  inside the moonpool. The  $m$ -th moonpool wetted hull surface is  $S_{bm}$  and the wetted surface of the body outside the moonpool is  $S_b$ . The  $m$ -th moonpool wetted hull surface and outside body wetted surface are separated by a multi-region matching surface  $S_{mm}$  at the bottom of the  $m$ -th moonpool. The free

surface outside the body is  $S_f$  and the sum of all free surfaces inside the moonpools is  $S_i = \sum_{m=1}^{N_m} S_{im}$ .

The whole boundary surface, including the wetted surfaces and all mean free surfaces inside the

moonpools, is expressed as  $S_w = S_b + \sum_{m=1}^{N_m} (S_{bm} + S_{im})$ , of which the normal vectors point into the fluid region when the surface integration is employed.

**Figure 4.3: Fluid Regions of Floating Structures with Moonpools**

Due to the significant water motion inside the moonpool and the assumption of low fluid particle motion outside the moonpools, different boundary conditions over the internal and external free surfaces should be satisfied separately:

$$\begin{aligned} -K\phi + \phi_z &= \frac{i\omega}{\rho g} p, \text{ on } S_i \\ -K\phi + \phi_z &= 0, \text{ on } S_f \end{aligned} \quad (4.113)$$

where  $K = \omega^2/g$ . Note that the incident wave frequency  $\omega$  is replaced by the encounter frequency  $\omega_e$  if the structure travels with a low forward speed and the simplified free surface boundary condition of [Equation 4.47 \(p. 70\)](#) is used.

Lee and Nielsen (1996) introduced the prescribed pressure modes on the mean free surface inside the moonpool. The pressure on  $S_{im}$  is expressed as the oscillatory pressure distribution of the prescribed modal shapes:

$$p_m = -\rho g \sum_{k=1}^{N_{pm}} \xi_{km} n_{km}(x, y) \quad (4.114)$$

where  $n_{km}(x, y)$  is the k-th non-dimensional pressure distribution modal shape,  $\xi_{km}$  is the pressure modal RAO, and  $N_{pm}$  is the number of pressure modes.

Without loss of generality, for a single structure with multiple moonpools, the total potential with unit incident wave amplitude is expressed as the summation of the potential components of the incident wave, diffraction wave, radiation waves and other waves due to the internal free surface pressure oscillation:

$$\phi = \phi_I + \phi_d + \sum_{j=1}^6 x_j \phi_{rj} + \sum_{m=1}^{N_m} \sum_{k=1}^{N_{pm}} \xi_{km} \phi_{km} \quad (4.115)$$

The boundary conditions of the radiation potentials due to structure motions and diffraction potential remain constant, as those discussed in the previous sections in this chapter.

The velocity potential  $\phi_{km}$ , due to the k-th pressure mode inside the m-th moonpool free surface, satisfies the Laplace equation in the fluid region and the following boundary conditions:

1. On free surfaces, it is given by

$$\begin{aligned} -K\phi_{km} + \frac{\partial}{\partial z}\phi_{km} &= -i\omega n_{km}, \text{ on } S_{im} \\ -K\phi_{km} + \frac{\partial}{\partial z}\phi_{km} &= 0, \text{ on } S_f + \sum_q^{q \neq m} S_{iq} \end{aligned} \quad (4.116)$$

where  $K = \frac{\omega^2}{g}$ .

2. The boundary condition on the wetted body surface is

$$\frac{\partial}{\partial n}\phi_{km} = 0, \text{ on } S_b + \sum_{m=1}^{N_m} S_{bm} \quad (4.117)$$

3. The seabed boundary and far field radiation condition should also be satisfied.

The coupling relationship between the potential components in [Equation 4.115 \(p. 85\)](#) is bound by the condition that the power transferred across the internal mean free surface is equal to the time-average of the rate of energy flux (Lee and Nielsen, 1996):

$$\frac{dE}{dt} = \sum_{m=1}^{N_m} \iint_{S_{im}} p_m \bar{\phi}_z dS \quad (4.118)$$

Inside a moonpool, the air pressure is assumed to be constant (atmospheric pressure) and the rate of energy flux is zero. From [Equation 4.118 \(p. 86\)](#), the general motion equation in the frequency domain is given by:

$$[-\omega^2(\mathbf{M}_s + \mathbf{M}_a) - i\omega\mathbf{C} + \mathbf{K}_{hys}] \begin{bmatrix} x_j \\ \xi_{km} \end{bmatrix} = \begin{bmatrix} F_j \\ F_{km} \end{bmatrix} \quad (4.119)$$

The dimension of the equation above is  $6 + \sum_{m=1}^{N_m} N_{pm}$ , corresponding to the six rigid body degrees of freedom and all pressure modes.  $\mathbf{M}_s$  is the extended structure mass matrix of which only the  $6 \times 6$  sub-matrix on the top left of the matrix is non-zero.

To create a more general expression of the added mass matrix  $\mathbf{M}_a = [A_{ij}]$ , hydrodynamic damping matrix  $\mathbf{C} = [B_{ij}]$ , hydrostatic stiffness matrix  $\mathbf{K}_{hys} = [K_{ij}]$  and the exciting force on the right hand side

of [Equation 4.119 \(p. 86\)](#), the sequence number of a degree of freedom  $j$  starts from 1 to  $6 + \sum_{m=1}^{N_m} N_{pm}$ .

The first six degrees of freedom are corresponding to the six rigid body motions of the structure and follow the internal free surface pressure modes of the moonpools. The generalized normal vector of each degree of freedom of the system is redefined on the boundary surfaces  $S_w$ , such as:

1. For the rigid body motions ( $j=1,6$ )

$$(n_1, n_2, n_3) = \begin{cases} \vec{n} & \text{on } S_b + \sum_{m=1}^{N_m} S_{bm} \\ 0 & \text{on } S_i \end{cases} \quad (4.120)$$

$$(n_4, n_5, n_6) = \begin{cases} \vec{x} \times \vec{n} & \text{on } S_b + \sum_{m=1}^{N_m} S_{bm} \\ 0 & \text{on } S_i \end{cases}$$

2. For the k-th free surface pressure mode inside the m-th moonpool

$$n_j = \begin{cases} 0, & \text{on } S_b + \sum_{q=1}^{N_m} S_{bq} + \sum_{q \neq m}^{q \neq m} S_{iq} \\ n_{km}, & \text{on } S_{im} \end{cases} \quad (4.121)$$

where  $j=6+\sum_{l=1}^{m-1} N_{pl}+k$ .

Employing the above definitions, the generalized added mass and damping coefficient is given by:

$$\omega^2 A_{ij} + i\omega B_{ij} = -i\omega\rho \iint_{S_w} \phi_i \phi_j ds \quad (4.122)$$

The hydrostatic stiffness coefficients  $K_{ij}$  for  $i \leq 6$  and  $j \leq 6$  are the same as the conventional seakeeping analysis definition, i.e. [Equation 3.19 \(p. 48\)](#), [Equation 3.39 \(p. 54\)](#), and [Equation 3.42 \(p. 54\)](#). For  $i \geq 7$  and  $j \geq 7$ , considering the buoyancy force acting on the air chamber (Lee and Newman, 2016),

$$C_{ij} = \rho g \iint_{S_i} n_i n_j ds \quad (4.123)$$

The wave exciting force component is

$$F_{Ij} = -i\omega\rho \iint_{S_w} \phi_I \phi_j ds$$

$$F_{dj} = -i\omega\rho \iint_{S_w} \phi_d \phi_j ds \quad (4.124)$$

### Note:

The velocity potential on the internal free surfaces of the moonpools is required.

Three types of prescribed internal free surface pressure modes could be defined:

1. Series of sine and cosine functions

$$n_k(x, y) = \begin{pmatrix} \sin[\frac{m\pi}{l}(x-x_f)] \\ \cos[\frac{m\pi}{l}(x-x_f)] \end{pmatrix} \cdot \begin{pmatrix} \sin[\frac{m\pi}{b}(y-y_f)] \\ \cos[\frac{m\pi}{b}(y-y_f)] \end{pmatrix} \quad (4.125)$$

where  $(x_f, y_f)$  is the center of the internal free surface of a moonpool,  $l$  is the characteristic length of the moonpool, and  $b$  is the characteristic breadth of the moonpool.

2. Series of Legendre polynomials

$$\begin{aligned}
 n_k(x,y) &= p_n\left(\frac{x-x_f}{l/2}\right)p_m\left(\frac{y-y_f}{b/2}\right) \\
 p_0(\xi) &= 1 \\
 p_1(\xi) &= \xi \\
 (i+1)p_{i+1}(\xi) &= (2i+1)\xi p_i(\xi) - i p_{i-1}(\xi)
 \end{aligned} \tag{4.126}$$

3. For an axisymmetric moonpool, the piston modes could be

$$n_k(r) = J_0(k_n r) \tag{4.127}$$

where  $J_0$  is the Bessel function of the first kind,  $k_n$  is the roots of  $J'_0(k_n R) = 0$ , and  $R$  is the radius of the cylinder and  $r = \sqrt{(x-x_f)^2 + (y-y_f)^2}$ .

### 4.12.3. Multi-region Matching Approach for Simulation of Moonpool Effects

Considering the differences between the internal and external free surface conditions and the possibly thin-walled moonpool structure, the multi-region matching approach is introduced.

As shown in [Figure 4.3: Fluid Regions of Floating Structures with Moonpools \(p. 85\)](#), a matching boundary surface below the m-th moonpool  $S_{mm}$  is added. The m-th moonpool internal fluid region is enclosed by  $S_m = S_{bm} + S_{im} + S_{mm}$ , while the external fluid region is bound by  $S_{out} = S_b + \sum_{m=1}^{N_m} S_{mm}$  alongside the free surface of  $S_f$ , the seabed surface and the far field surface at infinity.

Denoting the diffraction wave and radiation wave potential component in the moonpool fluid region as  $\phi_{dm}^{in}$  and  $\phi_{jm}^{in}$  ( $j=1, 6+\sum_{m=1}^{N_m} N_{pm}$ ) and the diffraction wave and radiation wave potential component in the external fluid region as  $\phi_d^{out}$  and  $\phi_j^{out}$  ( $j=1, 6+\sum_{m=1}^{N_m} N_{pm}$ ), the potential is determined by the source distribution approach:

$$\begin{aligned}
 \phi_m^{in}(\vec{x}) &= \frac{1}{4\pi} \int_{S_m} \sigma(\vec{\xi}) G(\vec{x}, \vec{\xi}) dS \\
 \phi_j^{out}(\vec{x}) &= \frac{1}{4\pi} \int_{S_{out}} \sigma(\vec{\xi}) G(\vec{x}, \vec{\xi}) dS
 \end{aligned} \tag{4.128}$$

where  $\sigma(\vec{\xi})$  is the source strength over the integral surfaces and  $G(\vec{x}, \vec{\xi})$  is the pulsating source Green function defined by [Equation 4.18 \(p. 63\)](#).

The potential of the m-th moonpool internal fluid regions is matched on  $S_{mm}$  with that of the external fluid region by the boundary conditions of

$$\begin{aligned}
 \phi_{dm}^{in} &= \phi_d^{out} \\
 \frac{\partial \phi_{dm}^{in}}{\partial n} &= \frac{\partial \phi_d^{out}}{\partial n} \\
 \phi_{jm}^{in} &= \phi_j^{out} \\
 \frac{\partial \phi_{jm}^{in}}{\partial n} &= \frac{\partial \phi_j^{out}}{\partial n}
 \end{aligned} \tag{4.129}$$

#### 4.12.4. Artificial Damping for Suspending Resonant Water Motion within Moonpools

In [Suspending Standing Waves \(p. 68\)](#), the artificial damping is introduced on the free surface of the restricted fluid region to suspend the overestimated standing wave motion within the restricted fluid region. This concept is extended in the moonpool hydrodynamic analysis to approximately account for the viscous damping effects. Similar to [Equation 4.36 \(p. 68\)](#), the artificial damping terms are added in [Equation 4.116 \(p. 86\)](#). The new free surface boundary condition on the mean free surface within all moonpools is expressed as:

$$\begin{aligned}
 K(\alpha_d^2 f_1 - 1) \phi_j^{in} - 2iK\alpha_d f_1 \phi_j^{in} + \frac{\partial \phi_j^{in}}{\partial z} &= -i\omega n_j, \\
 K(\alpha_d^2 f_1 - 1) \phi_d^{in} - 2iK\alpha_d f_1 \phi_d^{in} + \frac{\partial \phi_d^{in}}{\partial z} &= 0, \quad \text{on } S_i
 \end{aligned} \tag{4.130}$$

where  $\phi_j^{in}$  is the potential component due to a structure COG basic motion ( $j=1,6$ ) or an internal

free surface pressure mode ( $j=7,6+N_{pm}$ ),  $\phi_d^{in}$  is the diffraction wave potential,  $\alpha_d$  is the damping factor which is mainly determined by the model test involving the viscous scale effect (DNV, 2010) or the trial measurement,  $f_1$  is a function related to the lowest natural frequency  $\omega_0$  of the water motions in moonpools which is estimated by [Equation 4.111 \(p. 84\)](#) or [Equation 4.112 \(p. 84\)](#),

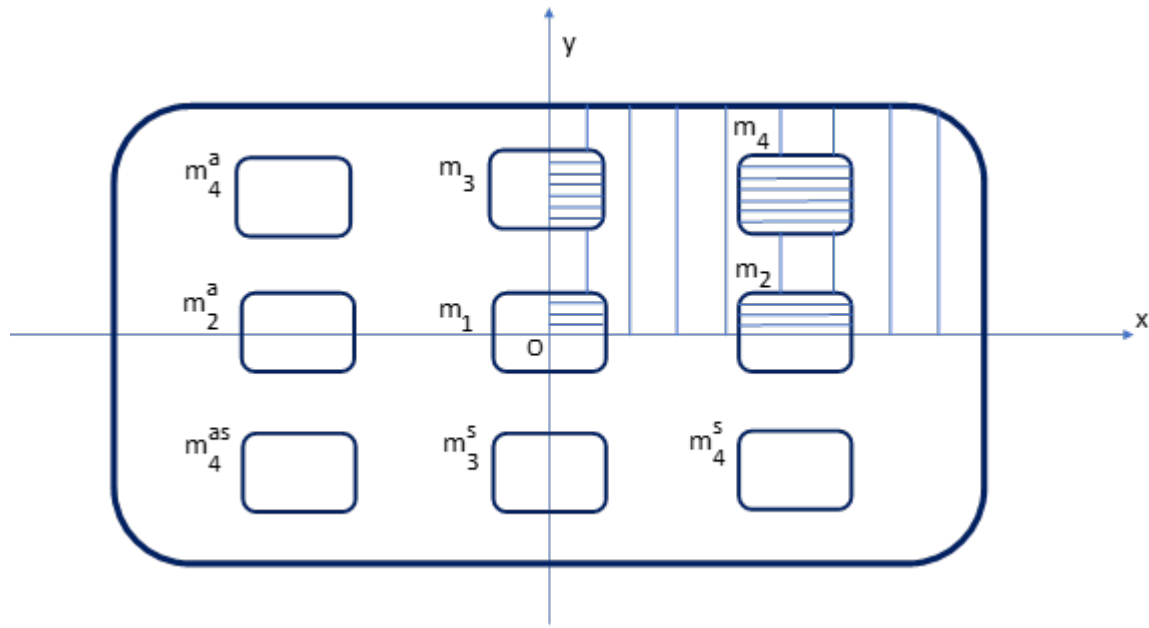
$$f_1 = \begin{cases} \sin^2(\frac{\pi}{2}\delta) & \text{where } \delta < 1 \\ 1 & \text{where } \delta \geq 1 \end{cases} \tag{4.131}$$

$$\delta = \frac{\omega}{\omega_0}$$

#### 4.12.5. Composite Source Distribution Method for Symmetric Moonpool Configuration

The composite source distribution method significantly increases the calculation efficiency when a model is symmetric. The approach is described in [Composite Source Distribution Method for Symmetric Structures \(p. 73\)](#) and is extended to estimate the velocity potential components of the waves due to the extended set of the internal mean free surface pressure modes.

As shown in [Figure 4.4: Symmetric Types of Moonpool Geometry \(p. 90\)](#), if the structure is of fore-aft and port-starboard symmetry, only a quarter of the surfaces related to this structure is required to be meshed when the composite source distribution method is employed. There are four possible types of the moonpool geometric symmetric forms and moonpool configurations:

**Figure 4.4: Symmetric Types of Moonpool Geometry**

1. A moonpool (Moonpool  $m_1$ ) is of fore-aft and port-starboard symmetry in FRA

Only a quarter of the moonpool boundaries is required to be meshed. The composite source distribution method discussed in [Composite Source Distribution Method for Symmetric Structures \(p. 73\)](#) is directly used for the potential due to the prescribed pressure modes on this moonpool's internal mean free surface.

2. A moonpool (Moonpool  $m_2$ ) is of port-starboard symmetry in FRA and there is an OYZ plane mirrored moonpool (Moonpool  $m_2^g$ )

The internal mean free surface area center is at  $(x_f, 0)$ . Only the port or starboard part of the  $m_2$ -th moonpool boundaries is required to be meshed.  $N_{pm}$  prescribed pressure modes on the  $m_2$ -th moonpool internal mean free surface are input and defined by [Equation 4.125 \(p. 87\)](#) through [Equation 4.127 \(p. 88\)](#). A set of the extended pressure mode on the  $m_2^a$ -th moonpool mean free surface  $S_{im_2^a}$  is mirrored from the predefined, based on the property of the prescribed pressure mode on  $S_{im_2}$ , i.e.

$$n_{km_2^a}(x^a - x_f^a, y^a) = n_{km_2}(x - x_f, y), \quad k=1, N_{pm} \quad (4.132)$$

where  $(x^a, y^a) = (-x, y)$  is the x- and y-coordinates of the point on  $S_{im_2^a}$  of which the area center is at  $(x_f^a, 0) = (-x_f, 0)$ .

[Equation 4.132 \(p. 90\)](#) can be further written as

$$n_{km_2^a}(x^a - x_f^a, y^a) = (-1)^{\kappa_a} n_{km_2}(x^a - x_f^a, y^a), \quad (4.133)$$

where  $\kappa_a=0$  if  $n_{km_2}$  is an even function of x and  $\kappa_a=1$  if  $n_{km_2}$  is an odd function of x.

To further define the composite potentials due to these pressure modes on either the port or starboard part of  $S_{im_2}$ , a set of the composite pressure modes on the free surface panel on defined half-part of  $S_{im_2}$  can be presented as

$$n_{km_2}^{(+,+)}(x-x_f, y) = n_{km_2}(x-x_f, y) + n_{km_2}(x-x_f, -y) + n_{km_2^a}(x^a-x_f^a, y) + n_{km_2^a}(x^a-x_f^a, -y) \quad (4.134)$$

$$n_{km_2}^{(+,-)}(x-x_f, y) = n_{km_2}(x-x_f, y) + n_{km_2}(x-x_f, -y) - n_{km_2^a}(x^a-x_f^a, y) - n_{km_2^a}(x^a-x_f^a, -y) \quad (4.135)$$

$$n_{km_2}^{(-,+)}(x-x_f, y) = n_{km_2}(x-x_f, y) - n_{km_2}(x-x_f, -y) + n_{km_2^a}(x^a-x_f^a, y) - n_{km_2^a}(x^a-x_f^a, -y) \quad (4.136)$$

$$n_{km_2}^{(-,-)}(x-x_f, y) = n_{km_2}(x-x_f, y) - n_{km_2}(x-x_f, -y) - n_{km_2^a}(x^a-x_f^a, y) + n_{km_2^a}(x^a-x_f^a, -y) \quad (4.137)$$

**Composite Source Distribution Method for Symmetric Structures (p. 73)** is applied to obtain the source strength and velocity potential on the whole boundary surface  $S_w$ .

3. A moonpool (Moonpool  $m_3$ ) is of fore-aft symmetry in FRA and there is an OXZ plane mirrored moonpool (Moonpool  $m_3^s$ )

The inside mean free surface area center is at  $(0, y_f)$ . Only the fore-aft part of the  $m_3$ -th moonpool boundaries is required to be meshed. Like the second moonpool type stated above, the extended pressure modes on the  $m_3^s$ -th moonpool mean free surface are derived from the prescribed pressure modes of the  $m_3$ -th moonpool:

$$n_{km_3^s}(x^s, y^s - y_f^s) = (-1)^{\kappa_s} n_{km_3}(x^s, y^s - y_f^s) \quad (4.138)$$

where  $(x^s, y^s)$  is the x- and y-coordinates of the point on the  $m_3^s$ -th moonpool mean free surface of which the area center is at  $(0, y_f^s) = (0, -y_f)$ ;  $\kappa_s=0$  if  $n_{km_3}$  is the even function of y and  $\kappa_s=1$  if  $n_{km_3}$  is the odd function of y.

A similar concept is applied for defining the composite boundary condition on the meshed part of

$$n_{km_3}^{(+,+)}(x, y - y_f) = n_{km_3}(x, y - y_f) + n_{km_3^s}(x, y^s - y_f^s) + n_{km_3}(-x, y - y_f) + n_{km_3^s}(-x, y^s - y_f^s) \quad (4.139)$$

$$n_{km_3}^{(+,-)}(x, y - y_f) = n_{km_3}(x, y - y_f) + n_{km_3^s}(x, y^s - y_f^s) - n_{km_3}(-x, y - y_f) - n_{km_3^s}(-x, y^s - y_f^s) \quad (4.140)$$

$$n_{km_3}^{(-,+)}(x, y - y_f) = n_{km_3}(x, y - y_f) - n_{km_3^s}(x, y^s - y_f^s) + n_{km_3}(-x, y - y_f) - n_{km_3^s}(-x, y^s - y_f^s) \quad (4.141)$$

$$n_{km_3}^{(-,-)}(x, y - y_f) = n_{km_3}(x, y - y_f) - n_{km_3^s}(x, y^s - y_f^s) - n_{km_3}(-x, y - y_f) + n_{km_3^s}(-x, y^s - y_f^s) \quad (4.142)$$

4. A moonpool (Moonpool  $m_4$ ) is not symmetric in FRA but has three mirrored moonpools (Moonpools  $m_4^a$ ,  $m_4^s$ ,  $m_4^{as}$ )

The whole boundary surfaces of the  $m_4$ -th moonpool should be meshed, the internal mean free surface area center is at  $(x_f, y_f)$ .

Based on  $N_{pm}$  prescribed pressure modes defined on the  $m_4$ -th moonpool mean free surface  $S_{im_4}$ , the other  $3N_{pm}$  pressure modes on the internal mean free surfaces within the mirrored moonpools are:

On  $S_{im_4^a}$ ,

$$n_{km_4^a}(x^a - x_f^a, y^a - y_f^a) = (-1)^{ka} n_{km_4}(x^a - x_f^a, y^a - y_f^a) \quad (4.143)$$

On  $S_{im_4^s}$ ,

$$n_{km_4^s}(x^s - x_f^s, y^s - y_f^s) = (-1)^{ks} n_{km_4}(x^s - x_f^s, y^s - y_f^s) \quad (4.144)$$

On  $S_{im_4^{as}}$ ,

$$n_{km_4^{as}}(x^{as} - x_f^{as}, y^{as} - y_f^{as}) = (-1)^{ka+ks} n_{km_4}(x^{as} - x_f^{as}, y^{as} - y_f^{as}) \quad (4.145)$$

where

$(x_f^a, y_f^a) = (-x_f, y_f)$  is the  $m_4^a$ -th moonpool mean free surface area center,

$(x_f^s, y_f^s) = (x_f, -y_f)$  is the  $m_4^s$ -th moonpool mean free surface area center,

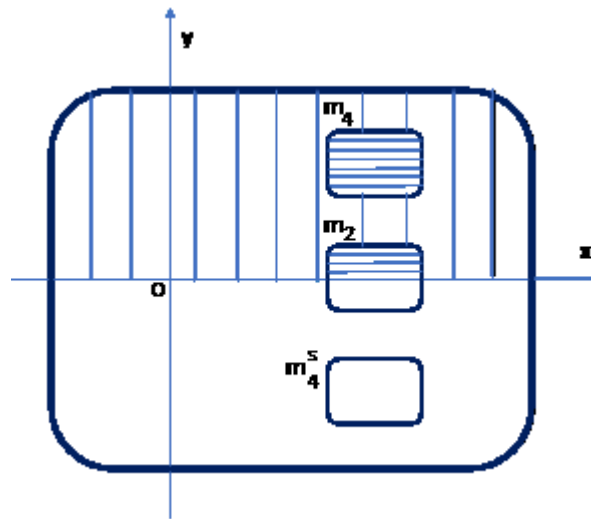
$(x_f^{as}, y_f^{as}) = (-x_f, -y_f)$  is the  $m_4^{as}$ -th moonpool mean free surface area center.

Similar to [Equation 4.134 \(p. 91\)](#) through [Equation 4.137 \(p. 91\)](#) on the meshed surface of  $S_{im_2}$ , the composite non-dimensional pressure modal shapes on the whole surface of  $S_{im_4}$  are

$$\begin{aligned} n_{km_4}^{(+,+)}(x - x_f, y - y_f) &= n_{km_4}(x - x_f, y - y_f) + n_{km_4^s}(x - x_f, y^s - y_f^s) \\ &\quad + n_{km_4^a}(x^a - x_f^a, y - y_f) + n_{km_4^{as}}(x^{as} - x_f^{as}, y^{as} - y_f^{as}) \\ n_{km_4}^{(+,-)}(x - x_f, y - y_f) &= n_{km_4}(x - x_f, y - y_f) + n_{km_4^s}(x - x_f, y^s - y_f^s) \\ &\quad - n_{km_4^a}(x^a - x_f^a, y - y_f) - n_{km_4^{as}}(x^{as} - x_f^{as}, y^{as} - y_f^{as}) \\ n_{km_4}^{(-,+)}(x - x_f, y - y_f) &= n_{km_4}(x - x_f, y - y_f) - n_{km_4^s}(x - x_f, y^s - y_f^s) \\ &\quad + n_{km_4^a}(x^a - x_f^a, y - y_f) - n_{km_4^{as}}(x^{as} - x_f^{as}, y^{as} - y_f^{as}) \\ n_{km_4}^{(-,-)}(x - x_f, y - y_f) &= n_{km_4}(x - x_f, y - y_f) - n_{km_4^s}(x - x_f, y^s - y_f^s) \\ &\quad - n_{km_4^a}(x^a - x_f^a, y - y_f) + n_{km_4^{as}}(x^{as} - x_f^{as}, y^{as} - y_f^{as}) \end{aligned} \quad (4.146)$$

As shown in [Figure 4.5: Port-Starboard Symmetric Types of Moonpool Geometry \(p. 92\)](#), a structure is of port-starboard symmetry only. There are two possible types of moonpool geometric symmetric forms and moonpool configurations, if the associated structure is only port-starboard symmetric.

**Figure 4.5: Port-Starboard Symmetric Types of Moonpool Geometry**



1. A moonpool (Moonpool  $m_2$ ) has port-starboard symmetry in FRA

The internal mean free surface area center is at  $(x_f, 0)$ . Only the port or starboard part of the  $m_2$ -th moonpool boundaries is required to be meshed.  $N_{pm}$  prescribed pressure modes on the  $m_2$ -th moonpool internal mean free surface is input and defined by [Equation 4.125 \(p. 87\)](#) through [Equation 4.127 \(p. 88\)](#).

The composite source distribution method discussed in [Composite Source Distribution Method for Symmetric Structures \(p. 73\)](#) is directly used for the potential due to the prescribed pressure modes on this moonpool's internal mean free surface.

2. A moonpool (Moonpool  $m_4$ ) is not symmetric in FRA but has one mirrored moonpool (Moonpool  $m_4^s$ )

The entire boundary surface of the  $m_4$ -th moonpool should be meshed, the internal mean free surface area center is at  $(x_f, y_f)$ .

Based on  $N_{pm}$  prescribed pressure modes defined on the  $m_4$ -th moonpool mean free surface  $S_{im_4}$ , the other  $N_{pm}$  pressure modes on the internal mean free surfaces within the mirrored moonpool are

$$n_{km_4^s}(x^s - x_f^s, y^s - y_f^s) = (-1)^{ks} n_{km_4}(x - x_f, y - y_f) \quad \text{on } S_{im_4^s} \quad (4.147)$$

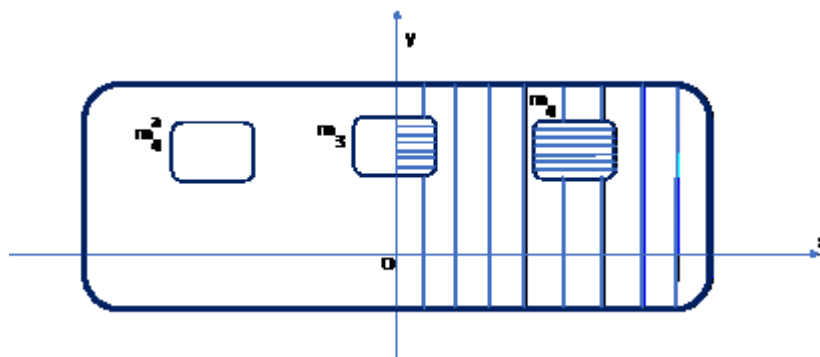
where  $(x_f^s, y_f^s) = (x_f, -y_f)$  is the  $m_4^s$ -th moonpool mean free surface area center,  $k=1, N_{pm}$ .

Similar to [Equation 4.146 \(p. 92\)](#) on the meshed surface of  $S_{im_4}$ , the composite non-dimensional pressure modal shapes for a port-starboard symmetric case are

$$\begin{aligned} n_{km_4}^{(+)}(x - x_f, y - y_f) &= n_{km_4}(x - x_f, y - y_f) + n_{km_4^s}(x - x_f, y^s - y_f^s) \\ n_{km_4}^{(-)}(x - x_f, y - y_f) &= n_{km_4}(x - x_f, y - y_f) - n_{km_4^s}(x - x_f, y^s - y_f^s) \end{aligned} \quad (4.148)$$

As shown in [Figure 4.6: Fore-aft Symmetric Types of Moonpool Geometry \(p. 93\)](#), a structure is of fore-aft symmetry only. There are two possible types of the moonpool geometric symmetric forms and moonpool configurations if the associated structure is only fore-aft symmetric.

**Figure 4.6: Fore-aft Symmetric Types of Moonpool Geometry**



1. A moonpool (Moonpool  $m_2$ ) is of fore-aft symmetry in FRA

The internal mean free surface area center is at  $(x_f, 0)$ . Only the fore-aft part of the  $m_2$ -th moonpool boundaries is required to be meshed.  $N_{pm}$  prescribed pressure modes on the  $m_2$ -th

moonpool internal mean free surface are input and defined by Equation 4.125 (p. 87) through Equation 4.127 (p. 88).

The composite source distribution method discussed in [Composite Source Distribution Method for Symmetric Structures \(p. 73\)](#) is directly used for the potential due to the prescribed pressure modes on this moonpool's internal mean free surface.

2. A moonpool (Moonpool  $m_4$ ) is not symmetric in FRA but has one mirrored moonpool (Moonpool  $m_4^a$ )

The entire boundary surface of the  $m_4$ -th moonpool should be meshed. The internal mean free surface area center is at  $(x_f, y_f)$ .

Based on  $N_{pm}$  prescribed pressure modes defined on the  $m_4$ -th moonpool mean free surface  $S_{im_4}$ , the other  $N_{pm}$  pressure modes on the internal mean free surfaces within the mirrored moonpool are

$$n_{km_4^a}(x^a - x_f^a, y^a - y_f^a) = (-1)^{ka} n_{km_4}(x - x_f, y - y_f) \quad \text{on } S_{im_4^a} \quad (4.149)$$

where  $(x_f^a, y_f^a) = (-x_f, y_f)$  is the  $m_4^a$ -th moonpool mean free surface area center,  $k=1, N_{pm}$ .

Similar to [Equation 4.148 \(p. 93\)](#) on the meshed surface of  $S_{im_4}$ , the composite non-dimensional pressure modal shapes for port-starboard symmetric case are

$$\begin{aligned} n_{km_4}^{(+)}(x - x_f, y - y_f) &= n_{km_4}(x - x_f, y - y_f) + n_{km_4^a}(x^a - x_f^a, y^a - y_f^a) \\ n_{km_4}^{(-)}(x - x_f, y - y_f) &= n_{km_4}(x - x_f, y - y_f) - n_{km_4^a}(x^a - x_f^a, y^a - y_f^a) \end{aligned} \quad (4.150)$$

In summary, the numbers of the described pressure modes of the moonpools on the defined quadrant or half-part of a vessel and their extended pressure modes on the mirrored moonpools are listed in [Table 4.1: Numbers of Pressure Modes due to Geometric Symmetry \(p. 94\)](#).

**Table 4.1: Numbers of Pressure Modes due to Geometric Symmetry**

| Vessel Symmetry             | Moonpool | Pre-described | Extended  | Total     |
|-----------------------------|----------|---------------|-----------|-----------|
| Fore-aft and port-starboard | $m_1$    | $N_{pm}$      | 0         | $N_{pm}$  |
|                             | $m_2$    | $N_{pm}$      | $N_{pm}$  | $2N_{pm}$ |
|                             | $m_3$    | $N_{pm}$      | $N_{pm}$  | $2N_{pm}$ |
|                             | $m_4$    | $N_{pm}$      | $3N_{pm}$ | $4N_{pm}$ |
| Port-starboard              | $m_2$    | $N_{pm}$      | <b>0</b>  | $N_{pm}$  |
|                             | $m_4$    | $N_{pm}$      | $N_{pm}$  | $2N_{pm}$ |
| Fore-aft                    | $m_3$    | $N_{pm}$      | <b>0</b>  | $N_{pm}$  |
|                             | $m_4$    | $N_{pm}$      | $N_{pm}$  | $2N_{pm}$ |

#### 4.12.6. Extended Hydrodynamic Coefficient Matrices of a Hydrodynamic Interaction Structure Group with Moonpools

In a hydrodynamic interaction structure group with moonpools, the total number of degrees of freedom includes:

the total number of the rigid body motions, which is  $6 \times M$ , where  $M$  is the number of the structures in the group;

the total number of the moonpool pressure modes in the group, which is  $N_p = \sum_{s=Str1}^{StrM} N_{ps} = \sum_{s=Str1}^{StrM} \sum_{m=1}^{N_{ms}} N_{pms}$ ,

where  $Str1$  and  $StrM$  are the global sequence numbers (within the whole model) of the starting and finishing structures of the hydrodynamic interaction structure group,  $StrM - Str1 + 1 = M$ ,  $N_{ms}$  is the number of moonpools associated with the  $s$ -th structure,  $N_{pms}$  is the number of the pressure modes

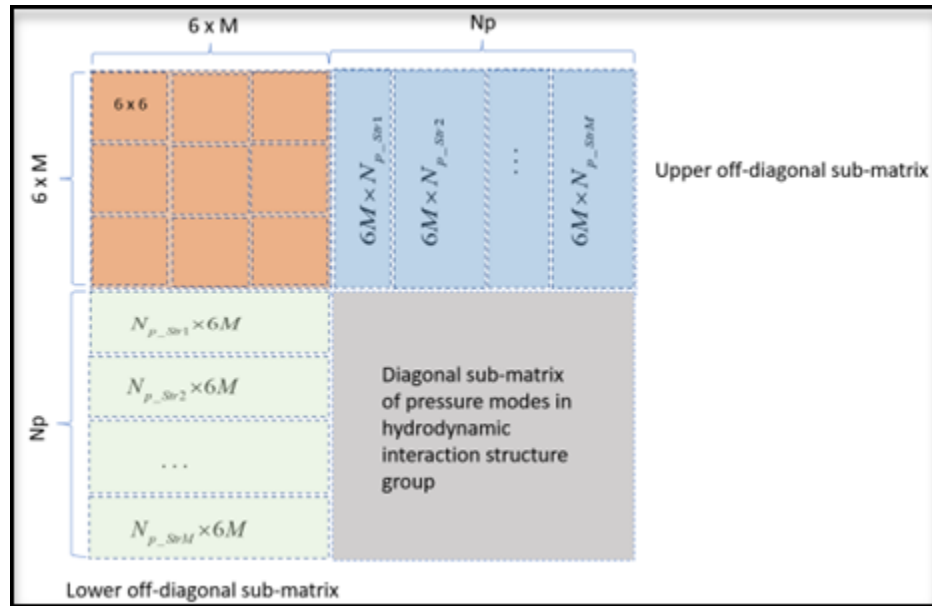
of the  $m$ -th moonpool associated with the  $s$ -th structure,  $N_{ps} = \sum_{m=1}^{N_{ms}} N_{pms}$  is the number of the pressure modes of the moonpools associated with the  $s$ -th structure.

The total unsteady fluid potential around the hydrodynamic interaction structure group is usually expressed as a superposition,

$$\varphi(\vec{X}) e^{-i\omega t} = [(\varphi_i + \varphi_d) + \sum_{s=Str1}^{StrM} \sum_{j=1}^6 x_{js} \varphi_{rjs} + \sum_{s=Str1}^{StrM} \sum_{m=1}^{N_{ms}} \sum_{k=1}^{N_{pms}} \xi_{kms} \varphi_{rkms}] e^{-i\omega t} \quad (4.151)$$

where  $\varphi_i$  is the isolated space dependent incident wave potential and  $\varphi_d$  is the diffraction wave potential,  $x_{js}$  is the RAO of the  $j$ -th rigid body motion of the  $s$ -th structure;  $\varphi_{rjs}$  is the radiation potential due to the unit  $j$ -th rigid motion of the  $s$ -th structure while other structures remain stationary;  $\xi_{kms}$  is the RAO of the  $k$ -th pressure mode of the  $m$ -th moonpool associated with the  $s$ -th structure.  $\varphi_{rkms}$  is the radiation potential due to the unit  $k$ -th pressure mode of the  $m$ -th moonpool associated with the  $s$ -th structure.

Corresponding to the definition of the radiation potential component sequences in [Equation 4.151 \(p. 95\)](#), the coefficients of the added mass and the hydrodynamic damping matrices are arranged in the form shown in [Coefficient Locations in Added Mass and Hydrodynamic Damping Matrices \(p. 96\)](#).

**Figure 4.7: Coefficient Locations in Added Mass and Hydrodynamic Damping Matrices**

# Chapter 5: Second Order Wave Excitation Forces

---

Estimation of the second order hydrodynamic effects is one of major design and analysis concerns for performance and safety in marine structures. Aqwa provides a numerical simulation to investigate these effects by means of both time domain and frequency domain analysis approaches.

In this chapter, a general description of the first and second order motions and forces is provided, and the formula of the far field solution of the second order mean wave drift force and moment coefficients in the horizontal plane under unidirectional waves are presented. Then the general forms of the second order forces (the quadratic transfer function (QTF) matrices) due to a pair of regular waves with different frequencies and directions are deduced based on the near field integration over the mean wetted hull surface. As a special case, the expressions of mean wave drift forces and moments (near field solution) are given for both unidirectional waves and bi-directional waves cases. Some simplified approaches applied in Aqwa, such as the extended Newman's approximation of the difference frequency second order forces and the Pinkster's approximation of the contribution of the second order potential on the second order forces, are also discussed.

By employing the generated QTF matrix database, the equilibrium position prediction, time domain response simulation and frequency domain response statistical analysis of marine structure systems with the second order force effects under irregular waves can be implemented. These topics are discussed in [Equilibrium Estimation and Stability Analysis of Structure System \(p. 171\)](#), [Frequency Domain Dynamic Simulation \(p. 179\)](#), and [Time Domain Dynamic Simulation \(p. 187\)](#).

## 5.1. Second Order Motion and Force

---

The concept of the second order wave exciting forces is based on the assumption of hydrodynamic responses of floating or fixed structure surrounding by an inviscid, irrotational, homogeneous, and incompressible fluid. In addition, both the fluid wave amplitude and the amplitude of the corresponding structural motion responses are small (see [37]).

Under these assumptions, the surrounding fluid can be expressed by the velocity potential function, and the perturbation approach is employed to express the fluid potential, wave elevation, and the position of a point on structure:

$$\begin{aligned}\Phi &= \varepsilon\Phi^{(1)} + \varepsilon^2\Phi^{(2)} + O(\varepsilon^3) \\ \zeta &= \zeta^{(0)} + \varepsilon\zeta^{(1)} + \varepsilon^2\zeta^{(2)} + O(\varepsilon^3) \quad \text{where } \varepsilon \rightarrow 0 \\ \vec{X} &= \vec{X}^{(0)} + \varepsilon\vec{X}^{(1)} + \varepsilon^2\vec{X}^{(2)} + O(\varepsilon^3)\end{aligned}\tag{5.1}$$

where the superscript (0) denotes the static values, and superscripts (1) and (2) indicate the first and the second order variations with respect to the perturbation parameter  $\varepsilon$ .

In [Equation 5.1 \(p. 97\)](#), the position of a point on a rigid floating structure is defined in a fixed reference axes OXYZ introduced in [Fixed Reference Axes \(p. 12\)](#). In that section the local structure axes Gxyz are also introduced, which are fixed on the structure at the center of gravity. At the initial equilibrium pos-

ition in the still water, the three axis directions of  $G_{xyz}$  are parallel to the axes of the fixed global system OXYZ. Employing these definitions, and from [Equation 1.8 \(p. 16\)](#) and [Equation 1.9 \(p. 16\)](#), the position on a structure point can be written as

$$\begin{aligned}\vec{X}^{(0)} &= \vec{X}_g^{(0)} + \vec{x} \\ \vec{X}^{(1)} &= \vec{X}_g^{(1)} + \vec{\alpha}^{(1)} \times \vec{x}\end{aligned}\quad (5.2)$$

where  $\vec{X}_g^{(0)}$  is the static position of the center of gravity in the fixed reference axes (FRA),  $\vec{x}$  is the position of the point in the local structure axes,  $\vec{X}_g^{(1)}$  is the first order translational motion of the center of gravity in the FRA, and  $\vec{\alpha}^{(1)}$  is the first order rotational motion of the center of gravity in the FRA. Only first order terms are discussed here. The second order terms in [Equation 5.1 \(p. 97\)](#) have the similar forms as those in [Equation 5.2 \(p. 98\)](#).

If the normal vector of the structure surface at the point  $\vec{x}$  is denoted as  $\vec{n}$  when a structure is at its equilibrium position in still water, then the first order velocity, acceleration responses at that point, and the first order component of the normal vector, are written as

$$\begin{aligned}\dot{\vec{X}}^{(1)} &= \dot{\vec{X}}_g^{(1)} + \dot{\vec{\alpha}}^{(1)} \times \vec{x} \\ \ddot{\vec{X}}^{(1)} &= \ddot{\vec{X}}_g^{(1)} + \ddot{\vec{\alpha}}^{(1)} \times \vec{x} \\ \vec{N}^{(1)} &= \vec{\alpha}^{(1)} \times \vec{n}\end{aligned}\quad (5.3)$$

where  $\vec{N}^{(1)}$  is the first order variation of the normal vector  $\vec{N}$  of a body surface location in the FRA,  $\vec{N} = \vec{N}^{(0)} + \varepsilon \vec{N}^{(1)} + \dots$  of which  $\vec{N}^{(0)} = \vec{n}$ .

The fluid pressure at a given point is determined by Bernoulli's equation and can be represented as a Taylor series,

$$\begin{aligned}p &= -\rho \frac{\partial \Phi}{\partial t} - \frac{1}{2} \rho \nabla \Phi \cdot \nabla \Phi - \rho g Z \\ &= p^{(0)} + p^{(1)} + p^{(2)} + O(\varepsilon^3)\end{aligned}\quad (5.4)$$

where

$$\begin{aligned}p^{(0)} &= -\rho g X_3^{(0)} \\ p^{(1)} &= -\rho g X_3^{(1)} - \rho \frac{\partial \Phi^{(1)}}{\partial t} \\ p^{(2)} &= -\frac{1}{2} \rho |\nabla \Phi^{(1)}|^2 - \rho \vec{X}^{(1)} \cdot \nabla \frac{\partial \Phi^{(1)}}{\partial t} - \rho \frac{\partial \Phi^{(2)}}{\partial t} - \rho g X_3^{(2)}\end{aligned}$$

In the fixed reference axes, the total fluid force and moment with respect to the center of gravity of the body have the general forms of

$$\begin{aligned}\vec{F}(t) &= - \iint_{S(t)} p \vec{N} dS \\ \vec{M}(t) &= - \iint_{S(t)} p [(\vec{X} - \vec{X}_g) \times \vec{N}] dS\end{aligned}\quad (5.5)$$

where  $S(t)$  is the instantaneous wetted surface of the body.

After the perturbation analysis of the above integrations over the wetted surface  $S(t)$ , the second order wave exciting force and moment can be written as (see [37])

$$\begin{aligned}
 \vec{F}^{(2)} &= -\frac{1}{2}\rho g \oint_{WL} \zeta_r^{(1)} \cdot \vec{\zeta}_r^{(1)} \vec{n} dl \quad \text{Water line integral} \\
 &+ \frac{1}{2}\rho \iint_{S_0} [\nabla \Phi^{(1)} \cdot \nabla \Phi^{(1)}] \vec{n} dS \quad \text{Bernoulli} \\
 &+ \rho \iint_{S_0} \left[ \vec{X}^{(1)} \cdot \nabla \frac{\partial \Phi^{(1)}}{\partial t} \right] \vec{n} dS \quad \text{Acceleration} \tag{a} \\
 &+ \vec{\alpha}^{(1)} \times \vec{F}^{(1)} \quad \text{Momentum} \\
 &+ \rho \iint_{S_0} \frac{\partial \Phi^{(2)}}{\partial t} \vec{n} dS \quad \text{2nd order potential} \\
 \vec{M}^{(2)} &= -\frac{1}{2}\rho g \oint_{WL} \zeta_r^{(1)} \cdot \vec{\zeta}_r^{(1)} (\vec{x} \times \vec{n}) dl \quad \text{Water line integral} \\
 &+ \frac{1}{2}\rho \iint_{S_0} [\nabla \Phi^{(1)} \cdot \nabla \Phi^{(1)}] (\vec{x} \times \vec{n}) dS \quad \text{Bernoulli} \\
 &+ \rho \iint_{S_0} \left[ \vec{X}^{(1)} \cdot \nabla \frac{\partial \Phi^{(1)}}{\partial t} \right] (\vec{x} \times \vec{n}) dS \quad \text{Acceleration} \tag{b} \\
 &+ \vec{\alpha}^{(1)} \times \vec{M}^{(1)} \quad \text{Momentum} \\
 &+ \rho \iint_{S_0} \frac{\partial \Phi^{(2)}}{\partial t} (\vec{x} \times \vec{n}) dS \quad \text{2nd order potential}
 \end{aligned} \tag{5.6}$$

where  $\zeta_r^{(1)} = \zeta^{(1)} - X_3^{(1)}_{WL}$  is the relative wave elevation along the mean undisturbed water line,  $S_0$  is the mean wetted surface, and  $\vec{F}^{(1)}$  and  $\vec{M}^{(1)}$  are the total first order fluid force and moment including the gravity variation relative to the body fixed axes, hydrostatic restoring, wave exciting, hydrodynamic radiation force and moment.

## 5.2. Unidirectional Mean Wave Drift Forces (Far Field Solution)

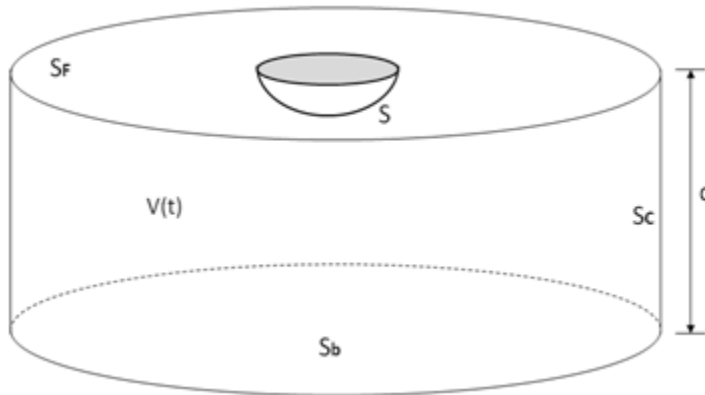
The mean wave drift forces on a floating body in the horizontal plane can be calculated by considering the rate of change of linear and angular momentum within a prescribed fluid domain. This is known as the far field solution. For more information, see [29].

As shown in [Figure 5.1: Floating Body and Vertical Control Surface at Infinity \(p. 100\)](#), denoting  $V(t)$  as the fluid volume which is enclosed by the floating body wetted surface  $S$ , seabed  $S_b$ , a vertical cylindrical surface  $S_C$  at infinity with the local z-axis of the floating body as its vertical axis, free surface  $S_F$ , and water depth  $d$ , the linear and angular momentums of the fluid in this volume are

$$\begin{aligned}
 \bar{G} &= \rho \iiint_{V(t)} \nabla \Phi dV \\
 \bar{H} &= \rho \iiint_{V(t)} (\vec{X} - \vec{X}_g) \times \nabla \Phi dV \tag{5.7}
 \end{aligned}$$

where  $\bar{G}$ ,  $\bar{H}$  are the linear and angular momentums,  $\rho$  is the fluid density,  $\Phi$  is the fluid potential,  $\vec{X}$  is the coordinates of a fluid domain point, and  $\vec{X}_g$  is the center of gravity of the floating body in the FRA.

**Figure 5.1: Floating Body and Vertical Control Surface at Infinity**



The rate of the change of linear momentum is written as

$$\begin{aligned}\frac{d\bar{G}}{dt} &= \rho \frac{d}{dt} \iiint_{V(t)} \nabla \Phi \, dV = \rho \iiint_{V(t)} \nabla \left( \frac{\partial \Phi}{\partial t} \right) \, dV + \rho \iint_{S_t} \nabla \Phi \cdot u_n \, dS \\ &= \rho \iint_{S_t} \left[ \frac{\partial \Phi}{\partial t} \vec{n} + \nabla \Phi \cdot u_n \right] \, dS\end{aligned}\quad (5.8)$$

where  $S_t = S + S_p + S_c + S_b$ ,  $u_n$  is the normal velocity of the boundary surface, and  $\vec{n}$  is the normal vector on the boundary surface pointing positively outwards from the fluid volume. A similar formula can be derived for the rate of the change of angular momentum.

When the second order mean forces in the horizontal plane are concerned, the second order potential has no contribution on them, so that the fluid potential thereafter only includes the first order components in this section. By taking the time average over a period of the incident wave and using the Stokes's equation, the horizontal mean drift forces and moment are expressed as

$$\begin{aligned}\bar{F}_1 &= -\frac{\rho}{2g} \int_I \left( \frac{\partial \Phi}{\partial t} \right)^2 n_1 dl - \rho \iint_{S_c} \left[ \frac{\partial \Phi}{\partial x} \frac{\partial \Phi}{\partial n} - \frac{1}{2} \nabla \Phi \cdot \nabla \Phi n_1 \right] \, dS \\ \bar{F}_2 &= -\frac{\rho}{2g} \int_I \left( \frac{\partial \Phi}{\partial t} \right)^2 n_2 dl - \rho \iint_{S_c} \left[ \frac{\partial \Phi}{\partial y} \frac{\partial \Phi}{\partial n} - \frac{1}{2} \nabla \Phi \cdot \nabla \Phi n_2 \right] \, dS \\ \bar{M}_6 &= -\frac{\rho}{2g} \int_I \left( \frac{\partial \Phi}{\partial t} \right)^2 n_6 dl - \rho \iint_{S_c} \left\{ \left[ (X - X_g) \frac{\partial \Phi}{\partial y} - (Y - Y_g) \frac{\partial \Phi}{\partial x} \right] \frac{\partial \Phi}{\partial n} - \frac{1}{2} \nabla \Phi \cdot \nabla \Phi n_6 \right\} \, dS \\ n_6 &= (X - X_g) n_2 - (Y - Y_g) n_1\end{aligned}\quad (5.9)$$

where  $I$  is the intersection between the control surface  $S_c$  and the mean free surface.

Let  $\vec{X} = (X, Y, Z)$  be the point on the cylindrical surface  $S_c$  at infinity and  $\vec{\xi} = (\xi, \eta, \zeta)$  be the point on the body surface  $S$ , their horizontal coordinates in a polar coordinate system of which the origin is at the center of gravity of the floating body are represented as

$$\begin{aligned}X &= r \cos \theta + X_g, \quad Y = r \sin \theta + Y_g \\ \xi &= r_q \cos \theta_q + X_g, \quad \eta = r_q \sin \theta_q + Y_g\end{aligned}\quad (5.10)$$

Using the same definition of incident regular wave as expressed in [Equation 2.2 \(p. 20\)](#) and [Equation 2.3 \(p. 20\)](#), and based on the source distribution method discussed in [Extended Hydrodynamic Coefficient Matrices \(p. 67\)](#), the total source strength at a source point on the mean wetted body surface due to the diffraction wave and radiation wave potentials is expressed as

$$\sigma_t(\vec{\xi}) = a_w [\sigma_d(\vec{\xi}) + \sum_{j=1}^6 \sigma_j(\vec{\xi}) x_j] \quad (5.11)$$

where  $\sigma_d(\vec{\xi})$  is the source strength due to diffraction wave potential,  $\sigma_j(\vec{\xi})$  is the radiation wave potential source strength due to the  $j$ -th motion,  $x_j$  is the  $j$ -th motion RAO with unit incident wave amplitude.

By using the asymptotic expression of the frequency domain pulsating Green's function when the field point is on the cylindrical surface  $S_C$  at infinity, the formula of the second order mean drift forces and moment for the horizontal motions due to an incident wave ( $a_w, \omega, k, \chi$ ) are written as

$$\begin{aligned} \bar{F}_1 &= -\frac{\rho g a_w}{v} \operatorname{Re}[A_B^*(\chi)] \cos \chi - \frac{\rho g}{2\pi v} \cdot \frac{(1+e^{-2kd})^2}{1-e^{-4kd}+4kde^{-2kd}} \int_0^{2\pi} |A_B(\theta)|^2 \cos \theta d\theta \\ \bar{F}_2 &= -\frac{\rho g a_w}{v} \operatorname{Re}[A_B^*(\chi)] \sin \chi - \frac{\rho g}{2\pi v} \cdot \frac{(1+e^{-2kd})^2}{1-e^{-4kd}+4kde^{-2kd}} \int_0^{2\pi} |A_B(\theta)|^2 \sin \theta d\theta \\ \bar{M}_6 &= -\frac{2apgka_w}{\sqrt{[\tan(kd)+kd-vdtanh(kd)]}} \operatorname{Re}(A_C) \\ &\quad - \frac{apgk}{\pi v} \cdot \frac{1}{[\tanh(kd)+kd-vdtanh(kd)]^2} \operatorname{Re} \left[ \int_0^{2\pi} A_C(\theta) A_B^*(\theta) d\theta \right] \end{aligned} \quad (5.12)$$

where the superscript \* denotes a conjugate of complex variable and

$$\begin{aligned} A_B(\theta) &= -\frac{2\pi}{g} \omega(k+v) \iint_{S_0} \sigma_t(\vec{\xi}) e^{-kd} \cosh[k(\zeta+d)] e^{-ikr_q \cos(\theta-\theta_q)} dS \\ A_C(\theta) &= -\frac{2\pi}{g} \omega(k+v) \iint_{S_0} \sigma_t(\vec{\xi}) e^{-kd} \cosh[k(\zeta+d)] r_q \sin(\theta-\theta_q) e^{-ikr_q \cos(\theta-\theta_q)} dS \\ a &= \frac{\sinh(2kd)+2kd}{2k[\cosh(2kd)+1]} \end{aligned}$$

The far field solution approach discussed above has the following limitations:

- It is only valid for a single floating body: the hydrodynamic interaction effects between different floating structures cannot be involved
- It can only estimate the second order mean drift force and moment in the horizontal plane
- It is only valid for unidirectional waves

### 5.3. General QTF Coefficient Matrix in Multiple Directional Waves

This section is only concerned with the second order force and moment due to the first order wave potential and the first order motion responses. The second order fluid potential components shown in

Equation 5.6 (p. 99) will be discussed separately in [Second Order Wave Potential and Its Simplification \(p. 106\)](#).

Extending the unidirectional incident wave definition to a more general multiple directional wave case, the fluid wave potential of an incident wave in the  $m$ -th wave direction is expressed in the complex form. For example, the first order incident regular wave elevation at a point on the mean water surface  $\vec{X}^{(0)} = (X, Y, 0)$  is represented as

$$\zeta_{jm}(\vec{X}^{(0)}, t) = a_{jm} e^{i(-\omega_{jm}t + k_{jm}X \cos \chi_m + k_{jm}Y \sin \chi_m + \alpha_{jm})} \quad (5.13)$$

where  $a_{jm}$  is the wave amplitude,  $\omega_{jm}$  is the frequency,  $k_{jm}$  is the wave number,  $\chi_m$  is the direction, and  $\alpha_{jm}$  is the phase.

All the variables in the second order force and moment expressions in [Equation 5.6 \(p. 99\)](#) are real numbers. The complex forms of the first order relative wave elevation, potential, displacement and acceleration of the body corresponding to the unit wave amplitude are:

$$\begin{aligned} \operatorname{Re}\left\{\zeta'_{rjm} e^{i(-\omega_{jm}t + \alpha_{jm})}\right\} &= \zeta_{rjm}^{(1)} \\ \operatorname{Re}\left\{\Phi'_{jm} e^{i(-\omega_{jm}t + \alpha_{jm})}\right\} &= \Phi_{jm}^{(1)} \\ \operatorname{Re}\left\{\vec{X}'_{jm} e^{i(-\omega_{jm}t + \alpha_{jm})}\right\} &= \vec{X}_{jm}^{(1)} \\ \operatorname{Re}\left\{\vec{\alpha}'_{jm} e^{i(-\omega_{jm}t + \alpha_{jm})}\right\} &= \vec{\alpha}_{jm}^{(1)} \\ \operatorname{Re}\left\{\vec{F}'_{jm} e^{i(-\omega_{jm}t + \alpha_{jm})}\right\} &= \vec{F}_{jm}^{(1)} \\ \operatorname{Re}\left\{\vec{M}'_{jm} e^{i(-\omega_{jm}t + \alpha_{jm})}\right\} &= \vec{M}_{jm}^{(1)} \end{aligned} \quad (5.14)$$

The second order wave exciting force/moment due to the first order waves and motion responses resulting from a pair of the regular incident waves with  $(a_{jm}, \omega_{jm}, \chi_m, \alpha_{jm})$  and  $(a_{kn}, \omega_{kn}, \chi_n, \alpha_{kn})$  can be written as

$$\begin{aligned} \vec{F}_{jkmn}^{(2)} = a_{jm} a_{kn} &\left\{ \vec{P}_{jkmn}^+ \cos[(\omega_{jm} + \omega_{kn})t - (\alpha_{jm} + \alpha_{kn})] \right. \\ &+ \vec{Q}_{jkmn}^+ \sin[(\omega_{jm} + \omega_{kn})t - (\alpha_{jm} + \alpha_{kn})] \\ &+ \vec{P}_{jkmn}^- \cos[(\omega_{jm} - \omega_{kn})t - (\alpha_{jm} - \alpha_{kn})] \\ &\left. + \vec{Q}_{jkmn}^- \sin[(\omega_{jm} - \omega_{kn})t - (\alpha_{jm} - \alpha_{kn})] \right\} \end{aligned} \quad (5.15)$$

where the coefficients for the second order wave force are:

$$\begin{aligned}
\left( \vec{P}_{jkmn}^+, \vec{Q}_{jkmn}^+ \right) &= -\frac{1}{4} \rho g \oint_{WL} \zeta'_{rjm} \cdot \zeta'_{rkn} \vec{n} dl + \frac{1}{4} \rho \iint_{S_0} [\nabla \Phi'_{jm} \cdot \nabla \Phi'_{kn}] \vec{n} dS \\
&+ \frac{1}{2} \rho \iint_{S_0} \left[ X'_{jm} \cdot \nabla \frac{\partial \Phi'_{kn}}{\partial t} \right] \vec{n} dS + \frac{1}{2} \vec{\alpha}'_{jm} \times \vec{F}'_{jm} \\
\left( \vec{P}_{jkmn}^-, \vec{Q}_{jkmn}^- \right) &= -\frac{1}{4} \rho g \oint_{WL} \zeta'_{rjm} \cdot \zeta'^*_{rkn} \vec{n} dl + \frac{1}{4} \rho \iint_{S_0} [\nabla \Phi'_{jm} \cdot \nabla \Phi'^*_{kn}] \vec{n} dS \\
&+ \frac{1}{2} \rho \iint_{S_0} \left[ X'_{jm} \cdot \nabla \frac{\partial \Phi'^*_{kn}}{\partial t} \right] \vec{n} dS + \frac{1}{2} \vec{\alpha}'_{jm} \times \vec{F}'^*_{jm}
\end{aligned} \tag{5.16}$$

and the coefficients for the second order wave moment are:

$$\begin{aligned}
\left( \vec{P}_{jkmn}^+, \vec{Q}_{jkmn}^+ \right) &= -\frac{1}{4} \rho g \oint_{WL} \zeta'_{rjm} \cdot \zeta'_{rkn} (\vec{x} \times \vec{n}) dl + \frac{1}{4} \rho \iint_{S_0} [\nabla \Phi'_{jm} \cdot \nabla \Phi'_{kn}] (\vec{x} \times \vec{n}) dS \\
&+ \frac{1}{2} \rho \iint_{S_0} \left[ \vec{X}'_{jm} \cdot \nabla \frac{\partial \Phi'_{kn}}{\partial t} \right] (\vec{x} \times \vec{n}) dS + \frac{1}{2} \vec{\alpha}'_{jm} \times \vec{M}'_{jm} \\
\left( \vec{P}_{jkmn}^-, \vec{Q}_{jkmn}^- \right) &= -\frac{1}{4} \rho g \oint_{WL} \zeta'_{rjm} \cdot \zeta'^*_{rkn} (\vec{x} \times \vec{n}) dl + \frac{1}{4} \rho \iint_{S_0} [\nabla \Phi'_{jm} \cdot \nabla \Phi'^*_{kn}] (\vec{x} \times \vec{n}) dS \\
&+ \frac{1}{2} \iint_{S_0} \left[ X'_{jm} \cdot \nabla \frac{\partial \Phi'^*_{kn}}{\partial t} \right] (\vec{x} \times \vec{n}) dS + \frac{1}{2} \vec{\alpha}'_{jm} \times \vec{M}'^*_{jm}
\end{aligned} \tag{5.17}$$

From [Equation 5.15 \(p. 102\)](#),  $\vec{Q}_{jkmn}^+$ ,  $\vec{P}_{jkmn}^+$  are used as the sum frequency force components, while  $\vec{Q}_{jkmn}^-$ ,  $\vec{P}_{jkmn}^-$  contribute only in the difference frequency force components. In cases with multiple directional irregular waves, the total second order wave exciting force (not including the component due to the second order potential) has a quadruple summation form,

$$\begin{aligned}
\vec{F}^{(2)}(t) &= \sum_{m=1}^{N_d} \sum_{n=1}^{N_d} \sum_{j=1}^{N_m} \sum_{k=1}^{N_n} \vec{F}_{jkmn}^{(2)} \\
&= \sum_{m=1}^{N_d} \sum_{n=1}^{N_d} \sum_{j=1}^{N_m} \sum_{k=1}^{N_n} a_{jm} a_{kn} \left\{ \vec{P}_{jkmn}^+ \cos[(\omega_{jm} + \omega_{kn}) t - (\alpha_{jm} + \alpha_{kn})] \right. \\
&\quad + \vec{Q}_{jkmn}^+ \sin[(\omega_{jm} + \omega_{kn}) t - (\alpha_{jm} + \alpha_{kn})] \\
&\quad + \vec{P}_{jkmn}^- \cos[(\omega_{jm} - \omega_{kn}) t - (\alpha_{jm} - \alpha_{kn})] \\
&\quad \left. + \vec{Q}_{jkmn}^- \sin[(\omega_{jm} - \omega_{kn}) t - (\alpha_{jm} - \alpha_{kn})] \right\}
\end{aligned} \tag{5.18}$$

where  $N_d$  is the number of wave directions, and  $N_m$  and  $N_n$  are the numbers of wave components in the  $m$ -th and the  $n$ -th wave directions respectively.

Further introducing a new set of matrices for a generalized multi-directional wave set, in which the so-called composite elements are defined:

$$\begin{aligned}
\vec{P}_{jkmn}^{+} &= \frac{1}{2} (\vec{P}_{jkmn}^{+} + \vec{P}_{kjm}^{+}) = \vec{P}_{kjm}^{+} \\
\vec{Q}_{jkmn}^{+} &= \frac{1}{2} (\vec{Q}_{jkmn}^{+} + \vec{Q}_{kjm}^{+}) = \vec{Q}_{kjm}^{+} \\
\vec{P}_{jkmn}^{-} &= \frac{1}{2} (\vec{P}_{jkmn}^{-} + \vec{P}_{kjm}^{-}) = \vec{P}_{kjm}^{-} \\
\vec{Q}_{jkmn}^{-} &= \frac{1}{2} (\vec{Q}_{jkmn}^{-} - \vec{Q}_{kjm}^{-}) = -\vec{Q}_{kjm}^{-}
\end{aligned} \tag{5.19}$$

in which the composite elements  $\vec{P}_{jkmn}^{+}$ ,  $\vec{Q}_{jkmn}^{+}$ ,  $\vec{P}_{jkmn}^{-}$  are symmetric against a pair of the waves with  $(a_{jm}, \omega_{jm}, \chi_m, \alpha_{jm})$  and  $(a_{kn}, \omega_{kn}, \chi_n, \alpha_{kn})$  and  $\vec{Q}_{jkmn}^{-}$  is skew-symmetric against this pair of waves.

Employing above definitions, [Equation 5.18 \(p. 103\)](#) can be rewritten as

$$\begin{aligned}
\vec{F}^{(2)}(t) = & \sum_{m=1}^{N_d} \sum_{n=1}^{N_d} \sum_{j=1}^{N_m} \sum_{k=1}^{N_n} a_{jm} a_{kn} \left\{ \vec{P}_{jkmn}^{+} \cos[(\omega_{jm} + \omega_{kn}) t - (\alpha_{jm} + \alpha_{kn})] \right. \\
& + \vec{Q}_{jkmn}^{+} \sin[(\omega_{jm} + \omega_{kn}) t - (\alpha_{jm} + \alpha_{kn})] \\
& + \vec{P}_{jkmn}^{-} \cos[(\omega_{jm} - \omega_{kn}) t - (\alpha_{jm} - \alpha_{kn})] \\
& \left. + \vec{Q}_{jkmn}^{-} \sin[(\omega_{jm} - \omega_{kn}) t - (\alpha_{jm} - \alpha_{kn})] \right\}
\end{aligned} \tag{5.20}$$

## 5.4. Mean Wave Drift Forces (Near Field Solution)

As discussed in [Unidirectional Mean Wave Drift Forces \(Far Field Solution\) \(p. 99\)](#), the far field solution approach has several limitations. However based on the mean wetted body surface integration approach, more general forms of the mean wave drift force and moment on a floating body in all motion directions can be given as a special case in [Equation 5.15 \(p. 102\)](#) through [Equation 5.20 \(p. 104\)](#) of which  $\omega_{jm}$  where  $j=k$  and the sum frequency force components are excluded.

In this case, the composite directional coupling mean drift force coefficient QTF matrices can be presented as

$$\begin{aligned}
\mathbf{P}_{jj}^{-} &= [P_{jjmn}^{-}] \\
\mathbf{Q}_{jj}^{-} &= [Q_{jjmn}^{-}] \text{ where } m=1, N_d \text{ and } n=1, N_d
\end{aligned} \tag{5.21}$$

of which  $\mathbf{P}_{jj}^{-}$  are symmetric matrices, while  $\mathbf{Q}_{jj}^{-}$  is a skew-symmetric matrix.

From [Equation 5.20 \(p. 104\)](#), the mean drift force and moment are expressed as the triple summation:

$$\begin{aligned}
\vec{F}^{(2)} &= \sum_{m=1}^{N_d} \sum_{n=1}^{N_d} \sum_{j=1}^{N_w} a_{jm} a_{jn} \left\{ \vec{P}_{jjmn}^{-} \cos(\alpha_{jm} - \alpha_{kn}) - \vec{Q}_{jjmn}^{-} \sin(\alpha_{jm} - \alpha_{kn}) \right\} \\
&= \sum_{m=1}^{N_d} \sum_{n=1}^{N_d} \sum_{j=1}^{N_w} \vec{f}^{(2)}(\omega_j; \beta_m, \beta_n)
\end{aligned} \tag{5.22}$$

where the numbers of wave components of every individual wave directions are the same ( $N_m=N_n=N_w$ ).

For a long crested wave case ( $N_d=1$ ), the mean drift force can be further simplified as

$$\overline{\vec{F}^{(2)}} = \sum_{j=1}^{N_w} a_j^2 \vec{P}_{jj11} \quad (5.23)$$

in which the out of phase item  $\vec{Q}_{jjmn}$  where  $m=n=1$  in [Equation 5.22 \(p. 104\)](#) is no longer included.

The above expressions are known as the near field solution, and valid for both a single and multiple floating structure system with or without hydrodynamic interaction effects.

## 5.5. Extended Newman's Approximation

In a time domain analysis, the wave directional angles  $\chi_m$  and  $\chi_n$  in [Equation 5.20 \(p. 104\)](#) should be treated as the relative directions between the wave propagating direction and the vessel orientation at each time step. Therefore the frequency domain database of  $\vec{P}_{jkmm}^\pm$ ,  $\vec{Q}_{jkmm}^\pm$  covering all the possible relative directions should be created prior to any time domain analysis. The values of  $\vec{P}_{jkmm}^\pm$ ,  $\vec{Q}_{jkmm}^\pm$  at any actual vessel position at a time step could be then estimated by the means of database interpolation. However even with this database interpolation treatment, the quadruple summation form given in [Equation 5.20 \(p. 104\)](#) is still prohibitively difficult to apply for the numerical time domain simulation procedure due to the large processing and memory requirements.

For the unidirectional wave case, Newman's approximation [28] is frequently used in practice. This takes the off-diagonal difference frequency QTF value to be an average of the corresponding diagonal values:

$$\vec{P}_{jkmm}'' = \frac{1}{2} [\vec{P}_{jjmm}^\pm + \vec{P}_{kkmm}^\pm] \text{ where } m=1 \quad (5.24)$$

The out of phase item  $\vec{Q}_{jkmm}''$  is excluded in this approximation for the difference frequency second order force calculation as  $\vec{Q}_{jjmm}^\pm = \vec{Q}_{kkmm}^\pm = 0$ .

Newman's approximation is normally accepted for the hydrodynamic analysis of moored offshore structures in moderate and deep water depth in long crested waves.

In Aqwa, Newman's approximation is extended to the multiple directional wave case for the difference frequency QTF element evaluation:

$$\begin{aligned} \vec{P}_{jkmm}'' &= \frac{1}{2} [\vec{P}_{jjmn}^\pm + \vec{P}_{kknm}^\pm] \\ \vec{Q}_{jkmm}'' &= \frac{1}{2} [\vec{Q}_{jjmn}^\pm - \vec{Q}_{kknm}^\pm] \end{aligned} \quad (5.25)$$

In the above equation, the out of phase item  $\vec{Q}_{jkmm}''$  is also defined, because  $\vec{Q}_{jjmn}^\pm, \vec{Q}_{kknm}^\pm$  where  $(m \neq n)$  are not necessarily zero. However it is easily observed that this extended approximation will be exactly the same as the original one shown in [Equation 5.24 \(p. 105\)](#) when long crested waves are concerned ( $m=n=1$ ). With the simplified expressions of the difference frequency QTF elements in [Equation 5.25 \(p. 105\)](#), the symmetric properties shown in [Equation 5.19 \(p. 104\)](#) still remain true with respect to a pair of waves with difference frequencies and wave directions:

$$\begin{aligned}\vec{P}_{jkmn}^{''} &= \vec{P}_{kjnm}^{''} \\ \vec{Q}_{jkmn}^{''} &= -\vec{Q}_{kjnm}^{''}\end{aligned}\quad (5.26)$$

Denoting  $c_{jm}=a_{jm}\sin(\omega_{jm}t-a_{jm})$  and  $s_{jm}=a_{jm}\cos(\omega_{jm}t-a_{jm})$  and substituting [Equation 5.25 \(p. 105\)](#) into [Equation 5.20 \(p. 104\)](#) for the difference frequency second order force and moment only, we have

$$\begin{aligned}\vec{F}^{(2)}(t) &= \frac{1}{2} \sum_{m=1}^{N_d} \sum_{n=1}^{N_d} \sum_{j=1}^{N_m} \sum_{k=1}^{N_n} \left\{ (c_{jm}c_{kn}+s_{jm}s_{kn})(\vec{P}_{jjmn}^{'}+\vec{P}_{kknm}^{'}) \right. \\ &\quad \left. +(s_{jm}c_{kn}-c_{jm}s_{kn})(\vec{Q}_{jjmn}^{'}+\vec{Q}_{kknm}^{'}) \right\} \\ &= \sum_{m=1}^{N_d} \left\{ \left( \sum_{j=1}^{N_m} c_{jm} \right) \times \left[ \sum_{n=1}^{N_d} \sum_{k=1}^{N_n} (c_{kn}\vec{P}_{kknm}^{'}-s_{kn}\vec{Q}_{kknm}^{'}) \right] \right\} \\ &\quad + \sum_{m=1}^{N_d} \left\{ \left( \sum_{j=1}^{N_m} s_{jm} \right) \times \left[ \sum_{n=1}^{N_d} \sum_{k=1}^{N_n} (s_{kn}\vec{P}_{kknm}^{'}+c_{kn}\vec{Q}_{kknm}^{'}) \right] \right\}\end{aligned}\quad (5.27)$$

Comparing the equation above to [Equation 5.20 \(p. 104\)](#) it is observed that the summation against the frequencies of the  $m$ -th directional waves has been uncoupled from summations against the frequencies of the  $n$ -th ( $n = 1, N_d$ ) directional waves, which converts the quadruple summations into triple summations and hence greatly increases the numerical calculation efficiency. In addition, instead of using the four dimensional elements of  $\vec{P}_{jkmn}^{'}$ ,  $\vec{Q}_{jkmn}^{'}$  for obtaining the difference frequency drift force, the directional coupling mean QTF matrices of  $\vec{P}_{kknm}^{'}$ ,  $\vec{Q}_{kknm}^{'}$  are required when employing [Equation 5.27 \(p. 106\)](#), which significantly reduces the memory buffer and hard disk requirements.

## 5.6. Second Order Wave Potential and Its Simplification

The second order wave potential does not contribute to the mean wave drift force component given in [Equation 5.6 \(p. 99\)](#). However, it has been reported that in shallow water the difference frequency drift force may be increased significantly by the second order potential contribution. Therefore, the inclusion of the second order potential would be necessary for the accurate evaluation of the second order wave exciting forces in shallow water.

In Aqwa this is done by using Pinkster's approximation for long crested wave case (see [37]). The second order force component induced by the second order potential corresponding to a pair of incident waves of  $(a_j, \omega_j, \chi, \alpha_j)$  and  $(a_k, \omega_k, \chi, \alpha_k)$  is given as

$$\begin{aligned}F_{jk}^{(2)}(t) &= \text{Re} \left\{ F_{jk}^{(2)} e^{-i(\omega_j-\omega_k)t+i(\alpha_j-\alpha_k)} \right\} \\ F_{jk}^{(2)} &= f_{jk} F^{(1)}(k_j-k_k)\end{aligned}\quad (5.28)$$

where  $F^{(1)}(k_j-k_k)$  is the first order wave exciting force induced by a regular wave with the wave number of  $(k_j-k_k)$  and unit wave amplitude, which can be directly calculated by [Equation 4.8 \(p. 61\)](#). The factor  $f_{jk}$  is expressed as

$$f_{jk} = \frac{a_j a_k A_{jk} (\omega_j - \omega_k)}{g} \quad (5.29)$$

where

$$\begin{aligned} A_{jk} &= \frac{1}{2} g^2 \frac{B_{jk} + C_{jk}}{(\omega_j - \omega_k)^2 - (k_j - k_k) g \tanh(k_j - k_k) d} \\ B_{jk} &= \frac{k_j^2}{\omega_j \cosh^2 k_j d} - \frac{k_k^2}{\omega_k \cosh^2 k_k d} \\ C_{jk} &= \frac{2k_j k_k (\omega_j - \omega_k)(1 + \tanh k_j d \tanh k_k d)}{\omega_j \omega_k} \end{aligned}$$

In Aqwa, this simplification is only applied for the long crested wave case when the full QTF matrix is required. When Newman's approximation is employed, this term is ignored.



# Chapter 6: Morison Element Forces

---

The Morison's equation approach is widely used for slender body components when the characteristic diameter of a structural component is less than 1/5<sup>th</sup> of the shortest wavelength. In this equation, the drag load component is induced by viscosity and proportional to the relative velocity between fluid particles and the structure surface, and becomes important when the structural members are slender and wave amplitude is large.

Morison element forces relate to all non-panel elements that can attract wave and current loading. In Aqwa, cylindrical tube (TUBE), slender tube with general cross section form (STUB) and disc (DISC) elements can be defined.

Aqwa employs a hybrid method to model the large-volume components of structure by diffracting panels and the rest of the small cross sectional components by Morison elements. The diffracting panel method is discussed in [Hydrodynamic Radiation and Diffraction Analysis by Source Distribution Method \(p. 59\)](#) and [Second Order Wave Excitation Forces \(p. 97\)](#).

## 6.1. Morison Equation

---

Morison's equation for the fluid forces acting on the cross section of a slender structural member is

$$\begin{aligned} dF &= \frac{1}{2} \rho D C_d |u_f - u_s| (u_f - u_s) + \rho A C_m \dot{u}_f - \rho A (C_m - 1) \dot{u}_s \\ &= \frac{1}{2} \rho D C_d |u_f - u_s| (u_f - u_s) + \rho A (1 + C_a) \dot{u}_f - \rho A C_a \dot{u}_s \end{aligned} \quad (6.1)$$

where  $C_d$  is the drag coefficient,  $D$  is the characteristic drag diameter,  $u_f$  is the transverse directional fluid particle velocity,  $u_s$  is the transverse directional structure velocity,  $C_m = C_a + 1$  is the inertia coefficient, and  $A$  is the cross-sectional area.

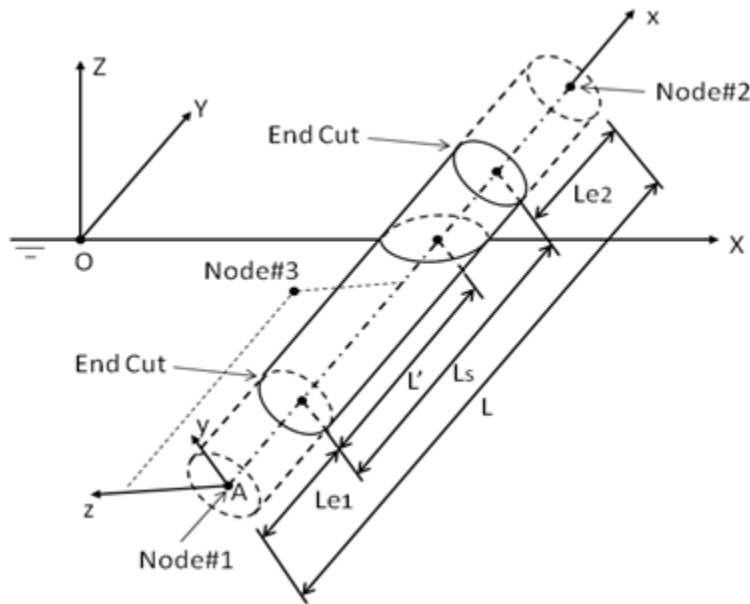
The inertia coefficient and the drag coefficient are estimated empirically and are influenced by several parameters including Reynolds number, Keulegan-Carpenter number and others. The Reynolds number effect on the tube drag coefficient can be considered in Aqwa and is discussed in the next chapter.

In practice, the inertia coefficient and the drag coefficient of a normal sized cylindrical tube could be approximated as 2.0 (or  $C_a = 1.0$ ) and 0.75 respectively. For a single side disc, the default values of inertia coefficient and drag coefficient could be 2.4 (or  $C_a = 1.4$ ) and 1.14 respectively. For a non-cylindrical tube, these coefficients could be dependent on the cross section directions.

As shown in [Figure 6.1: Local Tube Axis System \(p. 110\)](#), a tube local axis frame is used to define these directional dependent variables. In this right handed local axis frame, the origin A is located on the first node of the element, the local x-axis points towards the second node. For a non-cylindrical tube, the third node is away from the local x-axis and located on the local Axz plane. For a cylindrical tube, the local y-axis is in the global horizontal plane at right angle to the local x-axis, the local z-axis is orthogonal to the local x-y plane with z component in positive Z-direction; for a special case when the local x-axis is parallel to the global Z-axis, the local y-axis will be in the same direction as the global Y-axis.

Optionally, end-cuts ( $L_{ej}$  where  $j=1,2$ ) are used to leave gaps between the exposed ends and the nodes of tube element. These end-cut parts will not contribute on the tube structural mass and moment of inertia, and have no effect on the tube hydrostatic and hydrodynamic properties. For a fully submerged case, the submerged length of this tube element will be  $L'=L-L_{e1}-L_{e2}$ . For a partially submerged tube case, the submerged tube length  $L'$  is the distance between the center of the cross-water surface section and the end cut of the submerged node, as shown in [Figure 6.1: Local Tube Axis System \(p. 110\)](#).

**Figure 6.1: Local Tube Axis System**



The hydrodynamic forces and moments are calculated first with reference to the local tube axis system by the integration of the cross sectional force/moment over the submerged length of  $L'$ ,

$$\begin{aligned}
 F_y &= \int_{L_{e1}}^{L'+L_{e1}} \left\{ \frac{1}{2} \rho D_y C_{dy} |\vec{u}_f - \vec{u}_s| (u_{fy} - u_{sy}) + \rho A C_{my} \dot{u}_{fy} - \rho A (C_{my} - 1) \dot{u}_{sy} \right\} dx \\
 F_z &= \int_{L_{e1}}^{L'+L_{e1}} \left\{ \frac{1}{2} \rho D_z C_{dz} |\vec{u}_f - \vec{u}_s| (u_{fz} - u_{sz}) + \rho A C_{mz} \dot{u}_{fz} - \rho A (C_{mz} - 1) \dot{u}_{sz} \right\} dx \\
 M_y &= \int_{L_{e1}}^{L'+L_{e1}} \left\{ \frac{1}{2} \rho D_z C_{dz} |\vec{u}_f - \vec{u}_s| (u_{fz} - u_{sz}) + \rho A C_{mz} \dot{u}_{fz} - \rho A (C_{mz} - 1) \dot{u}_{sz} \right\} x dx \\
 M_z &= - \int_{L_{e1}}^{L'+L_{e1}} \left\{ \frac{1}{2} \rho D_y C_{dy} |\vec{u}_f - \vec{u}_s| (u_{fy} - u_{sy}) + \rho A C_{my} \dot{u}_{fy} - \rho A (C_{my} - 1) \dot{u}_{sy} \right\} x dx
 \end{aligned} \tag{6.2}$$

in which the hydrodynamic moments are with respect to the first node of the tube element, the subscripts  $y$  and  $z$  indicate the coefficients and velocity components in the  $y$ - or  $z$ -direction respectively.

In general a partially submerged tube which is arbitrarily inclined may have a section which is either completely submerged, partially submerged, or completely out of the water. Hence the integration in [Equation 6.2 \(p. 110\)](#) will be only over the submerged part.

In Aqwa, a three-point Gaussian integration scheme is employed to estimate the integral forms given by [Equation 6.2 \(p. 110\)](#). To ensure the accuracy of the numerical calculation of the tube force and moment, it is required that the tube element length be short enough. Following the general principle for the diffracting panel size requirement discussed in [Mesh Quality Check \(p. 65\)](#), the tube element size should preferably be less than 1/7<sup>th</sup> of the shortest wavelength.

The forces and moments on each tube element are then transformed to the fixed reference axes (FRA) and, in addition, the moments are with respect to the center of gravity of the structure. The total fluid load is the summation of forces on all the tube elements and the panel elements.

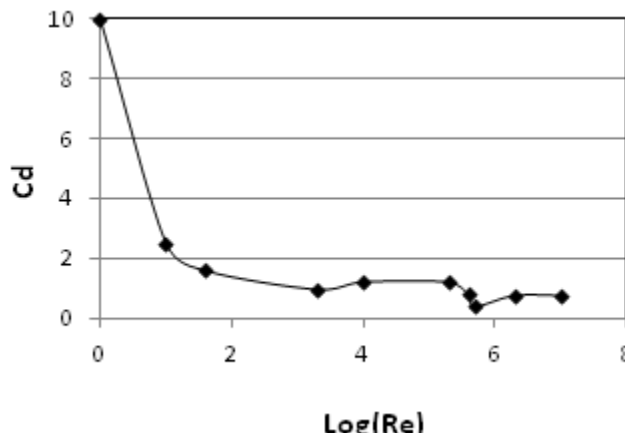
## 6.2. Scale Factor for Model Test Simulation

For a cylindrical tube in steady flow, the drag coefficient may vary with flow velocity, tube diameter, surface roughness. For a smooth cylinder, the drag coefficient can be expressed as a function of Reynolds number  $Re = \frac{UD}{\nu}$ . In this definition,  $\nu = 1.57 \times 10^{-6} (m^2 s^{-1})$  is the kinematic viscosity at sea water at 40 °C and  $U$  is the steady flow velocity. This function is known as the Wieselburger curve, as shown in [Figure 6.2: Drag Coefficients Versus Reynolds Numbers for Circular Cylinder \(p. 111\)](#). Barltrop and Adams [5] described that for small Reynolds numbers, the drag is mainly due to skin friction as a function of magnitude of flow velocity, hence the drag coefficient is relatively large. For larger Reynolds numbers, the drag force is mainly from low pressure in the wake as a function of velocity squared. The corrections with surface roughness and Keulegan-Carpenter number can be found in the literature (for example, [5]), in which Keulegan-Carpenter number is defined as  $K_C = \frac{\pi b}{D}$  where  $b$  is wave particle orbit size.

Aqwa normally assumes that the Reynolds Number is sufficiently large for the drag coefficient to be considered constant. The Morison element drag coefficients defined either directly by the user or automatically by Aqwa will be used.

However if this is not a reasonable assumption, a model test factor can be defined to calculate the local Reynolds number. Even though experimental evidence shows that the Reynolds number is not a simple function of the velocity and diameter for cylinders with arbitrary orientation to the direction of the fluid flow, considerable improvement in agreement with model tests has been obtained by using the scale factor to obtain a local Reynolds number and interpolating from classic experimental results.

**Figure 6.2: Drag Coefficients Versus Reynolds Numbers for Circular Cylinder**



The scale factor number is

$$S_C = \frac{L_0}{L_m} \quad (6.3)$$

where  $L_0$  is the characteristic length of the prototype structure,  $L_m$  is its testing model length.

If Reynolds number of a prototype tube is  $Re = \frac{UD}{\nu}$ , the local Reynolds number for the corresponding experimental model should be

$$Re' = \frac{Re}{(S_C)^{3/2}} = \frac{UD}{\nu} \cdot \frac{1}{(\sqrt{S_C})^3} \quad (6.4)$$

where  $U$  is the velocity transverse to the axis of the prototype tube with diameter of  $D$ .

Using this local Reynolds number and employing the Wieselburger curve given by [Figure 6.2: Drag Coefficients Versus Reynolds Numbers for Circular Cylinder \(p. 111\)](#), the actual drag coefficient for the model test case can be interpolated. In such special case, the drag coefficients for all Morison tube elements on all structures previously defined by user are ignored.

## 6.3. Morison Elements in Frequency Domain Dynamic Response Analysis

Linear Morison forces, which are applicable to small non-diffracting structures or parts of structures, are included in the Aqwa radiation/diffraction analysis and frequency domain statistic analysis. Therefore mixed models (diffracting and non-diffracting elements) may be analyzed. The contribution of the Morison elements on hydrostatic forces, hydrostatic stiffness matrices, and added mass and wave exciting forces, is calculated and written to the hydrodynamic database.

However, Morison drag forces, which are nonlinear, are not directly calculated in the radiation and diffraction analysis and the frequency domain statistic analysis. Linearization of drag forces can be optionally carried out if required.

## 6.4. Morison Drag Linearization

As observed from [Equation 6.1 \(p. 109\)](#), the drag force component in the Morison equation consists of the factor of  $|u_f - u_s| (u_f - u_s)$ . It is a nonlinear term in which  $|u_f - u_s|$  can be replaced by a factor multiplied by the root mean square of relative velocity in order to create an equivalent linear term. In the literature (for example, [6]) this factor is given by  $\alpha = \sqrt{\frac{8}{\pi}}$ . By choosing a proper factor  $\alpha$ , the linearized drag force at a cross section of a tube is expressed as

$$\begin{aligned} dF_{drag} &= \frac{1}{2} \rho DC_d \alpha u_{rms} (u_f - u_s) \\ &= \frac{1}{2} \rho DC_d \alpha u_{rms} u_f - \frac{1}{2} \rho DC_d \alpha u_{rms} u_s \end{aligned} \quad (6.5)$$

where  $u_{rms}$  is the root mean square of transverse directional relative velocity at that location.

The first item in the right hand side of [Equation 6.5 \(p. 112\)](#) is a linear function of fluid particle velocity and could be considered as the external fluid force acting on the structure. The corresponding total force and moment on the whole submerged tube element are

$$\begin{aligned} F_{df} &= \frac{1}{2} \rho D C_d \int_{Le1}^{L+Le1} \alpha u_{rms} u_f dx \\ M_{df} &= \frac{1}{2} \rho D C_d \int_{Le1}^{L+Le1} \alpha u_{rms} u_f x dx \end{aligned} \quad (6.6)$$

The second item in the right hand side of [Equation 6.5 \(p. 112\)](#) linearly relates to the structure velocity, so that its coefficient could be considered as the damping factor due to the linearized drag force.

Denoting the structural velocity vector of a tube in the tube local axis frame as

$$\mathbf{u}_s = [u_1, u_2, u_3, u_4, u_5, u_6]^T \quad (6.7)$$

where  $(u_1, u_2, u_3)$  is the translational velocity at node 1 in the local x-, y-, and z-directions and  $(u_4, u_5, u_6)$  is the rotational velocity of tube about the local x-, y-, and z-axes.

The damping force from the linearized drag in the local y-direction and the moment about the local z-axis at the location of  $(x, 0, 0)$  are

$$\begin{aligned} dF_{dy} &= -\frac{1}{2} \rho D_y C_{dy} \alpha_y u_{rms} u_{sy} = -\frac{1}{2} \rho D_y C_{dy} \alpha_y u_{rms} (u_2 + x u_6) \\ dM_{dz} &= -\frac{1}{2} \rho D_y C_{dy} \alpha_y u_{rms} u_{sy} x = -\frac{1}{2} \rho D_y C_{dy} \alpha_y u_{rms} (u_2 + x u_6) x \end{aligned} \quad (6.8)$$

the total damping force and moment on the whole submerged tube are

$$\begin{aligned} F_{dy} &= -\frac{1}{2} \rho D_y C_{dy} \left( \int_{Le1}^{L+Le1} \alpha_y u_{rms} dx \right) u_2 - \frac{1}{2} \rho D_y C_{dy} \left( \int_{Le1}^{L+Le1} \alpha_y u_{rms} x dx \right) u_6 \\ M_{dz} &= -\frac{1}{2} \rho D_y C_{dy} \left( \int_{Le1}^{L+Le1} \alpha_y u_{rms} x dx \right) u_2 - \frac{1}{2} \rho D_y C_{dy} \left( \int_{Le1}^{L+Le1} \alpha_y u_{rms} x^2 dx \right) u_6 \end{aligned} \quad (6.9)$$

Similarly the total z-direction damping force and moment about local y axis on the whole submerged tube are

$$\begin{aligned} F_{dz} &= -\frac{1}{2} \rho D_z C_{dz} \left( \int_{Le1}^{L+Le1} \alpha_z u_{rms} dx \right) u_3 + \frac{1}{2} \rho D_z C_{dz} \left( \int_{Le1}^{L+Le1} \alpha_z u_{rms} x dx \right) u_5 \\ M_{dy} &= \frac{1}{2} \rho D_z C_{dz} \left( \int_{Le1}^{L+Le1} \alpha_z u_{rms} x dx \right) u_3 - \frac{1}{2} \rho D_z C_{dz} \left( \int_{Le1}^{L+Le1} \alpha_z u_{rms} x^2 dx \right) u_5 \end{aligned} \quad (6.10)$$

Introducing a linearized drag damping coefficient matrix

$$C_{drag} = [C_{dij}] \text{ where } i=1,6 \text{ and } j=1,6 \quad (6.11)$$

and setting

$$\mathbf{F}_{drag}^L = \begin{bmatrix} F_{dx} \\ F_{dy} \\ F_{dz} \\ M_{dx} \\ M_{dy} \\ M_{dz} \end{bmatrix} = -\mathbf{C}_{drag} \mathbf{u}_s \quad (6.12)$$

from [Equation 6.6 \(p. 113\)](#), [Equation 6.9 \(p. 113\)](#), and [Equation 6.10 \(p. 113\)](#) we will have

$$\begin{aligned} C_{d11} &= \frac{1}{2} \rho S_w C_{dx} \alpha_x u_{rmsx} \\ C_{d22} &= \frac{1}{2} \rho D_y C_{dy} \left( \int_{L_{e1}}^{L'+L_{e1}} \alpha_y u_{rms} dx \right) \\ C_{d26} &= C_{d62} = \frac{1}{2} \rho D_y C_{dy} \left( \int_{L_{e1}}^{L'+L_{e1}} \alpha_y u_{rms} x dx \right) \\ C_{d66} &= \frac{1}{2} \rho D_y C_{dy} \left( \int_{L_{e1}}^{L'+L_{e1}} \alpha_y u_{rms} x^2 dx \right) \\ C_{d33} &= \frac{1}{2} \rho D_z C_{dz} \left( \int_{L_{e1}}^{L'+L_{e1}} \alpha_z u_{rms} dx \right) \\ C_{d35} &= C_{d53} = -\frac{1}{2} \rho D_z C_{dz} \left( \int_{L_{e1}}^{L'+L_{e1}} \alpha_z u_{rms} x dx \right) \\ C_{d55} &= -\frac{1}{2} \rho D_z C_{dz} \left( \int_{L_{e1}}^{L'+L_{e1}} \alpha_z u_{rms} x^2 dx \right) \\ C_{dij} &= 0 \text{ (otherwise)} \end{aligned} \quad (6.13)$$

where  $S_w$  is the tube wetted surface,  $C_{dx}$  is the axial drag coefficient,  $\alpha_x$  is the linearized factor in the axial direction, and  $u_{rmsx}$  is the root mean square of axial motion velocity. Aqwa sets  $C_{dx}=0.016$  as an unamendable default value for both circular tube and slender tube elements.

In the above discussion of the tube drag linearization method, the correlation effects between two transverse relative velocity components are not included, hence a one-dimensional linearization formula is employed. This method makes the total dissipating energy due to the linearized drag force approximately equal to the associated free energy dissipated in the exact time domain analysis. However, each dissipating energy component in either the local tube y-direction or z-direction may not be inherently compatible between the exact time domain analysis and the linearized frequency domain analysis.

Because of these limitations, Aqwa uses a two-dimensional method, which includes the correlation between two transverse relative velocities, which ensures equal dissipating energy components in both the local tube y- and z-directions between the time domain and the linearized frequency domain analyses.

In this two-dimensional approach, the linearized drag force at a cross-section position  $x$  in the local tube axes is given by

$$\begin{pmatrix} dF_{dy} \\ dF_{dz} \end{pmatrix} = \begin{bmatrix} \beta_{yy} & \beta_{yz} \\ \beta_{zy} & \beta_{zz} \end{bmatrix} \begin{pmatrix} u_{fy} - u_{sy} \\ u_{fz} - u_{sz} \end{pmatrix} \quad (6.14)$$

where the damping factors  $\beta_{yy}$ ,  $\beta_{zy}$ ,  $\beta_{yz}$ , and  $\beta_{zz}$  are the functions of the root of the mean square of structural motion at the position  $x$ , the tube cross-sectional geometric properties, and the drag coefficients of the tube in both local tube  $y$ - and  $z$ -directions.  $u_{fy}$  and  $u_{fz}$  are the fluid particle velocity components in the tube local  $y$ - and  $z$ -directions, and  $u_{sy}$  and  $u_{sz}$  are the structural velocity components in the local tube  $y$ - and  $z$ -directions.

From [Equation 6.14 \(p. 115\)](#), the linearized drag force/moment due to fluid particle velocity can be written as

$$\begin{aligned} \begin{pmatrix} F_{dfy} \\ F_{dfz} \end{pmatrix} &= \int_{L_{e1}}^{L'+L_{e1}} \begin{bmatrix} \beta_{yy} & \beta_{yz} \\ \beta_{zy} & \beta_{zz} \end{bmatrix} \begin{pmatrix} u_{fy} \\ u_{fz} \end{pmatrix} dx \\ \begin{pmatrix} M_{dfy} \\ M_{dfz} \end{pmatrix} &= \int_{L_{e1}}^{L'+L_{e1}} \begin{bmatrix} -\beta_{zy} & -\beta_{zz} \\ \beta_{yy} & \beta_{yz} \end{bmatrix} \begin{pmatrix} u_{fy} \\ u_{fz} \end{pmatrix} x dx \end{aligned} \quad (6.15)$$

In [Equation 6.14 \(p. 115\)](#), the term  $\begin{pmatrix} u_{fy} - u_{sy} \\ u_{fz} - u_{sz} \end{pmatrix}$  linearly relates to the structural velocity: its coefficient can be considered the damping factor due to linearized drag force. Employing [Equation 6.7 \(p. 113\)](#) as the definition of the structural velocity vector of a tube in the tube local axis frame, the linearized damping force and moment in/about the local  $y$ - and  $z$ -directions is written as

$$\begin{aligned} \begin{pmatrix} F_{dsy} \\ F_{dsz} \end{pmatrix} &= - \int_{L_{e1}}^{L'+L_{e1}} \begin{bmatrix} \beta_{yy} & \beta_{yz} \\ \beta_{zy} & \beta_{zz} \end{bmatrix} \begin{pmatrix} u_2 + xu_6 \\ u_3 - xu_5 \end{pmatrix} dx \\ &= - \int_{L_{e1}}^{L'+L_{e1}} \begin{bmatrix} 0 & \beta_{yy} & \beta_{yz} & 0 & -x\beta_{yz} & x\beta_{yy} \\ 0 & \beta_{zy} & \beta_{zz} & 0 & -x\beta_{zz} & x\beta_{zy} \end{bmatrix} dx \mathbf{u}_s \\ \begin{pmatrix} M_{dsy} \\ M_{dsz} \end{pmatrix} &= - \int_{L_{e1}}^{L'+L_{e1}} \begin{bmatrix} -\beta_{zy} & -\beta_{zz} \\ \beta_{yy} & \beta_{yz} \end{bmatrix} \begin{pmatrix} u_2 + xu_6 \\ u_3 - xu_5 \end{pmatrix} x dx \\ &= - \int_{L_{e1}}^{L'+L_{e1}} \begin{bmatrix} 0 & -\beta_{zy} & -\beta_{zz} & 0 & x\beta_{zz} & -x\beta_{zy} \\ 0 & \beta_{yy} & \beta_{yz} & 0 & -x\beta_{yz} & x\beta_{yy} \end{bmatrix} x dx \mathbf{u}_s \end{aligned} \quad (6.16)$$

Using the linearized drag damping coefficient matrix definition given in [Equation 6.11 \(p. 113\)](#) and [Equation 6.12 \(p. 114\)](#), the linearized tube damping coefficient matrix in the tube local axis frame can be derived from [Equation 6.16 \(p. 115\)](#):

$$\mathbf{C}_{drag} = [C_{ij}] = \int_{L_{e1}}^{L+L_{e1}} \begin{bmatrix} 0 & 0 & 0 & 0 & 0 & 0 \\ 0 & \beta_{yy} & \beta_{yz} & 0 & -x\beta_{yz} & x\beta_{yy} \\ 0 & \beta_{zy} & \beta_{zz} & 0 & -x\beta_{zz} & x\beta_{zy} \\ 0 & 0 & 0 & 0 & 0 & 0 \\ 0 & -x\beta_{zy} & -x\beta_{zz} & 0 & x^2\beta_{zz} & -x^2\beta_{zy} \\ 0 & x\beta_{yy} & x\beta_{yz} & 0 & -x^2\beta_{yz} & x^2\beta_{yy} \end{bmatrix} dx \quad (6.17)$$

Additionally, the axial translational motion linearized drag damping coefficient  $C_{11}$  defined by [Equation 6.13 \(p. 114\)](#) should be included.

Note that the drag damping coefficient matrix and the force and moment in [Equation 6.11 \(p. 113\)](#) through [Equation 6.17 \(p. 116\)](#) are defined in the tube local axis frame. They should be transferred to the fixed reference axes and with respect to the center of gravity of the attached floating structure when the motion response is solved. To do so, denote  $\vec{X}_t, \vec{X}_{gj}$  as the coordinates of the tube element's first node and the center of gravity of the structure respectively, the relative location vector

$$\vec{r}_t = \vec{X}_t - \vec{X}_{gj} = (x_t, y_t, z_t) \quad (6.18)$$

and the unit vectors of the tube local axes reference to the global axes as

$$\begin{aligned} \vec{e}_1 &= (e_{11}, e_{21}, e_{31}) \\ \vec{e}_2 &= (e_{12}, e_{22}, e_{32}) \\ \vec{e}_3 &= (e_{13}, e_{23}, e_{33}) \end{aligned} \quad (6.19)$$

From [Equation 6.12 \(p. 114\)](#), the linearized tube drag force and moment with respect to the center of gravity in the global axes is above equations can be expressed as

$$\mathbf{F}_{drag} = \begin{bmatrix} \mathbf{E} & \mathbf{0} \\ \mathbf{R}^T \mathbf{E} & \mathbf{E} \end{bmatrix} \mathbf{F}_{drag}^L \quad (6.20)$$

where

$$\begin{aligned} \mathbf{E} &= \begin{bmatrix} e_{11} & e_{12} & e_{13} \\ e_{21} & e_{22} & e_{23} \\ e_{31} & e_{32} & e_{33} \end{bmatrix} \\ \mathbf{R} &= \begin{bmatrix} 0 & z_t & -y_t \\ -z_t & 0 & x_t \\ y_t & -x_t & 0 \end{bmatrix} \end{aligned}$$

## 6.5. Effects of Morison Elements in Equilibrium and Static Stability Analysis

If a current is defined in the analysis, drag forces on Morison element due to current velocity are computed by using the Morison equation. In this case the structural velocity  $u_s$  is taken as zero. Inertial forces are also not computed since the static solution is required.

Similarly, for static stability calculations, only the tube drag force term in the above equation is considered since the structure and fluid accelerations are not included.

The force arising from components of velocity in line with the tube axis is assumed to be zero.

## 6.6. Effects of Morison Elements in a Time Domain Dynamic Response Analysis

All Morison force components are calculated at each time step, including the effects of variation of immersion as the analysis proceeds.

Optionally, the slamming force on tube can be included.

The value of the slamming force, for each element, is based on the premise that the slamming force and moment are equal to the rate of change of the added mass matrix (with time) multiplied by the velocity:

$$\mathbf{F}_{\text{slam}} = -f_{\text{slam}} \frac{d \mathbf{M}_a}{dt} \mathbf{u}_s \quad (6.21)$$

where  $f_{\text{slam}}$  is the user defined slamming multiplying factor,  $\mathbf{M}_a$  is the added mass matrix of tube, and  $\mathbf{u}_s$  is the structural velocity vector of a tube in the tube local axis frame defined in [Equation 6.7 \(p. 113\)](#).

This means that the time step must be sufficiently small to accurately represent the added mass at each stage of immersion and emergence. In general this will depend on the geometry of each element and its orientation to the water surface. In practice, this severe restriction of the size of the time step means that this option is only used when specifically investigating the effects of slam forces on individual elements during critical stages of the simulation period, as the momentum changes due to slamming forces are normally small and have little effect on the overall motion of the structure.

In Aqwa-Drift, the incident wave properties at a specified location ( $X, Y, Z_0$ ) on the Morison element beneath the instantaneous incident wave surface  $\zeta(X, Y; t)$  are calculated at the relative vertical position at  $(X, Y, Z)$ , in which

$$Z(X, Y; t) = Z_0 - \zeta(X, Y; t) \quad (6.22)$$

In Aqwa-Naut, the extended Wheeler stretching method is employed. See [Extended Wheeler Stretching Method \(p. 198\)](#) for more information.

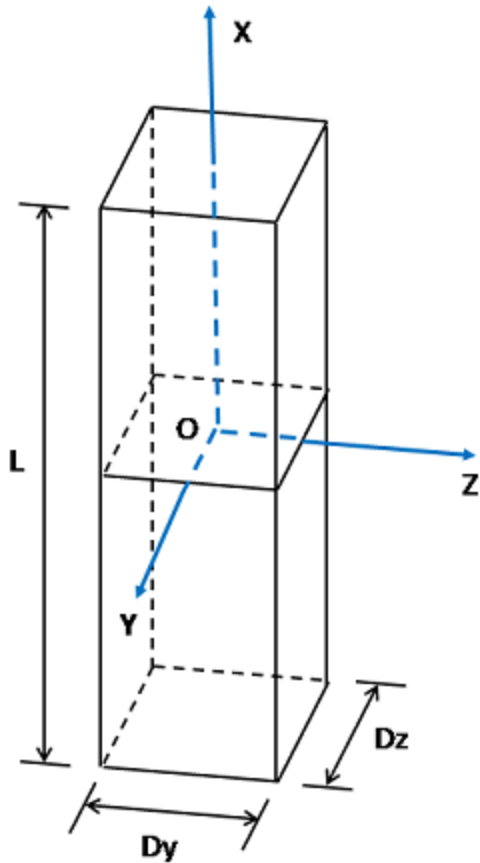
## 6.7. Properties of Typical Morison Elements

The mass and moment of inertia of a circular cross section tube, with respect to the center of the element in the local tube axes, are

$$\begin{aligned} m &= \rho_s \pi (D-t)tL \\ I_{yy} = I_{zz} &= \rho_s \frac{\pi}{4} \left( \frac{D^2}{2} - Dt + t^2 \right) \left( D-t \right) t L + \frac{1}{12} m L^2 \end{aligned} \quad (6.23)$$

where  $\rho_s$  is the material density of the tube,  $D$  is the tube diameter,  $t$  is the tube wall thickness, and  $L$  is the length of the tube element.

The slender tube properties are defined in the principal centroidal axes, as shown in [Figure 6.3: Slender Tube Definition \(p. 118\)](#).  $D_y$  and  $D_z$  are the effective diameters normal to the  $y$ - and  $z$ -directions, respectively.

**Figure 6.3: Slender Tube Definition**

The mass and moment of inertia of a slender tube with respect to the center of the element are

$$\begin{aligned} m &= m_L L \\ I_{yy} &= S_{yy} L + \frac{1}{12} m L^2 \\ I_{zz} &= S_{zz} L + \frac{1}{12} m L^2 \end{aligned} \quad (6.24)$$

where  $m_L$  is the mass per unit length,  $S_{yy}$  is the Y axis inertia per unit length, and  $S_{zz}$  is the Z axis inertia per unit length.

$$\begin{aligned} S_{yy} &= \rho_s \iint_{A_S} z^2 dA \\ S_{zz} &= \rho_s \iint_{A_S} y^2 dA \end{aligned} \quad (6.25)$$

in which  $\rho_s$  is the material density of the slender tube, and  $A_S$  is the structural cross sectional area.

There is neither hydrostatic force nor Froude-Krylov force acting on the circular disc element, as no disc thickness is taken into account. The added mass and drag force on one side of a completely submerged disc are given by

$$\begin{aligned} m_d &= \frac{1}{2} \left\{ \frac{1}{3} C_a \rho D^3 \right\} \\ F_{\text{drag}} &= \frac{1}{2} \left\{ \frac{1}{2} C_d \rho A V^2 \right\} \end{aligned} \quad (6.26)$$

where  $C_a$  is the added mass coefficient for a double-sided disc (1.0 by default),  $\rho$  is the water density,  $D$  is the diameter of the circular disc,  $C_d$  is the drag coefficient for a double-sided disc (1.14 by default),  $A = \frac{1}{4}\pi D^2$ , and  $V$  is the relative normal velocity between the fluid particles and the disc.

In [Equation 6.26 \(p. 118\)](#), the calculated forces are only for the single side of the disc which is subject to the hydrodynamic pressure. If both sides are subject to hydrodynamic pressure, taking into consideration that the pressure on one side is positive and the pressure on the other side is negative, the input  $C_d$  and  $C_a$  values should be doubled.



# Chapter 7: Hull Drag and Damping

Linear hydrodynamic damping caused by radiation potential is discussed in [Hydrodynamic Radiation and Diffraction Analysis by Source Distribution Method \(p. 59\)](#). In this chapter, some additional hull drag forces due to wind and current, nonlinear roll damping induced by bilge vortex shedding, and the wave drift damping due to the small forward speed, are discussed.

## 7.1. Current and Wind Hull Drag

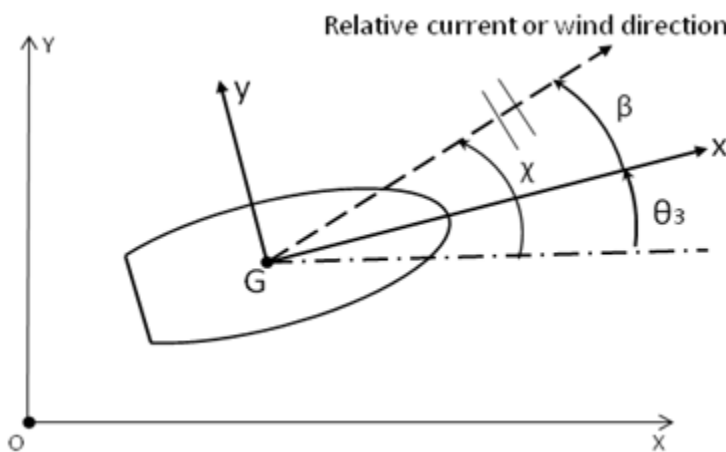
Theoretically predicting current and wind loads on three dimensional marine structures with sufficient accuracy is difficult. However, when the Reynolds number  $Re = \frac{UD}{\nu}$  (in which  $U$  is the characteristic free-stream velocity and  $D$  is the characteristic length of a prototype marine structure) is relatively high (for example, it is in the order of 10<sup>7</sup> for a full scale semi-submersible with diameter 15m, current flow velocity of 1m/s or wind speed of 40m/s, see [15]), the current or wind forces in the current or wind direction on the structure can be approximately expressed in the form of

$$F = C_d |u| u \quad (7.1)$$

where  $C_d$  is the current or wind drag coefficient and  $u$  is the relative current or wind velocity in the current or wind travelling direction.

The hull drag force and moment are normally the functions of the relative heading angle between the current or wind propagating direction and the investigated structure, which can be defined by  $\beta = \chi - \theta_3$ , where  $\chi$  is the current or wind directional angle in the global fixed frame and  $\theta_3$  is the yaw angle of the structure, as shown in [Figure 7.1: Relative Directional Angle Between Current/Wind and Structure \(p. 121\)](#).

**Figure 7.1: Relative Directional Angle Between Current/Wind and Structure**



At a given relative heading, the hull drag force and moment can be more generally written as

$$F_j(\beta) = C_{dj}(\beta) |u| u \text{ where } j=1,6 \quad (7.2)$$

where the subscript  $j$  ( $j = 1,3$ ) represents the force components in the local structure x, y and z directions respectively, the subscript  $j$  ( $j = 4,6$ ) indicates the moment components about the local structure x, y and z directions respectively.

According to the above definition, the coefficients are dimensional so you must conform to a consistent set of units.

The relative wind or current velocity in the above expression is calculated to be the relative velocity between the wind or current velocity and the structure motion velocity along the wind/current direction. In reality, the time scale of the mean wind and current flow is much longer than the typical wave periods, so the wind and current flows do not have time to develop in response to the wave frequency variations of position. In Aqwa, an option can be used to employ the slow velocity (drift frequency velocity) for the hull drag calculation, instead of the total velocity (drift frequency velocity plus wave frequency velocity).

For a floating structure system the relative heading angle may vary at each time step, hence the hull drag coefficients at such headings are required. In order to efficiently evaluate the hull drag force and moment, Aqwa requires the user to define the wind and current hull drag coefficients for a range of relative heading angles. This creates a database which is then accessed during the analysis to interpolate the coefficients at any specified relative heading angle at each time step.

The wind and current drag are both calculated in a similar manner from a set of user-derived environmental load coefficients, covering a range of heading angles. Aqwa is based on the potential theory, so these hull drag coefficients should come from CFD numerical prediction results, empirical formulas, or model test data. For example, if under the condition of a known relative heading angle  $\beta_k$  and known wind or current speed  $u$ , the force and moment about structure COG in the structure local axis frame,  $F_j(\beta_k)$  where  $k=1,6$ , are obtained by means of experimental or CFD or empirical approach, then the drag coefficients at this specific heading angle can be converted by

$$C_{dj}(\beta_k) = \frac{F_j(\beta_k)}{u^2} \quad (7.3)$$

## 7.2. Nonlinear Roll Damping

Linear potential theories have proved to be efficient tools to predict linear floating structure motions. A known exception to this is the roll motion of ship-like structures near the resonant frequency range, where codes based on potential theories commonly overestimate the responses.

The roll damping moment could include a number of components, such as the wave induced, lift, friction, eddy, and the appendage contributions. The wave and lift components are linear, and are proportional to the roll angular velocity. The hull surface frictional damping for a full size ship-like structure is negligible; the major contributions are the radiation damping, nonlinear bilge vortex shedding damping, and bilge keel damping [21].

It is common practice for the calculation of nonlinear roll damping to use estimation methods or experimental data to account for the viscosity effect.

### 7.2.1. Nonlinear Bilge Vortex Shedding Damping

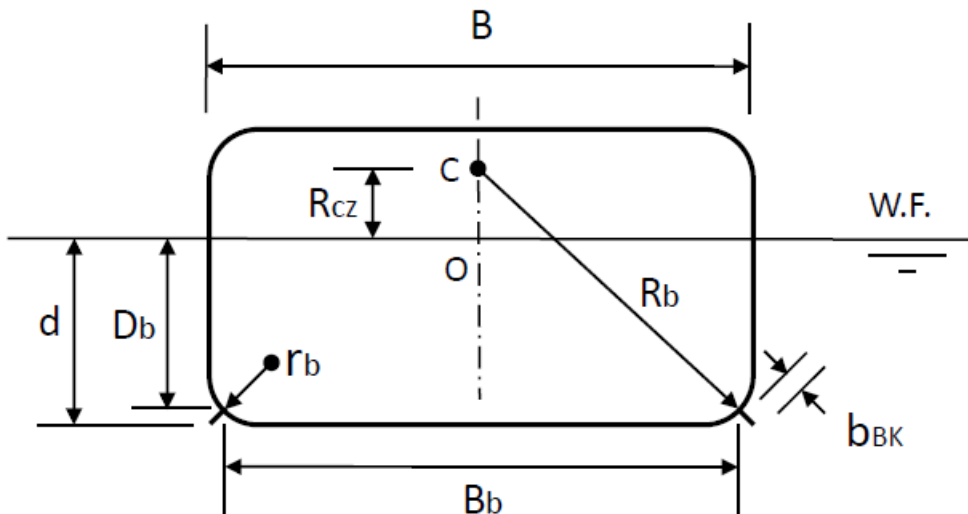
To take into account the effect of vortex shedding from the bilges of a vessel, a nonlinear roll damping moment can be calculated in Aqwa time domain analysis. The method used is based on the work of Robinson and Stoddart [41].

[Figure 7.2: Ship-Like Cross Section with Bilge \(p. 123\)](#) shows a ship-like cross section where the nonlinear damping is taken into account. To check whether vortex shedding from the bilge is occurring, the relative flow velocity at the bilge, the roll natural frequency of the vessel, and the bilge radius are involved. To do so, the Keulegan-Carpenter number at each time step is used, which is defined as:

$$K_{cb} = \frac{R_b |\dot{\phi}| T_R}{2r_b} \quad (7.4)$$

where (as shown in [Figure 7.2: Ship-Like Cross Section with Bilge \(p. 123\)](#))  $R_b$  is the distance from the roll center to the turn of the bilge,  $r_b$  is the bilge radius,  $\dot{\phi}$  is the relative angular roll velocity to the wave slope, and  $T_R$  is the roll period at resonance.

**Figure 7.2: Ship-Like Cross Section with Bilge**



The roll moment due to bilge vortex shedding induced nonlinear damping at each time step is calculated with the following correction to account for the bilge Keulegan-Carpenter number:

$$M_{4B} = -\frac{1}{2} \rho \gamma C_{db} B_b^4 L_b |\dot{\phi}| \dot{\phi} \quad (7.5)$$

where  $L_b$  is the bilge length,  $B_b$  is the breadth of the turn of the bilge,  $C_{db}$  is the non-dimensional roll damping coefficient, and  $\gamma$  is the correction factor, which is defined as:

$$\gamma = \begin{cases} 1 & K_{cb} \geq 10 \\ \sin\left(\frac{\pi}{2} \cdot \frac{K_{cb}}{10}\right) & K_{cb} < 10 \end{cases}$$

The non-dimensional roll damping coefficient  $C_{db}$  in [Equation 7.5 \(p. 123\)](#) is interpolated from a database, which is a function of the bilge geometric properties:

$$C_{db} = C_{db} \left( \frac{B_b}{D_b}, \frac{R_{cz}}{D_b} \right) \quad (7.6)$$

where  $D_b$  is the draft of the turn of the bilge and  $R_{cz}$  is the vertical distance from the roll center to the still water surface, as shown in [Figure 7.2: Ship-Like Cross Section with Bilge \(p. 123\)](#).

The roll damping coefficient database is listed in the following table:

**Table 7.1: Database of Non-Dimensional Roll Damping Coefficient  $C_{db}(R_{BD}, R_{RD})$**

| <b>R<sub>BD</sub></b> | <b>2.00</b> | <b>2.29</b> | <b>2.71</b> | <b>3.25</b> | <b>3.97</b> | <b>10.45</b> | <b>59.55</b> |        |
|-----------------------|-------------|-------------|-------------|-------------|-------------|--------------|--------------|--------|
| <b>R<sub>RD</sub></b> | -1.00       | 0.0031      | 0.0051      | 0.0072      | 0.0090      | 0.0104       | 0.0100       | 0.0047 |
|                       | -0.80       | 0.0180      | 0.0183      | 0.0183      | 0.0178      | 0.0171       | 0.0119       | 0.0048 |
|                       | -0.60       | 0.0499      | 0.0429      | 0.0362      | 0.0307      | 0.0260       | 0.0135       | 0.0049 |
|                       | -0.40       | 0.1042      | 0.0818      | 0.0627      | 0.0484      | 0.0376       | 0.0153       | 0.0050 |
|                       | -0.20       | 0.1862      | 0.1381      | 0.0990      | 0.0715      | 0.0520       | 0.0172       | 0.0051 |
|                       | 0.00        | 0.3012      | 0.2148      | 0.1468      | 0.1008      | 0.0695       | 0.0193       | 0.0052 |
|                       | 0.20        | 0.4544      | 0.3148      | 0.2075      | 0.1370      | 0.0906       | 0.0215       | 0.0052 |
|                       | 0.40        | 0.6513      | 0.4412      | 0.2827      | 0.1808      | 0.1155       | 0.0239       | 0.0053 |
|                       | 0.60        | 0.8970      | 0.5969      | 0.3798      | 0.2330      | 0.1445       | 0.0265       | 0.0054 |
|                       | 0.80        | 1.1968      | 0.7850      | 0.4823      | 0.2941      | 0.1779       | 0.0292       | 0.0055 |
|                       | 1.00        | 1.5662      | 1.0084      | 0.6097      | 0.3650      | 0.2161       | 0.0321       | 0.0056 |
|                       | 2.00        | 4.4301      | 2.7601      | 1.5832      | 0.8901      | 0.4887       | 0.0497       | 0.0061 |
|                       | 4.00        | 17.6827     | 10.6352     | 5.8107      | 3.0764      | 1.5664       | 0.1018       | 0.0071 |
|                       | 6.00        | 45.3549     | 26.8347     | 14.3268     | 7.3668      | 3.6119       | 0.1816       | 0.0082 |
|                       | 8.00        | 92.7427     | 54.3531     | 28.6293     | 14.4685     | 6.9341       | 0.2948       | 0.0094 |

**Note:**

$$R_{BD} = \frac{B_b}{D_b} \text{ and } R_{RD} = \frac{R_{cz}}{D_b}$$

## 7.2.2. Bilge Keel Damping

The bilge keel damping is usually the largest contribution in the total roll damping, which consists of four components:

1. Nonlinear normal force component
2. Pressure on the hull surface created by the bilge keels
3. Lift force acting on the bilge keel due to forward speed
4. Wave making contribution for bilge keels

Among them, the nonlinear normal force component on bilge keels and the hull pressure component make a major contribution to the bilge keel damping moment [22].

The Keulegan-Carpenter number is used in the estimation of the bilge keel damping, which is defined as:

$$K_{CBK} = \frac{U_{\max} T}{2b_{BK}} = \frac{\pi R_b \phi_a}{b_{BK}} \quad (7.7)$$

where  $T$  and  $U_{\max} = R_b \phi_a \omega = \frac{2\pi R_b \phi_a}{T}$  are the period of motion and the amplitude of velocity of periodic motion;  $R_b$  and  $b_{BK}$  are the distance from the roll center to the tip of the bilge keel and the bilge keel breadth respectively, as shown in [Figure 7.2: Ship-Like Cross Section with Bilge \(p. 123\)](#), and  $\phi_a$  is the amplitude of roll motion.

ITTC [21] recommends that the drag moment due to the nonlinear normal force on a bilge keel is expressed approximately as:

$$\begin{aligned} M_{4BKNO} &= -\rho R_b^3 b_{BK} L_{BK} f C_D |\dot{\phi}| \dot{\phi} \\ C_D &= 22.5 \frac{b_{BK}}{\pi R_b \phi_a f} + 2.4 \end{aligned} \quad (7.8)$$

where  $\rho$  and  $L_{BK}$  are the water density and the length of the bilge keel respectively,  $f = 1 + 0.3e^{-160(1-C_m)}$  is the correction factor to take into account the increment of flow velocity at the bilge, where  $C_m = \frac{A_j}{Bd}$  is the mid-ship section coefficient of which  $A_j$  is the area of the mid-ship cross section.

Note that the drag coefficient depends on the Keulegan-Carpenter number. Substituting [Equation 7.7 \(p. 125\)](#) into [Equation 7.8 \(p. 125\)](#) we have:

$$C_D = 22.5 \frac{1}{K_{CBK} f} + 2.4 \quad (7.9)$$

In Aqwa time domain analysis, the Keulegan-Carpenter number is further defined as:

$$K_{CBK}(t) = \frac{R_b |\dot{\phi}(t)| T_R}{2b_{BK}} \quad (7.10)$$

where  $T_R$  is the roll period at resonance.

By employing the ITTC [21] recommended method, the coefficient of pressure on the front and back hull faces of the bilge keels and the length of the negative pressure region are given by:

$$\begin{aligned} C_p^+ &= 1.2 \\ C_p^- &= 1.2 - C_D \\ S_0 &= \left( 0.3 \frac{\pi R_b \phi_a f}{b_{BK}} + 1.95 \right) b_{BK} = \left( 0.3 K_{CBK} f + 1.95 \right) b_{BK} \end{aligned} \quad (7.11)$$

The roll drag moment is:

$$M_{4BKHO} = -\frac{1}{2} \rho R_b^2 L_{BK} f^2 \int C_p l_p dG |\dot{\phi}| \dot{\phi} \quad (7.12)$$

where  $G$  is the length along the girth of the cross section and  $l_p$  is the moment lever.

Combining [Equation 7.5 \(p. 123\)](#), [Equation 7.8 \(p. 125\)](#), and [Equation 7.12 \(p. 125\)](#), the total roll drag coefficient due to bilge vortex shedding and bilge keels is:

$$C_{droll} = \frac{1}{2}\rho\gamma C_{db}B_b^4L_b + \frac{1}{2}\rho R_b^2L_{BK}f^2 \int C_{pl}p dG + \rho R_b^3 b_{BK}L_{BK}f C_D \quad (7.13)$$

if the nonlinear drag moment is expressed as  $M_{roll} = -C_{droll}|\dot{\phi}| \dot{\phi}$

### 7.2.3. User-Defined Quadratic Roll Damping

The friction, eddy, and appendage induced roll damping components are nonlinear and could be assumed to be proportional to the square of roll angular velocity, which is expressed as the quadratic:

$$M_{roll} = -C_{droll}|\dot{\phi}(t)|\dot{\phi}(t) \quad (7.14)$$

in the local structure axes (LSA), where  $\dot{\phi}(t)$  is the roll angular velocity at time  $t$  and  $C_{droll}$  is the quadratic roll damping coefficient which can be derived from experimental data or given by any empirical formula other than the forms discussed in [Nonlinear Bilge Vortex Shedding Damping \(p. 123\)](#) and [Bilge Keel Damping \(p. 124\)](#).

## 7.3. Yaw Rate Drag Force

When calculated as described in [Current and Wind Hull Drag \(p. 121\)](#), the wind and current loads have no dependence on yaw rotational velocity. This contribution is calculated separately and the yaw rate drag moment is given by [43]:

$$M_{yaw} = C_{dyaw} \int_{X_{min}}^{X_{max}} \left[ u_y |u| - (u_y + x\dot{\beta}) \sqrt{u_x^2 + (u_y + x\dot{\beta})^2} \right] dx \quad (7.15)$$

where  $C_{dyaw}$  is the yaw rate drag coefficient which is force per unit length per unit velocity squared,  $\beta$  is the relative heading angle between current or wind propagating direction and the analyzed structure as shown in [Figure 7.1: Relative Directional Angle Between Current/Wind and Structure \(p. 121\)](#),  $u_x = u \cos \beta$  and  $u_y = u \sin \beta$  are the relative current velocity components in the structure local x- and y-axes respectively. The integration is along the length of the structure between  $X_{min}$  and  $X_{max}$  in the structure local axis frame Gxyz.

If the center of gravity is not at the geometric center of the structure's projection on the water surface, the yaw rate drag will have a lateral component given by a very similar expression:

$$F_{sway} = C_{dyaw} \int_{X_{min}}^{X_{max}} \left[ u_y |u| - (u_y + x\dot{\beta}) \sqrt{u_x^2 + (u_y + x\dot{\beta})^2} \right] dx \quad (7.16)$$

## 7.4. Morison Hull Drag Force

Aqwa also provides a facility for hull drag force and moment on a diffracting structure to be calculated in a similar way to that for Morison element, i.e. the structure motion in six degrees of freedom is taken into account in the drag force calculation, such as

$$[F_{dmj}] = C_{dm} [|u_j| u_j] \text{ where } j=1,6 \quad (7.17)$$

where  $[F_{dmj}]$  is a  $6 \times 1$  matrix consisting of three Morison hull drag force components and three Morison hull drag moment components,  $\mathbf{C}_{dm}$  is a  $6 \times 6$  Morison drag coefficient matrix, and  $u_j$  ( $j = 1, 6$ ) is the relative translational or rotational velocity component in the structure local axis frame.

By default, the translational relative velocity  $u_j$  ( $j = 1, 3$ ) in [Equation 7.17 \(p. 126\)](#) is the difference between the steady fluid velocity (current speed only without fluid particle velocity due to waves) and the structural motion velocity,

$$u_j = U_{cj} - u_{sj} \text{ where } j=1,3 \quad (7.18)$$

where  $u_{cj}$  and  $u_{sj}$  are the current velocity and structure motion velocity along the  $j$ -th direction of structure local axis frame.

This default definition of translational relative velocity can be optionally changed by only taking structure motion velocity components:

$$u_j = -u_{sj} \text{ where } j=1,3 \quad (7.19)$$

However, the rotational relative velocity components in [Equation 7.17 \(p. 126\)](#) are always in the form of

$$u_j = -u_{sj} \text{ where } j=4,6 \quad (7.20)$$

## 7.5. Wave Drift Damping

Wave drift damping is induced by nonlinear surface wave effects, which provides additional damping for the slow-drift motions, along with above mentioned nonlinear drag forces. It is employed in Aqwa time domain analysis when the first and second order wave exciting forces are included (Aqwa-Drift).

For a long crested wave case, the wave drift damping coefficients used in Aqwa are based on the work of Kim and Sclavounos [23], in which the Aranha's formulae are employed. The wave drift damping coefficient  $B_{jj}$  is defined in the drift matrix equation for a floating structure with small forward speed:

$$\begin{Bmatrix} \bar{F}_{x,U}(\omega, \beta) \\ \bar{F}_{y,U}(\omega, \beta) \\ \bar{M}_{z,U}(\omega, \beta) \end{Bmatrix} = \begin{Bmatrix} \bar{F}_x(\omega, \beta) \\ \bar{F}_y(\omega, \beta) \\ \bar{M}_z(\omega, \beta) \end{Bmatrix} - \begin{Bmatrix} B_{11}(\omega, \beta) & B_{12}(\omega, \beta) & B_{16}(\omega, \beta) \\ B_{21}(\omega, \beta) & B_{22}(\omega, \beta) & B_{26}(\omega, \beta) \\ B_{61}(\omega, \beta) & B_{62}(\omega, \beta) & B_{66}(\omega, \beta) \end{Bmatrix} \begin{Bmatrix} u_1 \\ u_2 \\ u_6 \end{Bmatrix} \quad (7.21)$$

where  $\bar{F}_{x,U}$ ,  $\bar{F}_{y,U}$ ,  $\bar{M}_{z,U}$  are the drift forces and moment when floating structure has a relative speed  $u_1, u_2, u_6$ , and  $\beta$  is the incident wave angle relative to the structure local axis frame Gxyz.

For a deep water case, the drift damping coefficients are estimated by

$$\begin{aligned} B_{11}(\omega, \beta) &= \frac{\omega}{g} \left[ \omega \frac{\partial \bar{F}_x}{\partial \omega} \cos \beta - 2 \frac{\partial \bar{F}_x}{\partial \beta} \sin \beta + 4 \bar{F}_x \cos \beta \right] \\ B_{12}(\omega, \beta) &= \frac{\omega}{g} \left[ \omega \frac{\partial \bar{F}_x}{\partial \omega} \sin \beta + 2 \frac{\partial \bar{F}_x}{\partial \beta} \cos \beta + 4 \bar{F}_x \sin \beta \right] \\ B_{21}(\omega, \beta) &= \frac{\omega}{g} \left[ \omega \frac{\partial \bar{F}_y}{\partial \omega} \cos \beta - 2 \frac{\partial \bar{F}_y}{\partial \beta} \sin \beta + 4 \bar{F}_y \cos \beta \right] \\ B_{22}(\omega, \beta) &= \frac{\omega}{g} \left[ \omega \frac{\partial \bar{F}_y}{\partial \omega} \sin \beta + 2 \frac{\partial \bar{F}_y}{\partial \beta} \cos \beta + 4 \bar{F}_y \sin \beta \right] \\ B_{61}(\omega, \beta) &= \frac{\omega}{g} \left[ \omega \frac{\partial \bar{M}_z}{\partial \omega} \cos \beta - 2 \frac{\partial \bar{M}_z}{\partial \beta} \sin \beta + 4 \bar{M}_z \cos \beta \right] \\ B_{62}(\omega, \beta) &= \frac{\omega}{g} \left[ \omega \frac{\partial \bar{M}_z}{\partial \omega} \sin \beta + 2 \frac{\partial \bar{M}_z}{\partial \beta} \cos \beta + 4 \bar{M}_z \sin \beta \right] \end{aligned} \quad (7.22)$$

The drifting damping coefficients due to the yaw motion are given by Aranha and Martins [3] and are based on the slender-body approximation

$$\begin{aligned} B_{16}(\omega, \beta) &= B_{61}(\omega, \beta - \frac{\pi}{2}) \\ B_{26}(\omega, \beta) &= B_{62}(\omega, \beta) \\ B_{66}(\omega, \beta) &= \Gamma B_{22}(\omega, \beta) \end{aligned} \quad (7.23)$$

where

$$\Gamma = \frac{\int_L^L \xi^2 [1 - (\frac{db(\xi)}{d\xi})^2] d\xi}{\int_L^L [1 - (\frac{db(\xi)}{d\xi})^2] d\xi}$$

in which  $b(\xi)$  is the water-line profile of the ship with length  $L$ .

For the finite depth water of  $d$ , Equation 7.22 (p. 127) is extended as

$$\begin{aligned} B_{11}(\omega, \beta) &= k \frac{\partial \bar{F}_x}{\partial \omega} \cos \beta - \frac{1}{C_g} \frac{\partial \bar{F}_x}{\partial \beta} \sin \beta + \frac{2K}{C_g} \bar{F}_x \cos \beta \\ B_{12}(\omega, \beta) &= k \frac{\partial \bar{F}_x}{\partial \omega} \sin \beta + \frac{1}{C_g} \frac{\partial \bar{F}_x}{\partial \beta} \cos \beta + \frac{2K}{C_g} \bar{F}_x \sin \beta \\ B_{21}(\omega, \beta) &= k \frac{\partial \bar{F}_y}{\partial \omega} \cos \beta - \frac{1}{C_g} \frac{\partial \bar{F}_y}{\partial \beta} \sin \beta + \frac{2K}{C_g} \bar{F}_y \cos \beta \\ B_{22}(\omega, \beta) &= k \frac{\partial \bar{F}_y}{\partial \omega} \sin \beta + \frac{1}{C_g} \frac{\partial \bar{F}_y}{\partial \beta} \cos \beta + \frac{2K}{C_g} \bar{F}_y \sin \beta \\ B_{61}(\omega, \beta) &= k \frac{\partial \bar{M}_z}{\partial \omega} \cos \beta - \frac{1}{C_g} \frac{\partial \bar{M}_z}{\partial \beta} \sin \beta + \frac{2K}{C_g} \bar{M}_z \cos \beta \\ B_{62}(\omega, \beta) &= k \frac{\partial \bar{M}_z}{\partial \omega} \sin \beta + \frac{1}{C_g} \frac{\partial \bar{M}_z}{\partial \beta} \cos \beta + \frac{2K}{C_g} \bar{M}_z \sin \beta \end{aligned} \quad (7.24)$$

where

$$\begin{aligned} C_g &= \frac{d\omega}{dk} = \frac{\omega}{2k} \left[ 1 + \frac{2kd}{\sinh(2kd)} \right] \\ K &= 1 - \frac{kd(\sinh 2kd - 2kd \cosh 2kd)}{(\sin 2kd + 2kd) \sinh 2kd} \end{aligned}$$

The drift damping coefficients due to the yaw motion for finite depth water have the same forms as those given by Equation 7.23 (p. 128).

For a multiple directional wave case, the mean drift force component is written as

$$\bar{F}_i^{(2)} = \sum_{m=1}^{N_d} \sum_{n=1}^{N_d} \sum_{j=1}^{N_w} \bar{f}_1^{(2)}(\omega_j; \beta_m, \beta_n), (j=1, 6) \quad (7.25)$$

As discussed by Kim et al [24], the damping coefficient  $B_{11}$  in Equation 7.24 (p. 128) is extended as

$$B_{11} = \sum_{m=1}^{N_d} \sum_{n=1}^{N_d} \sum_{j=1}^{N_w} \bar{E}_{11}(\omega_j; \beta_m, \beta_n) \bar{f}_1^{(2)}(\omega_j; \beta_m, \beta_n) \quad (7.26)$$

where

$$\begin{aligned}\Xi_{11}(\omega_j; \beta_m, \beta_n) &= \frac{1}{2} \left\{ (\cos \beta_m + \cos \beta_n) \cdot (k_j \frac{\partial}{\partial \omega_j} + \frac{2K_j}{C_{gj}}) - \frac{1}{C_{gj}} (\sin \beta_m \frac{\partial}{\partial \beta_m} + \sin \beta_n \frac{\partial}{\partial \beta_n}) \right\} \\ k_j &= \frac{\omega_j^2}{g} \\ C_{gj} &= \frac{\omega_j}{2k_j} \left[ 1 + \frac{2k_j d}{\sinh(2k_j d)} \right] \\ K_j &= 1 - \frac{k_j d (\sinh 2k_j d - 2k_j d \cosh 2k_j d)}{(\sin 2k_j d + 2k_j d) \sin 2k_j d}\end{aligned}$$

$N_d$  is the total number of wave directions,

$N_w$  is the number of frequencies.

Other damping terms in [Equation 7.24 \(p. 128\)](#) have the similar forms as that expressed in [Equation 7.25 \(p. 128\)](#) for the multiple directional wave case.



# Chapter 8: Articulation and Constraint

Offshore engineering structure systems frequently contain various types of connections between structural components, as well as external constraints on the motions of one or more structures. Connections are represented using articulations in Aqwa, while external constraints are enforced by eliminating freedoms of motion at the center of gravity.

## 8.1. Articulations Between Structures

Articulations between structures are used to physically connect one structure to another by means of an articulated joint. These connections are referred to as constraints, for which only rotational freedoms exist. There is no relative translational motion at the articulated joint between the linked structures. The term 'structure' is used in this context to mean either a floating structure or a fixed position in the fixed reference axes (FRA), for example an anchored plinth on the sea bed.

Four types of articulation can be modelled by Aqwa, as listed in [Table 8.1: Constraint Types \(p. 131\)](#). The local articulation axis system has been described in [Local Articulation Axes \(p. 12\)](#).

**Table 8.1: Constraint Types**

| Type        | Description   |
|-------------|---|
| Ball/Socket | 3 rotational degrees of freedom                         |
| Universal   | 2 rotational degrees of freedom in 2 perpendicular axes |
| Hinge       | 1 rotational degree of freedom in 1 axis                |
| Locked      | No relative rotational motion                           |

### 8.1.1. Motion Restriction due to Articulation

Denoting  $\vec{X}_{gj}$ ,  $\vec{X}_{gk}$  as the locations of the centers of gravity of the  $j$ -th and  $k$ -th structures respectively, and  $\vec{X}_p$  as the connecting point in the global axes, the vectors between the joint point and the  $j$ -th and  $k$ -th structures are written as

$$\begin{aligned}\vec{r}_j &= \vec{X}_p - \vec{X}_{gj} = (x_j, y_j, z_j) \\ \vec{r}_k &= \vec{X}_p - \vec{X}_{gk} = (x_k, y_k, z_k)\end{aligned}\tag{8.1}$$

Let us further denote the translational and rotational movements of these two linked structures as  $(\vec{u}_j, \vec{\theta}_j)$  and  $(\vec{u}_k, \vec{\theta}_k)$  and the unit vectors of the local articulation axes with respect to the global axes as

$$\begin{aligned}\vec{e}_1 &= (e_{11}, e_{21}, e_{31}) \\ \vec{e}_2 &= (e_{12}, e_{22}, e_{32}) \\ \vec{e}_3 &= (e_{13}, e_{23}, e_{33})\end{aligned}\quad (8.2)$$

For the locked constraint case, the constraint boundary conditions in the local articulation frame are

$$\begin{aligned}(\vec{u}_j + \vec{\theta}_j \times \vec{r}_j) \cdot \vec{e}_m &= (\vec{u}_k + \vec{\theta}_k \times \vec{r}_k) \cdot \vec{e}_m \\ \vec{\theta}_j \cdot \vec{e}_m &= \vec{\theta}_k \cdot \vec{e}_m \text{ where } m=1,3\end{aligned}\quad (8.3)$$

Introducing the matrix form, the above equations can be expressed as

$$\begin{bmatrix} \mathbf{E}^T & \mathbf{E}^T \mathbf{R}_j \\ 0 & \mathbf{E}^T \end{bmatrix} \mathbf{U}_j - \begin{bmatrix} \mathbf{E}^T & \mathbf{E}^T \mathbf{R}_k \\ 0 & \mathbf{E}^T \end{bmatrix} \mathbf{U}_k = 0 \quad (8.4)$$

where

$$\begin{aligned}\mathbf{E} &= \begin{bmatrix} e_{11} & e_{12} & e_{13} \\ e_{21} & e_{22} & e_{23} \\ e_{31} & e_{32} & e_{33} \end{bmatrix} \\ \mathbf{R}_j &= \begin{bmatrix} 0 & z_j & -y_j \\ -z_j & 0 & x_j \\ y_j & -x_j & 0 \end{bmatrix} \\ \mathbf{R}_k &= \begin{bmatrix} 0 & z_k & -y_k \\ -z_k & 0 & x_k \\ y_k & -x_k & 0 \end{bmatrix} \\ \mathbf{U}_j &= (\vec{u}_j, \vec{\theta}_j) \\ \mathbf{U}_k &= (\vec{u}_k, \vec{\theta}_k)\end{aligned}$$

For the hinge constraint case, in which the rotation about the local articulation x-axis is free, the boundary conditions are similarly given by

$$\begin{bmatrix} \mathbf{E}^T & \mathbf{E}^T \mathbf{R}_j \\ 0 & \mathbf{G}^T \end{bmatrix} \mathbf{U}_j - \begin{bmatrix} \mathbf{E}^T & \mathbf{E}^T \mathbf{R}_k \\ 0 & \mathbf{G}^T \end{bmatrix} \mathbf{U}_k = 0 \quad (8.5)$$

where

$$\mathbf{G} = \begin{bmatrix} 0 & e_{12} & e_{13} \\ 0 & e_{22} & e_{23} \\ 0 & e_{32} & e_{33} \end{bmatrix}$$

For the universal constraint case in which rotations about the local articulation x- and y-axes are free, the boundary conditions have the same form as [Equation 8.5 \(p. 132\)](#) but

$$\mathbf{G} = \begin{bmatrix} 0 & 0 & e_{13} \\ 0 & 0 & e_{23} \\ 0 & 0 & e_{33} \end{bmatrix} \quad (8.6)$$

Finally for the ball/socket constraint case, the boundary conditions have the same form as [Equation 8.5 \(p. 132\)](#) but

$$\mathbf{G} = \begin{bmatrix} 0 & 0 & 0 \\ 0 & 0 & 0 \\ 0 & 0 & 0 \end{bmatrix} \quad (8.7)$$

[Equation 8.4 \(p. 132\)](#) for the locked constraint case can be converted into the same form of [Equation 8.5 \(p. 132\)](#) by simply defining  $\mathbf{G}=\mathbf{E}$ .

From the above discussion, the boundary conditions of all constraint types can be defined by [Equation 8.5 \(p. 132\)](#), differing only in the form of the  $\mathbf{G}$  matrix. Further denoting

$$\mathbf{H}_j = \begin{bmatrix} \mathbf{E}^T & \mathbf{E}^T \mathbf{R}_j \\ 0 & \mathbf{G}^T \end{bmatrix} \quad (8.8)$$

[Equation 8.5 \(p. 132\)](#) is rewritten as

$$\mathbf{H}_j \mathbf{U}_j - \mathbf{H}_k \mathbf{U}_k = 0 \quad (8.9)$$

Denoting the constraint reaction force/moment matrix acting on the  $j$ -th structure at the articulation point in the local articulation axes as  $\mathbf{R}_C$ , the motion including the reaction forces and moments of the two linked structures can be determined from

$$\begin{bmatrix} \mathbf{K}_{jj} & \mathbf{K}_{jk} & -\mathbf{H}_j^T \\ \mathbf{K}_{kj} & \mathbf{K}_{kk} & \mathbf{H}_k^T \\ \mathbf{H}_j & -\mathbf{H}_k & \mathbf{0} \end{bmatrix} \begin{bmatrix} \mathbf{U}_j \\ \mathbf{U}_k \\ \mathbf{R}_C \end{bmatrix} = \begin{bmatrix} \mathbf{F}_j \\ \mathbf{F}_k \\ 0 \end{bmatrix} \quad (8.10)$$

where  $\begin{bmatrix} \mathbf{K}_{jj} & \mathbf{K}_{jk} \\ \mathbf{K}_{kj} & \mathbf{K}_{kk} \end{bmatrix}$  is the total stiffness matrix of these two structures, and  $\mathbf{F}_j$  and  $\mathbf{F}_k$  are the forces and moments acting on the  $j$ -th and  $k$ -th structures respectively (excluding the reaction force component).

### 8.1.2. Effect of Articulation Stiffness, Damping and Friction

Articulation stiffness, damping, and friction can be defined for all of the relevant articulation types, including ball/socket, universal, and hinge.

As articulations only allow rotational motion, only the rotational stiffness, damping, and friction need to be specified. These are defined with respect to the local articulation axes.

To define any articulation stiffness the input values should have units of moment per radian. The corresponding restoring moment acting on the  $j$ -th structure in the local articulation axes is

$$\mathbf{M}_{js} = - \begin{bmatrix} k_1 & 0 & 0 \\ 0 & k_2 & 0 \\ 0 & 0 & k_3 \end{bmatrix} [0, \mathbf{G}^T] [\mathbf{U}_j - \mathbf{U}_k] \quad (8.11)$$

where  $k_m$  ( $m = 1, 3$ ) are the stiffness coefficients of relative rotations along the local articulation axes and  $[0, \mathbf{G}^T]$  is a  $3 \times 6$  matrix.

Denoting  $c_m$  ( $m = 1, 3$ ) as the damping coefficients of relative rotations along the local articulation axes, the moment due to articulation damping acting on the  $j$ -th structure in this local axis system is similarly expressed as

$$\mathbf{M}_{jd} = - \begin{bmatrix} c_1 & 0 & 0 \\ 0 & c_2 & 0 \\ 0 & 0 & c_3 \end{bmatrix} [0, \mathbf{G}^T] [\dot{\mathbf{U}}_j - \dot{\mathbf{U}}_k] \quad (8.12)$$

Coulomb friction can be optionally defined in time domain analyses, and always uses a local right hand axis system  $Ax'y'z'$  (where the  $x'$ -axis is aligned with the direction of the instantaneous relative rotational velocity of the two articulated structures). For a hinge, this will always be the hinge axis; for universal or ball/socket joints it will vary as the two structures move relative to one another. The frictional moment is given by

$$M_f = \varepsilon [f_1 \sqrt{F_y^2 + F_z^2} + f_2 \sqrt{M_y^2 + M_z^2} + f_3 F_x + f_4] \quad (8.13)$$

where  $\varepsilon=0$  if the relative rotational velocity is less than 0.001 rad/s and  $\varepsilon=1$  otherwise, while  $f_m$  ( $m = 1, 4$ ) are the input friction coefficients. These are not conventional dimensionless friction coefficients (as used in the general friction force equation  $F=\mu R$ ), but are factors to be applied to the appropriate reaction forces ( $F_x', F_y', F_z'$ ) and moments ( $M_y', M_z'$ ) to give the frictional moment.  $f_1$  and  $f_3$  must not be negative, and the maximum permissible value of any element of  $f$  is 0.025 when a [kg, m, s] unit system is used in the analysis. If another unit system is used this maximum value criterion will be adjusted to  $\frac{0.025g}{g_{SI}}$ , where  $g$  is the acceleration due to gravity expressed in the current unit system and  $g_{SI}$  is the acceleration due to gravity expressed in the [kg, meter, second] unit system. However, according to [Equation 8.13 \(p. 134\)](#), the factor  $f_2$  is non-dimensional; hence it is simply required to be less than 0.025 (but may also be negative).

Once this frictional moment is calculated, it will be transformed into the local articulation axes (LAA), local structure axes (LSA), or fixed reference axes (FRA) as appropriate.

To calculate the motions and reaction forces of the articulation-linked structures, the articulation stiffness, damping, and friction moments expressed in [Equation 8.11 \(p. 133\)](#) through [Equation 8.13 \(p. 134\)](#) should be converted into the fixed reference axes (FRA) and should then be assembled into [Equation 8.10 \(p. 133\)](#).

## 8.2. Elimination of Freedoms at the Center of Gravity

Elimination of freedoms at the center of gravity is used to remove one or more of the six degrees of freedom at the center of gravity. For example, if the analysis is one- or two-dimensional, then the user may eliminate the appropriate five or three degrees of freedom respectively. This facility is extremely useful when data for a full three-dimensional analysis is unavailable, or when a simple model is being analyzed. This is achieved by the use of the deactivated freedom function in Aqwa.

If an offshore structure system consists of  $M$  structures and the general matrix form of the equations of motion in the time domain is expressed as

$$\mathbf{M} \ddot{\mathbf{U}} = \mathbf{F} \quad (8.14)$$

where  $\mathbf{M}=[M_{jk}]$  is a  $6M \times 6M$  structural mass matrix and  $\mathbf{F}=[F_j]$  is the external force  $6M \times 1$  matrix, then the deactivation of the  $m$ -th degree of freedom in the whole structure system leads to the corresponding coefficients and force components in [Equation 8.14 \(p. 134\)](#) to be adjusted as

$$\begin{aligned} M_{mj} &= \begin{cases} 0 & \text{where } j=1,6 \times M \text{ and } j \neq m \\ 1 & \text{where } j=m \end{cases} \\ F_m &= 0 \end{aligned} \quad (8.15)$$

With these corrections, the acceleration response of the  $m$ -th degree of freedom is guaranteed to be zero in a time domain analysis procedure.

It should be noted that the deactivated degree of freedom refers to motion of the center of gravity in the fixed reference axes (FRA), not the local structure axes (LSA) described in [Local Structure Axes \(p. 12\)](#).



---

# Chapter 9: Moorings and Fenders

---

Mooring systems, fenders, drum winches, and pulleys are widely applied in marine and harbor engineering operations. Aqwa provides a comprehensive set of mooring or hawser configurations to numerically simulate these marine structure auxiliaries. The types of mooring lines available include both linear and nonlinear cables. These can be summarized as follows:

- Linear Cables:
  - Linear elastic cable
  - Winch cable
  - Constant force cable
  - Pulley
  - Drum winch cable
- Nonlinear Cables:
  - Steel wire cable
  - Nonlinear cable (described by a polynomial of up to fifth order or 2-D load extension database)
  - Quasi-static composite catenary cable (with intermediate buoys and clump weights)
  - Dynamic composite catenary cable (with bending stiffness, intermediate buoys, and clump weights)
- Nonlinear Fenders:
  - Fixed and floating fenders (with nonlinear stiffness properties)

In Aqwa frequency domain analysis and equilibrium prediction, one or more mooring lines may be set to be broken under any specified environment configuration. In Aqwa time domain analysis, the user may further set the time at which the mooring line breaks, and/or provide the breaking tensions at mooring attachment points.

---

## 9.1. Linear Elastic Cable

---

A linear elastic cable is the simplest numerical model of an actual mooring line. It is defined by the stiffness, initial unstretched length and two attachment points of the mooring line on the linked structures. This line is assumed to have no mass and is therefore represented geometrically by a straight line.

Denoting  $k$  as the mooring line stiffness and  $L_0$  as its initial unstretched length, and  $\vec{X}_1(t), \vec{X}_2(t)$  as the attachment points on the two structures (in the fixed reference axes, where one structure may be a fixed location, for instance an anchor point), the tension on the mooring line is defined as

$$T = \begin{cases} k(L-L_0) & \text{if } L > L_0 \\ 0 & \text{if } L \leq L_0 \end{cases} \quad (9.1)$$

where the stretched length of the mooring line is  $L=|\vec{X}_1(t)-\vec{X}_2(t)|$ .

It is understood from [Equation 9.1 \(p. 138\)](#) that this type of mooring line bears tension but not compression.

## 9.2. Pulley

A linear pulley cable can also be modeled in Aqwa. Pulley line stiffness  $k$  and initial unstretched length  $L_0$  are defined similarly to the linear elastic cable described in [Linear Elastic Cable \(p. 137\)](#). Either pulley sliding friction or bearing friction can be optionally included in a pulley model.

### 9.2.1. Pulley with Sliding Friction

We assume that there is no rotation between a pulley and its axle, but the rope tends to slip over the pulley sheave surface with a friction effect.

As shown in [Figure 9.1: Pulley with Sheave Surface Sliding Friction \(p. 139\)](#), a pulley system in an equilibrium state is acted upon by two end tension forces  $\vec{T}_1, \vec{T}_2$  ( $T_2 > T_1$ ), where no inertia force on the pulley is considered.

Considering the pulley system in an equilibrium state, the total force and moment about the pulley axle center must be zero.

We assume that tension variation over the pulley sheave surface obeys the following form

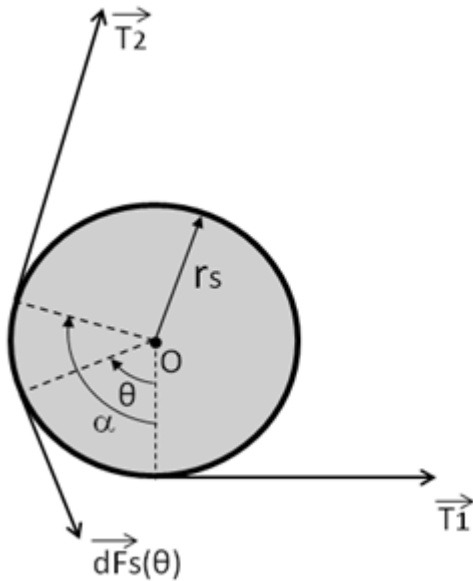
$$T(\theta)=T_1e^{\mu_s\theta} \text{ where } \theta \in [0, \alpha] \quad (9.2)$$

where  $\mu_s$  is the average sliding friction coefficient along the rope attachment section.

Denoting the radius of the sheave as  $r_s$  and the friction force over a pulley sheave surface segment  $r_s d\theta$  as  $d\vec{F}_s(\theta)$ , the friction force ensuring a load balance across this segment is

$$dF_s(\theta)=[T(\theta)+dT]\cos\frac{d\theta}{2}-T(\theta)\cos\frac{d\theta}{2}=dT=\mu_s T_1 e^{\mu_s\theta} d\theta \quad (9.3)$$

**Figure 9.1: Pulley with Sheave Surface Sliding Friction**



By integrating over the whole attached pulley sheave surface, the total friction force is:

$$\begin{aligned}\vec{F}_s &= (F_l, F_n) \\ &= \frac{\mu_s}{\mu_s^2 + 1} [\mu_s (T_2 \cos \alpha - T_1) + T_2 \sin \alpha, -\mu_s T_2 \sin \alpha - T_1 + T_2 \cos \alpha]\end{aligned}\quad (9.4)$$

where the total friction force components along the  $\vec{T}_1$  inline and normal directions are

$$\begin{aligned}F_l &= \int_0^\alpha dF_s(\theta) \cos \theta \quad \text{aligned with } \vec{T}_1 \\ F_n &= - \int_0^\alpha dF_s(\theta) \sin \theta \quad \text{normal to } \vec{T}_1\end{aligned}$$

If the tension ratio  $C_T = \frac{T_2}{T_1}$  is defined as an input pulley property when  $\alpha = \pi$ , the friction factor  $\mu_s$  can be evaluated from [Equation 9.2 \(p. 138\)](#) as

$$\mu_s = \frac{1}{\pi} \ln C_T \quad (9.5)$$

Based on the above equations, the reaction force and pulley line end tensions on a pulley system can be evaluated, as long as the attachment points and pulley axle center location are known at the current time step or iteration stage.

## 9.2.2. Pulley with Bearing Friction

Alternatively, if we assume that there is no rope slippage over the pulley surface, the pulley instead tends to rotate about its axle.

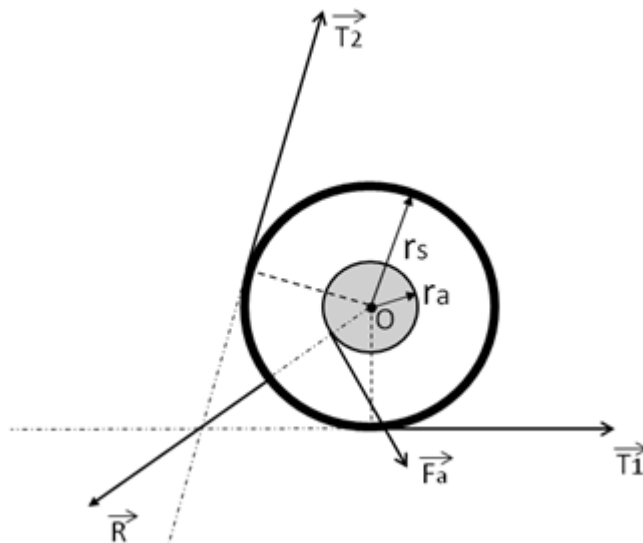
As shown in [Figure 9.2: Pulley with Axle Surface Bearing Friction \(p. 140\)](#), the radii of the pulley sheave and axle are not the same ( $r_s > r_a$ ). In this case, without considering the inertia force on the pulley, the total reaction force and moment about the axle center should be null, for example

$$\vec{R} = -(\vec{T}_2 + \vec{T}_1) \quad (9.6)$$

$$F_a r_a = \mu'_b |\vec{R}| r_a = (T_2 - T_1) r_s$$

where  $\mu'_b$  is the average bearing friction coefficient of the pulley axle.

**Figure 9.2: Pulley with Axle Surface Bearing Friction**



If the tension ratio  $C_T = \frac{T_2}{T_1}$  is defined as an input pulley property when  $\alpha=\pi$  the equivalent average bearing friction coefficient  $\mu_b$  can be determined by

$$\mu_b = \mu'_b \frac{r_a}{r_s} = \frac{C_T - 1}{C_T + 1} \quad (9.7)$$

The reaction force and pulley line end tensions on a pulley system may then be evaluated from the given attachment points and pulley axle center location at the current time step or iteration stage.

### 9.3. Linear Drum Winch

A winch or drum (winding in or paying out a linear elastic line starting at a specified time) can be modeled in Aqwa by a linear drum winch. This line is assumed to have no mass, and is therefore represented geometrically by a straight line between the drum and the attachment point.

The linear drum winch is defined by the initial length, final length, and winch speed. Positive speed indicates a paying out condition, while a negative speed means winding in.

In the paying out condition, the final length is the maximum permissible length of the line. If this length is reached, or is shorter than the initial length, all winching action will cease for the rest of the simulation.

In the winding in condition, the final length is the minimum permissible length of the line. If this length is reached, or is longer than the initial length, all winching action will cease for the rest of the simulation.

A maximum tension can also be defined to model the locked winch situation: if at any time the tension exceeds this value, all winching action will cease until the line tension drops below this value.

Denoting  $k$  as the mooring line stiffness and  $L_0$  as the unstretched length at the initial stage, the product of the Young's modulus and the cross-sectional area,  $EA$ , is assumed to be a constant and

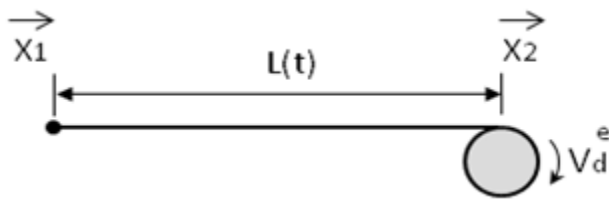
$$EA=kL_0 \quad (9.8)$$

The drum speed at a time moment  $t>t_s$ , where  $t_s$  is the specified time at which winding in or paying out starts, is defined as

$$V_d = \frac{dL_u(t)}{dt} \text{ where } t>t_s \quad (9.9)$$

where  $L_u(t)$  is the unstretched length of free line corresponding to the stretched length  $L(t)$ , as shown in [Figure 9.3: Winding in Drum Winch \(p. 141\)](#).

**Figure 9.3: Winding in Drum Winch**



Denoting  $\vec{X}_1(t), \vec{X}_2(t)$  as the attachment points on the two structures (in the fixed reference axes, where one structure may be a fixed location, for instance an anchor point), this stretched length is

$$L(t) = |\vec{X}_1(t) - \vec{X}_2(t)| \quad (9.10)$$

Based on [Equation 9.9 \(p. 141\)](#), the unstretched free line segment length is

$$L_u(t) = L_0 + V_d(t-t_s) \text{ where } t>t_s \quad (9.11)$$

The tension of the drum line is

$$T = \begin{cases} \frac{EA}{L_u(t)} [L(t) - L_u(t)] = EA\varepsilon(t) & \text{if } L(t) > L_u(t) \\ 0 & \text{if } L(t) \leq L_u(t) \end{cases} \quad (9.12)$$

In [Equation 9.9 \(p. 141\)](#), the drum speed measures the rate of change of the unstretched line length. For lines that have significant strain  $\varepsilon(t)$ , the effective speed of the drum in terms of stretched length should be considered.

When winding in, the line wound on to the drum will have the same tension as the free line segment at any particular time. This means that in order to maintain the speed defined in [Equation 9.9 \(p. 141\)](#), the effective drum speed must be increased, such that

$$V_d^e = \frac{d\{L_u(t)[1+\varepsilon(t)]\}}{dt} \approx V_d[1+\varepsilon(t)] \text{ where } t>t_s \quad (9.13)$$

This is done automatically in Aqwa. If you wish to simulate a stretched line speed for winding in, the speed specified should be input with a reduction factor of  $\frac{1}{1+\varepsilon}$ , where  $\varepsilon$  is the average strain of the line.

When paying out, the adjustment of speed is not straightforward. The elastic energy of the line on the drum will depend on exactly how the line was wound on to the drum originally. This 'energy' stored on the drum is unknown and is assumed to be zero, i.e. the line on the drum is assumed to be un-stretched. The effective winch speed is defined as

$$V_d^e = \frac{d\{L_u(t)[1 + \frac{1}{2}\varepsilon(t)]\}}{dt} \approx V_d[1 + \frac{1}{2}\varepsilon(t)] \text{ where } t > t_s \quad (9.14)$$

If you wish to simulate a stretched line speed for paying out, the speed specified should be input with a reduction factor of  $\frac{2}{2+\varepsilon}$  where  $\varepsilon$  is the average strain of the line.

It should be noted that the linear drum winch is considered as a time-history feature, and is therefore only available in Aqwa time domain analysis. An Aqwa frequency domain analysis or equilibrium simulation will treat it as a normal linear elastic line.

## 9.4. Winch Line and Force Line

A winch adjusted to constant tension and a force line representing a constant force can also be defined. These mooring lines are assumed to have no mass and are therefore represented geometrically by a straight line.

Denoting  $T_s$  as the constant tension on a winch line,  $L_0$  as the initial line length, and  $\vec{X}_1(t), \vec{X}_2(t)$  as the attachment points on the two structures (in the fixed reference axes, where one structure may be a fixed location, for instance an anchor point), this stretched length is defined by [Equation 9.1 \(p. 138\)](#). The tension on the winch is

$$T = \begin{cases} T_s & \text{if } L > L_0 \\ 0 & \text{if } L \leq L_0 \end{cases} \quad (9.15)$$

When a winding-in factor  $F_w$  (where  $F_w \geq 0$ ) is given, the tension in [Equation 9.15 \(p. 142\)](#) will be replaced by

$$T = \begin{cases} T_s(1 - F_w) & \text{if } L > L_0 \\ 0 & \text{if } L \leq L_0 \end{cases} \quad (9.16)$$

When a paying-out factor  $F_p$  (where  $F_p \geq 0$ ) is given, the tension in [Equation 9.15 \(p. 142\)](#) will be replaced by

$$T = \begin{cases} T_s(1 + F_p) & \text{if } L > L_0 \\ 0 & \text{if } L \leq L_0 \end{cases} \quad (9.17)$$

A constant force cable represents a mooring line whose second attachment point is automatically adjusted so that the force vector acting on the connecting node of the attached structure is constant. Although the first attachment point moves with the structure during the analysis, the magnitude and direction of the force acting at that point remains constant in the fixed reference axes (FRA). This type of cable therefore represents a force of constant magnitude and direction throughout the analysis.

Denoting  $F$  as the magnitude of the constant force acting on the connecting node of the attached structure and  $\vec{X}_1^0, \vec{X}_2^0$  as the initial attachment nodal locations in the fixed reference axes (of which  $\vec{X}_1^0$  is on a structure and  $\vec{X}_2^0$  is at a fixed location), the constant force acting on the connecting node of the attached structure is

$$\vec{F} = F \frac{\vec{X}_2^0 - \vec{X}_1^0}{|\vec{X}_2^0 - \vec{X}_1^0|} \quad (9.18)$$

Although presented as a type of cable, in practice a constant force cable may be used to represent any external force acting at a point on a structure whose magnitude and direction is constant. For example, a constant force cable could represent the force exerted by wind on a superstructure.

## 9.5. Weightless Nonlinear Mooring Line

Weightless nonlinear mooring line properties can be defined using the following three forms in Aqwa. These nonlinear mooring lines are assumed to have no mass and are therefore represented geometrically by a straight line.

### 9.5.1. Steel Wire

A steel wire cable with nonlinear properties can be modeled in Aqwa. Denoting  $k_a$  as the asymptotic stiffness,  $d_a$  as the asymptotic offset,  $L_0$  as the initial unstretched mooring length, and  $\vec{X}_1(t), \vec{X}_2(t)$  as the attachment points on the two structures (in the fixed reference axes, where one structure may be a fixed location, for instance an anchor point), the tension on the steel wire cable is defined as

$$T = \begin{cases} k_a(L - L_t) & \text{if } L > L_t \\ 0 & \text{if } L \leq L_t \end{cases} \quad (9.19)$$

where

$$L = |\vec{X}_1(t) - \vec{X}_2(t)|$$

$$L_t = L_0 + d_a \tanh\left(\frac{L - L_0}{d_a}\right)$$

The names of the constants  $k_a$  and  $d_a$  arise from the fact that at large extensions,  $\tanh\left(\frac{L - L_0}{d_a}\right)$  tends to unity and [Equation 9.19 \(p. 143\)](#) tends to the asymptotic form of

$$T = \begin{cases} k_a(L - L_0 - d_a) & \text{if } L > L_0 + d_a \\ 0 & \text{if } L \leq L_0 + d_a \end{cases} \quad (9.20)$$

### 9.5.2. Polynomial Nonlinear Mooring Line

Denoting  $L_0$  as the initial unstretched mooring line length and  $\vec{X}_1(t), \vec{X}_2(t)$  as the attachment points on the two structures (in the fixed reference axes, where one structure may be a fixed location, for instance an anchor point), the tension as a polynomial function of the mooring line extension is defined as

$$T = \begin{cases} k_1 \Delta L + k_2 (\Delta L)^2 + k_3 (\Delta L)^3 + k_4 (\Delta L)^4 + k_5 (\Delta L)^5 & \text{if } \Delta L > 0 \\ 0 & \text{if } \Delta L \leq 0 \end{cases} \quad (9.21)$$

where  $k_j$  ( $j = 1, 5$ ) are the coefficients of the polynomial function and

$$L = |\vec{X}_1(t) - \vec{X}_2(t)|$$

$$\Delta L = L - L_0$$

When a polynomial nonlinear line is used as a winch line, the winch tension  $T_s$  can be specified together with a winding in factor  $F_w$  or paying out factor  $F_p$ . The tension in the polynomial winch line when winding in is given by:

$$T_w = T_s(1 - |F_w|) \quad (9.22)$$

When paying out, the tension is given by:

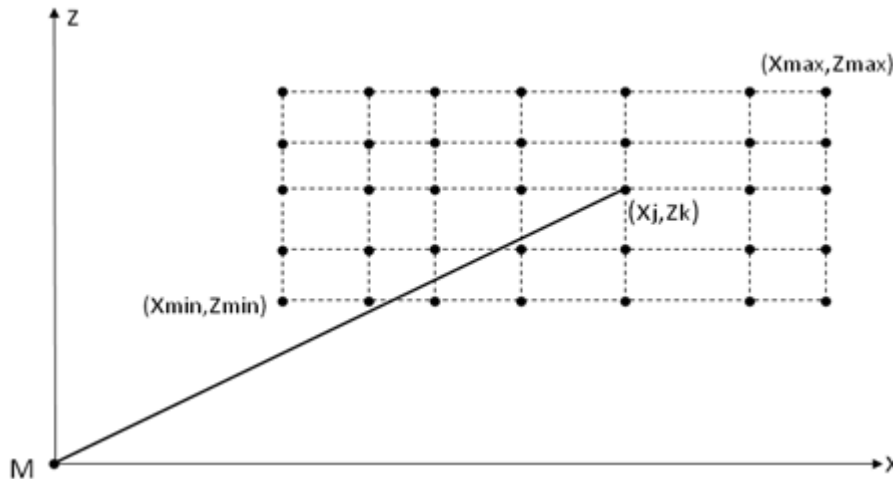
$$T_p = T_s(1 + |F_p|) \quad (9.23)$$

### 9.5.3. Nonlinear Mooring with 2-Dimensional Load Extension Database

The nonlinear properties of a mooring line can be defined by a set of load extension characteristics.

To define these properties, a mooring line local Cartesian coordinate system Mxyz is introduced, where the origin is the lower attachment point of the mooring line, the z-axis points vertically upwards, and the mooring line is in the local Mxz plane, as shown in [Figure 9.4: 2-D Load Extension Database \(p. 144\)](#).

**Figure 9.4: 2-D Load Extension Database**



To build a 2-D extension database a number of z-levels are chosen; in other words,  $z_k \in [z_{\min}, z_{\max}]$  for  $k=1, N$ . On each z-level a number of points are selected as  $(x_j, z_k)$  where  $x_j \in [x_{\min}, x_{\max}]$  for  $j=1, M$ . The mooring tension components  $(H_{jk}, V_{jk})$  along the local x- and z-axes are then given at those points. The stiffness matrix that can be formed from the 2-D load/extension database is evaluated as follows:

$$\mathbf{K} = \begin{bmatrix} k_{xx} & k_{xy} & k_{xz} \\ k_{yx} & k_{yy} & k_{yz} \\ k_{zx} & k_{zy} & k_{zz} \end{bmatrix} = \begin{bmatrix} \frac{\partial H}{\partial x} & 0 & \frac{\partial H}{\partial z} \\ 0 & \frac{H}{x} & 0 \\ \frac{\partial V}{\partial x} & 0 & \frac{\partial V}{\partial z} \end{bmatrix} \quad (9.24)$$

It should be considered that the values of  $\frac{\partial H}{\partial z}$  and  $\frac{\partial V}{\partial x}$  for a completely elastic mooring line must be equal. You must input values of  $(H_{jk}, V_{jk})$  at  $(x_j, z_k)$  that obey this condition. Failure to do so will result in an unphysical mooring system that generates or absorbs energy.

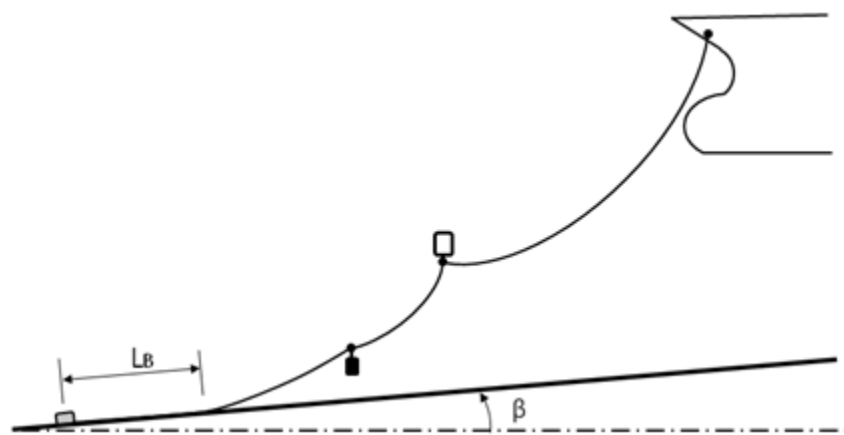
## 9.6. Quasi-Static Composite Catenary Mooring Line

The quasi-static composite catenary model permits multi-segment elastic catenary lines, which can connect a body and the (sloped) sea bed, or join two bodies.

Each catenary segment is specified by its length, mass per unit length, equivalent cross-sectional area (which is numerically equal to the volume of water displaced per unit length of the line), and its linear or nonlinear axial stiffness properties. Intermediate buoys and clump weights can be attached at catenary segment joints. Two attachment points should be provided for each catenary segment. The sea bed slope may optionally be introduced if the mooring connects a body to the sloped sea bed. An example of a quasi-static composite mooring line anchored to a sloped sea bed is demonstrated in [Figure 9.5: Composite Catenary Mooring Line \(p. 145\)](#).

In [Figure 9.5: Composite Catenary Mooring Line \(p. 145\)](#),  $L_B$  denotes the laid length of the mooring line on the seabed; the friction force acting on this mooring line section is ignored.

**Figure 9.5: Composite Catenary Mooring Line**



An iterative procedure is involved in the simulation of a multiple-segment catenary mooring line fitted with intermediate buoys and clump weights, based on the catenary segment solution with either linear or nonlinear axial elasticity.

Current drag and inertia force on the quasi-static line itself are ignored.

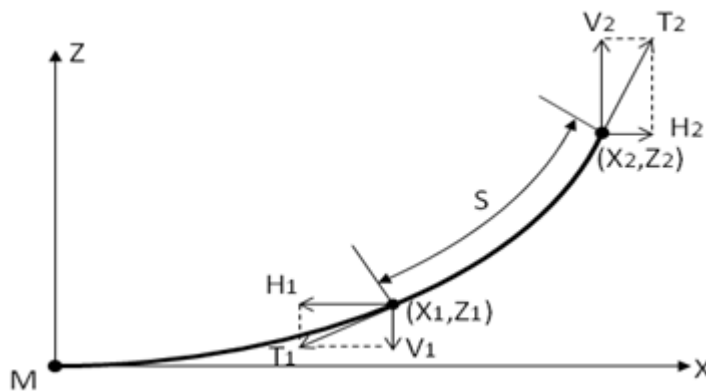
### 9.6.1. Catenary Segment with Influence of Axial Linear Elasticity

Each catenary segment in Aqwa is considered to be uniform. As the solution of the catenary equations is well documented (for example, as described in [4]) a summary of the solution is presented in this manual.

The equations can be expressed in a mooring local axis system Mxyz, whose local x-axis is a projection on to the sea bed of the vector joining the two attachment points and whose z-axis points vertically

upwards. At the origin the catenary line profile has zero slope, i.e.  $\frac{dY}{dX}=0$ , as shown in [Figure 9.6: Catenary Solution \(p. 146\)](#).

**Figure 9.6: Catenary Solution**



For a catenary which has zero slope at the contact/attachment point on the sea bed these equations can be written as

$$\begin{aligned} H_2 &= AE \sqrt{\left(\frac{T_2}{AE} + 1\right)^2 - \frac{2wZ_2}{AE}} - AE = H \\ X_2 &= \frac{H_2}{w} \sinh^{-1}\left(\frac{wL}{H_2}\right) + \frac{H_2 L}{AE} \\ V_2 &= wL \\ T_2 &= \sqrt{H_2^2 + V_2^2} \end{aligned} \quad (9.25)$$

where  $L$  is the unstretched suspended length from the origin to the attachment point  $(X_2, Z_2)$  (for a given tension force  $\vec{T}_2 = (H_2, V_2) = (H, V_2)$  at the point  $(X_2, Z_2)$ , for instance at the fairlead),  $w$  is the submerged weight per unit length, and  $EA$  is the stiffness per unit length.

The stretched length of the suspended catenary line is

$$L' = L + \frac{1}{2wAE} \left\{ wL \sqrt{H^2 + (wL)^2} + H^2 \ln[wL + \sqrt{H^2 + (wL)^2}] - H^2 \ln|H| \right\} \quad (9.26)$$

When the unstretched length of a catenary segment from its top right end  $(X_2, Z_2)$  is  $S$ , where  $S$  is shorter than the theoretical unstretched suspended length  $L$ , and the tension force at the top right end is known, the position of the bottom left end of this segment is

$$\begin{aligned} X_1 &= \frac{H}{w} \ln \frac{V_2 + T_2}{V_1 + T_1} + \frac{HS}{AE} \\ Y_1 &= \frac{V_2 + V_1}{T_2 + T_1} S + S \frac{V_2 + V_1}{2AE} \end{aligned} \quad (9.27)$$

The horizontal and vertical components of the tension at the left-hand end are

$$\begin{aligned} H_1 &= H \\ V_1 &= V_2 - wS \\ T_1 &= \sqrt{H_1^2 + T_1^2} \end{aligned} \quad (9.28)$$

The stretched length of this catenary segment is

$$S' = S + \frac{1}{2wAE} (V_2 T_2 - V_1 T_1 + H^2 \ln \frac{V_2 + T_2}{V_1 + T_1}) \quad (9.29)$$

The extension of this segment is

$$\Delta S = S' - S \quad (9.30)$$

### 9.6.2. Catenary Segment with Influence of Axial Nonlinear Elasticity

For a catenary segment with nonlinear axial stiffness, as a standard input data format the nonlinear axial stiffness property is defined in the form of

$$EA = EA(\text{constant}) + a\varepsilon + b\varepsilon^2 + c\varepsilon^3 \quad (9.31)$$

in the range  $0 \leq \varepsilon \leq \varepsilon_{\max}$ .

From the above definition, the tension on the cable can be expressed as

$$\begin{aligned} T(\varepsilon) &= \int_0^{\varepsilon} EA d\varepsilon \\ &= EA(\text{constant})\varepsilon + \frac{1}{2}a\varepsilon^2 + \frac{1}{3}b\varepsilon^3 + \frac{1}{4}c\varepsilon^4 \end{aligned} \quad (9.32)$$

Numerically, the series form of the strain function with respect to the tension can be derived from Equation 9.32 (p. 147):

$$\varepsilon(T) = \sum_{j=0} B_j (T - T_0)^j \quad (9.33)$$

in the range  $0 \leq \varepsilon \leq \varepsilon_{\max}$ , where  $T_0 = T(\varepsilon_0)$ .

An intermediate tension is introduced here, which is

$$T_{12} = \frac{\bar{V}\Delta y + H\Delta x}{S} \quad (9.34)$$

where

$$\begin{aligned} \Delta x &= \frac{H}{w} \ln \frac{V_2 + T_2}{V_1 + T_1} \\ \Delta y &= \frac{T_2 - T_1}{w} \\ \bar{V} &= \frac{V_2 + V_1}{2} \end{aligned}$$

An equivalent nonlinear tension is also introduced:

$$\varepsilon_2 = \frac{1}{2} [\bar{\varepsilon}(T_1, T_{12}) + \bar{\varepsilon}(T_{12}, T_2)] \quad (9.35)$$

where

$$\bar{\varepsilon}(f_1, f_2) = \frac{1}{F_2 - F_1} \int_{F_1}^{F_2} \varepsilon(T) dT$$

in which

$$\begin{aligned}F_2 &= \max(f_2 - f_1) \\F_1 &= \min(f_2 - f_1)\end{aligned}$$

In addition, the equivalent tension is denoted as

$$T^e = \frac{1}{2S} [\bar{T}S + \bar{V}\Delta y + H\Delta x] \quad (9.36)$$

$$\text{where } \bar{T} = \frac{T_2 + T_1}{2}$$

Finally, the bottom left-hand positions and extension of the nonlinear axial stiffness catenary line segment can be expressed as

$$\begin{aligned}X_1 &= \Delta x + S \frac{H}{AE^e} \\Y_1 &= \Delta y + \frac{\text{sgn}(\bar{V})}{|w|} \int_{T_1'}^{T_2'} \varepsilon(T) dT \\AS &= S \frac{T^e}{AE^e}\end{aligned} \quad (9.37)$$

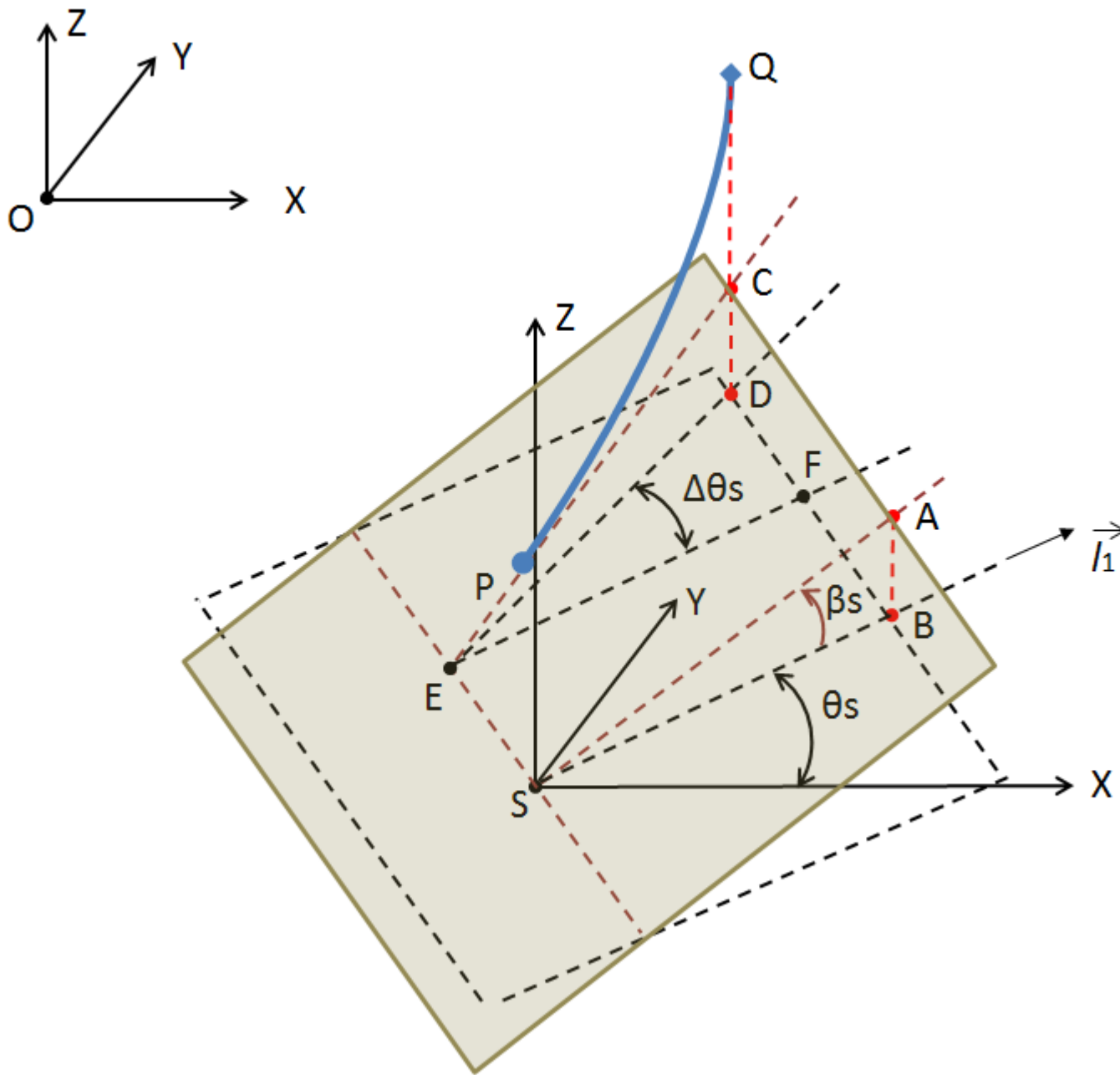
where  $T_2' = \max(T_1, T_2)$ ,  $T_1' = \min(T_1, T_2)$ , and the equivalent nonlinear stiffness is defined as

$$AE^e = \frac{T^e}{\varepsilon_2} \quad (9.38)$$

### 9.6.3. Cable on Global Sloped Seabed

A global sloped seabed can be defined for quasi-static composite cable analysis.

As shown in [Figure 9.7: Global Sloped Seabed Definition \(p. 149\)](#), a local seabed right-hand Cartesian frame SXYZ is defined, in which the origin is on the seabed reference point S and the local axes are parallel to the corresponding axes of the fixed reference axes. The seabed slope angle  $\beta_S$  is the angle between the steepest upward path on the seabed and the horizontal plane. The seabed azimuth angle  $\theta_S$  is the angle between the projection of the steepest path on the horizontal plane and the local x-axis.

**Figure 9.7: Global Sloped Seabed Definition**

To express the relevant geometric information of the seabed and the composite cable, point A is designated as a point on the line passing through a reference point S and being in the steepest upward direction on the seabed. Point B is the intersection point between the horizontal SXY plane and the vertical line across point A. The angle between line SA and line SB defines the seabed slope angle  $\beta_s$ , the angle between line SB and the x-axis of SXYZ gives the seabed azimuth angle  $\theta_s$ .

By denoting the anchor point on the seabed as P:  $\vec{X}_P = (X_P, Y_P, Z_P)$  in the global fixed reference frame, the following equation is satisfied:

$$Z_P = Z_S + (X_P - X_S, Y_P - Y_S, 0) \cdot \vec{l}_1 \tan \beta_s \quad (9.39)$$

where  $\vec{l}_1 = (\cos \theta_S, \sin \theta_S, 0)$  is the seabed azimuth directional vector in the fixed reference axes.

Assuming that the attachment point of a composite mooring Q:  $\vec{X}_Q = (X_Q, Y_Q, Z_Q)$  is above the seabed but not on the vertical line across point P, the mooring vertical plane which point P and point Q are on can be uniquely determined. Defining the vertical line across point Q, this line has an intersection point with the seabed at point C and an intersection point with the SXY plane at point D. Point E is the intersection point of the SXY plane and the line crossing points C and P. Line EF parallels to line SB, and the relative azimuth angle of the mooring vertical plane and the seabed direction is  $\Delta\theta_S$ .

Based on the definitions above, the coordinate of point C:  $\vec{X}_C = (X_C, Y_C, Z_C)$  is determined by:

$$\begin{aligned} X_C &= X_Q \\ Y_C &= Y_Q \\ Z_C &= Z_S + (X_Q - X_S, Y_Q - Y_S, 0) \cdot \vec{l}_1 \tan \beta_S \end{aligned} \quad (9.40)$$

The coordinate of point D:  $\vec{X}_D = (X_D, Y_D, Z_D)$  is:

$$\vec{X}_D = (X_Q, Y_Q, 0) \quad (9.41)$$

and the coordinate of point E:  $\vec{X}_E = (X_E, Y_E, Z_E)$  is:

$$\vec{X}_E = \frac{Z_P}{Z_P - Z_C} (\vec{X}_C - \vec{X}_P) + \vec{X}_P \quad (9.42)$$

In the general case of  $Z_P \neq Z_C$ , the relative azimuth angle of the mooring vertical plane is given by:

$$\Delta\theta_S = \tan^{-1}\left(\frac{Z}{X}\right) \quad (9.43)$$

where

$$\begin{aligned} x &= \vec{l}_1 \cdot (\vec{X}_D - \vec{X}_E) \\ (0, 0, z) &= \vec{l}_1 \times (\vec{X}_D - \vec{X}_E) \end{aligned}$$

From [Equation 9.42 \(p. 150\)](#) it can be observed that point E does not exist if  $Z_P = Z_C$ . In this special case, the relative azimuth angle of the mooring vertical plane is:

$$\Delta\theta_S = \pm \frac{\pi}{2} \quad (9.44)$$

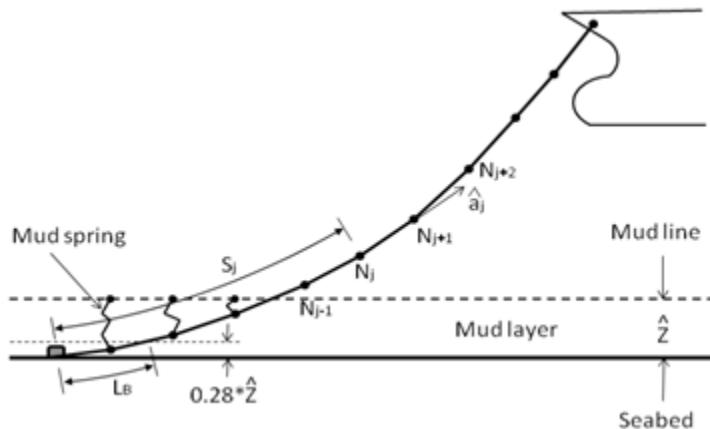
## 9.7. Dynamic Composite Catenary Mooring Line

When the dynamics of a cable are included in the cable motion analysis, the effects of the cable mass, drag forces, inline elastic tension, and bending moment are considered. Forces on the cable will vary in time, and the cable will generally respond in a nonlinear manner. The solution is fully coupled: the cable tensions and motions of the vessel are considered to be mutually interactive, where cables affect vessel motion and vice versa.

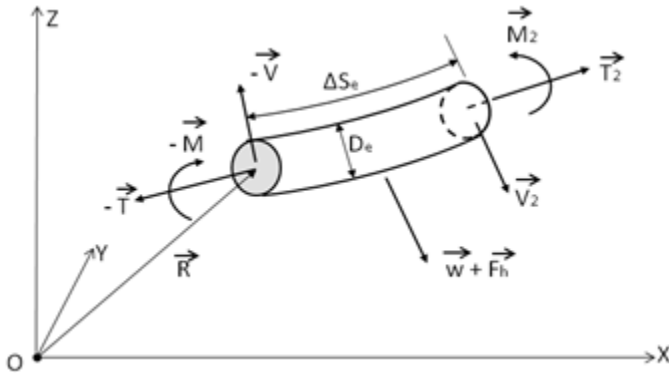
The simulation of cable dynamics in Aqwa uses a discretization along the cable length and an assembly of the mass and applied/internal forces. In principle, this approach should give the same solution as any of the methods applied in Aqwa that have been described previously. However, in the case of a dynamic cable the inline stiffness is extremely large compared with the transverse stiffness. In addition, the sea bed is modeled with nonlinear springs and dampers, chosen to minimize discontinuities and energy losses at the touchdown point due to the discretization. Forces on each element of the cable are determined and assembled into a symmetric banded global system ready for solution directly (in the static/frequency domain) or by integrating in time.

**Figure 9.8: Modeling of a Dynamic Cable (p. 151)** shows the configuration of a dynamic cable in discrete form in the fixed reference axes (FRA). Each dynamic mooring line is modeled as a chain of Morison-type elements subjected to various external forces.  $\hat{a}_j = (a_1, a_2, a_3)$  denotes the unit axial vector from the  $j$ -th node to the  $(j+1)$ -th node in the fixed reference axes, while  $S_j$  is the unstretched cable length from the anchor point (or the first attachment point on the structure) to the  $j$ -th node. The sea bed is assumed to be horizontal and flat. The reaction force of the sea bed on the mooring line is modeled by mud line springs at each node. Each mud line spring is attached between the top of the artificial mud layer and the cable element node, if the node is located below the mud line level. The depth of the mud layer is  $\hat{z}$  above the seabed. The laid length  $L_B$  of a dynamic mooring line on the sea bed is measured from the anchor to the touchdown point, which is defined as  $0.28\hat{z}$  above the seabed.

**Figure 9.8: Modeling of a Dynamic Cable**



A single element of a circular slender cable is shown in [Figure 9.9: Forces on a Cable Element \(p. 152\)](#), which is subjected to external hydrodynamic loadings as well as to structural inertia loading. Torsional deformation is not included in Aqwa dynamic cable analysis.

**Figure 9.9: Forces on a Cable Element**

The motion equation of this cable element is

$$\begin{aligned} \frac{\partial \vec{T}}{\partial s_e} + \frac{\partial \vec{V}}{\partial s_e} + \vec{w} + \vec{F}_h &= m \frac{\partial^2 \vec{R}}{\partial t^2} \\ \frac{\partial \vec{M}}{\partial s_e} + \frac{\partial \vec{R}}{\partial s_e} \times \vec{V} &= -\vec{q} \end{aligned} \quad (9.45)$$

where  $m$  is the structural mass per unit length,  $\vec{q}$  is the distributed moment loading per unit length,  $\vec{R}$  is the position vector of the first node of the cable element,  $\Delta S_e$  and  $D_e$  are the length and diameter of the element respectively,  $\vec{w}$  and  $\vec{F}_h$  are the element weight and external hydrodynamic loading vectors per unit length respectively,  $\vec{T}$  is the tension force vector at the first node of the element,  $\vec{M}$  is the bending moment vector at the first node of the element, and  $\vec{V}$  is the shear force vector at the first node of the element.

The bending moment and tension are related to the bending stiffness  $EI$  and the axial stiffness  $EA$  of the cable material through the following relations:

$$\begin{aligned} M &= EI \frac{\partial \vec{R}}{\partial s_e} \times \frac{\partial^2 \vec{R}}{\partial s_e^2} \\ T &= EA \varepsilon \end{aligned} \quad (9.46)$$

where  $\varepsilon$  is the axial strain of the element.

To ensure a unique solution to [Equation 9.45 \(p. 152\)](#), pinned connection boundary conditions are imposed at the top and bottom ends:

$$\begin{aligned} \vec{R}(0) &= \vec{P}_{bot} \\ \vec{R}(L) &= \vec{P}_{top} \\ \frac{\partial^2 \vec{R}(0)}{\partial s_e^2} &= \vec{0} \\ \frac{\partial^2 \vec{R}(L)}{\partial s_e^2} &= \vec{0} \end{aligned} \quad (9.47)$$

where  $\vec{P}_{bot}$ ,  $\vec{P}_{top}$  are the locations of the cable attachment points and  $L$  is the total unstretched length of the cable.

The dynamic response of the cable with bending governed by [Equation 9.45 \(p. 152\)](#), [Equation 9.46 \(p. 152\)](#), and [Equation 9.47 \(p. 152\)](#) is solved numerically by employing the discrete Lump-Mass model. As shown

in [Figure 9.8: Modeling of a Dynamic Cable \(p. 151\)](#), the cable is discretized into a number of finite elements where the mass of each element is concentrated into a corresponding node.

The unit axial vector  $\hat{a}_j$  of an element  $j$ , which corresponds to the slope of that element, from one element to the next, is given by:

$$\hat{a}_j = \frac{\vec{R}_{j+1} - \vec{R}_j}{L_j} \quad (9.48)$$

where the unstretched element length is  $\Delta S_{ej} \approx L_j = |\vec{R}_{j+1} - \vec{R}_j|$ .

The curvature vector at node  $j$  is given by the rate of change of slope, which can be calculated from the cross product of the unit vectors along two adjacent elements, i.e.

$$\vec{C}_j = -\frac{\partial \vec{R}}{\partial s_e} \times \frac{\partial^2 \vec{R}}{\partial s_e^2} \Big|_j = \frac{1}{L_j} \hat{a}_j \times \hat{a}_{j-1} \quad (9.49)$$

where the effective length of the  $j$ -th node in this context is  $\bar{L}_j = \frac{L_j + L_{j-1}}{2}$ .

$EI$  is assumed to be constant between two adjacent elements. From [Equation 9.46 \(p. 152\)](#) the bending moment at node  $j$  is:

$$\vec{M}_j = -(EI)_j \vec{C}_j \quad (9.50)$$

For the general configuration of cables, the axial stiffness  $EA$  is of a higher order than the bending stiffness  $EI$ , so that we may assume that the axial strain is small and the bending stiffness factor  $\frac{(EI)_j}{\bar{L}_j}$  is constant.

The  $3 \times 3$  axial and normal directional tensors are now introduced, as

$$\begin{aligned} \mathbf{A}_j &= \hat{a}_j^T \hat{a}_j \\ \mathbf{N}_j &= \mathbf{I} - \mathbf{A}_j \end{aligned} \quad (9.51)$$

If the distributed bending moment is zero, from [Equation 9.45 \(p. 152\)](#) and [Equation 9.51 \(p. 153\)](#) the matrix form of the shear force on element  $j$  is expressed as

$$[V_{(j)}] = -\frac{1}{\bar{L}_j} \mathbf{N}_j [(EI)_{j+1} \frac{1}{\bar{L}_{j+1}} \hat{a}_{j+1}^T + (EI)_j \frac{1}{\bar{L}_j} \hat{a}_{j-1}^T] \quad (9.52)$$

Integrating both sides of the motion equation given in [Equation 9.45 \(p. 152\)](#), for an element  $j$ , the motion of that element with respect to its two ends can be expressed in a matrix form:

$$\begin{bmatrix} -T_j \hat{a}_j^T \\ T_{j+1} \hat{a}_j^T \end{bmatrix} + \begin{bmatrix} -[V_j] \\ [V_{j+1}] \end{bmatrix} + \frac{L_j}{2} \begin{bmatrix} [\vec{w} + \vec{F}_h]^T \\ [\vec{w} + \vec{F}_h]^T \end{bmatrix} = \frac{mL_j}{2} \frac{\partial^2}{\partial t^2} \begin{bmatrix} \vec{R}_j^T \\ \vec{R}_{j+1}^T \end{bmatrix} \quad (9.53)$$

in which  $[V_j] = [V_{(j-1)}] - [V_{(j)}]$  is the shear force at node  $j$ , which is calculated from the two adjacent elements. Note that in the current notation, an index in parentheses e.g.  $(j)$  refers to an element, while an index without the parentheses refers to a node.

To maintain generality, assume that there is an intermediate clump weight/buoy attached at node  $j$ , but no clump/buoy mass is attached at node  $j+1$ . The mass of this clump weight/buoy is  $M$ . Then the total gravity forces at node  $j$  and node  $j+1$  for the element ( $j$ ), in a  $6 \times 1$  matrix form and in the fixed reference axes, are

$$\mathbf{w} = (\vec{w}_j, \vec{w}_{j+1})^T = \left\{ 0, 0, -\frac{1}{2}(mL_j + M)g, 0, 0, -\frac{1}{2}mL_j g \right\}^T \quad (9.54)$$

where  $g$  is the acceleration due to gravity. We assume that half of the gravitational force due to the clump weight/buoy will act on the other (i.e. the adjacent) element to which the  $j$ -th node is attached.

The wave excitation force on a dynamic cable is ignored. Hence in [Equation 9.53 \(p. 153\)](#) the hydrodynamic force,  $\mathbf{F}_h$ , acting on a cable element consists of the buoyant force, the drag force, and the (added mass related) radiation force, for example

$$\mathbf{F}_h = \mathbf{F}_b + \mathbf{F}_d - \mathbf{m}_a [\vec{a}_j, \vec{a}_{j+1}]^T \quad (9.55)$$

where  $\mathbf{m}_a$  is the cable element added mass matrix including the added mass contribution of the attached intermediate clump weight/buoy, and  $\vec{a}_j$  is the acceleration of the cable at node  $j$ .

Denoting the equivalent cross-sectional area of the mooring line as  $A_{cj}$  and the displaced mass of water of the intermediate clump weight/buoy as  $M_b$ , the element buoyant force matrix is

$$\mathbf{F}_b = \left\{ 0, 0, \frac{1}{2}(\rho_w A_{cj} L_j + M_b)g, 0, 0, \frac{1}{2}\rho_w A_{cj} L_j g \right\}^T \quad (9.56)$$

where  $\rho_w$  is the density of water.

The time-dependent drag force on the mooring line element is expressed in a simplified form as

$$\mathbf{F}_d(t) = \begin{cases} \mathbf{f}_d(j) - \frac{1}{2} C_{dc} S_c \rho_w |\mathbf{U}_j(t) - \mathbf{V}_j(t)| \{\mathbf{U}_j(t) - \mathbf{V}_j(t)\} \\ \mathbf{f}_d(j+1) \end{cases} \quad (9.57)$$

where  $\mathbf{V}_j(t) = (v_{xj}(t), v_{yj}(t), v_{zj}(t))^T$  is the matrix form of the structural velocity at node  $j$  at time  $t$ ,  $\mathbf{U}_j = \vec{U}_j^T = (U_{xj}, U_{yj}, 0)^T$  is the matrix form of the current velocity at the location of node  $j$ ,  $C_{dc}$  is the drag coefficient of the clump weight/buoy (attached at node  $j$ ) which has corresponding projected surface area  $S_c$ , and the drag force on node  $j$  connected to a mooring line element is

$$\begin{aligned} \mathbf{f}_d(j) = & -\frac{1}{4} C_x \rho_w D_j L_j |\mathbf{A}_j \{\mathbf{U}_j(t) - \mathbf{V}_j(t)\}| \mathbf{A}_j \{\mathbf{U}_j(t) - \mathbf{V}_j(t)\} \\ & -\frac{1}{4} C_d \rho_w D_j L_j |\mathbf{N}_j \{\mathbf{U}_j(t) - \mathbf{V}_j(t)\}| \mathbf{N}_j \{\mathbf{U}_j(t) - \mathbf{V}_j(t)\} \end{aligned}$$

in which  $C_d$  and  $C_x$  are the transverse and inline drag coefficients respectively.

[Equation 9.57 \(p. 154\)](#) provides a simplified form of the drag force on a mooring line element; a more accurate form may be applied by integrating the drag force over the length of the element to take the variation of the current velocity along the element into account. This is performed in Aqwa using a Gaussian integration scheme.

The reaction force of the sea bed on the mooring line is modeled by a mud line spring at each node within the mud layer. If the position of node  $j$  is  $\vec{R}_j = (x_j, y_j, z_j)$ , the water depth is  $d$ , and the depth

of the mud layer is  $\hat{z}$ , the magnitude of the reaction force due to the mud spring on node  $j$  is defined as

$$F_{zj} = \begin{cases} 0, & \text{if node } j \text{ is above mud line,} \\ \frac{mg}{\hat{z}} \left[ -d - z_j + \hat{z} - \frac{\hat{z}}{\pi} \sin 2\theta \right], & \text{if node } j \text{ is in mud layer,} \\ \frac{mg}{\hat{z}} \left[ \hat{z} - 2(d + z_j) \right], & \text{if node } j \text{ is beneath seabed,} \end{cases} \quad (9.58)$$

where  $m'$  is the net mass at node  $j$ , i.e.  $m' = \text{structural mass} - \text{displaced mass of water}$ , and

$$\theta = -\frac{\pi(d + z_j - \hat{z})}{2\hat{z}}.$$

It is also assumed that the mud line springs are critically damped, where the damping force at node  $j$  in the vertical direction is defined as

$$F_{zsdj} = \begin{cases} 0 & \text{if node } j \text{ is above the mud line} \\ -4m_{tj}v_{sj}(t)\sin^2\theta & \text{if node } j \text{ is in the mud layer} \\ -4m_{tj}v_{sj}(t) & \text{if node } j \text{ is beneath the sea bed} \end{cases} \quad (9.59)$$

where  $m_{tj}$  is the sum of the structural mass and added mass at node  $j$ .

The Coulomb friction model is applied for the estimation of sea bed friction force on dynamic cables. The Coulomb function is written as:

$$F_f = \mu F_z \quad (9.60)$$

where  $\mu$  is the constant friction coefficient, and  $F_z$  is the magnitude of the normal reaction force of the sea bed.

The direction of the friction force is opposite to the in-plane velocity of the cable on the sea bed, so [Equation 9.60 \(p. 155\)](#) could be rewritten as

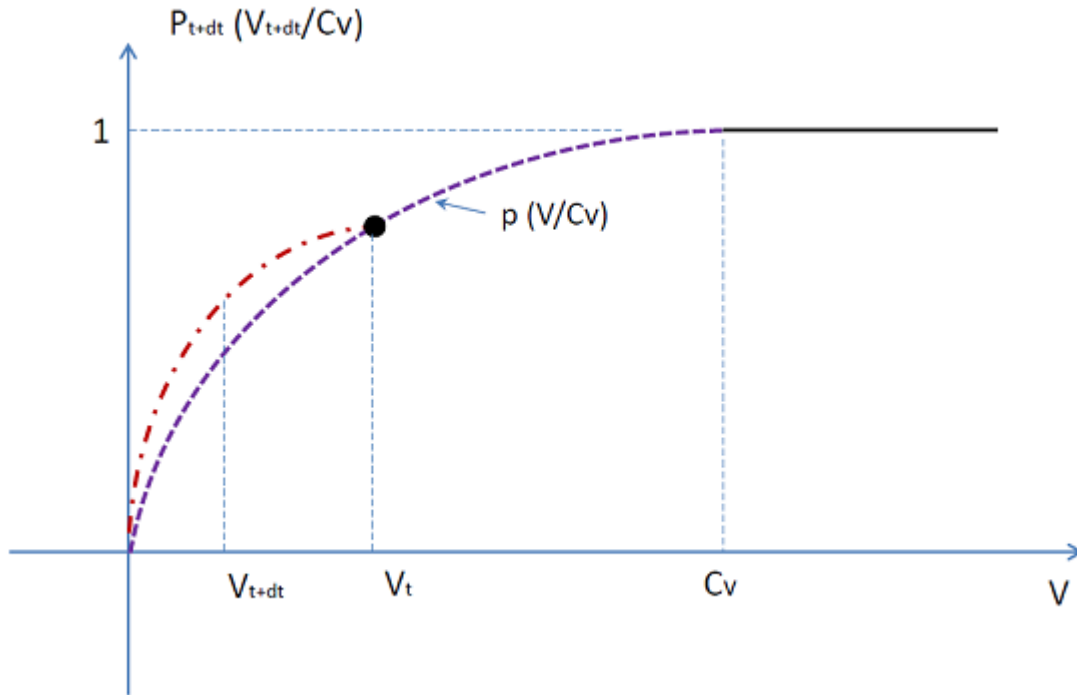
$$\mathbf{F}_f = -\mu F_z \frac{\mathbf{V}}{V} \quad (9.61)$$

where  $\mathbf{V}$  is the in-plane velocity of the laid-down segment of a mooring line on the sea bed and  $V = |\mathbf{V}|$ .

To avoid numerical instability problems when the slip velocity or the movement changes direction, the friction force is set to be linear or nonlinear varying within a transition zone [35]. By introducing a single parameter transition function, the extended Coulomb friction model is expressed as:

$$\mathbf{F}_f = -\mu F_z p\left(\frac{V}{C_v}\right) \frac{\mathbf{V}}{V} \quad (9.62)$$

where  $C_v$  is the ramp velocity threshold (or critical velocity),  $p\left(\frac{V}{C_v}\right)$  is the transition function, which satisfies  $p(0)=0, p(1)=1$ , as shown in [Figure 9.10: Double Quadratic Transition Function \(p. 156\)](#).

**Figure 9.10: Double Quadratic Transition Function**

In the Aqwa time domain dynamic cable analysis, the ramp velocity threshold is defined as:

$$C_v = \frac{\pi}{8T} D \quad (9.63)$$

where  $D$  is the diameter of the cable and  $T$  is the zero-cross or characteristic wave period.

A second-order polynomial form of the transition function is introduced by Ostergaard et al. [35], which is determined with an additional condition of  $\frac{dp}{dV} = 0$  when  $V = C_v$ :

$$p\left(\frac{V}{C_v}\right) = \begin{cases} \frac{V}{C_v} \left(2 - \frac{V}{C_v}\right) & V < C_v \\ 1 & V \geq C_v \end{cases} \quad (9.64)$$

A double quadratic extension Coulomb friction mode, as shown in [Figure 9.10: Double Quadratic Transition Function \(p. 156\)](#), is introduced in Aqwa time domain analysis to smooth the variation of friction when the magnitude of node velocity decreases compared to the previous time step.

The double quadratic transition function in Aqwa time domain analysis is expressed as:

$$(1) \mathbf{V}_t \cdot \mathbf{V}_{t+dt} \geq 0 \quad P_{t+dt} = \begin{cases} \max \left\{ p\left(\frac{V_{t+dt}}{C_v}\right), P_t \right\} & V_{t+dt} \geq \max \{V_t, C_v\} \\ P_t \cdot p\left(\frac{V_{t+dt}}{C_v}\right) & V_{t+dt} < V_t \end{cases}$$

$$(2) \mathbf{V}_t \cdot \mathbf{V}_{t+dt} < 0 \quad P_{t+dt} = p\left(\frac{V_{t+dt}}{C_v}\right)$$
(9.65)

In [Equation 9.65 \(p. 156\)](#), the single parameter transition function  $p$  is given by [Equation 9.64 \(p. 156\)](#).

If the axial and lateral friction coefficients  $\mu_a$  and  $\mu_l$  are different, the equivalent friction coefficient is defined as:

$$\mu^e = \frac{\sqrt{(v_a \mu_a)^2 + (v_l \mu_l)^2}}{\sqrt{v_a^2 + v_l^2}} \quad (9.66)$$

where  $v_a$  and  $v_l$  are the cable velocity components in the sea bed inline and lateral directions, respectively.

It is found from [Equation 9.66 \(p. 157\)](#) that  $\mu^e = \mu$  if  $\mu_a = \mu_l = \mu$ .

It is assumed that the friction force may exist once a cable segment node (node  $j$ ) touches down:

$$Z_j \leq -d + 0.28\hat{Z} \quad (9.67)$$

where  $d$  is the water depth at the  $j$ -th node location and  $\hat{Z}$  is the depth of the mud layer shown in [Figure 9.8: Modeling of a Dynamic Cable \(p. 151\)](#).

The element bending stiffness matrix can be determined directly from the derivative of the shear force:

$$\begin{aligned} [dV] &= [\nabla^T \vec{V}]^T [u] \\ &= -\mathbf{K}_b [u] \end{aligned} \quad (9.68)$$

From [Equation 9.52 \(p. 153\)](#), it can be seen that the shear force on element  $j$  is a function of the positions of four nodes,  $j-1, j, j+1$ , and  $j+2$  (for the evaluation of  $\hat{a}_{j-1}$  and  $\hat{a}_{j+1}$ , defined by [Equation 9.48 \(p. 153\)](#)) so that  $\mathbf{K}_b$  is a  $12 \times 12$  matrix. Denoting the movements at these four nodes as  $[u_{j-1}], [u_j], [u_{j+1}], [u_{j+2}]$  and substituting [Equation 9.52 \(p. 153\)](#) into [Equation 9.68 \(p. 157\)](#), we have

$$\begin{aligned} [dV_{(j)}] &= \sum_{m=j-1}^{j+2} [\nabla_m^T \vec{V}_{(j)}]^T [u_m] \\ &= \sum_{m=j-1}^{j+2} -\mathbf{K}_m [u_m] \end{aligned} \quad (9.69)$$

where

$$\mathbf{K}_m^T = \frac{1}{L_j} [\mathbf{\Xi}_j \nabla_m]^T \mathbf{A}_j + (\nabla_m^T \frac{1}{L_j}) \mathbf{\Xi}_j^T \mathbf{N}_j + \frac{1}{L_j} (\nabla_m^T \mathbf{\Xi}_j^T) \mathbf{N}_j \quad (9.70)$$

in which  $\nabla_m = (\frac{\partial}{\partial x}, \frac{\partial}{\partial y}, \frac{\partial}{\partial z}) \Big|_m$  is the gradient operator with respect to the displacement at node  $m$  and

$$\mathbf{\Xi}_j = - \left\{ (EI)_{j+1} \frac{1}{L_{j+1}} [\hat{a}_{j+1} - \hat{a}_j]^T - (EI)_j \frac{1}{L_j} [\hat{a}_j - \hat{a}_{j-1}]^T \right\}$$

The axial elastic force on element  $(j)$  is a function of the deformations of two nodes, i.e.  $[u_j], [u_{j+1}]$ ,

$$-\mathbf{K}_a \begin{bmatrix} [u_j] \\ [u_{j+1}] \end{bmatrix} = d \mathbf{F} \quad (9.71)$$

where  $\mathbf{K}_a$  is the  $6 \times 6$  stiffness matrix of the mooring line element:

$$\mathbf{K}_a = \begin{bmatrix} \mathbf{K}_{33} & -\mathbf{K}_{33} \\ -\mathbf{K}_{33} & \mathbf{K}_{33} \end{bmatrix} \text{ where } \mathbf{K}_{33} = k_x \mathbf{A}_j + \frac{T_j}{L_j} \mathbf{N}_j \quad (9.72)$$

In which  $k_x$  is the inline linear stiffness or the equivalent inline stiffness for a nonlinear axial stiffness cable, which is discussed in [Catenary Segment with Influence of Axial Nonlinear Elasticity \(p. 147\)](#).

Assembling the matrices of all the elements and applying boundary conditions on the two attachment points of the mooring line, the static solution can be solved by

$$\mathbf{K}[u] = \mathbf{F}_{total} \quad (9.73)$$

where  $\mathbf{F}_{total}$  is the assembled total static force matrix.

In a time domain analysis, the solution of dynamic cable motion at the given attachment locations can be obtained by solving the following equation

$$\mathbf{M}[\ddot{u}] = \mathbf{F}_{total} \quad (9.74)$$

where  $\mathbf{F}_{total}$  and  $\mathbf{M}$  are the assembled total force matrix and the total mass matrix (including structural and added masses) respectively.

In a frequency domain analysis, all of the nonlinear terms are linearized such that

$$\{-\omega^2 \mathbf{M} - i\omega \mathbf{C} + \mathbf{K}\}[u] = \mathbf{F}_{total}(\omega) \quad (9.75)$$

where  $\mathbf{C}$  is the linearized damping matrix.

In [Equation 9.75 \(p. 158\)](#), the linearized damping is obtained from the root mean square of the relative velocity for multiple frequency solutions. The numerical approach is similar to the Morison drag linearization discussed in [Morison Drag Linearization \(p. 112\)](#).

In summary, the forces applied on the dynamic cable in the different analysis procedures are listed in [Table 9.1: Summary of Force Components on Dynamic Cable \(p. 158\)](#).

**Table 9.1: Summary of Force Components on Dynamic Cable**

| Forces applied   | Equilibrium | Frequency domain | Time domain |
|--|-------------|------------------|-------------|
| Gravitational force (cable and clump weight/buoy)      | ✓           | -                | ✓           |
| Buoyant force (cable and clump weight/buoy)            | ✓           | -                | ✓           |
| Structural inertia force (cable and clump weight/buoy) | -           | ✓                | ✓           |
| Radiation force due to added mass                      | -           | ✓                | ✓           |
| Drag force due to current and/or cable motion          | ✓           | Linearized       | ✓           |
| Linear or nonlinear axial tension                      | ✓           | Linearized       | ✓           |
| Bending moment due to cable bending stiffness          | ✓           | ✓                | ✓           |
| Seabed effect by mud-layer spring stiffness            | ✓           | Linearized       | ✓           |
| Seabed effect by mud-layer spring damping              | -           | Linearized       | ✓           |
| Seabed friction  | -           | -                | ✓           |
| Wave excitation force on cable                         | -           | -                | -           |
| Torsional moment                                       | -           | -                | -           |

| Forces applied              | Equilibrium | Frequency domain | Time domain |
|-----------------------------|-------------|------------------|-------------|
| Reaction forces at two ends | ✓           | ✓                | ✓           |

**Note:**

The check mark ' ✓ ' indicates the item is included, ' - ' indicates the item is excluded.

## 9.8. Fender

A fender can have nonlinear stiffness, friction and damping. It acts only in compression between a point on one structure and a contact plane on another.

Denoting  $L_0$  as the fender initial uncompressed size, the magnitude of the fender axis-directional compression force is defined as a polynomial function of the compression, as

$$T = \begin{cases} k_1\Delta L + k_2(\Delta L)^2 + k_3(\Delta L)^3 + k_4(\Delta L)^4 + k_5(\Delta L)^5 & \text{if } \Delta L > 0 \\ 0 & \text{if } \Delta L \leq 0 \end{cases} \quad (9.76)$$

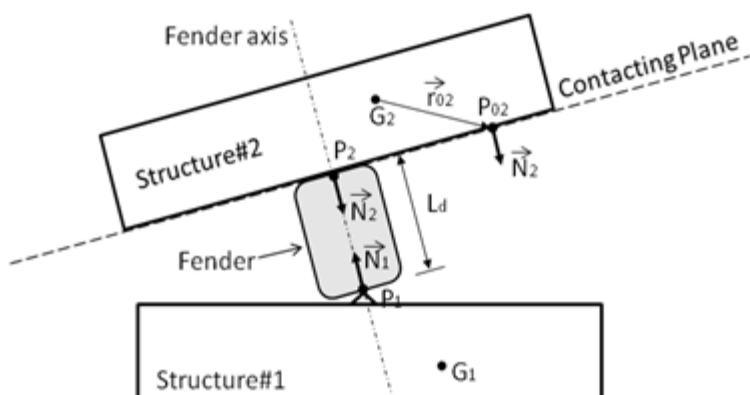
where  $k_j$  ( $j = 1, 5$ ) are the coefficients of the polynomial function and  $\Delta L = L_0 - L_d$ , where  $L_d$  is the distance between the two contacting points of the fender.

Fixed fenders and floating fenders can be defined in Aqwa. The contacting points of a fender and the directions of the fender force acting on each contacted structure depend on the type of fender.

### 9.8.1. Fixed Fender

As shown in [Figure 9.11: Fixed Fender \(p. 159\)](#), the fender is fixed at the point  $P_1$  on Structure 1 and may touch a contacting plane on Structure 2. This contacting plane is fixed on Structure 2 through a point  $P_{02}$  with a normal direction of  $\vec{n}_2 = (n_{12}, n_{22}, n_{32})$  expressed in the local structure axes (LSA) of Structure 2.

**Figure 9.11: Fixed Fender**



Denoting  $\vec{r}_{02}$  as the location of the point  $P_{02}$  in the local structure axes, and  $\mathbf{E}_2$  as the Euler rotation matrix between the local structure axes of Structure 2 and the fixed reference axes (as defined in

[Axis Transformation and Euler Rotations \(p. 14\)](#)), the location of the point  $P_{02}$  in the fixed reference axes is expressed as

$$\vec{R}_{02}^T = \vec{X}_{g2}^T + \mathbf{E}_2 \vec{r}_{02}^T \quad (9.77)$$

where  $\vec{X}_{g2}^T = (X_{g2}, Y_{g2}, Z_{g2})^T$  is the coordinate of the Structure 2 center of gravity in the fixed reference axes.

The unit normal directional vector of the contacting plane in the fixed reference axes is

$$\vec{N}_2^T = \mathbf{E}_2 \vec{n}_2^T \quad (9.78)$$

When the fender is in compression, the fender compression force acting at the fixed point  $P_1$  on Structure 1 is in the direction of

$$\vec{N}_1 = -\vec{N}_2 \quad (9.79)$$

and the coordinate of the actual contacting point  $P_2$  on the contacting plane in the fixed reference axes can be determined from

$$\vec{R}_2 = \vec{R}_1 - L_d \vec{N}_2 \quad (9.80)$$

where  $\vec{R}_1$  is the coordinate of the fixed point on Structure 1 in the fixed reference axes, and the distance  $L_d$  between the two contacting points of the fender is given by

$$L_d = (\vec{R}_1 - \vec{R}_{02}) \cdot \vec{N}_2 \quad (9.81)$$

The fender compression force acting at the actual contacting point  $P_2$  on Structure 2 is in the direction of  $\vec{N}_2$ , while the magnitude of the force is evaluated from [Equation 9.76 \(p. 159\)](#).

The optional friction and fender damping force components can also be defined, and will be discussed separately in [Fender Friction and Damping \(p. 162\)](#).

## 9.8.2. Floating Fender

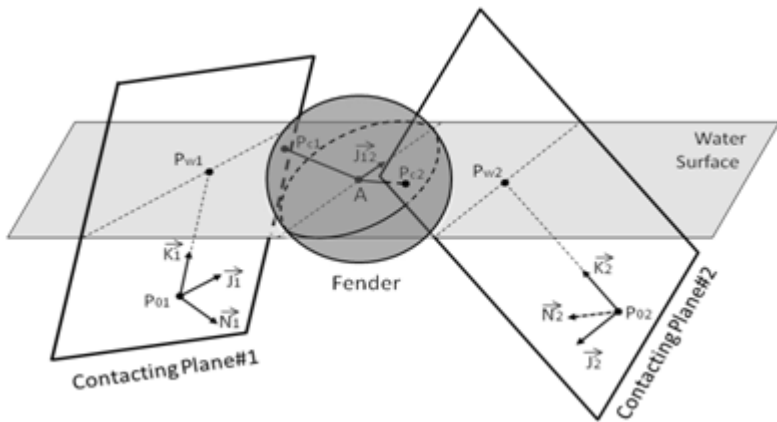
Floating fenders are normally applied to provide side protection to offshore structures and submarine docks. This type of fender can be modeled in Aqwa by the following approach.

Similar to the fixed fender definition, one contacting plane is positioned on Structure 2 through a point  $P_{02}$  with a normal direction of  $\vec{n}_2 = (n_{12}, n_{22}, n_{32})$  in the corresponding local structure axes (LSA), as shown in [Figure 9.12: Floating Fender \(p. 161\)](#). The location of the point  $P_{02}$  and this normal vector in the global axes are given by [Equation 9.77 \(p. 160\)](#) and [Equation 9.78 \(p. 160\)](#). Similarly, a contacting plane is positioned on Structure 1, passing through an associated point  $P_{01}$  whose location in the local structure axes is given as  $\vec{r}_{01}$ . The location of the point  $R_{01}$  in the fixed reference axes can be expressed as

$$\vec{R}_{01}^T = \vec{X}_{g1}^T + \mathbf{E}_1 \vec{r}_{01}^T \quad (9.82)$$

where  $\vec{X}_{g1}^T = (X_{g1}, Y_{g1}, Z_{g1})^T$  is the coordinate of the Structure 1 center of gravity in the fixed reference axes (FRA) and  $\mathbf{E}_2$  is the Euler rotation matrix between the local structure axes of Structure 1 and the fixed reference axes.

**Figure 9.12: Floating Fender**



If the normal vector of the contacting plane on Structure 1 is not specified, by default it is assumed to be in the direction opposite to the normal direction of the contacting plane on Structure 2, as given in [Equation 9.79 \(p. 160\)](#). Otherwise, if the normal direction of the contacting plane on Structure 1 is defined in the corresponding local structure axes as  $\vec{n}_1 = (n_{11}, n_{21}, n_{31})$ , it can be expressed in the fixed reference axes as

$$\vec{N}_1^T = \mathbf{E}_1 \vec{n}_1^T \quad (9.83)$$

It is assumed that the actual fender axle of a floating fender is always at the level of the mean water surface. To determine this fender axle position, Cartesian coordinate systems local to the two contacting planes are introduced as shown in [Figure 9.12: Floating Fender \(p. 161\)](#). The origin of this local axis system on Structure 1 is at the associated point  $P_{01}$ , the local x-axis direction is  $\vec{N}_1$ , while the local y-axis direction  $\vec{J}_1$  runs parallel to the intersection between the contacting plane and the mean water surface, and the vertical component of the local z-axis direction  $\vec{K}_1$  is set to be positive in the fixed reference axes. The crossing point  $P_{w1}$  of the local z-axis and the intersection of the mean water surface on the contact plane can be expressed in the fixed reference axes as

$$\vec{R}_{w1} = \vec{R}_{01} - \frac{Z_{01}}{K_{31}} \vec{K}_1 \quad (9.84)$$

where  $\vec{R}_{01} = (X_{01}, Y_{01}, Z_{01})$ ,  $\vec{K}_1 = (K_{11}, K_{21}, K_{31})$

The local axis system on Structure 2 and the mean water surface point  $P_{w2}$  along its local z-axis can be similarly defined.

The fender axle is assumed to lie on the mean water surface and points in the direction of

$$\vec{J}_{12} = \frac{\vec{J}_1 - \vec{J}_2}{|\vec{J}_1 - \vec{J}_2|} \quad (9.85)$$

This fender axle crosses through the point  $A$ , which lies on the mean water surface and is equidistant from the contacting points  $P_{c1}$  and  $P_{c2}$  on the two contacting planes. If these three points are expressed in the fixed reference axes as  $\vec{R}_A = (X_A, Y_A, 0)$ ,  $\vec{R}_{C1}$ ,  $\vec{R}_{C2}$  respectively, they should satisfy the following conditions:

$$\begin{aligned} (\vec{R}_{C1} - \vec{R}_{01}) \cdot \vec{N}_1 &= 0 \\ (\vec{R}_{C2} - \vec{R}_{02}) \cdot \vec{N}_2 &= 0 \\ \vec{R}_A - \vec{R}_{C1} &= d_1 \vec{N}_1 \\ \vec{R}_A - \vec{R}_{C2} &= d_2 \vec{N}_2 \\ d_1 &= d_2 \end{aligned} \quad (9.86)$$

The compressed length of the fender is given by

$$L_d = d_1 + d_2 \quad (9.87)$$

The magnitude of the compression force is evaluated from [Equation 9.76 \(p. 159\)](#), and the fender compression forces act in the direction of a line crossing through the two contacting points  $P_{c1}$  and  $P_{c2}$ .

### 9.8.3. Fender Friction and Damping

The fender friction force on the contacting surface is given by

$$F_f = \mu T \quad (9.88)$$

where  $\mu$  is the friction coefficient, and  $T$  is the normal compression reaction found from [Equation 9.76 \(p. 159\)](#).

It should be noted that fender friction works best in situations where the friction force is smaller than other forces in the same direction. Friction will slow down relative motion between two structures, but is not suitable for keeping them fixed together. When the relative velocity changes sign the friction force must also change sign, but to avoid an instantaneous change in this force (and therefore an instantaneous change in acceleration) a smoothing function is applied. This means that when the relative velocity is very small the friction force is also small, which may allow some relative motion between the two structures.

A fender damping force is only applied in the direction of the fender compression force, and is modeled by a linear material damping, as

$$F_d = \beta K_f \frac{dL_d}{dt} \quad (9.89)$$

where  $\beta$  is the damping coefficient and  $k_f$  is the fender stiffness.

# Chapter 10: Tethers

---

A time history simulation of tethers during towing-out, as well as static or time domain simulations of tethers once installed, can be performed in Aqwa for both regular and irregular waves.

Tethers are considered by Aqwa as flexible cylindrical tubes whose diameters are small compared to the wavelength of the waves, and are described by a series of elements along each tether. Each element may have different geometric and/or material properties.

The analysis of towed tethers is an independent process, and requires no hydrodynamic database from an Aqwa hydrodynamic diffraction analysis. As all tethers are regarded as a mooring capability in Aqwa, a nominal structure must be input to define the position of the axis system, in which the towed tether displacements are output and the eigenvalue solution is performed. The nominal structure plays no other part in the analysis.

An installed tether system is often applied for anchoring a tension leg platform (TLP) to the sea bed, as it prevents vertical motion but allows lateral motion due to environmental loadings. With a sufficient tether axial stiffness, the tether-hull system keeps the heave, pitch and roll natural frequencies above the wave energy frequencies. For an installed tether system, the hydrodynamic database from an Aqwa hydrodynamic diffraction analysis is required for the diffracting structures. For non-diffracting structures, however, a tube model can be used.

The tether modeling techniques are based on the following limitations and assumptions.

- No axial deformation

Bending and lateral motion only are considered, omitting translation and rotation in the axial direction.

- Zero axial tension in towed tether

Both the wall and effective tensions in a towed tether are assumed to be zero, and hence the bending stiffness is purely structural.

- Small motions

It is assumed that the lateral and rotational deformations of the tether from the defined tether axes are small. This means that the analysis is unsuitable for large rotations about the transverse axes, for example for the upending of a structure.

- Mass/stiffness

The mass/stiffness ratio of any element must not be too small. Very short elements inherently have small mass/stiffness ratios, which gives rise to very high natural frequencies. These high frequencies may cause stability problems and roundoff errors in the analysis. As a general rule, natural periods of less than 1/100<sup>th</sup> of a second are not allowed.

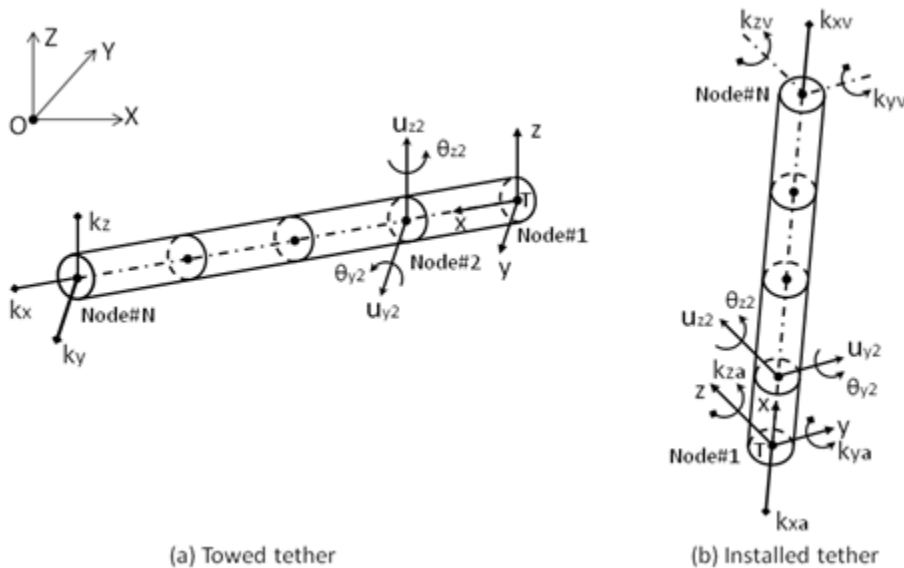
- Time step width

In a time domain analysis, the time step width must be small enough to resolve the response motion of the tether. This includes any transients that may be present either initially or, more importantly, throughout the analysis. A good rule of thumb is that the time step width should be less than 1/10<sup>th</sup> of the period of any response.

## 10.1. Mass and Stiffness Matrices

The tether element Cartesian coordinate system (TEA), Txyz, is defined as shown in [Figure 10.1: Tether Element Axes and Nodal Displacement \(p. 164\)](#).

**Figure 10.1: Tether Element Axes and Nodal Displacement**



As shown in [Figure 10.1: Tether Element Axes and Nodal Displacement \(p. 164\)](#) (a), a towed tether initially lies in the horizontal plane of the fixed reference axes (FRA), and the TEA x-axis coincides with the zero current wave direction. The node sequence numbers along the tether increase with positive x-value, where the first node, at the trailing end of the tether, lies at the TEA origin.

For an installed tether, shown in [Figure 10.1: Tether Element Axes and Nodal Displacement \(p. 164\)](#) (b), the TEA is parallel to the global if the tether is vertical. Otherwise, in general, the TEA x-axis goes from the anchor node to the vessel attachment node, the y-axis direction is perpendicular to the TEA x-axis in the XY plane of the fixed reference frame, and the z-axis follows the right-hand rule. The TEA origin is at the anchor node.

The tether local axes (TLA) is introduced for data input and results output:

- For a towed tether, the TLA is the same as the TEA.
- For an installed tether, the TLA x-, y-, and z-axes are in the TEA y-, z-, and x-axes directions.

As the displacements along the tether are rotations and translations at each node, the nodal displacement vector of the j-th element in the tether element axes can be expressed as

$$\mathbf{U}_e = [u_{yj}, u_{zj}, \theta_{yj}, \theta_{zj}; u_{yj+1}, u_{zj+1}, \theta_{yj+1}, \theta_{zj+1}]^T \quad (10.1)$$

An 8x2 cubic shape function matrix is employed to define the displacement at the point  $(x, 0, 0)$  along the  $j$ -th tether element axes, i.e.

$$\mathbf{T} = \begin{bmatrix} 1-a^2(3-2a) & 0 \\ 0 & 1-a^2(3-2a) \\ 0 & -La(1-a)^2 \\ La(1-a)^2 & 0 \\ a^2(3-2a) & 0 \\ 0 & a^2(3-2a) \\ 0 & -La^2(1-a) \\ La^2(1-a) & 0 \end{bmatrix} \quad (10.2)$$

where  $a=\frac{(x-x_j)}{L}$ , in which  $L$  is the length of this element.

Using this shape function, the structural mass matrix of the tether elements is defined by an 8x8 matrix as follows:

$$\mathbf{M}_s = \frac{m_s}{420} \begin{bmatrix} 156L & 0 & 0 & 22L^2 & 54L & 0 & 0 & -13L^2 \\ 0 & 156L & -22L^2 & 0 & 0 & 54L & 13L^2 & 0 \\ 0 & -22L^2 & 4L^3 & 0 & 0 & -13L^2 & -3L^3 & 0 \\ 22L^2 & 0 & 0 & 4L^3 & 13L^2 & 0 & 0 & -3L^3 \\ 54L & 0 & 0 & 13L^2 & 156L & 0 & 0 & -22L^2 \\ 0 & 54L & -13L^2 & 0 & 0 & 156L & 22L^2 & 0 \\ 0 & 13L^2 & -3L^3 & 0 & 0 & 22L^2 & 4L^3 & 0 \\ -13L^2 & 0 & 0 & -3L^3 & -22L^2 & 0 & 0 & 4L^3 \end{bmatrix} \quad (10.3)$$

where  $m_s$  is the structural mass per unit length.

The added mass for completely submerged tether elements will be the same as above, where the mass per unit length will be equal to the displaced mass per unit length. However, for partially submerged elements, the added mass is calculated by integrating the following function along the submerged length by a Gaussian integration scheme, such as

$$\mathbf{M}_a = \int_{L_1}^{L_2} \mathbf{T} \mathbf{m}_a \mathbf{T}^T dx \quad (10.4)$$

where  $\mathbf{m}_a$  is a diagonal 2x2 matrix of added mass per unit length, which depends on the level of submersion of the tether element:

$$\mathbf{m}_a = \begin{bmatrix} m_y & 0 \\ 0 & m_z \end{bmatrix} \quad (10.5)$$

The structural stiffness matrix is given by:

$$\mathbf{K} = \frac{EI}{L^3} \begin{bmatrix} 12 & 0 & 0 & 6L & -12 & 0 & 0 & 6L \\ 0 & 12 & -6L & 0 & 0 & -12 & -6L & 0 \\ 0 & -6L & 4L^2 & 0 & 0 & 6L & 2L^2 & 0 \\ 6L & 0 & 0 & 4L^2 & -6L & 0 & 0 & 2L^2 \\ -12 & 0 & 0 & -6L & 12 & 0 & 0 & -6L \\ 0 & -12 & 6L & 0 & 0 & 12 & 6L & 0 \\ 0 & -6L & 2L^2 & 0 & 0 & 6L & 4L^2 & 0 \\ 6L & 0 & 0 & 2L^2 & -6L & 0 & 0 & 4L^2 \end{bmatrix} \quad (10.6)$$

where  $E$  is the Young's modulus of elasticity and  $I$  is the second moment of cross-sectional area.

## 10.2. Boundary Conditions and Constraints

For a towed tether, one tether end is attached to a nominal structure with three spring stiffnesses in the translational directions, which are assumed to represent a soft mooring line stiffness between the tether and its attached structure. As shown in [Figure 10.1: Tether Element Axes and Nodal Displacement \(p. 164\)](#) (a), those three stiffnesses are denoted as  $k_x$ ,  $k_y$ , and  $k_z$ .

For an installed tether, between the vessel end of the tether and its corresponding vessel attachment point, three spring stiffnesses ( $k_{xv}$ ,  $k_{yv}$ , and  $k_{zv}$ ) are defined as the inline stiffness and two rotational stiffnesses about the TEA y- and z-axes respectively. These are used to determine the relative translational displacement in the TEA x-direction and rotations about the TEA y- and z-axes between the vessel end of the tether and the vessel attachment point. The relative translational displacements in the TEA y- and z-axial directions are set to zero at the vessel attachment point.

Similar to the vessel end of an installed tether, three spring stiffnesses ( $k_{xa}$ ,  $k_{ya}$ , and  $k_{za}$ ), between the anchor end of the tether and the corresponding fixed point on the sea bed, are defined as the inline stiffness and two rotational stiffnesses about the TEA y- and z-axes. The relative translational displacements in the TEA y- and z-directions are set to be zero at the anchor point.

As a special case, if the anchor inline stiffness  $k_{xa}$  is positive but small, the tether can be considered to be free-hanging. In this case, a tether lower stop distance can be introduced to define a stop point below the anchor end. The anchor end of the tether is restricted to be no lower than this point.

Several other constraints at the specified tether element nodes can be defined, such as the tether fixed lateral constraint, the tether fixed rotational constraint, the tether rotational vessel constraint (representing an encastre condition on the vessel) and the tether lateral vessel constraint. It should be noted that the two above-mentioned rotational constraints are rarely used, as they will cause large bending moments at the attachment points. A tether lateral vessel constraint defines a gap to represent an opening on the vessel that is wider than the tether. This is assumed to be a frictionless circular gap in the structure, below the vessel end of the tether along the TEA x-axis direction. If the total lateral movement relative to the center of the gap is greater than the specified gap distance, it is assumed that the tether node at the gap is constrained laterally by the structure.

## 10.3. Total Applied Forces

The total applied force  $\mathbf{F}_e$  on a tether element consists of the components

$$\mathbf{F}_e = \mathbf{F}_k + \mathbf{F}_s + \mathbf{F}_i + \mathbf{F}_m \quad (10.7)$$

where  $\mathbf{F}_k$  is the internal force due to bending structural stiffness,  $\mathbf{F}_s$  represents the externally-applied forces due to the springs at the end nodes,  $\mathbf{F}_i$  represents the integrated forces, which consist of gravity, hydrostatic forces, drag, wave inertia, the Froude-Krylov force and slam forces, and  $\mathbf{F}_m$  is the force due to the calculation being performed in a moving reference frame, which applies to installed tethers only.

The integrated forces vector  $\mathbf{F}_i$  includes the contributions  $\mathbf{F}_a$  due to lateral forces and  $\mathbf{F}_r$  due to applied moments. Similar to the mass matrix calculation in [Equation 10.4 \(p. 165\)](#), these are integrated along the element, i.e.

$$\begin{aligned}\mathbf{F}_a &= \int_{L_1}^{L_2} T f_a dx \\ \mathbf{F}_r &= \int_{L_1}^{L_2} B f_r dx\end{aligned}\quad (10.8)$$

where  $f_a = (f_y, f_z)^T$  is the lateral force at a point  $(x, 0, 0)$  along the element, due to the 6 different types of integrated forces mentioned previously, and  $f_r = (m_y, m_z)^T$  is the moment at a point along the element, to which only the hydrostatic force contributes (as it may not act on or at right angles to the axis of the element).

In [Equation 10.8 \(p. 167\)](#), the  $8 \times 2$  matrix  $\mathbf{B}$  (which is similar to the shape function matrix  $\mathbf{T}$  defined in [Equation 10.2 \(p. 165\)](#)) is the transfer function for the forces/momenta at the element ends due to an applied moment at a point along the element, and is given by

$$\mathbf{B} = \begin{bmatrix} 0 & -6a(1-a)/L \\ 6a(1-a)/L & 0 \\ 1+3a^2-4a & 0 \\ 0 & 1+3a^2-4a \\ 0 & 6a(1-a)/L \\ -6a(1-a)/L & 0 \\ 3a^2-2a & 0 \\ 0 & 3a^2-2a \end{bmatrix} \quad (10.9)$$

The moving reference frame force vector  $\mathbf{F}_m$  is given by

$$\mathbf{F}_m = \mathbf{M}_s \mathbf{a}_f \quad (10.10)$$

where  $\mathbf{a}_f$  is the acceleration of the moving reference frame.

For each element, the equations of motion are assembled to give the global equations of motion for the whole tether with respect to the fixed reference axes (FRA). As each element mass is stored in an  $8 \times 8$  matrix form, the global mass matrix should be a symmetric banded matrix with a semi-bandwidth of 8. The assembled equation has  $4 \times (\text{number of nodes})$  unknown acceleration variables (for a time domain analysis) or displacement variables (for an equilibrium analysis).

The axial stresses due to an impact are considered to act simultaneously along the whole of the installed tether member, as the time for the shock wave to propagate is small (i.e. speed of the shock wave is large) compared to the time step width. The initial stress caused by the tether impact is assumed to be proportional to the velocity of the impact, and to subsequently decay exponentially as

$$\sigma(t) = A_{imp} V e^{-0.693 \frac{t}{T_h}} \quad (10.11)$$

where  $A_{imp}$  is the stress impact factor,  $V$  is the velocity on impact and  $T_h$  is the half-life duration of the impact.

## 10.4. Integration in Time of Motion Equation

The global equation of motion in the time domain is given by:

$$\mathbf{M}\mathbf{A} = \mathbf{F}_t \quad (10.12)$$

where  $\mathbf{M}$  is the assembled structural and added mass matrix in the fixed reference axes,  $\mathbf{A}$  is the unknown acceleration vector, and  $\mathbf{F}_t$  is the total applied force vector on all of the element nodes.

Due to the high frequencies present in the higher modes of vibration, a semi-implicit two-stage predictor corrector scheme is used to integrate in time for velocity and displacement.

The higher frequencies, and hence the semi-implicit aspect of the formulation, involve the forces due to structural bending. We thus rewrite [Equation 10.12 \(p. 168\)](#) as

$$\mathbf{M}\mathbf{A} = \mathbf{F} - \mathbf{K}\mathbf{U} \quad (10.13)$$

where  $\mathbf{K}$  the is assembled structural stiffness matrix,  $\mathbf{U}$  is the displacement vector over all nodes, and  $\mathbf{F}$  is a vector representing forces other than those due to structural stiffness.

At the first stage of the integration scheme, we write

$$\begin{aligned} \mathbf{M}(t)\mathbf{A}_1 &= \mathbf{F}(t) - \mathbf{K}\mathbf{U}\left(t + \frac{dt}{2}\right) \\ &= \mathbf{F}(t) - \mathbf{K}\left\{\mathbf{U}(t) - \frac{dt}{2}\mathbf{V}(t) + \left(\frac{dt}{2}\right)^2 \mathbf{A}_1\right\} \end{aligned} \quad (10.14)$$

where  $\mathbf{U}(t)$  and  $\mathbf{V}(t)$  are the known displacement and velocity vectors, respectively, of nodes at time  $t$ .

This equation leads to a solution for acceleration at the predictor stage, from which predictions  $\mathbf{V}^*(t+dt)$  and  $\mathbf{U}^*(t+dt)$  for nodal velocities and displacements at time  $t+dt$  may be made:

$$\begin{aligned} \left\{\mathbf{M}(t) + \left(\frac{dt}{2}\right)^2 \mathbf{K}\right\}\mathbf{A}_1 &= \mathbf{F}(t) - \mathbf{K}(t)\left\{\mathbf{U}(t) + \mathbf{V}(t)\frac{dt}{2}\right\} \\ \mathbf{V}^*(t+dt) &= \mathbf{V}(t) + \mathbf{A}_1 dt \\ \mathbf{U}^*(t+dt) &= \mathbf{U}(t) + (\mathbf{V}(t) + \mathbf{V}^*(t+dt))\frac{dt}{2} \end{aligned} \quad (10.15)$$

At the corrector stage, the acceleration is determined from

$$\left\{\mathbf{M}(t+dt) + \left(\frac{dt}{2}\right)^2 \mathbf{K}\right\}\mathbf{A}_2 = \mathbf{F}(t+dt) - \mathbf{K}(t)\left\{\mathbf{U}(t) + \mathbf{V}(t)\frac{dt}{2}\right\} \quad (10.16)$$

where the added mass and forces at  $t+dt$  are calculated using  $\mathbf{U}^*(t+dt)$  and  $\mathbf{V}^*(t+dt)$ .

The final solutions for velocity and displacement at time  $t+dt$  are then given by

$$\begin{aligned} \mathbf{V}(t+dt) &= \mathbf{V}(t) + \{\mathbf{A}_1 + \mathbf{A}_2\}\frac{dt}{2} \\ \mathbf{U}(t+dt) &= \mathbf{U}(t) + \{\mathbf{V}(t) + \mathbf{V}(t+dt)\}\frac{dt}{2} \end{aligned} \quad (10.17)$$

For some extreme cases of loading, the above time-centered scheme may be unstable. A factor  $b$  is therefore introduced to make the formulation non-time-centered, which increases the stability but reduces the accuracy. Introducing  $b$  gives:

$$\begin{aligned} \left\{ \mathbf{M}(t) + 2b \left( \frac{dt}{2} \right)^2 \mathbf{K} \right\} \mathbf{A}_1 &= \mathbf{F}(t) - \mathbf{K}(t) \left\{ \mathbf{U}(t) + b \mathbf{V}(t) dt \right\} \\ \left\{ \mathbf{M}(t+dt) + 2b \left( \frac{dt}{2} \right)^2 \mathbf{K} \right\} \mathbf{A}_2 &= \mathbf{F}(t+dt) - \mathbf{K}(t) \left\{ \mathbf{U}(t) + b \mathbf{V}(t) dt \right\} \end{aligned} \quad (10.18)$$

When the value of  $b$  is 0.5, the expressions for  $\mathbf{A}_1$  and  $\mathbf{A}_2$  in [Equation 10.18 \(p. 169\)](#) equate to the formulas given by [Equation 10.15 \(p. 168\)](#) and [Equation 10.16 \(p. 168\)](#) respectively. Tests have shown that the optimum value for  $b$  is 0.54, which gives the best trade-off of stability and accuracy when employing [Equation 10.18 \(p. 169\)](#).

## 10.5. Fatigue/Extreme Value Statistical Post-Processing for Towed Tethers

The fatigue life along a towed tether can be estimated in a time domain analysis. The formula used to calculate the fatigue life is

$$\text{Fatigue life (days)} = \frac{A}{\sum_{j=1}^m \sigma_j (S_{cf})^m N_j} \quad (10.19)$$

where  $\sigma_j$  is the stress range computed from a rainflow count of time history stresses,  $N_j$  is the number of cycles per day for this stress range from a probability distribution by a rainflow count,  $S_{cf}$  is the stress concentration factor, and  $m$  and  $A$  are the S-N curve slope and the S-N curve intercept coefficient respectively.

The extreme values of stress are based on the assumption that stress has a Rayleigh distribution. The peak stress is given by

$$\text{Peak stress in K hours} = |\bar{\sigma}| + \sigma_{rms} \sqrt{2 \ln(K \cdot N)} \quad (10.20)$$

where  $\bar{\sigma}$  is the mean stress,  $\sigma_{rms}$  is the root mean square of the stress, and  $N$  is the number of cycles per hour (based on the mean number of positive and negative peaks per hour in the stress time history).



# Chapter 11: Equilibrium Estimation and Stability Analysis of Structure System

Aqwa can calculate the equilibrium configuration and stability properties (both static and dynamic), of a system of one or more floating bodies under the influence of mooring lines, steady wind, current, thrusters and wave drifting forces.

The static equilibrium configuration then forms the basis for subsequent dynamic analyses of floating systems.

## 11.1. External Static Forces

The external forces and stiffnesses acting on each body are specified with respect to the local structure axes (LSA) for that body, whose origin is located at, and moves with, the center of gravity of the body, while the axes remain parallel to the fixed reference axes (see [Axes Conventions \(p. 11\)](#)). Aqwa employs an iterative approach for determining the equilibrium position of the floating system.

Gravitational forces acting on structures are included in the equilibrium position estimation.

At each iterative step, Aqwa calculates hydrostatic forces and moments directly from the integral of hydrostatic pressure over all the elements comprising the submerged part of the body (in the same manner as used in the radiation/diffraction analysis, see [Hydrostatic Forces and Moments \(p. 43\)](#)). You may also directly input a buoyancy force, which is assumed to be constant throughout the analysis.

In multi-directional waves, the mean drift forces are determined from [Equation 5.22 \(p. 104\)](#) by the superposition of wave component series with the same frequency increment.

Aqwa assigns a unique set of pseudo-random numbers to describe the wave component phases within each sub-directional spectrum. However, as Aqwa can only allow a finite number of wave components for each spectrum, the numerical results may be sensitive to the selected wave component number. Statistically, given that the wave component phases follow a uniform random distribution in the range [0, 360] degrees, the mean drift force could be written as:

$$\bar{F}^{(2)} = \sum_{m=1}^{N_d} \sum_{n=1}^{N_a} \sum_{j=1}^{N_w} a_{jm} a_{jn} \left\{ \bar{P}_{jjmn} \lim_{N \rightarrow \infty} \frac{1}{N} \sum_{s=1}^N \cos(\alpha_{jm} - \alpha_{jn}) - \bar{Q}_{jjmn} \lim_{N \rightarrow \infty} \frac{1}{N} \sum_{s=1}^N \sin(\alpha_{jm} - \alpha_{jn}) \right\} \quad (11.1)$$

where  $s$  is the sample sequence number. For a pair of sub-directions (where  $m \neq n$ ), in the limit:

$$\lim_{N \rightarrow \infty} \frac{1}{N} \sum_{s=1}^N \cos(\alpha_{jm} - \alpha_{jn}) = 0 \quad (11.2)$$

$$\lim_{N \rightarrow \infty} \frac{1}{N} \sum_{s=1}^N \sin(\alpha_{jm} - \alpha_{jn}) = 0$$

This means that as the number of samples tends to infinity, the mean drift force is independent of any directional coupling effect. Taking this observation into account, for any specified sea state, we introduce

$$\bar{F}^{(2)} = \sum_{m=1}^{N_d} \sum_{n=1}^{N_d} \sum_{j=1}^{N_w} a_{jm} a_{jn} \left\{ \bar{P}_{jjmn} \frac{1}{N} \sum_{s=1}^N \cos(\alpha_{jm} - \alpha_{jn}) - \bar{Q}_{jjmn} \frac{1}{N} \sum_{s=1}^N \sin(\alpha_{jm} - \alpha_{jn}) \right\} \quad (11.3)$$

where  $N$  is the number of random phase settings.

With this form, the numerical results for mean drift forces due to directional coupling are less sensitive to the selected wave component number. [Equation 11.3 \(p. 172\)](#) could alternatively be considered as the summation of the  $N$  sub-components within a normal wave component frequency range.

In order to estimate the multi-directional coupling mean drift force, the same starting and finishing wave frequencies, and frequency increment are required for all wave directions. Denoting the starting and finishing frequencies of each sub-directional wave spectrum as  $\omega_{start}^{sp}$  and  $\omega_{finish}^{sp}$  respectively, and the number of wave components as  $N_{spl}^{sp}$ , the corresponding values for the whole wave spectral group are determined as

$$\begin{aligned} \omega_{start}^{sg} &= \min\{\omega_{start}^{sp}\} \\ \omega_{finish}^{sg} &= \max\{\omega_{finish}^{sp}\} \\ \Delta\omega &= \min\left\{\frac{\omega_{finish}^{sp} - \omega_{start}^{sp}}{N_{spl}^{sp}}\right\} \\ N_w &= \min\left\{N_w^{\max}, \frac{\omega_{finish}^{sg} - \omega_{start}^{sg}}{\Delta\omega}\right\} \\ \Delta\omega^{sg} &= \frac{\omega_{finish}^{sg} - \omega_{start}^{sg}}{N_w} \end{aligned} \quad (11.4)$$

where  $\Delta\omega^{sg}$  is the constant frequency increment within the wave spectral group, and  $N_w^{\max}$  is the maximum number of wave components allowed in Aqwa.

A number of thruster forces ( $f_{xt}$ ,  $f_{yt}$ ,  $f_{zt}$ ) may be included in the equilibrium calculation and can be specified at the positions ( $x_t$ ,  $y_t$ ,  $z_t$ ) on each structure in the local structure axes (LSA). The magnitudes of the thruster forces are assumed to be constant throughout the analysis. The three components ( $f_{xt}$ ,  $f_{yt}$ ,  $f_{zt}$ ) define the thruster direction relative to the structure, which is also assumed to be constant. This means that the thruster direction relative to the fixed reference axis system (FRA) will change with the structure position.

As discussed in [Axis Transformation and Euler Rotations \(p. 14\)](#), the Euler rotation matrix at an intermediate position in the iterative process may be defined from [Equation 1.7 \(p. 16\)](#). Further introducing a 3x3 matrix based on the thruster position in the local structure axes (LSA), i.e.

$$\mathbf{R} = \begin{bmatrix} 0 & z_t & -y_t \\ -z_t & 0 & x_t \\ y_t & -x_t & 0 \end{bmatrix} \quad (11.5)$$

the thruster force and corresponding moments about the structure center of gravity in the fixed reference axes (FRA) can be given by

$$\mathbf{F}_t = \begin{bmatrix} \mathbf{E} \\ \mathbf{ER}^T \end{bmatrix} \begin{bmatrix} f_{xt} \\ f_{yt} \\ f_{zt} \end{bmatrix} \quad (11.6)$$

where  $\mathbf{F}_t$  is a  $6 \times 1$  matrix consisting of three thruster force components and three thruster moment components about the structure center of gravity in the FRA.

Drag effects on mooring lines are ignored if cable dynamics are not used for composite catenary lines.

Steady wind and current drag forces and moments are included, as discussed in [Current and Wind Hull Drag \(p. 121\)](#), as well as drag forces and moments on Morison elements (see [Effects of Morison Elements in Equilibrium and Static Stability Analysis \(p. 116\)](#)).

Mooring forces and articulation reaction forces are also included.

## 11.2. Equilibrium Analysis

The equilibrium position of each body is described by three translational and three rotational components of the center of gravity of the body, with respect to the origin of the fixed reference axes (FRA). To move a body towards equilibrium requires a number of iterative steps, where in each step the total stiffness matrix and the force vector are re-calculated. In general, the stiffness matrix is nonlinear.

The computed equilibrium configuration may be used as a starting point for subsequent frequency domain or time domain hydrodynamic analyses carried out by Aqwa. It is also used as an input to the static and dynamic stability computations.

### 11.2.1. The Stiffness Matrix

Aqwa computes all of the stiffness contributions directly from analytical expressions for the load/displacement derivatives, or through the use of numerical differentiation.

The global stiffness matrix is nonlinear and is composed of hydrostatic restoring stiffness, mooring stiffness, and 'stiffness' due to the heading variation in wind, current and wave drifting forces and moments.

The cut water-plane area, together with the locations of the center of buoyancy and the center of gravity of the body, determine the hydrostatic stiffness matrix. As each body is moved towards equilibrium, the hydrostatic properties are recalculated at each iterative step based on the new submerged volume. However, there are instances where a detailed geometry of the bodies is not available or not required. You may therefore directly input a hydrodynamic stiffness matrix, which will be assumed to be constant throughout the analysis.

The hydrostatic stiffness components  $K_{46}$  and  $K_{56}$  will be zero and the stiffness matrix will be symmetric if the center of buoyancy and the center of gravity are located on the same vertical line. For a free-floating body in equilibrium, this is automatically the case. However, if the body is in equilibrium under the influence of mooring lines and/or articulations, the center of buoyancy and the center of gravity will not necessarily be located on the same vertical line. In this case, the hydrostatic stiffness matrix will be asymmetric, although the global system stiffness matrix will still be symmetric.

Steady wind, current and wave drift forces are functions of the heading angle only, and their stiffness contributions are therefore found only in changes in the yaw coordinate (i.e. components  $K_{16}$  and  $K_{26}$  of the stiffness matrix).

The fixed reference axes (FRA) are used for the equilibrium analysis of the floating system. If force/moment vectors and stiffness matrices are initially evaluated in the local structure axis system (LSA), they will be transformed into the FRA prior to the calculation of equilibrium. As an example, a thruster force (defined in the LSA of the body on which the thruster is acting) is transformed into a force/moment about the structure center of gravity in the FRA by [Equation 11.6 \(p. 173\)](#).

The formulation of a vector translation may be applied directly to translate the stiffness matrix,  $\mathbf{K}$ , from the point of definition to the center of gravity. It should be noted, however, that if the stiffness matrix is defined in a fixed axis system that does not rotate with the structure, an additional stiffness term is required to account for the change of moment created by a constant force applied at a point when the structure is rotated.

As an example, at an intermediate position in the iterative process, denote  $\mathbf{K}$  as a  $3 \times 3$  structure-anchor mooring line stiffness matrix corresponding to the translational movements of the attachment point at  $(X_a, Y_a, Z_a)$  on the structure in the FRA. We also denote  $(P_{xa}, P_{ya}, P_{za})$  as the X, Y and Z components of the tension in the mooring line at  $(X_a, Y_a, Z_a)$ . The full  $6 \times 6$  stiffness matrix  $\mathbf{K}_g$  for each mooring line, relating displacements of the center of gravity of the structure, located at  $(X_{ga}, Y_{ga}, Z_{ga})$ , to the change in forces and moments acting on the center of gravity, is therefore given by

$$\mathbf{K}_g = \begin{bmatrix} \mathbf{I} \\ \mathbf{R}_a^T \end{bmatrix} [\mathbf{K}] [\mathbf{I} \quad \mathbf{R}_a] + \begin{bmatrix} 0 & 0 \\ 0 & \mathbf{P}_a \mathbf{R}_a^T \end{bmatrix} \quad (11.7)$$

where

$$\mathbf{R}_a = \begin{bmatrix} 0 & Z_a - Z_{ga} & -(Y_a - Y_{ga}) \\ -(Z_a - Z_{ga}) & 0 & X_a - X_{ga} \\ Y_a - Y_{ga} & -(X_a - X_{ga}) & 0 \end{bmatrix}$$

$$\mathbf{P}_a = \begin{bmatrix} 0 & P_{za} & -P_{ya} \\ -P_{za} & 0 & P_{xa} \\ P_{ya} & -P_{xa} & 0 \end{bmatrix}$$

For a mooring line joining two structures this causes a fully-coupled stiffness matrix, where the displacement of one structure causes a force on the other. This stiffness matrix may be obtained simply by considering that the displacement of the attachment point on one structure is equivalent to a negative displacement of the attachment point on the other structure. Extending the definitions in [Equation 11.7 \(p. 174\)](#), the alternative  $12 \times 12$  stiffness matrix  $\mathbf{K}_g$  is given by

$$\mathbf{K}_g = \begin{bmatrix} \mathbf{I} \\ \mathbf{R}_a^T \\ -\mathbf{I} \\ -\mathbf{R}_b^T \end{bmatrix} [\mathbf{K}] [\mathbf{I} \ \mathbf{R}_a \ -\mathbf{I} \ -\mathbf{R}_b] + \begin{bmatrix} 0 & 0 & 0 & 0 \\ 0 & \mathbf{P}_a \mathbf{R}_a^T & 0 & 0 \\ 0 & 0 & 0 & 0 \\ 0 & 0 & 0 & \mathbf{P}_b \mathbf{R}_b^T \end{bmatrix} \quad (11.8)$$

where

$$\mathbf{R}_b = \begin{bmatrix} 0 & Z_b - Z_{gb} & -(Y_b - Y_{gb}) \\ -(Z_b - Z_{gb}) & 0 & X_b - X_{gb} \\ Y_b - Y_{gb} & -(X_b - X_{gb}) & 0 \end{bmatrix}$$

$$\mathbf{P}_b = \begin{bmatrix} 0 & P_{zb} & -P_{yb} \\ -P_{zb} & 0 & P_{xb} \\ P_{yb} & -P_{xb} & 0 \end{bmatrix}$$

in which  $(X_b, Y_b, Z_b)$  are the coordinates of the attachment point on the second structure with its center of gravity located at  $(X_{gb}, Y_{gb}, Z_{gb})$ , and  $(P_{xb}, P_{yb}, P_{zb})$  are the X, Y and Z components of the tension in the mooring line at the attachment point on the second structure.

### 11.2.2. Iteration Towards Equilibrium

Considering a multi-body floating system consisting of  $N$  structures, let the initial estimate of the structure positions and orientations be represented by the vector  $\mathbf{X}^{(0)}$ ,

$$\mathbf{X}^{(0)} = (X_{g1}^{(0)}, Y_{g1}^{(0)}, Z_{g1}^{(0)}, \theta_{11}^{(0)}, \theta_{21}^{(0)}, \theta_{31}^{(0)}, \dots, X_{gN}^{(0)}, Y_{gN}^{(0)}, Z_{gN}^{(0)}, \theta_{1N}^{(0)}, \theta_{2N}^{(0)}, \theta_{3N}^{(0)}) \quad (11.9)$$

where  $(X_{gj}^{(0)}, Y_{gj}^{(0)}, Z_{gj}^{(0)})$  are the coordinates of the  $j$ -th structure center of gravity with respect to the FRA, and  $(\theta_{1j}^{(0)}, \theta_{2j}^{(0)}, \theta_{3j}^{(0)})$  are the finite angular rotations describing the orientation of this structure; the superscripts denote the iteration step. The displacement required in step 1 is given by

$$d\mathbf{X}^{(1)} = \mathbf{K}^{-1}(\mathbf{X}^{(0)}) \mathbf{F}(\mathbf{X}^{(0)}) \quad (11.10)$$

and the new position of the body  $\mathbf{X}^{(1)}$  is given by

$$\mathbf{X}^{(1)} = d\mathbf{X}^{(1)} + \mathbf{X}^{(0)} \quad (11.11)$$

The process is repeated until the  $m$ -th iterative step, when  $d\mathbf{X}^{(m)}$  is smaller than the prescribed limit for convergence.

It is possible to have more than one equilibrium position: for example, a capsized ship can still float in equilibrium, if buoyancy is preserved. It is therefore important to start the iterative process with an initial estimate  $\mathbf{X}^{(0)}$  that is close to the required solution. Furthermore, because of the nonlinearities in the system, it is also possible to overshoot the intended equilibrium position. In practice,  $d\mathbf{X}^{(m)}$  may therefore be scaled by a specified under-relaxation factor to ensure stability in the iterative scheme.

Before equilibrium is reached, a set of unbalanced residual forces and moments will act on the bodies. These include hydrostatic forces, weights of the structures, mooring tensions, wind and current drag,

thruster forces, steady wave drift forces, and constraint reaction forces as described in [External Static Forces \(p. 171\)](#) and [Articulations Between Structures \(p. 131\)](#).

## 11.3. Static Stability Analysis

Aqwa extracts the eigenvalues of the linearized stiffness matrix at the equilibrium position by the standard Jacobi successive rotation method. The following equation is solved:

$$\mathbf{K}\mathbf{X} - \lambda\mathbf{X} = 0 \quad (11.12)$$

of which positive eigenvalues of  $\lambda$  imply stable equilibrium, and zero eigenvalues imply neutral stability. If any of the eigenvalues are negative the body will not return to its equilibrium position after a small disturbance in any of the corresponding modes. As a special case, these eigenvalues are analogous to the metacentric height, GM, in transverse stability analysis of a free-floating ship.

At present, Aqwa only provides valid stability information for small displacements about the equilibrium position. You should be aware of this limitation, and the corresponding risk associated with extrapolating such data to large displacements from the equilibrium position.

However, it is possible to generate a stability report, for a single structure acted on by gravity and hydrostatic forces only (see [Large Angle Stability \(p. 47\)](#)). Such a report gives a list of positions of the structure and the corresponding forces at each position.

## 11.4. Dynamic Stability Analysis

Given the static equilibrium position of the floating system,  $\mathbf{X}_B$ , an equation of small motions of the system about its equilibrium position can be written as

$$\mathbf{M}\ddot{\mathbf{U}} = \mathbf{F}(t) \quad (11.13)$$

where  $\ddot{\mathbf{U}}$  is the acceleration vector,  $\mathbf{M}$  is the mass matrix, and  $\mathbf{F}(t)$  is the total external force vector evaluated at the position  $\mathbf{X}_B + \mathbf{U}$ .

Neglecting terms of second order or higher, the linearized equation of motion of the system can be expressed in terms of a general force, as

$$\mathbf{M}_t \ddot{\mathbf{U}} + \mathbf{C} \dot{\mathbf{U}} + \mathbf{K} \mathbf{U} = \mathbf{F} \quad (11.14)$$

where  $\mathbf{M}(t)$  is the total mass matrix, including the structural mass and the hydrodynamic added mass.

This equation of motion may also be rewritten in the Hamiltonian form

$$\begin{bmatrix} \mathbf{M}_t & \mathbf{0} \\ \mathbf{0} & \mathbf{M}_t \end{bmatrix} \begin{bmatrix} \dot{\mathbf{V}} \\ \mathbf{U} \end{bmatrix} + \begin{bmatrix} \mathbf{C} & \mathbf{K} \\ -\mathbf{M}_t & \mathbf{0} \end{bmatrix} \begin{bmatrix} \mathbf{V} \\ \mathbf{U} \end{bmatrix} = \begin{bmatrix} \mathbf{F} \\ \mathbf{0} \end{bmatrix} \quad (11.15)$$

where  $\mathbf{V} = \dot{\mathbf{U}}$  is the velocity vector.

Denoting

$$\begin{bmatrix} \mathbf{V} \\ \mathbf{U} \end{bmatrix} = \begin{bmatrix} \mathbf{V}_0 \\ \mathbf{U}_0 \end{bmatrix} e^{\lambda t} \quad (11.16)$$

$$\lambda = f + i\omega_n$$

the eigenvalues of [Equation 11.15 \(p. 176\)](#) can be determined from

$$\begin{bmatrix} \mathbf{M}_t^{-1}\mathbf{C} & \mathbf{M}_t^{-1}\mathbf{K} \\ -\mathbf{I} & \mathbf{0} \end{bmatrix} \begin{Bmatrix} \mathbf{V}_0 \\ \mathbf{U}_0 \end{Bmatrix} + \lambda \begin{Bmatrix} \mathbf{V}_0 \\ \mathbf{U}_0 \end{Bmatrix} = \begin{Bmatrix} 0 \\ 0 \end{Bmatrix} \quad (11.17)$$

Eigenvalues of the system given by [Equation 11.16 \(p. 176\)](#) and [Equation 11.17 \(p. 177\)](#) will indicate the modes of motion of the system, and may be interpreted as follows:

- $f < 0$ , stable
- $f > 0$  and  $\omega_n = 0$ , unstable
- $f > 0$  and  $\omega_n \neq 0$ , fishtailing

The natural period  $T_n$  of a mode of motion is given by:

$$T_n = \frac{2\pi}{\omega_n} \quad (11.18)$$

The critical damping percentage of a mode of motion is defined as

$$\zeta_c = -\frac{f}{\sqrt{f^2 + \omega_n^2}} \times 100\% \quad (11.19)$$

The normalized eigenvector output in Aqwa is defined as

$$\mathbf{U}_e = 10 \frac{\mathbf{U}_0}{|\mathbf{U}_0|} \quad (11.20)$$

For a single degree of freedom system, the equation of motion is written as

$$M\ddot{U} + C\dot{U} + KU = F \quad (11.21)$$

which may alternatively be expressed as

$$\ddot{U} + 2\omega_n\zeta_c\dot{U} + \omega_n^2U = \frac{F}{M} \quad (11.22)$$

where  $\omega_n = \sqrt{\frac{K}{M}}$  and  $\zeta_c = \frac{C}{2\omega_n M}$ .

The percentage of critical damping can then be simplified as

$$\zeta_c = -\frac{C}{2\sqrt{MK}} \times 100\% \quad (11.23)$$

The total mass matrix and linearized damping matrix may be frequency dependent. As an approximation, constant added mass and damping matrices at 'drift frequencies' with a wave period of 200 seconds are used in [Equation 11.17 \(p. 177\)](#). In order to evaluate a more accurate natural frequency and its corresponding mode of motion, an iterative approach may be employed. This picks up the hydrodynamic added mass and damping at a frequency close to that natural frequency, and is implemented in the Aqwa Graphical Supervisor (AGS) online dynamic stability calculation.



# Chapter 12: Frequency Domain Dynamic Simulation

The determination of the motions of a moored floating structure system in response to environmental forces (i.e. wind, waves, and current) and structure control mechanisms is a complex procedure, which may include system nonlinearities (such as mooring line nonlinearities) and position-dependent environmental loads, as well as any motion control mechanisms. For a systematic parametric study, given the large number of possible combinations of environmental conditions, a time domain analysis would be prohibitively time-consuming; however, a frequency domain evaluation of the system response can provide a simple and fast tool to fulfill this requirement.

## 12.1. Linearization

It is assumed that a frequency domain analysis is carried out when the analyzed structure system is at its equilibrium location, which should either be imported from the previous estimation (discussed in [Equilibrium Estimation and Stability Analysis of Structure System \(p. 171\)](#)) or directly defined by the user. Mooring line stiffness, hydrostatic stiffness and the stiffness due to reaction forces at articulations are re-estimated at this equilibrium location. An Aqwa frequency domain evaluation of the system response does not directly include system nonlinearities in its analysis. Some nonlinearities, such as wind drag force, the drag force on Morison elements, or dynamic cables, are firstly linearized and then applied to the motion response calculations.

### 12.1.1. Wind Drag Linearization

As described in [Wind \(p. 35\)](#), the wind speed generally consists of a mean velocity over a given period of time (usually 1 hour) at a standard height above the water surface (usually 10m), and a turbulent time-varying wind speed about the mean speed in a constant direction with respect to the fixed reference axes, as expressed in [Equation 2.67 \(p. 36\)](#). In a frequency domain analysis we assume that the displacement response of a structure from its equilibrium position is small, and that the turbulent time-varying wind speed is small compared to the mean wind speed. Based on these assumptions, and by substituting [Equation 2.71 \(p. 37\)](#) into [Equation 7.2 \(p. 122\)](#), for the wind hull drag force:

$$F_{wj} = C_{wdj}(\beta) |\bar{V}_Z| \left\{ \bar{V}_Z + 2 \sum_{k=1}^{N_w} \sqrt{2S(f_k)\Delta f_k} \cos(2\pi f_k t + \alpha_k) - 2V_s \right\} \text{ where } j=1,6 \quad (12.1)$$

where the subscript  $j$  ( $j = 1, 3$ ) represents the force components in the local structure x-, y- and z-directions respectively, the subscript  $j$  ( $j = 4, 6$ ) represents the moment components about the local structure x-, y- and z-directions respectively,  $\beta$  is the relative angle between the wind direction and the structure at its equilibrium position,  $C_{wdj}(\beta)$  ( $j = 1, 6$ ) are the wind hull drag coefficients at  $\beta$ , and  $V_s$  is the velocity of the structure in the wind direction.

The first term of [Equation 12.1 \(p. 179\)](#) involves the signed square of the mean wind velocity, the components of which will not directly affect the frequency-dependent response. However, this term

does contribute to the stiffness due to small yaw motion. In the local structure axis system (LSA), the additional stiffness matrix components due to the constant wind drag forces and yaw motion are

$$\begin{aligned} K_{w16} &= C_{wd2}(\beta) |\bar{V}_Z| \bar{V}_Z \\ K_{w26} &= -C_{wd1}(\beta) |\bar{V}_Z| \bar{V}_Z \end{aligned} \quad (12.2)$$

From [Equation 12.1 \(p. 179\)](#), the amplitude of the linear frequency-dependent wind force at a frequency point  $k$  ( $k = 1, N_w$ ) is

$$F_{wj}(f_k) = 2C_{wdj}(\beta) |\bar{V}_Z| \sqrt{2S(f_k) \Delta f_k} \text{ where } j=1,6 \quad (12.3)$$

Finally, the linear wind drag damping force is

$$F_{wdj} = -2C_{wdj}(\beta) |\bar{V}_Z| V_s \text{ where } j=1,6 \quad (12.4)$$

### 12.1.2. Dynamic Cable Drag Linearization

When including the current speed effect, the linearized drag factor on a dynamic cable takes the form

$$\delta = \sqrt{(\alpha u_{rms})^2 + \gamma u_c^2} \quad (12.5)$$

where  $u_{rms}$  and  $u_c$  are the root mean square of the cable velocity and the current velocity respectively, in either the transverse or axial direction, and:

$$\begin{aligned} \alpha &= \sqrt{\frac{8}{\pi}} \\ \gamma &= 2(2 - e^{-r}) \\ r &= \frac{u_c}{u_{rms}} \end{aligned}$$

The linearized drag force due to current velocity may be written as

$$F_{drag} = \frac{1}{2} (\rho A C_d \delta) u \quad (12.6)$$

where  $\rho$  is the density of water,  $A$  is the cross-sectional area of the cable,  $C_d$  is the drag coefficient, and  $u$  is the velocity of a cable section in either the transverse or axial direction.

To estimate the root mean square of the cable velocity in multi-directional waves, the average motion RAOs at the attachment ends of a dynamic cable are used to calculate the harmonic response of that cable.

Denoting  $S_{wm}(\omega_j)$  as the wave spectral ordinate at the  $j$ -th wave component ( $j = 1, N_w$ ) of the  $m$ -th sub-directional wave spectrum ( $m = 1, N_d$ ), and the complex value  $U_m(\omega_j)$  as the motion RAO of the mooring attachment end at position  $(x, y, z)$  due to wave component  $\omega_j$  in the  $m$ -th wave direction  $\chi_m$ , the average RAO at the wave frequency  $\omega_j$  is expressed as

$$U(\omega_j) = \sum_{m=1}^{N_d} \sqrt{S_{wm}(\omega_j)} U_m(\omega_j) e^{i[k_x x \cos \chi_m + k_y y \sin \chi_m + \alpha_{jm}]} / \sum_{m=1}^{N_d} \sqrt{S_{wm}(\omega_j)} \quad (12.7)$$

where  $\alpha_{jm}$  is the random phase of the wave component  $(\omega_j, \chi_m)$ , and  $N_d$  is the total number of sub-directional wave spectra.

The total wave energy at a frequency  $\omega_j$  is assumed to be the summation of all of the wave component energies at that frequency:

$$E(\omega_j) = \sum_{m=1}^{N_d} S_{wm}(\omega_j) \Delta\omega_j \quad (12.8)$$

Using [Equation 12.7 \(p. 180\)](#) to determine RAOs at the ends of the cable, the average motion RAOs at the nodes  $u_n(\omega_j)$  of each of the cable elements can be calculated. The root mean square of the nodal motion velocity is then determined by

$$u_{rms} = \sqrt{\sum_{j=1}^{N_w} E(\omega_j) \omega_j^2 |u_n(\omega_j)|^2} \quad (12.9)$$

which will subsequently be used in [Equation 12.5 \(p. 180\)](#) to determine the linearized drag factor by means of an iterative procedure.

### 12.1.3. Morison Element Drag Linearization

Linearized drag on a Morison element is optionally included in frequency domain dynamic simulations. The detailed numerical approach is discussed in [Morison Drag Linearization \(p. 112\)](#).

### 12.1.4. Current Hull Drag Linearization

The current or wind drag forces on a structure in the relative current or wind direction can be expressed in the form of [Equation 7.17 \(p. 126\)](#).

Denoting the horizontal structure translational velocity in the local structure axes (LSA) as  $\vec{u}_s = (u_{s1}, u_{s2})$  and ignoring the constant component of the hull drag force for the frequency domain analysis, the linearized hull drag force is given by

$$\mathbf{F} = \mathbf{D}_H \mathbf{u}_s = \mathbf{D}_H \begin{bmatrix} u_{s1} \\ u_{s2} \end{bmatrix} \quad (12.10)$$

where  $\mathbf{F}$  is the  $6 \times 1$  force/moment matrix, and  $\mathbf{D}_H$  is the  $6 \times 2$  linearized damping matrix.

The fundamental requirement of the hull drag linearization is an equal dissipation of associated energy between the exact time domain analysis and the linearized hull drag frequency domain analysis. The energy dissipation ratio (EDR), which represents the ratio of energy in the time history to the linearized drag dissipated energy in the frequency domain, must have a unit value. By employing [Equation 12.10 \(p. 181\)](#) and [Equation 7.2 \(p. 122\)](#), this requirement can be expressed as

$$EDR(\text{total}) = \frac{\int \{\mathbf{D}_H \mathbf{u}_s\} \cdot \mathbf{V}_s dt}{\int \mathbf{F}_H \cdot \mathbf{V}_s dt} \rightarrow 1 \quad (12.11)$$

Where  $\mathbf{V}_s$  is the  $6 \times 1$  matrix of structure translational and rotational motions.

By satisfying the above requirement the linearized damping matrix can be calculated. This matrix relates to the current and wind speed, the user-defined hull drag coefficient database, and the root mean square values of the structure horizontal translational (surge and sway) motions.

As discussed in [Yaw Rate Drag Force \(p. 126\)](#), the current drag load components that depend on yaw rotational velocity are called yaw rate drag.

By satisfying the equivalence of energy dissipation requirement, the total damping matrix due to the yaw rate drag in the local structure axes is expressed as

$$\mathbf{D}_{YRD} = \mathbf{D}_0 - \int_{x_{min}}^{x_{max}} \mathbf{D}_1(x) dx \quad (12.12)$$

where the damping matrix due to the constant term without integration is

$$\mathbf{D}_0 = \begin{bmatrix} 0 & 0 & 0 & 0 & 0 & 0 \\ 0 & 1 & 0 & 0 & 0 & 0 \\ 0 & 0 & 0 & 0 & 0 & 0 \\ 0 & 0 & 0 & 0 & 0 & 0 \\ 0 & 0 & 0 & 0 & 0 & 0 \\ 0 & \frac{x_{max} + x_{min}}{2} & 0 & 0 & 0 & 0 \end{bmatrix} \begin{bmatrix} 0 & 0 & 0 & 0 & 0 & 0 \\ d_{21} & d_{22} & 0 & 0 & 0 & 0 \\ 0 & 0 & 0 & 0 & 0 & 0 \\ 0 & 0 & 0 & 0 & 0 & 0 \\ 0 & 0 & 0 & 0 & 0 & 0 \\ 0 & 0 & 0 & 0 & 0 & 0 \end{bmatrix} \quad (12.13)$$

in which  $d_{21}$  and  $d_{22}$  are functions of the current and wind speed, the user defined yaw rate drag coefficient, and the root mean square values of the surge and sway motions at the center of gravity of the structure. The integrand in [Equation 12.12 \(p. 182\)](#) at a point along the line between  $[x_{min}, x_{max}]$  is given by

$$\mathbf{D}_1(x) = \begin{bmatrix} 0 & 0 & 0 & 0 & 0 & 0 \\ 0 & 1 & 0 & 0 & 0 & 0 \\ 0 & 0 & 0 & 0 & 0 & 0 \\ 0 & 0 & 0 & 0 & 0 & 0 \\ 0 & 0 & 0 & 0 & 0 & 0 \\ 0 & x & 0 & 0 & 0 & 0 \end{bmatrix} \begin{bmatrix} 0 & 0 & 0 & 0 & 0 & 0 \\ d_{21}(x) & d_{22}(x) & 0 & 0 & 0 & 0 \\ 0 & 0 & 0 & 0 & 0 & 0 \\ 0 & 0 & 0 & 0 & 0 & 0 \\ 0 & 0 & 0 & 0 & 0 & 0 \\ 0 & 0 & 0 & 0 & 0 & 0 \end{bmatrix} \begin{bmatrix} 0 & 0 & 0 & 0 & 0 & 0 \\ 0 & 1 & 0 & 0 & 0 & x \\ 0 & 0 & 0 & 0 & 0 & 0 \\ 0 & 0 & 0 & 0 & 0 & 0 \\ 0 & 0 & 0 & 0 & 0 & 0 \\ 0 & 0 & 0 & 0 & 0 & 0 \end{bmatrix} \quad (12.14)$$

where  $d_{21}(x)$  and  $d_{22}(x)$  are functions of the current and wind speed, the user defined yaw rate drag coefficient, and the root mean square values of the structure horizontal translational motion components normal to the line between  $[x_{min}, x_{max}]$  at that point.

The Morison hull drag force and moment components expressed by [Equation 7.17 \(p. 126\)](#) can also be linearized for a frequency domain analysis. The linearized damping matrix in the local structure axes is given by

$$\mathbf{D}_{MOR} = \mathbf{C}_{dm} \boldsymbol{\alpha} \quad (12.15)$$

where

$$\boldsymbol{\alpha} = \begin{bmatrix} \alpha_1 & 0 & 0 & 0 & 0 & 0 \\ 0 & \alpha_2 & 0 & 0 & 0 & 0 \\ 0 & 0 & \alpha_3 & 0 & 0 & 0 \\ 0 & 0 & 0 & \alpha_4 & 0 & 0 \\ 0 & 0 & 0 & 0 & \alpha_5 & 0 \\ 0 & 0 & 0 & 0 & 0 & \alpha_6 \end{bmatrix}$$

in which the coefficients  $\alpha_j$  ( $j = 1,6$ ) are a function of the current speed (for  $j = 1,2$  only) and the root mean square value of the structure motion in the  $j$ -th degree of freedom.

For a given relative heading, the steady hull drag force and moment components can be expressed in the local structure axes by [Equation 7.2 \(p. 122\)](#). Similar to the wind drag force-induced stiffness in [Equation 12.2 \(p. 180\)](#), the additional stiffness matrix components due to the constant current drag forces and yaw motion are

$$\begin{aligned} K_{c16} &= C_{cd2}(\beta) |U_c| U_c \\ K_{c26} &= -C_{cd1}(\beta) |U_c| U_c \end{aligned} \quad (12.16)$$

where  $C_{cdj}(\beta)$  ( $j = 1, 2$ ) are the wind hull drag coefficients at the relative angle  $\beta$ , and  $U_c$  is the current velocity at a specified water depth.

### 12.1.5. Nonlinear Roll Damping Linearization

For the irregular wave case, to minimize the least squares error of energy dissipation, the equivalent linear roll damping with respect to the local roll axis is:

$$C_{roll} = \sqrt{\frac{8}{\pi}} \sigma_{\dot{\phi}} C_{droll} \quad (12.17)$$

where  $\sigma_{\dot{\phi}}$  is the RMS of roll angular velocity and  $C_{droll}$  is the quadratic roll damping coefficient defined in either [Equation 7.13 \(p. 126\)](#) or [Equation 7.14 \(p. 126\)](#).

When the bilge vortex shedding roll drag is included, the Keulegan-Carpenter number for bilge is amended from [Equation 7.4 \(p. 123\)](#) as:

$$K_{cb} = \sqrt{\frac{8}{\pi}} \frac{R_b \sigma_{\dot{\phi}} T_R}{2r_b} \quad (12.18)$$

## 12.2. Response Spectral Density

In a linear dynamic system consisting of  $N$  structures, the equation of motion in the frequency domain is written as

$$[-\omega^2 \mathbf{M} - i\omega \mathbf{C} + \mathbf{K}] \mathbf{U} = \mathbf{F} \quad (12.19)$$

where  $\mathbf{M}$ ,  $\mathbf{C}$ , and  $\mathbf{K}$  are the  $6N \times 6N$  mass, damping, and stiffness matrices respectively,  $\mathbf{U}$  is the  $6N \times 1$  motion response, and  $\mathbf{F}$  is the  $6N \times 1$  external force, at frequency  $\omega$ .

In [Equation 12.19 \(p. 183\)](#),  $[-\omega^2 \mathbf{M} - i\omega \mathbf{C} + \mathbf{K}]$  is called the impedance matrix, while the receptance matrix is defined as

$$\mathbf{H} = [-\omega^2 \mathbf{M} - i\omega \mathbf{C} + \mathbf{K}]^{-1} \quad (12.20)$$

The motion response in complex values can then be expressed as

$$\mathbf{U} = \mathbf{H} \mathbf{F} \quad (12.21)$$

It should be noted that if the external force in [Equation 12.19 \(p. 183\)](#) only consists of the first order wave excitation force induced by a regular wave with unit amplitude, and the stiffness matrix includes both the hydrostatic and structural stiffness components (for example, the stiffness due to mooring lines and articulations), the motion responses given by [Equation 12.21 \(p. 183\)](#) are referred to as the fully-coupled response amplitude operators (RAOs).

In multi-directional waves, denoting the ordinate of the  $m$ -th directional wave spectrum in direction  $\chi_m$  at frequency  $\omega$  as  $S_{wm}(\omega)$ , the  $6N \times 6N$  general transform function due to the first order wave excitation is defined as

$$\mathbf{T}(\omega) = \sum_{m=1}^{N_d} S_{wm}(\omega) \mathbf{U}^*(\omega, \chi_m) \mathbf{U}^T(\omega, \chi_m) \quad (12.22)$$

where the superscripts \* and  $T$  indicate the conjugate transpose and non-conjugate transpose of a matrix respectively, and  $N_d$  is the number of wave directions. The diagonal terms of the real part of the general transform function matrix are the motion response spectral densities, i.e.

$$S_{U_j}(\omega) = \sum_{m=1}^{N_d} S_{wm}(\omega) |U_j(\omega, \chi_m)|^2 \text{ where } j=1, 6N \quad (12.23)$$

The first order wave excitation force spectral density is

$$S_{F_j^{(1)}}(\omega) = \sum_{m=1}^{N_d} S_{wm}(\omega) |F_j^{(1)}(\omega, \chi_m)|^2 \text{ where } j=1, 6N \quad (12.24)$$

The difference frequency second order force spectral density in multi-directional waves is expressed as

$$S_{F_j^{(2)}}(\omega) = 8 \sum_{m=1}^{N_d} \sum_{n=1}^{N_d} \left\{ \int_0^\infty S_{wm}(\mu) S_{wn}(\mu+\omega) \left[ |P_{mn}^-(\mu, \mu+\omega)|^2 + |Q_{mn}^-(\mu, \mu+\omega)|^2 \right] d\mu \right\} \quad (12.25)$$

For the relative motion of a pair of nodes in the global axes, denoting the relative motion response as  $[u_{rj}(\omega, \chi_m)] = [u_{nj}(\omega, \chi_m, \vec{X}_{n1}) - u_{nj}(\omega, \chi_m, \vec{X}_{n2})]$ , ( $j=1, 3$ ), where  $[u_{nj}(\omega, \chi_m, \vec{X}_{n1})]$ ,  $[u_{nj}(\omega, \chi_m, \vec{X}_{n2})]$  are the nodal motion responses at a pair of nodes  $\vec{X}_{n1}$ ,  $\vec{X}_{n2}$  (either on the same structure, or on different structures), at frequency  $\omega$  and along wave direction  $\chi_m$ , the relative motion response spectrum is

$$S_{u_{rj}}(\omega) = \sum_{m=1}^{N_d} S_{wm}(\omega) |u_{rj}(\omega, \chi_m)|^2 \text{ where } j=1, 3 \quad (12.26)$$

For nodal motion relative to the wave surface, denoting the wave elevation of a unit amplitude regular wave at the location of the node as  $\zeta(\omega, \chi_m, \vec{X}_n)$ , the relative vertical motion response spectrum can be obtained from

$$S_{u_{n3}}(\omega) = \sum_{m=1}^{N_d} S_{wm}(\omega) |u_{n3}(\omega, \chi_m, \vec{X}_n) - \zeta(\omega, \chi_m, \vec{X}_n)|^2 \quad (12.27)$$

## 12.3. Significant Value Calculation

An Aqwa frequency domain dynamic analysis outputs the significant amplitudes of forces and responses

$$R_s = 2\sqrt{m_0} \quad (12.28)$$

where  $m_0 = \int_0^\infty S_R(\omega) d\omega$  in which  $S_R(\omega)$  is a force or response spectral density.

The significant amplitude given by [Equation 12.28 \(p. 184\)](#) can be used to estimate the probable maximum value over a given duration. If the force or response spectral density is assumed to be Rayleigh-distributed, and the mean zero crossing period of the force or response is assumed to be similar to the mean zero crossing period  $T_z$  of the wave spectrum (as computed according to [Irregular Waves \(p. 26\)](#)), the number of independent maxima  $N$  over the duration  $T$  can be estimated as

$$N = \frac{T}{T_z} \quad (12.29)$$

Assuming that  $N$  is large, the probable maximum value  $R_{\max}$  can be determined from

$$R_{\max} = \alpha R_s \quad (12.30)$$

where the scaling factor  $\alpha$  is defined as

$$\alpha = \left( \frac{\ln N}{2} \right)^{\frac{1}{2}} \quad (12.31)$$

To similarly estimate a  $p$ -fractile (or percentile) extreme value of the force or response this scaling factor can be modified as

$$\alpha = \left( \frac{\ln N - \ln(-\ln p)}{2} \right)^{\frac{1}{2}} \quad (12.32)$$

where  $0.0 < p < 1.0$ . Using the formulation, the median extreme value can be estimated by setting  $p=0.5$ , while the expected extreme is estimated with  $p=0.5703$  [11](#).

Numerically, the density integration of spectral densities is performed over a finite frequency range. When the wave frequency responses only are concerned, this numerical integrating wave frequency range is given by  $[\omega_{start}^{sg}, \omega_{finish}^{sg}]$  (as defined in [Equation 11.4 \(p. 172\)](#) for a specified wave spectral group). When the total is required, consisting of both the wave frequency and drift frequency responses, the wave frequency range is given by  $[0, \omega_{finish}^{sg}]$ .

Integration of the response spectral density is achieved using a 3-point Gaussian quadrature algorithm within program-selected frequency intervals. These intervals are chosen based on the natural frequencies of the equations of motion and the peak of the spectrum, as described below.

Let us assume that there are  $M$  natural frequencies falling into the frequency range of integration as defined above. Denoting  $\omega_{nj}$  as the  $j$ -th natural frequency of the structural system with a critical damping percentage  $\zeta_{Cj}$ , the frequency at the peak value of the receptance function of the  $j$ -th single degree of freedom system is

$$\omega_{pj} = \omega_{nj} \sqrt{1 - 2\zeta_{Cj}^2} \quad (12.33)$$

The effective critical damping percentage and effective natural frequency of each sub-directional wave spectrum are defined as

$$\begin{aligned} \zeta_{Cj} &= 0.3849 \frac{S_{wj}(\omega_{pj})}{\omega_{pj} \max \left\{ \frac{dS_{wj}}{d\omega} \right\}} \text{ where } j = M+1, M+N_d \\ \omega_{nj} &= \omega_{pj} \end{aligned} \quad (12.34)$$

where  $\omega_{pj}$  is the peak frequency of the  $j$ -th sub-directional wave spectrum.

If the starting integration frequency is  $\omega_0$ , then the frequency interval from this starting frequency is determined by

$$\Delta\omega_0 = \min\{\Delta\omega_{0j}\} \text{ where } j=1, M+N_d \quad (12.35)$$

where

$$\Delta\omega_{0j} = \begin{cases} 0.75 \times |\omega_{pj} - \omega_0| + 0.375 \zeta_{Cj} \omega_{nj}, & \text{if } |\omega_0 - \omega_{pj}| > 1.5 \zeta_{Cj} \omega_{nj} \\ 1.5 \zeta_{Cj} \omega_{nj}, & \text{if } |\omega_0 - \omega_{pj}| \leq 1.5 \zeta_{Cj} \omega_{nj} \end{cases}$$

Three Gaussian evaluation points are chosen within the frequency interval of  $[\omega_0, \omega_0 + \Delta\omega_0]$ .

Subsequently, the starting frequency for the  $k$ -th 3-point Gaussian quadrature integration is found from

$$\omega_k = \omega_{k-1} + \Delta\omega_{k-1} \quad (12.36)$$

where  $\omega_k < \omega_{finish}^{sg}$ , and the frequency interval  $\omega_k$  is defined as

$$\Delta\omega_k = \min\{\Delta\omega_{kj}\} \text{ where } j=1, M+N_d \quad (12.37)$$

where

$$\Delta\omega_{kj} = \begin{cases} 0.75 \times |\omega_{pj} - \omega_k| + 0.375 \zeta_{Cj} \omega_{nj}, & \text{if } |\omega_k - \omega_{pj}| > 1.5 \zeta_{Cj} \omega_{nj} \\ 1.5 \zeta_{Cj} \omega_{nj}, & \text{if } |\omega_k - \omega_{pj}| \leq 1.5 \zeta_{Cj} \omega_{nj} \end{cases}$$

It should be noted that in order to limit the integration to a reasonable number of intervals, a minimum critical damping percentage of 0.5% assumed.

# Chapter 13: Time Domain Dynamic Simulation

---

Aqwa can generate a time history of the simulated motions of floating structures, arbitrarily connected by articulations or mooring lines, under the action of wind, wave and current forces. The positions and velocities of the structures are determined at each time step by integrating the accelerations due to these forces in the time domain, using a two stage predictor-corrector numerical integration scheme (see [Integration in Time of Motion Equation \(p. 168\)](#)).

Aqwa can employ one of two main simulation approaches in the time domain:

- Irregular wave responses with slow drift (Aqwa-Drift)

This analysis is used to simulate the real-time motion of a floating body or bodies while operating in irregular waves. Wave-frequency motions and low period oscillatory drift motions may be considered. Wind and current loading may also be applied.

The difference frequency and sum frequency second order forces are calculated at each time step in the simulation, together with the first order wave frequency forces and instantaneous values of all other forces. These are applied to the structures and the resulting accelerations are calculated, from which the structure positions and velocities are determined at the subsequent time step. The system properties at the end of one time step are then the starting conditions for the next, and so a time history of the motion of each structure is constructed.

As well as the instantaneous values of all other forces (i.e. wind and current drag, cable tension, etc.), one of four options can be selected to define forces due to the sea state: slow drift only, wave frequency response only, wave frequency response with slow drift, and wave frequency response with slow drift and sum frequency second order force excitation. The Aqwa-Drift analysis is normally applicable for low and moderate sea states.

- Severe wave responses (Aqwa-Naut)

This analysis is used to simulate the real-time motion of a floating body or bodies while operating in regular or irregular waves. Nonlinear Froude-Krylov and hydrostatic forces are estimated under an instantaneous incident wave surface. Wind and current loads may also be considered.

The analysis involves meshing the total surface of a structure to create a hydrodynamic and hydrostatic model. Nonlinear hydrostatic and Froude-Krylov wave forces can then be calculated from this model at each time step in a simulation, along with instantaneous values of all other forces. These forces are then applied to structures via a mathematical model (i.e. a set of nonlinear equations of motion), and the resulting accelerations are determined.

As well as instantaneous values of all other forces (i.e. wind and current drag, cable tensions, etc.), either regular or irregular wave response may be selected to define forces due to the sea state. Airy wave theory or second order Stokes wave theory, in finite-depth or deep water, can be applied for the regular wave response analysis. The Aqwa-Naut analysis is normally applicable for severe sea states, or if the wetted surface of a structure changes significantly during the simulated time (for example, during the analysis of a jacket structure launching and installation).

## 13.1. Radiation Force by Convolution Integration

If the external force  $\mathbf{F}(t)$  in a time domain analysis is not periodic with constant amplitude, the equation of motion in the frequency domain (i.e. [Equation 12.19 \(p. 183\)](#)) cannot be directly converted into the following form in the time domain:

$$\mathbf{M}\ddot{\mathbf{X}}(t) + \mathbf{C}\dot{\mathbf{X}}(t) + \mathbf{K}\mathbf{X}(t) = \mathbf{F}(t) \quad (13.1)$$

as the added mass in the mass matrix  $\mathbf{M}$  and the hydrodynamic damping in the damping matrix  $\mathbf{C}$  are frequency dependent.

Instead, the equation of motion of the floating structure system is expressed in a convolution integral form [10]

$$\{\mathbf{m} + \mathbf{A}_\infty\}\ddot{\mathbf{X}}(t) + \mathbf{c}\dot{\mathbf{X}}(t) + \mathbf{K}\mathbf{X}(t) + \int_0^t \mathbf{R}(t-\tau)\dot{\mathbf{X}}(\tau) d\tau = \mathbf{F}(t) \quad (13.2)$$

where  $\mathbf{m}$  is the structural mass matrix,  $\mathbf{A}_\infty$  is the fluid added mass matrix at infinite frequency,  $\mathbf{c}$  is the damping matrix except the linear radiation damping effects due to diffraction panels,  $\mathbf{K}$  is the total stiffness matrix, and  $\mathbf{R}$  is the velocity impulse function matrix.

Alternatively, the acceleration impulse function matrix can be employed in the equation of motion, such as

$$\{\mathbf{m} + \mathbf{A}_\infty\}\ddot{\mathbf{X}}(t) + \mathbf{c}\dot{\mathbf{X}}(t) + \mathbf{K}\mathbf{X}(t) + \int_0^t \mathbf{h}(t-\tau)\ddot{\mathbf{X}}(\tau) d\tau = \mathbf{F}(t) \quad (13.3)$$

in which the acceleration impulse function matrix is defined by

$$\mathbf{h}(t) = \frac{2}{\pi} \int_0^\infty \mathbf{B}(\omega) \frac{\sin(\omega t)}{\omega} d\omega = \frac{2}{\pi} \int_0^\infty \{\mathbf{A}(\omega) - \mathbf{A}_\infty\} \cos(\omega t) d\omega \quad (13.4)$$

where  $\mathbf{A}_\omega$  and  $\mathbf{B}_\omega$  are the added mass and hydrodynamic damping matrices, respectively, defined in [Equation 4.48 \(p. 70\)](#).

Because the complex function  $\{\mathbf{A}(\omega) - \mathbf{A}_\infty\} + \frac{i}{\omega} \mathbf{B}(\omega)$  is analytic in the upper half plane, the real and imaginary parts of this function are the Cauchy principle values of the Hilbert transforms of each other:

$$\begin{aligned} \{\mathbf{A}(\omega) - \mathbf{A}_\infty\} &= \frac{1}{\pi} cv \int_{-\infty}^{\infty} \frac{[\mathbf{B}(f)]}{f(f-\omega)} df \\ [\frac{1}{\omega} \mathbf{B}(\omega)] &= -\frac{1}{\pi} cv \int_{-\infty}^{\infty} \frac{\{\mathbf{A}(\omega) - \mathbf{A}_\infty\}}{(f-\omega)} df \end{aligned} \quad (13.5)$$

where  $cv$  denotes the Cauchy principle value. Generally, the values of the added damping coefficients at zero frequency and infinite frequency are null. It is therefore more practical to use the added damping coefficient matrix in [Equation 13.4 \(p. 188\)](#) to obtain the required impulse response function matrix.

The integration of [Equation 13.4 \(p. 188\)](#) is numerically truncated at a finite upper frequency limit. In Aqwa, this upper limit  $\omega_u$  is set to be approximately 10 radians/s, or a 0.5 second period, for a relatively

large structure. For a small diffracting structure with  $L < 20$ , where  $L$  is the characteristic structure size (in meters), this upper limit is increased by a factor of  $\sqrt{\frac{20}{L}}$ .

The selected frequency region  $[\omega_0, \omega_n]$  applied for the calculation of the diffraction and radiation potential in a conventional three-dimensional frequency domain hydrodynamic analysis may not correspond exactly to the total required range  $[0, \omega_u]$ . An automatic extrapolation is therefore carried out to estimate the added damping values in the extended frequency ranges of  $[0, \omega_0]$  and  $[\omega_n, \omega_u]$ .

The extended set of added damping coefficients in the frequency region of  $[0, \omega_u]$  is also used in the Hilbert transform shown in [Equation 13.5 \(p. 188\)](#) to obtain the fitted frequency-dependent added mass matrix  $\{\mathbf{A}'(\omega) - \mathbf{A}_\infty\}$ . A best fit is then obtained between the fitted added mass transformed from the damping coefficients and the directly-calculated added mass from an Aqwa hydrodynamic analysis. This gives the effective asymptotic added mass matrix  $\mathbf{A}_\infty$  at infinite frequency.

The average 'fitting quality' of the added mass coefficient  $A_{jk}$  is defined as

$$A_{Vjk} = 1 - \frac{\sum_{m=1}^{N_f} |A_{jk}(\omega_m) - A'_{jk}(\omega_m)|}{\alpha_{jk} N_f} \quad (13.6)$$

where  $N_f$  is the number of frequency points in the hydrodynamic database and  $\alpha_{jk}$  is the normalized mass factor, which may be related to the structure and added mass matrices as

$$\begin{aligned} \alpha_{jk} &= \sqrt{A_j A_k} \\ A_j &= m_{jj} + \frac{1}{\omega_{N_f} - \omega_1} \int_{\omega_1}^{\omega_{N_f}} A_{jj}(\omega) d\omega \\ A_k &= m_{kk} + \frac{1}{\omega_{N_f} - \omega_1} \int_{\omega_1}^{\omega_{N_f}} A_{kk}(\omega) d\omega \end{aligned} \quad (13.7)$$

where  $m_{jj}$  and  $m_{kk}$  are the diagonal elements of the structure mass matrix in the  $j$ -th and  $k$ -th degrees of freedom,  $A_{jj}(\omega)$  and  $A_{kk}(\omega)$  are the diagonal elements of the added mass matrix in the  $j$ -th and  $k$ -th degrees of freedom, and  $\omega_1$  and  $\omega_{N_f}$  are the first and last frequency points in the hydrodynamic database used for the impulse function calculation.

The [generalized damping \(p. 75\)](#) is also checked when the convolution method is used. It should generally be positive.

The impulse function convolution described above provides a more rigorous approach to the radiation force calculation in the time domain, and enhances the capability of the program in handling the nonlinear response of structures.

Alternatively, the RAO-based radiation forces at each time step can be estimated by the following approach. Denoting  $\vec{X}_g(t) = (X_g, Y_g, Z_g)$  as the position of the structure center of gravity and  $\theta_3(t)$  as the yaw angle at time  $t$  (both in the fixed reference axes), when the incident wave elevation is numerically expressed by [Equation 2.28 \(p. 26\)](#) and [Equation 2.29 \(p. 27\)](#), the free-floating structure RAO-based radiation force is given by

$$\mathbf{F}_r(t) = \sum_{m=1}^{N_d} \sum_{j=1}^{N_m} \operatorname{Re} \left\{ a_{jm} [\omega_{jm}^2 \mathbf{A}(\omega_{jm}) + i\omega_{jm} \mathbf{B}(\omega_{jm})] \mathbf{U}(\omega_{jm}, \beta_m) \cdot e^{i(k_{jm} X_g \cos \chi_m + k_{jm} Y_g \sin \chi_m - \omega_{jm} t + \alpha_{jm})} \right\} \quad (13.8)$$

where  $\mathbf{U}(\omega_{jm}, \beta_m)$  represents the motion RAOs at frequency  $\omega_{jm}$  and relative wave direction  $\beta_m = \chi_m - \theta_3(t)$ , as calculated by a frequency domain hydrodynamic diffraction analysis.

The motion RAOs appearing in [Equation 13.8 \(p. 190\)](#) do not include the nonlinear effects of mooring lines, articulations and other non-harmonic external forces. It is also assumed that at time  $t$ , the structure steadily oscillates with the incident wave component frequencies. Hence the RAO-based radiation force calculation of [Equation 13.8 \(p. 190\)](#) is considered to be a simplified, but approximate, method.

## 13.2. Sloshing Forces by Convolution Integration

The convolution integration approach discussed in [Radiation Force by Convolution Integration \(p. 188\)](#) can be used in the time domain analysis for estimating the sloshing force of the internal tank.

The added mass matrix is selected to calculate the impulse function defined by [Equation 13.4 \(p. 188\)](#),

$$\mathbf{h}_g^t(\tau) = \frac{2}{\pi} \int_0^\infty \sum \{\mathbf{A}_g^t(\omega) - \mathbf{A}_g^t(\infty)\} \cos(\omega t) d\omega \quad (13.9)$$

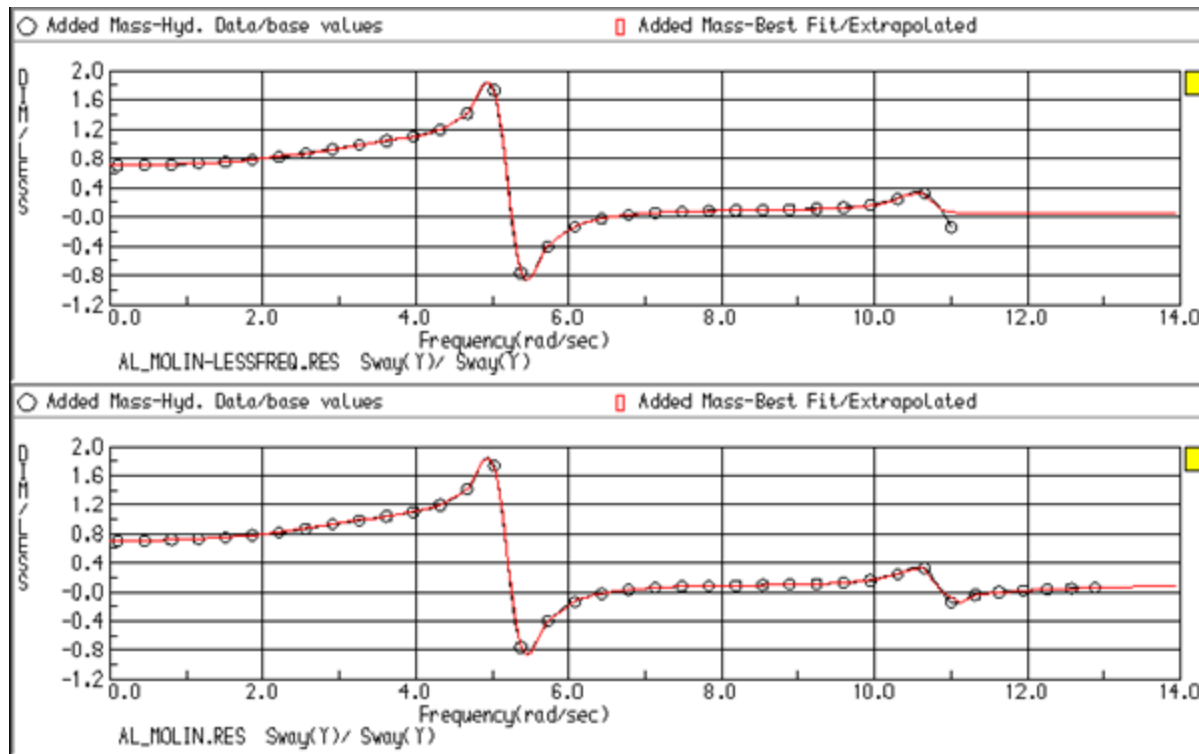
where  $\mathbf{A}_g^t(\omega)$  is the added mass matrix of the internal tank with respect to the LSA origin motions in the FRA which is define by [Equation 4.107 \(p. 83\)](#),  $\Sigma$  indicates the summation of the added mass matrices of the internal tanks attached on that structure.  $\mathbf{A}_g^t(\infty)$  is the added mass matrix at infinite frequency, which should have been calculated in the frequency domain analysis.

The equation of motion expressed in [Equation 13.3 \(p. 188\)](#) is still valid for the structures with internal tanks. Note that the assembled matrices of  $\mathbf{A}_\infty$ ,  $\mathbf{K}$  and  $\mathbf{h}$ , which consist of the contributions of both the external water and the internal tank liquids, must be employed in this equation.

If the RAO-based radiation and sloshing forces are required for motion response calculation at each time, the assembled added and damping matrices including the internal tank effects should be used in [Equation 13.8 \(p. 190\)](#).

### Note:

The maximum frequency in the hydrodynamic database should not be close to any of the internal tank's sloshing resonant frequencies in order to give a better quality of the added mass extrapolation to calculate the impulse function in [Equation 13.9 \(p. 190\)](#). As shown in [Figure 13.1: Added Mass and its Extrapolation for Impulse Function Estimation \(p. 191\)](#), the maximum frequency of the hydrodynamic database in the top graph is close to the second sloshing frequency, which for this model is centered at 11.0 rad/s; the extrapolation curve is not properly fitted to the trend of the added mass. In the bottom graph, the maximum frequency of the hydrodynamic database is 13.0 rad/s, and the extrapolated values are much closer to the original data.

**Figure 13.1: Added Mass and its Extrapolation for Impulse Function Estimation**

### 13.3. Optional Additional External Forces

Constant tensions/forces (see [Winch Line and Force Line \(p. 142\)](#)) or thruster forces (see [External Static Forces \(p. 171\)](#)) acting at specified locations on a structure can be defined as necessary.

Additional structure stiffness forces can also be defined as necessary with respect to the fixed reference axes:

$$\mathbf{F}_e(t) = \mathbf{F}_{e0} - \mathbf{K}_a \{ \mathbf{X}_g(t) - \mathbf{X}_{g0} \} \quad (13.10)$$

where  $\mathbf{K}_a$  is the additional structure stiffness matrix of the structure system,  $\mathbf{X}_{g0}$  is the equilibrium position of the origin of GXYZ of each structure, and  $\mathbf{F}_{e0}$  is the force at the equilibrium position.

External forces can also be defined in a time domain analysis by importing a time history record of those forces, and/or by an external force dynamic link library named `user_force.dll`.

The time history record of any additional external forces and moments acting at the center of gravity or the combined COG of a structure (expressed in the local structure axes (LSA) of that structure) can be stored in a file and imported for an Aqwa time domain analysis. The times defined in this imported record of external forces do not need to match the time steps of the time domain analysis, as Aqwa will interpolate the forces when necessary (using a cubic spline interpolation technique). However, when periods of constant forces are included in the record, an adequate number of data points must be provided to satisfy the interpolation method.

The dummy variables of `user_force.dll` consist of a series of constant integer and real parameters that you input, as well as the current time  $t$  and time interval  $\Delta t$ , the position and orientation array  $\mathbf{X}_g$ , and the velocity array  $\mathbf{V}_g$ , for each structure at that time in the fixed reference axes (FRA). The additional

external force matrix in the fixed reference axes can be defined as a function of the known structure positions and velocities, such as

$$\mathbf{F}_e(t) = \mathbf{F}(t, \Delta t, \mathbf{X}_g, \mathbf{V}_g, \mathbf{I}_u, \mathbf{R}_u) \quad (13.11)$$

where  $\mathbf{I}_u$  and  $\mathbf{R}_u$  are sets of user-defined constant integer and real parameters.

Alternatively, if the external forces in the structure local axis system (LSA) are defined as a function of the velocities,

$$\mathbf{F}_e^L(t) = \mathbf{F}^L(t, \Delta t, \mathbf{X}_g, \mathbf{H}^T \mathbf{V}_g, \mathbf{I}_u, \mathbf{R}_u) \quad (13.12)$$

where  $\mathbf{H} = \begin{bmatrix} \mathbf{E} & 0 \\ 0 & \mathbf{E} \end{bmatrix}$ ,  $\mathbf{E}$  is the Euler transformation matrix between the local structure axes (LSA) and the fixed reference axis (FRA) (as given by [Equation 1.7 \(p. 16\)](#)), and  $\mathbf{H}^T \mathbf{V}_g$  is therefore the structure velocity in the LSA.

The external force matrix in the FRA is then:

$$\mathbf{F}_e(t) = \mathbf{H} \mathbf{F}_e^L(t) \quad (13.13)$$

The external forces, which are linearly proportional to the structure acceleration, can be defined via the additional added mass matrix, as the accelerations are unknown variables. Similar to the external force definitions in [Equation 13.11 \(p. 192\)](#) through [Equation 13.13 \(p. 192\)](#), the additional added mass matrix in the global axes can be expressed in a general form:

$$\mathbf{M}_e(t) = \begin{cases} \mathbf{M}(t, \Delta t, \mathbf{X}_g, \mathbf{V}_g, \mathbf{I}_u, \mathbf{R}_u) & \text{directly defined in FRA} \\ \mathbf{H} \mathbf{M}^L(t, \Delta t, \mathbf{X}_g, \mathbf{H}^T \mathbf{V}_g, \mathbf{I}_u, \mathbf{R}_u) \mathbf{H}^T & \text{first defined in LSA} \end{cases} \quad (13.14)$$

[Equation 13.11 \(p. 192\)](#) through [Equation 13.14 \(p. 192\)](#) can be employed in both the prediction and correction stages of the predictor-corrector numerical time integration scheme.

## 13.4. Inertia Forces in Time Domain Analysis

Consider the model of an arbitrary mass whose center of gravity moves with the velocity array  $\mathbf{V}_g$  in the fixed reference axes (FRA). This velocity array at time  $t$  can be written as

$$\mathbf{V}_g^T(t) = \begin{bmatrix} \mathbf{v}(t) \\ \boldsymbol{\omega}(t) \end{bmatrix}^T = (v_x, v_y, v_z, \omega_x, \omega_y, \omega_z) \quad (13.15)$$

which consists of three translational and three rotational velocity components.

The momentum at time  $t$  is expressed as

$$\mathbf{P}(t) = \mathbf{M}(t) \mathbf{V}_g(t) \quad (13.16)$$

where  $\mathbf{M}(t)$  is the mass matrix at time  $t$  in the fixed reference axes.

At the next time step  $t + \Delta t$ , the momentum can be found from

$$\begin{aligned} \mathbf{P}(t + \Delta t) &= \mathbf{M}(t + \Delta t) \mathbf{V}_g(t + \Delta t) \\ &= \begin{bmatrix} \mathbf{D}^T(t) & 0 \\ 0 & \mathbf{D}^T(t) \end{bmatrix} \mathbf{M}(t) \begin{bmatrix} \mathbf{D}(t) & 0 \\ 0 & \mathbf{D}(t) \end{bmatrix} \left\{ \mathbf{V}_g(t) + \dot{\mathbf{V}}_g(t) \Delta t \right\} \end{aligned} \quad (13.17)$$

where the matrix  $\mathbf{D}(t)$  is the direction cosine matrix of the structure from its location at time  $t$  to its position at the next time step  $t+\Delta t$ . The first order direction cosine matrix with respect to  $\Delta t$  can be simplified as

$$\begin{bmatrix} \mathbf{D} & 0 \\ 0 & \mathbf{D} \end{bmatrix} = \begin{bmatrix} \mathbf{I} + \boldsymbol{\Omega} \Delta t & 0 \\ 0 & \mathbf{I} + \boldsymbol{\Omega} \Delta t \end{bmatrix} \quad (13.18)$$

where  $\boldsymbol{\Omega} = \begin{bmatrix} 0 & \omega_z & -\omega_y \\ -\omega_z & 0 & \omega_x \\ \omega_y & -\omega_x & 0 \end{bmatrix}$ .

As  $\boldsymbol{\Omega}$  is skew symmetric, i.e.

$$\boldsymbol{\Omega}^T = -\boldsymbol{\Omega} \quad (13.19)$$

and by substituting [Equation 13.18 \(p. 193\)](#) and [Equation 13.19 \(p. 193\)](#) into [Equation 13.17 \(p. 192\)](#)

$$\mathbf{P}(t+\Delta t) = \begin{bmatrix} \mathbf{I} - \boldsymbol{\Omega} \Delta t & 0 \\ 0 & \mathbf{I} - \boldsymbol{\Omega} \Delta t \end{bmatrix} \mathbf{M}(t) \begin{bmatrix} \mathbf{I} + \boldsymbol{\Omega} \Delta t & 0 \\ 0 & \mathbf{I} + \boldsymbol{\Omega} \Delta t \end{bmatrix} \left\{ \mathbf{V}_g(t) + \dot{\mathbf{V}}_g(t) \Delta t \right\} \quad (13.20)$$

Further splitting this expression into terms up to the first order with respect to  $\Delta t$ , we have

$$\begin{aligned} \mathbf{P}(t+\Delta t) = & \mathbf{M}(t) \mathbf{V}_g(t) - \left\{ \begin{bmatrix} \boldsymbol{\Omega} & 0 \\ 0 & \boldsymbol{\Omega} \end{bmatrix} \mathbf{M}(t) \mathbf{V}_g(t) - \right. \\ & \left. \mathbf{M}(t) \begin{bmatrix} \boldsymbol{\Omega} & 0 \\ 0 & \boldsymbol{\Omega} \end{bmatrix} \mathbf{V}_g(t) - \mathbf{M}(t) \mathbf{V}_g(t) \right\} \Delta t \end{aligned} \quad (13.21)$$

Between the times  $t$  and  $\Delta t$ , the variation of the structure position is  $(v_x, v_y, v_z)\Delta t$ . Due to this vector change in position, there is an additional rotational momentum term that may be written (up to the first order with respect to  $\Delta t$ ):

$$\mathbf{P}_r(t+\Delta t) = - \begin{bmatrix} 0 & 0 \\ \mathbf{V} & 0 \end{bmatrix} \mathbf{M}(t) \mathbf{V}_g(t) \Delta t \quad (13.22)$$

where  $\mathbf{V} = \begin{bmatrix} 0 & v_z & -v_y \\ -v_z & 0 & v_x \\ v_y & -v_x & 0 \end{bmatrix}$

As  $\mathbf{F} = -\frac{d\mathbf{P}}{dt}$ , the force at the center of gravity can be written up to the first order with respect to  $\Delta t$  as

$$\mathbf{F} = \begin{bmatrix} \boldsymbol{\Omega} & 0 \\ \mathbf{V} & \boldsymbol{\Omega} \end{bmatrix} \mathbf{M}(t) \mathbf{V}_g(t) - \mathbf{M}(t) \begin{bmatrix} \boldsymbol{\Omega} & 0 \\ 0 & \boldsymbol{\Omega} \end{bmatrix} \mathbf{V}_g(t) - \mathbf{M}(t) \dot{\mathbf{V}}_g(t) \quad (13.23)$$

If the added mass is omitted, the mass matrix in [Equation 13.23 \(p. 193\)](#) only includes the structure mass and moment of inertia matrix at the center of gravity:

$$\begin{aligned} \mathbf{M}(t) = & \begin{bmatrix} \mathbf{m}_{11} & 0 \\ 0 & \mathbf{m}_{22} \end{bmatrix} \\ \mathbf{m}_{11} = & m \mathbf{I} \end{aligned} \quad (13.24)$$

where  $m$  is the structure mass.

Substituting [Equation 13.24 \(p. 193\)](#) into [Equation 13.23 \(p. 193\)](#), we have

$$\mathbf{F} = \begin{bmatrix} 0 & 0 \\ 0 & \boldsymbol{\Omega} \end{bmatrix} \begin{bmatrix} \mathbf{m}_{11} & 0 \\ 0 & \mathbf{m}_{22} \end{bmatrix} \mathbf{V}_g(t) - \begin{bmatrix} \mathbf{m}_{11} & 0 \\ 0 & \mathbf{m}_{22} \end{bmatrix} \dot{\mathbf{V}}_g(t) \quad (13.25)$$

It is observed that there is no translational force component in the first term on the right hand side of [Equation 13.25 \(p. 193\)](#). The moment component in this term is named as the structural gyroscopic moment.

For each Morison element, the fluid forces and moments are calculated individually in the Morison element local axes, and then moved to the center of gravity. In such a case, the mass matrix  $\mathbf{M}(t)$  in [Equation 13.23 \(p. 193\)](#) is replaced by  $\mathbf{A}(t)$  representing the added mass matrix of the Morison element and the internal fluid mass matrix for flooded tubes, while  $\mathbf{V}_g(t)$  is the tube velocity in the Morison element local axes.

The fluid gyroscopic force and moment with respect to the origin of the Morison element local axis system are defined as

$$\mathbf{F}_{gyro}^L = \begin{bmatrix} \Omega & 0 \\ 0 & \Omega \end{bmatrix} \mathbf{A}(t) \begin{bmatrix} 0 \\ \omega(t) \end{bmatrix} \quad (13.26)$$

The fluid momentum force and wave inertia force are denoted as

$$\begin{aligned} \mathbf{F}_{mom}^L &= \begin{bmatrix} \Omega & 0 \\ \mathbf{V} & \Omega \end{bmatrix} \mathbf{A}(t) \mathbf{V}_g(t) - \mathbf{A}(t) \begin{bmatrix} \Omega & 0 \\ 0 & \Omega \end{bmatrix} \mathbf{V}_g(t) - \mathbf{F}_{gyro}^L \\ \mathbf{F}_{winer}^L &= -\mathbf{A}(t) \dot{\mathbf{V}}_g(t) \end{aligned} \quad (13.27)$$

The corresponding forces and moments with respect to the center of gravity of the structure in the fixed reference axes can be determined by transformations similar to those applied in [Equation 6.20 \(p. 116\)](#).

## 13.5. Irregular Wave Responses with Slow Drift (Aqwa-Drift)

Nonlinear hydrodynamic problems of marine floating structures in moderate sea waves can be analyzed by employing second order wave force theory.

### 13.5.1. Wave Excitation Forces and Motion Equation

Nonlinear wave excitation forces can be determined by the perturbation approach, with the wave amplitude as a small parameter, as discussed in [Second Order Wave Excitation Forces \(p. 97\)](#).

When the multi-directional wave elevation is generally represented by [Equation 2.28 \(p. 26\)](#) and [Equation 2.29 \(p. 27\)](#), the first order wave excitation force and moment, i.e. the sum of the Froude-Krylov and diffracting forces and moments, can be simply written as

$$\begin{aligned} \mathbf{F}^{(1)}(t) &= \sum_{m=1}^{N_d} \sum_{j=1}^{N_m} a_{jm} \mathbf{E}(t) \left\{ \mathbf{F}_I(\omega_{jm}, \beta_m) + \right. \\ &\quad \left. \mathbf{F}_d(\omega_{jm}, \beta_m) \right\} e^{j(k_{jm}X_g \cos \chi_m + k_{jm}Y_g \sin \chi_m - \omega_{jm}t + \alpha_{jm})} \end{aligned} \quad (13.28)$$

where  $\mathbf{E}(t)$  is the Euler rotation matrix defined by [Equation 1.7 \(p. 16\)](#) at a time  $t$ ,  $\beta_m = \chi_m - \theta_3(t)$  is the relative heading angle of the  $m$ -th sub-directional wave (relative to the structure, where  $\theta_3(t)$  is the instantaneous yaw angle of the structure), and  $\mathbf{F}_I + \mathbf{F}_d$  is the total first order wave excitation force induced by an unit amplitude incident wave with frequency  $\omega_{jm}$  and wave direction  $\beta_m$ . The components of this excitation force are expressed in [Equation 4.48 \(p. 70\)](#) and are calculated by a hydrodynamic diffraction analysis (Aqwa-Line) prior to the present time domain analysis.

From [Equation 5.20 \(p. 104\)](#), the second order wave excitation force in the fixed reference axes is given by

$$\begin{aligned} \mathbf{F}^{(2)}(t) = & \sum_{m=1}^{N_d} \sum_{n=1}^{N_d} \sum_{j=1}^{N_m} \sum_{k=1}^{N_n} a_{jm} a_{kn} \mathbf{E} \left\{ \mathbf{P}_{jk}^+(\beta_m, \beta_n) \cos[(\omega_{jm} + \omega_{kn}) t - (\varepsilon_{jm} + \varepsilon_{kn})] \right. \\ & + \mathbf{Q}_{jk}^+(\beta_m, \beta_n) \sin[(\omega_{jm} + \omega_{kn}) t - (\varepsilon_{jm} + \varepsilon_{kn})] \\ & + \mathbf{P}_{jk}^-(\beta_m, \beta_n) \cos[(\omega_{jm} - \omega_{kn}) t - (\varepsilon_{jm} - \varepsilon_{kn})] \\ & \left. + \mathbf{Q}_{jk}^-(\beta_m, \beta_n) \sin[(\omega_{jm} - \omega_{kn}) t - (\varepsilon_{jm} - \varepsilon_{kn})] \right\} \end{aligned} \quad (13.29)$$

where  $\varepsilon_{jm} = k_{jm} X_g \cos \chi_m + k_{jm} Y_g \sin \chi_m + \alpha_{jm}$  and  $\varepsilon_{kn} = k_{kn} X_g \cos \chi_n + k_{kn} Y_g \sin \chi_n + \alpha_{kn}$ .

Substituting the first and second order wave forces into [Equation 13.3 \(p. 188\)](#), the following equation of motion is solved:

$$\begin{aligned} \{\mathbf{m} + \mathbf{A}_\infty\} \ddot{\mathbf{X}}(t) = & \mathbf{F}^{(1)}(t) + \mathbf{F}^{(2)}(t) + \mathbf{F}_c(t) + \mathbf{F}_w(t) + \mathbf{F}_b(t) + \\ & \mathbf{F}_t(t) + \mathbf{F}_e(t) - \mathbf{c} \dot{\mathbf{X}}(t) - \mathbf{K} \mathbf{X}(t) - \int_0^t \mathbf{h}(t-\tau) \ddot{\mathbf{X}}(\tau) d\tau \end{aligned} \quad (13.30)$$

in which the total stiffness matrix  $\mathbf{K}$  includes the linear hydrostatic stiffness as well as all other stiffnesses, for example from mooring lines or articulations,  $\mathbf{F}_c(t)$  is the current hull drag force,  $\mathbf{F}_w(t)$  is the wind drag force,  $\mathbf{F}_b(t)$  is the nonlinear bilge roll damping force,  $\mathbf{F}_t(t)$  is the mooring and articulation force, and  $\mathbf{F}_e(t)$  represents additional external forces. The wave drift damping coefficients are optionally included in the damping matrix  $\mathbf{c}$ .

The structure responses due to mean and slowly-varying wave loads can be estimated from [Equation 13.30 \(p. 195\)](#) by including only the low frequency drift forces, i.e. the difference frequency terms of  $\mathbf{P}_{jk}^-(\beta_m, \beta_n)$ ,  $\mathbf{Q}_{jk}^-(\beta_m, \beta_n)$  in [Equation 13.29 \(p. 195\)](#).

If only the first order wave excitation force is involved in [Equation 13.30 \(p. 195\)](#), the wave frequency responses can be calculated.

Wave frequency response with slow drift can be analyzed from [Equation 13.30 \(p. 195\)](#) by including the first order wave excitation force together with the difference frequency second order drift forces.

The sum frequency second order force and moment components without directional coupling effects can be considered when the first order wave excitation force and both the difference frequency and sum frequency second order forces are included. The sum frequency second order force may only be included if the full quadratic transfer function (QTF) option has been applied in the hydrodynamic diffraction analysis (Aqwa-Line) prior to this time domain analysis.

### 13.5.2. Motions at Drift Frequency

Because of their large mass and flexible or soft moorings, large floating structures that are moored at sea tend to have natural periods of oscillation in the horizontal degrees of freedom that are of the order of minutes. At these periods there is no first order spectral energy, so they are not appreciably excited by first order forces in these degrees of freedom. However, the difference frequency drift forces vary with very low frequencies, implying large periods that may coincide with the natural period of oscillation of a large floating structure. Excitation at periods close to resonance results in

large amplification factors in the motions of the structure. These motions are the drift frequency motions.

From [Equation 13.30 \(p. 195\)](#), the drift frequency equation of motion is:

$$\{\mathbf{m} + \mathbf{A}_d\}\ddot{\mathbf{X}}(t) = \mathbf{F}_{sv}(t) + \mathbf{F}_c(t) + \mathbf{F}_w(t) + \mathbf{F}_b(t) + \mathbf{F}_t(t) + \mathbf{F}_e(t) + \mathbf{F}_h(t) + \mathbf{F}_r(t) \quad (13.31)$$

where  $\mathbf{A}_d$  is the drift frequency added mass,  $\mathbf{F}_{sv}(t)$  is the difference frequency force component of the second order force  $\mathbf{F}_{(2)}(t)$  given in [Equation 13.29 \(p. 195\)](#), and  $\mathbf{F}_h(t)$  and  $\mathbf{F}_r(t)$  are the hydrostatic force and radiation force components given by the impulse function integration, respectively.

It is assumed that the values of drift added mass and damping are constant.

When only drift wave forces are present, the structure will experience drift oscillations. This is termed the slow motion, with a corresponding slow position.

### 13.5.3. Motions at Drift and Wave Frequency

As well as being excited by drift forces, the structure will be subjected to first order wave frequency forces. Since the added mass and damping are not constant over the wave frequency range, [Equation 13.30 \(p. 195\)](#) should be employed directly.

When both drift and wave frequency forces are present, the structure will still experience drift oscillations, but these will be accompanied by wave frequency oscillations about the slow position. These latter oscillations are termed the wave frequency motion, with a corresponding wave frequency position. The sum of the slow position and the wave frequency position is called the total position, which is referred to simply as the position.

In cases where both drift and wave frequency motions exist, the current drag and wave drift forces are applied to the structure in an axis system that follows the slow position. However, wind forces are applied using an axis system that follows the total position.

The slow position is obtained by applying a low-pass filter to the total position, which removes the high frequency (fast) oscillations. This is achieved by integrating the following equation at each time step:

$$\ddot{\mathbf{X}}_s(t) + 2\omega_f \mathbf{c} \dot{\mathbf{X}}_s(t) + \omega_f^2 \{ \mathbf{X}_s(t) - \mathbf{X}(t) \} = 0 \quad (13.32)$$

where  $\mathbf{X}_s(t)$  is the slow position,  $\omega_f$  is the filtering frequency,  $\mathbf{c}$  is the filter damping, and  $\mathbf{X}(t)$  is the total position.

The filtering frequency is chosen automatically to eliminate the wave frequency effects. The damping is set to be 20% of the critical damping.

The difference between the unfiltered (total) and filtered (slow) positions is the wave frequency position  $\mathbf{X}_w(t)$ , i.e.

$$\mathbf{X}_w(t) = \mathbf{X}(t) - \mathbf{X}_s(t) \quad (13.33)$$

The response amplitude operator-based (RAO-based) position can also be estimated in a time domain analysis. As discussed in [Response Amplitude Operators \(p. 70\)](#), an RAO is determined from a frequency domain hydrodynamic analysis. A time history of the RAO-based position can be constructed by

combining RAOs at a series of frequencies with the wave spectrum. This is done for each degree of freedom as follows:

$$\mathbf{X}_{RAO}(t) = \sum_{m=1}^{N_d} \sum_{j=1}^{N_m} \operatorname{Re} \left\{ a_{jm} \mathbf{x}(\omega_{jm}, \beta_m) e^{i(k_{jm} X_g \cos \chi_m + k_{jm} Y_g \sin \chi_m - \omega_{jm} t + \alpha_{jm})} \right\} \quad (13.34)$$

where  $\mathbf{x}(\omega_{jm}, \beta_m)$  is the motion RAO at frequency  $\omega_{jm}$  and relative wave direction  $\beta_m = \chi_m - \theta_3(t)$ , as calculated by a hydrodynamic diffraction analysis.

This RAO-based position is used to calculate the initial fast position to minimize transients.

A similar expression is used to calculate the RAO-based velocity and acceleration, such as

$$\begin{aligned} \dot{\mathbf{X}}_{RAO}(t) &= \sum_{m=1}^{N_d} \sum_{j=1}^{N_m} \operatorname{Im} \left\{ a_{jm} \omega_{jm} \mathbf{x}(\omega_{jm}, \beta_m) e^{i(k_{jm} X_g \cos \chi_m + k_{jm} Y_g \sin \chi_m - \omega_{jm} t + \alpha_{jm})} \right\} \\ \ddot{\mathbf{X}}_{RAO}(t) &= \sum_{m=1}^{N_d} \sum_{j=1}^{N_m} \operatorname{Re} \left\{ -a_{jm} \omega_{jm}^2 \mathbf{x}(\omega_{jm}, \beta_m) e^{i(k_{jm} X_g \cos \chi_m + k_{jm} Y_g \sin \chi_m - \omega_{jm} t + \alpha_{jm})} \right\} \end{aligned} \quad (13.35)$$

For simple cases, the RAO-based position will be very similar to the wave frequency position defined by [Equation 13.33 \(p. 196\)](#). This can provide a useful check on the wave frequency position in runs where wave frequency forces are included.

### 13.5.4. Initial Position and Transients

[Equation 13.30 \(p. 195\)](#) represents the second order differential equations of motion for each structure. This is solved using the semi-implicit two stage predictor-corrector integration scheme described in [Integration in Time of Motion Equation \(p. 168\)](#). The resulting accelerations are then integrated to form a time history of structure motions. In order to begin this integration, the solver requires initial conditions for the total and slow positions at time  $t=t_0$ . It is also important that the transient experienced by the structure is as small as possible.

The initial conditions for the slow motion are relatively intuitive, since these relate to the general motion of the structure about its equilibrium position. The wave frequency motions, however, are in response to randomly-phased wave frequency forces that generally cannot be specified. In this case the program automatically computes an initial wave frequency position from [Equation 13.34 \(p. 197\)](#) at time  $t=t_0$ , which is added to the defined slow position to form an initial total position. The initial wave frequency velocity is estimated from [Equation 13.35 \(p. 197\)](#). These treatments ensure that the total initial conditions contain a fast (wave frequency) component equal to the steady state solution in response to the wave frequency forces at that instant; the transients can thus be minimized.

## 13.6. Motion Response in Severe Sea State (Aqwa-Naut)

Variations in the wetted hull surface due to severe sea waves and/or large amplitude motions may contribute significantly to nonlinear hydrodynamic loads. In such cases, the perturbation approach with wave amplitude and motion as small parameters (that is, the second order wave force theory) may no longer be valid.

Analysis of motion response in severe sea states is performed with Aqwa-Naut, which involves meshing the total surface of a structure to create a hydrodynamic and hydrostatic model. Nonlinear hydrostatic

and Froude-Krylov wave forces over the instantaneous wetted surface (i.e. beneath the incident wave surface) can then be calculated from this model. This calculation is performed at each time step of the simulation, along with instantaneous values of all other forces. These forces are then applied to structures, via a mathematical model (i.e. a set of nonlinear equations of motion), and the resulting accelerations are determined. The position and velocity at the subsequent time step are found by integrating these accelerations in the time domain, using a two stage predictor-corrector numerical integration scheme.

However, for large floating structures modeled by diffracting panel elements, the diffraction and radiation components are of comparable magnitude and are linear quantities.

The diffraction force in short crest waves contributed by all the diffracting panels is:

$$F_d(t) = E(t) \sum_{N_d}^{m=1} \sum_{N_m}^{j=1} a_{jm} F_d(\omega_{jm}, \beta_m) e^{i(k_{jm} X_g \cos \chi_m + k_{jm} Y_g \sin \chi_m - \omega_{jm} t + \alpha_{jm})} \quad (13.36)$$

where  $E(t)$  is the Euler rotation matrix at time  $t$  defined by [Equation 1.7 \(p. 16\)](#),  $\beta_m = \chi_m - \theta_3(t)$  is the relative heading angle of the wave direction with respect to the structure where  $\theta_3(t)$  is the yaw motion angle of the structure, and  $F_d(\omega_{jm}, \beta_m)$  is the diffraction wave force induced by a unit amplitude incident wave with frequency  $\omega_{jm}$  and relative wave direction  $\beta_m$ . The components of the diffraction wave excitation force are expressed in [Equation 4.48 \(p. 70\)](#) and are calculated by a hydrodynamic analysis prior to the current time domain analysis,  $N_d$  is the number of wave directions and  $N_m$  is the number of wave components in the  $m$ -th wave direction.

The radiation force consists of the impulse function convolution and the inertia force due to the added mass at infinite frequency, which are the same as those in [Equation 13.30 \(p. 195\)](#).

### 13.6.1. Extended Wheeler Stretching Method

Nonlinear hydrostatic and Froude-Krylov forces, as well as Morison forces, are evaluated by integrating the fluid pressure over the instantaneous wetted surface or by employing the Morison equation on tube/disc elements of a floating structure in rough waves. Accurate dynamic or kinematic properties of fluid particles beneath the wave surface are thus required for this purpose.

Du et al. [13] discussed and developed several approaches for a more accurate estimation of the fluid pressure and fluid particle velocity. Among these approaches, Wheeler stretching [42] for the first order approximation, as well as extended Wheeler stretching for the second order approximation, are selected for their efficiency and ease of completion in an Aqwa time domain analysis of severe waves. These ensure that the total pressure at the instantaneous incident wave surface (consisting of the incident wave pressure and the hydrostatic pressure) is zero.

#### 13.6.1.1. Wheeler Stretching for Regular Linear Airy Waves

This first order wave formula for an incident wave is derived from the perturbation expression beneath the mean free surface. The main properties of a regular linear Airy wave in finite-depth water, such as the fluid potential, hydrodynamic pressure, velocity and acceleration of a fluid particle, and the wave elevation, are expressed in first order terms:

$$\begin{aligned}
\varphi(x,y,z;t) &= -\frac{iga_w}{\omega} \frac{\cosh[k(z+d)]}{\cosh(kd)} e^{-i\omega t + ik(x\cos\chi + y\sin\chi) + i\alpha} \\
p &= -\rho \frac{\partial \varphi(x,y,z;t)}{\partial t} = i\omega \rho \varphi(x,y,z;t) \\
\vec{V} &= \nabla \varphi(x,y,z;t) = k\varphi(x,y,z;t) (i\cos\chi, i\sin\chi, \tanh[k(z+d)]) \\
\vec{a} &= \frac{\partial \vec{V}}{\partial t} = -i\omega k \varphi(x,y,z;t) (i\cos\chi, i\sin\chi, \tanh[k(z+d)]) \\
\zeta(x,y,t) &= a_w e^{-i\omega t + ik(x\cos\chi + y\sin\chi) + i\alpha}
\end{aligned} \tag{13.37}$$

where  $a_w$  is the wave amplitude,  $\omega$  is the wave frequency (in rad/s),  $k$  is the wave number,  $\chi$  is the wave propagation direction,  $\alpha$  is the wave phase,  $d$  is the water depth, and  $(x,y,z)$  is the position vector in the fixed reference axes.

The linear perturbation expression beneath the mean free surface implies that a point defined by  $(x,y,z)$  in Equation 13.37 (p. 199), at a given time  $t$ , is not exactly at that physical location but resides at the equilibrium position where the velocity potential is determined. The exact location corresponding to this equilibrium position  $(x,y,z)$  at time  $t$  is thus denoted as  $(x,y,z)_0$  in the fixed reference axes, of which the origin is on the mean water level, and where the z-axis points upwards. Employing Wheeler stretching [42], the coordinate transformation from  $z_0$  to  $z$  is

$$z(x,y,t) = d \frac{z_0 + d}{\operatorname{Re}[\zeta(x,y,t)] + d} - d \tag{13.38}$$

Rotate the coordinate system about the z-axis such that the x-axis points in the wave propagation direction:

$$\begin{aligned}
X &= x\cos\chi + y\sin\chi \\
Y &= -x\sin\chi + y\cos\chi \\
Z &= z
\end{aligned} \tag{13.39}$$

With these transformations, the main properties of a regular linear Airy wave at a specified location  $(X,Y,Z_0)$  beneath the instantaneous incident wave surface are simplified as

$$\begin{aligned}
\operatorname{Re}\{\vec{V}\} &= \omega a_w \frac{\cosh[k(Z+d)]}{\sinh(kd)} \left\{ \cos\psi, 0, \sin\psi \tanh[k(Z+d)] \right\} \\
\operatorname{Re}\{\vec{a}\} &= \omega^2 a_w \frac{\cosh[k(Z+d)]}{\sinh(kd)} \left\{ \sin\psi, 0, -\cos\psi \tanh[k(Z+d)] \right\} \\
\operatorname{Re}\{\zeta\} &= a_w \cos\psi \\
\operatorname{Re}\{p_I\} &= \rho g a_w \frac{\cosh[k(Z+d)]}{\cosh(kd)} \cos\psi \\
p_s &= -\rho g Z_0 \\
p_t(t) &= \operatorname{Re}\{p_I\} + p_s
\end{aligned} \tag{13.40}$$

where  $\psi = kX - \omega t + \alpha$  and  $p_t(t)$  is the sum of the incident wave pressure and the hydrostatic pressure.

For a deep water case where  $d \rightarrow \infty$ , the Wheeler stretching transformation is simplified as

$$Z(X,Y,t) = Z_0 - \operatorname{Re}[\zeta(X,Y,t)] \tag{13.41}$$

The main properties of a regular linear Airy wave in deep water are then expressed as

$$\begin{aligned}
\operatorname{Re}\{\vec{V}\} &= \omega a_w e^{kZ} \{ \cos\psi, 0, \sin\psi \} \\
\operatorname{Re}\{\vec{a}\} &= \omega^2 a_w e^{kZ} \{ \sin\psi, 0, -\cos\psi \} \\
\operatorname{Re}\{\zeta\} &= a_w \cos\psi \\
\operatorname{Re}\{p_I\} &= \rho g a_w e^{kZ} \cos\psi \\
p_s &= -\rho g Z_0 \\
p_t &= \operatorname{Re}\{p_I\} + p_s
\end{aligned} \tag{13.42}$$

From [Equation 13.40 \(p. 199\)](#) and [Equation 13.42 \(p. 200\)](#), it is easily proved that  $p_t = \operatorname{Re}\{p_I\} + p_s = 0$  at a point  $(X, Y, Z_0)$  on the instantaneous incident wave surface, for both the finite-depth and deep water cases.

### 13.6.1.2. Wheeler Stretching for Irregular Airy Waves

Employing [Equation 13.39 \(p. 199\)](#), irregular linear long-crested waves can be expressed as the summation of a series of regular incident waves based on the first order perturbation beneath the mean free surface, that is,

$$\begin{aligned}
\varphi(X, Y, Z; t) &= \sum_{j=1}^{N_w} \left\{ -\frac{i g a_j}{\omega_j} \frac{\cosh[k_j(Z+d)]}{\cosh(k_j d)} e^{-i\omega_j t + ik_j X + i\alpha_j} \right\} \\
\zeta(X, Y; t) &= \sum_{j=1}^{N_w} \{ a_j e^{-i\omega_j t + ik_j X + i\alpha_j} \}
\end{aligned} \tag{13.43}$$

where  $N_w$  is the total number of wave components.

Employing Wheeler stretching ([Equation 13.38 \(p. 199\)](#)) at an actual location  $(X, Y, Z_0)$  in the fixed reference axes (FRA), at time  $t$ , [Equation 13.43 \(p. 200\)](#) can be extended for irregular long-crested waves in finite-depth water, such as

$$\begin{aligned}
\operatorname{Re}\{\vec{V}\} &= \sum_{j=1}^{N_w} \omega_j a_j \frac{\cosh[k_j(Z+d)]}{\sinh(k_j d)} \{ \cos\psi_j, 0, \tanh[k_j(Z+d)] \sin\psi_j \} \\
\operatorname{Re}\{\vec{a}\} &= \sum_{j=1}^{N_w} \omega_j^2 a_j \frac{\cosh[k_j(Z+d)]}{\sinh(k_j d)} \{ \sin\psi_j, 0, -\tanh[k_j(Z+d)] \cos\psi_j \} \\
\operatorname{Re}\{\zeta\} &= \sum_{j=1}^{N_w} a_j \cos\psi_j \\
\operatorname{Re}\{p_I\} &= \rho g \sum_{j=1}^{N_w} a_j \frac{\cosh[k_j(Z+d)]}{\cosh(k_j d)} \cos\psi_j \\
p_s &= -\rho g Z_0 \\
p_t &= \operatorname{Re}\{p_I\} + p_s
\end{aligned} \tag{13.44}$$

where  $\psi_j = k_j X - \omega_j t + \alpha_j$ .

For deep water irregular waves, the Wheeler stretching given by [Equation 13.41 \(p. 199\)](#) is used, such that [Equation 13.44 \(p. 200\)](#) may be simplified as

$$\begin{aligned}
 \text{Re}\{\vec{V}\} &= \sum_{j=1}^{N_w} \omega_j a_j e^{k_j Z} \left\{ \cos\psi_j, 0, \sin\psi_j \right\} \\
 \text{Re}\{\vec{a}\} &= \sum_{j=1}^{N_w} \omega_j^2 a_j e^{k_j Z} \left\{ \sin\psi_j, 0, -\cos\psi_j \right\} \\
 \text{Re}\{\zeta\} &= \sum_{j=1}^{N_w} a_j \cos\psi_j \\
 \text{Re}\{p_I\} &= \rho g \sum_{j=1}^{N_w} a_j e^{k_j Z} \cos\psi_j \\
 p_s &= -\rho g Z_0 \\
 p_t &= \text{Re}\{p_I\} + p_s
 \end{aligned} \tag{13.45}$$

### 13.6.1.3. Extended Wheeler Stretching for Second Order Stokes Waves

The potential and wave elevation of second order Stokes waves with set-down terms are given in [Equation 2.15 \(p. 22\)](#).

The velocity of a fluid particle at the equilibrium position  $(X, Y, Z)$  is

$$\begin{aligned}
 \vec{V}(X, Y, Z; t) &= \vec{V}^{(1)}(X, Y, Z; t) + \vec{V}^{(2)}(X, Y, Z; t) \\
 &= k\varphi^{(1)}(X, Y, Z; t) (i, 0, \tanh[k(Z+d)]) \\
 &\quad + 2k\varphi^{(2)}(X, Y, Z; t) (i, 0, \tanh[2k(Z+d)])
 \end{aligned} \tag{13.46}$$

The acceleration of a fluid particle up to the second order may be written as:

$$\begin{aligned}
 \vec{a}(X, Y, Z; t) &= \frac{\partial}{\partial t} \vec{V}(X, Y, Z; t) + [\text{Re}(\vec{V}) \cdot \nabla] \text{Re}(\vec{V}) + i[\text{Im}(\vec{V}) \cdot \nabla] \text{Im}(\vec{V}) \\
 &= \frac{\partial}{\partial t} [\vec{V}^{(1)}(X, Y, Z; t) + \vec{V}^{(2)}(X, Y, Z; t)] \\
 &\quad + [\text{Re}(\vec{V}^{(1)}) \cdot \nabla] \text{Re}(\vec{V}^{(1)}) + i[\text{Im}(\vec{V}^{(1)}) \cdot \nabla] \text{Im}(\vec{V}^{(1)}) + O(\varepsilon^3)
 \end{aligned} \tag{13.47}$$

where  $\varepsilon = ka_w$  is assumed to be a small perturbation variable.

Employing Wheeler stretching, the real parts of the fluid pressure components up to the second order at a point  $(X, Y, Z_0)$ ,  $Z_0 \leq \text{Re}[\zeta(X, Y; t)]$  are expressed as:

$$\begin{aligned}
 \text{Re}\{p_d\} &= \text{Re}\left\{ i\rho\omega\varphi^{(1)}(X, Y, Z; t) + i2\rho\omega\varphi^{(2)}(X, Y, Z; t) \right\} \\
 &\quad - \frac{1}{2}\rho \left\{ \text{Re}(\vec{V}^{(1)}) \cdot \text{Re}(\vec{V}^{(1)}) \right\} \\
 &\quad - \rho(Z_0 - Z) \frac{\partial}{\partial Z} \left[ \frac{\partial \text{Re}(\varphi^{(1)})}{\partial t} \right] + \rho g(C + D), \\
 p_s(X, Y, Z_0; t) &= -\rho g Z_0.
 \end{aligned} \tag{13.48}$$

Note that in [Equation 13.48 \(p. 201\)](#), a new partial differential term  $\frac{\partial}{\partial Z} \left[ \frac{\partial \text{Re}(\varphi^{(1)})}{\partial t} \right]$  is introduced to account for the first order dynamic pressure variation in the vertical direction, from the equilibrium position to the actual position.

The explicit forms of the real parts of the fluid particle velocity, acceleration and pressure terms are

$$\begin{aligned} \text{Re}\left\{\vec{V}^{(1)}\right\} &= \frac{\omega a_w}{\sinh(kd)} \left\{ \cosh[k(Z+d)] \cos(kX-\omega t), 0, \sinh[k(Z+d)] \sin(kX-\omega t) \right\} \\ \text{Re}\left\{\vec{V}^{(2)}\right\} &= \frac{3}{4} \omega k a_w^2 \frac{\cosh[2k(Z+d)]}{\sinh^4(kd)} \left\{ \cos[2(kX-\omega t)], 0, \tanh[2k(Z+d)] \sin[2(kX-\omega t)] \right\} \\ \text{Re}\left\{\frac{\partial}{\partial Z} \frac{\partial(\varphi^{(1)})}{\partial t}\right\} &= -\frac{\omega^2 a_w}{\sinh(kd)} \left\{ \sinh[k(Z+d)] \cos(kX-\omega t) \right\} \\ \left[ \text{Re}\left\{\vec{V}^{(1)}\right\} \cdot \nabla \right] \text{Re}\left\{\vec{V}^{(1)}\right\} &= k(\omega a_w)^2 \frac{1}{(1-e^{-2kd})^2} \left\{ -2e^{-2kd} \sin[2(kX-2\omega t)], 0, (e^{2kZ}-e^{-2k(Z+d)}e^{-2kd}) \right\} \end{aligned} \quad (13.49)$$

With the above form, the real part of the fluid particle velocity at time  $t$  is

$$\begin{aligned} \text{Re}\left\{\vec{V}\right\} &= \frac{\omega a_w}{\sinh(kd)} \left\{ \cosh[k(Z+d)] \cos(kX-\omega t), 0, \sinh[k(Z+d)] \sin(kX-\omega t) \right\} \\ &\quad + \frac{3}{4} \omega k a_w^2 \frac{\cosh[2k(Z+d)]}{\sinh^4(kd)} \left\{ \cos[2(kX-\omega t)], 0, \tanh[2k(Z+d)] \sin[2(kX-\omega t)] \right\} \end{aligned} \quad (13.50)$$

While the real part of the acceleration is

$$\begin{aligned} \text{Re}\left\{\vec{a}\right\} &= \omega^2 a_w \frac{\cosh[k(Z+d)]}{\sinh(kd)} \left\{ \sin(kX-\omega t), 0, -\cos(kX-\omega t) \tanh[k(Z+d)] \right\} \\ &\quad + \frac{3}{2} \omega^2 k a_w^2 \frac{\cosh[2k(Z+d)]}{\sinh^4(kd)} \left\{ \sin[2(kX-\omega t)], 0, -\tanh[2k(Z+d)] \cos[2(kX-\omega t)] \right\} \\ &\quad + \frac{k}{2} \left[ \frac{\omega a_w}{\sinh(kd)} \right]^2 \left\{ -\sin[2(kX-2\omega t)], 0, \sinh[2k(Z+d)] \right\} \end{aligned} \quad (13.51)$$

The first order part of  $Z_0-Z$  is

$$Z_0-Z = \frac{\min[Z_0, \zeta^{(1)}]+d}{\zeta^{(1)}+d} \zeta^{(1)} + O(\varepsilon^2) \quad (13.52)$$

Including only the first order term, the real part of the extended hydrodynamic pressure is

$$\begin{aligned} \text{Re}\left\{p_d\right\} &= \rho g a_w \frac{\cosh[k(Z+d)]}{\cosh(kd)} \cos(kX-\omega t) \\ &\quad + \frac{3}{2} \rho g k a_w^2 \frac{\cosh[2k(Z+d)]}{\sinh^2(kd) \sinh(2kd)} \cos[2(kX-\omega t)] \\ &\quad - \frac{1}{2} \rho g k a_w^2 \frac{1}{\sinh(2kd)} \left\{ \cosh[2(kZ+d)] + \cos[2(kX-\omega t)] \right\} + \rho g(C+D) \\ &\quad + \rho g k a_w^2 \frac{\min[Z_0, \zeta_a \cos(kX-\omega t)]+d}{a_w \cos(kX-\omega t)+d} \cdot \frac{\sinh[k(Z+d)]}{\cosh(kd)} \cos[2(kX-\omega t)] + O(\varepsilon^3) \\ p_s &= -\rho g Z_0. \end{aligned} \quad (13.53)$$

From [Equation 13.53 \(p. 202\)](#), it is observed that the hydrodynamic incident wave pressure not only includes the partial derivatives of the first and second order potentials with respect to time, but also has the nonlinear Bernoulli term and a new perturbation term against the vertical shifting of

the location. This equation is employed directly to calculate the nonlinear Froude-Krylov and hydrostatic forces on a floating structure modeled by a series of panels.

For the deep water case, where  $d \rightarrow \infty$ , the velocity and acceleration of a fluid particle at the equilibrium position  $(X, Y, Z)$  is

$$\begin{aligned} \text{Re}\{\vec{V}\} &= \omega a_w e^{kZ} [\cos(kX - \omega t), 0, \sin(kX - \omega t)] \\ \text{Re}\{\vec{a}\} &= \omega^2 a_w e^{kZ} \{ \sin(kX - \omega t), 0, -\cos(kX - \omega t) \} + k\omega^2 a_w^2 e^{2kZ} \{ 0, 0, 1 \} \end{aligned} \quad (13.54)$$

The real parts of the modified hydrodynamic pressure and the hydrostatic pressure beneath the instantaneous incident wave surface are

$$\begin{aligned} \text{Re}\{p_I\} &= \rho g a_w e^{kZ} \cos(kX - \omega t) - \frac{1}{2} \rho g k a_w^2 e^{2kZ} + \rho g k a_w^2 e^{kZ} \cos^2(kX - \omega t) \\ p_s &= -\rho g Z_0 \end{aligned} \quad (13.55)$$

### 13.6.2. Second Order Correction of Linear Irregular Waves

By doing the perturbation up to the second order at a location close to the mean wave surface, the wave elevation and its partial derivatives can be further written as

$$\eta \approx \eta^{(1)} \left( 1 - \frac{1}{g} a_z^{(1)} \right) \Big|_{Z=0} - \frac{1}{2g} \vec{V}^{(1)} \cdot \vec{V}^{(1)} \Big|_{Z=0} \quad (13.56)$$

where  $\eta^{(1)}$  is the first order incident wave elevation,  $\vec{V}^{(1)}$  is the first order incident wave fluid particle velocity at the mean water surface, and  $a_z^{(1)}$  is the first order incident wave fluid particle acceleration at the mean water surface.

Denoting  $(X, Y, Z_0)$  as a field point beneath the instantaneous incident wave surface in the fixed reference axes, the Wheeler stretching at this location is determined by

$$\begin{aligned} X &= X_0 \\ Y &= Y_0 \\ Z &= \frac{Z_0 - \eta}{d + \eta} d \end{aligned} \quad (13.57)$$

Where  $d$  is the water depth and the wave elevation  $\eta$  up to the second order is given by [Equation 13.56 \(p. 203\)](#).

The second order correction of the dynamic pressure at this point is written as:

$$p_I \approx p_I^{(1)}((X_0, Y_0, Z)) \left[ 1 - \frac{1}{g} a_z^{(1)}(X_0, Y_0, Z) \right] - \frac{1}{2} \rho \left[ \vec{V}^{(1)}(X_0, Y_0, Z) \cdot \vec{V}^{(1)}(X_0, Y_0, Z) \right] \quad (13.58)$$

Similarly, the second order correction of the fluid particle velocity and acceleration are expressed as

$$\begin{aligned} \vec{V} &\approx \nabla \varphi^{(1)}(X_0, Y_0, Z) + \frac{p_I^{(1)}(X_0, Y_0, Z)}{\rho g} \frac{\partial}{\partial Z} \nabla \varphi^{(1)}(X_0, Y_0, Z) \\ \vec{a} &\approx \vec{a}^{(1)}(X_0, Y_0, Z) + \frac{p_I^{(1)}(X_0, Y_0, Z)}{\rho g} \frac{\partial}{\partial Z} \vec{a}^{(1)}(X_0, Y_0, Z) \end{aligned} \quad (13.59)$$

### 13.6.3. Wave Ramp

A wave ramp is introduced to reduce the transient motion of the structure in severe waves at the beginning of a time domain analysis. When it is optionally applied, the wave ramp factor is determined from

$$f(t) = \begin{cases} \sin^2\left(\frac{\pi t}{2t_w}\right) & 0 \leq t < t_w \\ 1 & t \geq t_w \end{cases} \quad (13.60)$$

where  $t_w$  is the time before which the wave ramp is effective.

If you do not specify  $t_w$ , a default value is selected automatically. For a regular wave case, this default is the wave period; for irregular waves, it will be the highest period of all of the wave components in the spectrum.

The amplitude of the regular wave, or of each wave component in a spectrum of irregular waves, is then modified as

$$a_j(t) = a_j f(t), \quad (j=1, N_w) \quad (13.61)$$

Subsequently, wave-related forces will also be multiplied with this ramp factor.

### 13.6.4. Hydrodynamic pressure and disturbed wave elevation

In the frequency domain, the total fluid pressure at the point  $\vec{x}$  on the hull surface can be expressed as

$$p_t(\vec{x}, \omega) = p_i(\vec{x}, \omega) + p_d(\vec{x}, \omega) + p_r(\vec{x}, \omega) + p_s(\vec{x}, \omega) \quad (13.62)$$

where  $p_i$ ,  $p_d$ ,  $p_r$ ,  $p_s$  are the incident wave, diffraction wave, radiation wave pressure, and hydrostatic components respectively.

In the time domain analysis, the incident wave pressure and hydrostatic pressure are defined in [Extended Wheeler Stretching Method \(p. 198\)](#) and [Second Order Correction of Linear Irregular Waves \(p. 203\)](#).

In the regular wave case, based on the incident wave definition in [Equation 13.37 \(p. 199\)](#) the diffraction pressure is expressed as

$$p_d(\vec{x}, t) = \text{Re}\left\{ p_d(\vec{x}, \omega) e^{-i\omega t + i\alpha} \right\} \quad (13.63)$$

In the irregular wave case, based on the irregular incident wave definition in [Equation 13.43 \(p. 200\)](#) the diffraction pressure is linearly expressed as

$$p_d(\vec{x}, t) = \sum_{j=1}^{N_w} \left\{ p_d(\vec{x}, \omega_j) e^{-i\omega_j t + i\alpha_j} \right\} \quad (13.64)$$

In the multiple structure hydrodynamic interaction case, the total degrees of rigid body motions are  $6 \times M$  where  $M$  is the number of structures in a hydrodynamic interaction group. The radiation wave pressure is usually expressed as

$$p_r(\vec{x}, \omega) = \sum_{m=1}^M \sum_{j=1}^6 p_{jm}(\vec{x}, \omega) x_{jm}(\omega) \quad (13.65)$$

where  $p_{jm}$  is the radiation pressure due to the unit j-th motion of the m-th structure whilst other structures remain stationary, and  $x_{jm}$  is the motion RAO.

The inverse Fourier transform of the radiation pressure in frequency domain is

$$\begin{aligned} p_r(\vec{x}, t) &= \sum_{m=1}^M \sum_{j=1}^6 \int_{-\infty}^{\infty} p_{jm}(\vec{x}, \omega) x_{jm}(\omega) e^{-i\omega t} d\omega \\ &= \sum_{m=1}^M \sum_{j=1}^6 \left\{ \int_{-\infty}^{\infty} \left[ -p_{jm}(\vec{x}, \omega) \frac{1}{\omega^2} - \psi_{jm}(\vec{x}) \right] a_{jm}(\omega) e^{-i\omega t} d\omega + H_{jm}(\vec{x}) a_{jm}(t) \right\} \\ &= \sum_{m=1}^M \sum_{j=1}^6 \left\{ \int_0^t h_{jm}(\vec{x}, t-\tau) a_{jm}(\tau) d\tau + H_{jm}(\vec{x}) a_{jm}(t) \right\} \end{aligned} \quad (13.66)$$

where  $a_{jm}(\omega) = -\omega^2 x_{jm}(\omega)$  is the acceleration RAO,  $\Psi_{jm}(\vec{x}) = \lim_{\omega_e \rightarrow \infty} \left\{ -\frac{1}{\omega^2} p_{jm}(\vec{x}, \omega) \right\}$ ,  $a_{jm}(t)$  is the acceleration in time domain, and the impulse function of the acceleration related is

$$h_{jm}(\vec{x}, \tau) = \frac{2}{\pi} \int_0^{\infty} \operatorname{Re} \left\{ -\frac{1}{\omega^2} p_{jm}(\vec{x}, \omega) - \Psi_{jm}(\vec{x}) \right\} \cos(\omega\tau) d\omega \quad (13.67)$$

and

$$H_{jm}(\vec{x}) = \operatorname{Re} \left\{ \Psi_{jm}(\vec{x}) \right\} \quad (13.68)$$

The wave elevation components due to radiation wave and diffraction wave in the time domain can be estimated by

$$\begin{aligned} \zeta_r(\vec{x}, t) &= \frac{1}{\rho g} p_r(\vec{x}, t), \\ \zeta_d(\vec{x}, t) &= \frac{1}{\rho g} p_d(\vec{x}, t), \quad \text{on } z=0 \end{aligned} \quad (13.69)$$

## 13.7. Nodal Motion Response

If the position of the center of gravity and the orientation of a structure at a time  $t$  is known, the nodal location in the fixed reference axes (FRA) can be determined from [Equation 1.7 \(p. 16\)](#) and [Equation 1.8 \(p. 16\)](#), i.e.

$$\mathbf{x}_N(t) = \mathbf{x}_g(t) + \mathbf{E} \begin{bmatrix} x \\ y \\ z \end{bmatrix} \quad (13.70)$$

where  $\mathbf{x}_g(t) = (X_g, Y_g, Z_g)^T$  is the position of the center of gravity of the structure in the fixed reference axes and  $[x, y, z]^T$  is the location of the node in the local structure axes.

Employing the notations in [Equation 13.15 \(p. 192\)](#) and [Equation 13.18 \(p. 193\)](#), the nodal velocity response in the fixed reference axes is

$$\mathbf{v}_N(t) = \mathbf{v}(t) - \boldsymbol{\Omega} [\mathbf{x}_N(t) - \mathbf{x}_g(t)] \quad (13.71)$$

and the acceleration is

$$\mathbf{a}_N(t) = \dot{\mathbf{v}}(t) - \boldsymbol{\Omega} [\mathbf{v}_N(t) - \mathbf{v}(t)] - \ddot{\boldsymbol{\Omega}} [\mathbf{x}_N(t) - \mathbf{x}_g(t)] \quad (13.72)$$

## 13.8. Morison Tube Element and Nodal Loads

Loads on Morison elements can be calculated and output in a time domain analysis. This is only available for tube elements.

There are two basic forms of Morison element nodal load output. The first is for space frames, where all elements are assumed to attached via encastre joints, and where more than two elements can be joined at a single node. The second is for riser-type structures, where riser geometry is assumed and, by definition, only two tube elements can join at a single node.

### 13.8.1. Nodal Loads of Tube Elements in Space Frames

Tube element loads are calculated with respect to the local tube axis system, which is defined in [Morison Equation \(p. 109\)](#) and displayed in [Figure 6.1: Local Tube Axis System \(p. 110\)](#).

The tube diameter is  $D$ , the tube wall thickness is  $T$ , and the tube structural material density is  $\rho_s$ . In the local tube axis system, the structural mass and moment of inertia with respect to the geometric center of the tube are

$$\begin{aligned} m_t &= \rho_s \pi (D - T) T L_s \\ I_{xx} &= \frac{m_t}{8} [D^2 + (D - 2T)^2] \\ I_{yy} = I_{zz} &= \frac{m_t}{12} L_s^2 + \frac{1}{2} I_{xx} \end{aligned} \quad (13.73)$$

where  $L_s = L - L_{e1} - L_{e2}$ , as shown in [Figure 6.1: Local Tube Axis System \(p. 110\)](#). The matrix of structural mass and moment of inertia is

$$\mathbf{m} = \begin{bmatrix} \mathbf{m}_{11} & 0 \\ 0 & \mathbf{m}_{22} \end{bmatrix} \quad (13.74)$$

where the  $3 \times 3$  sub-matrices are  $\mathbf{m}_{11} = \mathbf{m}_t I$  and  $\mathbf{m}_{22} = \begin{bmatrix} I_{xx} & 0 & 0 \\ 0 & I_{yy} & 0 \\ 0 & 0 & I_{zz} \end{bmatrix}$

Denoting  $\mathbf{E}_t$  as the directional cosine matrix of the local tube axis system with respect to the fixed reference axes and  $\mathbf{x}_c(t)$  as the position of the geometric center of the tube in the fixed reference axes, the velocity and acceleration at the tube geometric center in the fixed reference axes can be found from [Equation 13.71 \(p. 205\)](#) and [Equation 13.72 \(p. 205\)](#):

$$\begin{aligned} \mathbf{v}_c &= \mathbf{v}(t) - \boldsymbol{\Omega} [\mathbf{x}_c(t) - \mathbf{x}_g(t)] \\ \mathbf{a}_c &= \dot{\mathbf{v}}(t) - \boldsymbol{\Omega} [\mathbf{v}_c(t) - \mathbf{v}(t)] - \dot{\boldsymbol{\Omega}} [\mathbf{x}_c(t) - \mathbf{x}_g(t)] \end{aligned} \quad (13.75)$$

The total tube element structural force and moment components with respect to the geometric center of the tube, in the local tube axes, are

$$\mathbf{F}_{sc}(t) = -\mathbf{m} \mathbf{E}_t^T \begin{bmatrix} \mathbf{a}_c - \mathbf{g} \\ \dot{\boldsymbol{\omega}} \end{bmatrix} + \begin{bmatrix} 0 \\ \mathbf{E}_t^T \boldsymbol{\Omega} \mathbf{m}_{22} \mathbf{E}_t^T \boldsymbol{\omega} \end{bmatrix} \quad (13.76)$$

where  $\mathbf{g} = (0, 0, -g)^T$  represents the acceleration due to gravity in the fixed reference axes. The above forces and moments are the sum of the structural inertia force and moment, the gravitational force, and the structural gyroscopic moment.

Denoting the distance between the geometric center of the tube and the origin of the local tube axes (i.e. the first node of tube) as  $r$ , the force and moment with respect to the origin of the local tube axes may be expressed as

$$\mathbf{F}_s(t) = \begin{bmatrix} \mathbf{I} & 0 \\ -\mathbf{R}_r & \mathbf{I} \end{bmatrix} \mathbf{F}_{sc}(t) \quad (13.77)$$

where  $\mathbf{R}_r = \begin{bmatrix} 0 & 0 & 0 \\ 0 & 0 & r \\ 0 & -r & 0 \end{bmatrix}$

The tube element fluid force and moment matrix  $\mathbf{F}_f(t)$  consists of the following components:

- Morison drag, Froude-Krylov, wave inertia and radiation (added mass-related) force and moment, as expressed in [Equation 6.2 \(p. 110\)](#), where the fluid mass and moment of inertia of an internal flooded tube are included in the added mass matrix when the radiation force and moment are calculated.
- Fluid gyroscopic and momentum force, as given in [Equation 13.26 \(p. 194\)](#) and [Equation 13.27 \(p. 194\)](#), respectively.
- Slamming force and moment on tube, as defined in [Equation 6.21 \(p. 117\)](#).
- Hydrostatic force and moment, as calculated from [Equation 3.4 \(p. 43\)](#).

The total tube element force and moment with respect to the origin of the local tube axes are

$$(F_x, F_y, F_z, M_x, M_y, M_z)^T = \mathbf{F}_s(t) + \mathbf{F}_f(t) \quad (13.78)$$

The equivalent nodal forces and moments at the two tube ends are defined in the local tube axes as

$$\mathbf{F}_{Nj}^e = (F_{xj}, F_{yj}, F_{zj}, M_{xj}, M_{yj}, M_{zj})^T, \quad (j=1,2) \quad (13.79)$$

Considering the terms of [Equation 13.79 \(p. 207\)](#) individually:

$$\begin{aligned} F_{x1} &= F_{x2} = \frac{1}{2} F_x \\ M_{x1} &= M_{x2} = \frac{1}{2} M_x \end{aligned} \quad (13.80)$$

which are the forces in the x-axis direction and the moment about the x-axis.

$$\begin{aligned} F_{y1} &= -\frac{L}{20} (7f_1 + 3f_2) \\ F_{y2} &= -\frac{L}{20} (3f_1 + 7f_2) \\ M_{z1} &= -\frac{L^2}{60} (3f_1 + 2f_2) \\ M_{z2} &= \frac{L^2}{60} (2f_1 + 3f_2) \end{aligned} \quad (13.81)$$

where  $f_1 = -\frac{1}{L} (4F_y - \frac{6}{L} M_z)$  and  $f_2 = \frac{1}{L} (2F_y - \frac{6}{L} M_z)$  are the equivalent forces per unit length in the local xy-plane.

$$\begin{aligned}
 F_{z1} &= -\frac{L}{20}(7f_3 + 3f_4) \\
 F_{z2} &= -\frac{L}{20}(3f_3 + 7f_4) \\
 M_{y1} &= \frac{L^2}{60}(3f_3 + 2f_4) \\
 M_{y2} &= -\frac{L^2}{60}(2f_3 + 3f_4)
 \end{aligned} \tag{13.82}$$

where  $f_3 = -\frac{1}{L}(4F_z + \frac{6}{L}M_y)$  and  $f_4 = \frac{1}{L}(2F_z + \frac{6}{L}M_y)$  are the equivalent forces per unit length in the local xz-plane.

The tube end cap forces, which are due to the sum of the hydrostatic and incident wave pressures over the tube end cross-sections, can also be split from the nodal forces in [Equation 13.80 \(p. 207\)](#). The end cap forces in the local tube x-axis direction are

$$\begin{aligned}
 F_{cap1} &= A_{cap} [\operatorname{Re}\{p_{d1}\} + p_{s1}] \\
 F_{cap2} &= -A_{cap} [\operatorname{Re}\{p_{d2}\} + p_{s2}]
 \end{aligned} \tag{13.83}$$

where the subscripts 1 and 2 indicate the node number,  $\operatorname{Re}\{p_{dj}\}$  and  $p_{sj}$  ( $j = 1, 2$ ) are the incident wave and hydrostatic pressures at the  $j$ -th node of a tube element, respectively, and the end cap area is

$$A_{cap} = \begin{cases} \frac{\pi}{4}D^2 & \text{for a non-flooded tube} \\ \pi(D-T)T & \text{for a flooded tube} \end{cases}$$

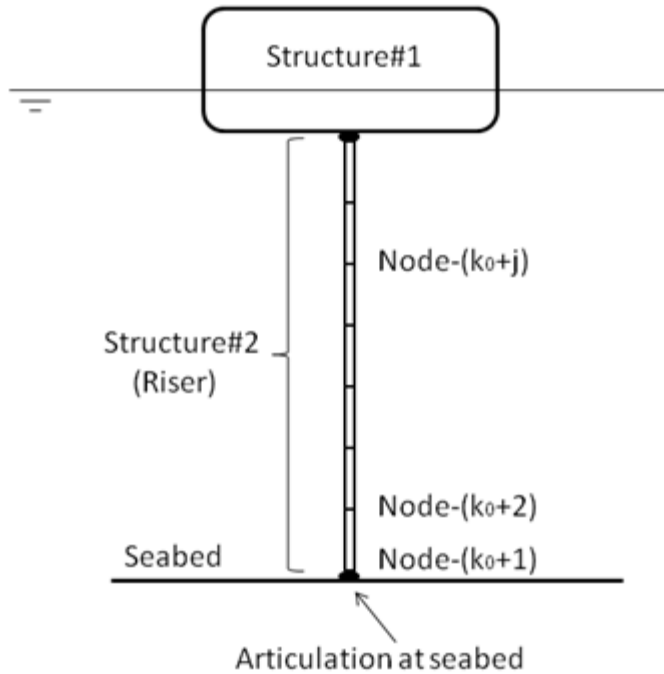
At the position of a user-defined node number  $k$ , where more than two elements of a space frame may be joined, the total tube element load is the summation of the nodal loads for all of the joined elements at that node, and is represented in the local structure axes (LSA) as:

$$\mathbf{F}_{Node-k} = \mathbf{E}^T \sum \mathbf{E}_t \mathbf{F}_{Nj}^e \tag{13.84}$$

where  $\mathbf{E}$  is the Euler transformation matrix from the local structure axes to the fixed reference axes.

### 13.8.2. Nodal Loads of Tube Elements in Riser-Type Structures

Inter-element forces can also be calculated at the nodes of a riser-type structure. As shown in [Figure 13.2: Loads at Riser Nodes \(p. 209\)](#), Structure #2 is assumed to be a riser structure consisting only of a number of tube elements. The first node (with the user-defined node number  $k_0+1$ ) of the first tube in this structure is located at the seabed; subsequently, the first node of the next element along the riser structure must be the second node of the previous element. A fixed point on the seabed constrains the riser via an articulation that links the point to the first node of the first tube element.

**Figure 13.2: Loads at Riser Nodes**

Denoting  $\mathbf{R}_C$  as the reaction force and moment matrix due to the articulation at the seabed in the local structure axes (LSA), and  $\mathbf{X}_{k_0+j} = (x_{k_0+j}, y_{k_0+j}, z_{k_0+j})^T$  as the coordinate of node  $(k_0+j)$  in the LSA, the nodal loads in the LSA for a riser-type structure can be calculated from the total tube elemental loads at each node, given by [Equation 13.84 \(p. 208\)](#), as

$$\mathbf{F}_{k_0+j} = \begin{bmatrix} \mathbf{I} & 0 \\ \mathbf{R}_{j-1} & \mathbf{I} \end{bmatrix} \mathbf{R}_C + \sum_{k=1}^j \begin{bmatrix} \mathbf{I} & 0 \\ \mathbf{R}_{j-k} & \mathbf{I} \end{bmatrix} \mathbf{F}_{\text{Node-}(k_0+k)} \quad (13.85)$$

where the  $3 \times 3$  sub-matrix  $\mathbf{R}_{j-k}$  is defined as

$$\mathbf{R}_{j-k} = \begin{bmatrix} 0 & z_{k_0+j}-z_{k_0+k} & -y_{k_0+j}+y_{k_0+k} \\ -z_{k_0+j}+z_{k_0+k} & 0 & x_{k_0+j}-x_{k_0+k} \\ y_{k_0+j}-y_{k_0+k} & -x_{k_0+j}+x_{k_0+k} & 0 \end{bmatrix} \text{ where } k=1, j$$

## 13.9. Integration in Time of Motion Equation

The global equation of motion in the time domain is given by:

$$\mathbf{MA} = \mathbf{F}_t \quad (13.86)$$

where  $\mathbf{M}$  is the assembled structural and added mass matrix described in [Equation 13.3 \(p. 188\)](#) in the fixed reference axes,  $\mathbf{A}$  is the unknown acceleration vector, and

$$\mathbf{F}_t = \mathbf{F}(t) - \mathbf{c}\dot{\mathbf{X}}(t) - \mathbf{K}\mathbf{X}(t) - \int_0^t \mathbf{h}(t-\tau)\ddot{\mathbf{X}}(\tau)d\tau$$

is the total applied force vector.

In order to integrate the estimated acceleration for the structure velocity and position, Aqwa uses a 2-stage predictor-corrector algorithm.

## Stage 1 - Predictor Stage

First, the total applied force  $\mathbf{F}_t$  is calculated, typically a function of the known time, position, and velocity:

$$\mathbf{F}_t(t) = \mathbf{f}(t, \mathbf{X}(t), \mathbf{V}(t)) \quad (13.87)$$

If a user-defined external force routine is used, the external routine is called at this point with stage = 1.

The acceleration is solved by substituting [Equation 13.87 \(p. 210\)](#) into [Equation 13.86 \(p. 209\)](#). The results are output at this point (during the first stage of the calculation).

The predicted velocity  $\mathbf{V}^*$  and position  $\mathbf{X}^*$  at time  $t + dt$  are given by:

$$\begin{aligned}\mathbf{V}^*(t+dt) &= \mathbf{V}(t) + \mathbf{A}(t)dt \\ \mathbf{X}^*(t+dt) &= \mathbf{X}(t) + \mathbf{V}(t)dt + \mathbf{A}(t)\frac{dt^2}{2}\end{aligned} \quad (13.88)$$

where the superscript \* indicates intermediate results in the predictor-corrector algorithm.

## Stage 2 - Corrector Stage

To begin stage 2, the total applied force  $\mathbf{F}_t^*$  is estimated at time  $t + dt$ :

$$\mathbf{F}^*(t+dt) = \mathbf{f}(t+dt, \mathbf{X}^*(t+dt), \mathbf{V}^*(t+dt)) \quad (13.89)$$

If a user-defined external force routine is used, the external routine is called at this point with stage = 2.

The acceleration  $\mathbf{A}^*(t+dt)$  at time  $t + dt$  is solved by substituting [Equation 13.89 \(p. 210\)](#) into [Equation 13.86 \(p. 209\)](#).

The corrected velocity and position is calculated at time  $t + dt$ , using Taylor's theorem:

$$\begin{aligned}\mathbf{V}(t+dt) &= \mathbf{V}(t) + \frac{\mathbf{A}(t) + \mathbf{A}^*(t+dt)}{2}dt \\ \mathbf{X}(t+dt) &= \mathbf{X}(t) + \mathbf{V}(t)dt + \frac{2\mathbf{A}(t) + \mathbf{A}^*(t+dt)}{6}dt^2\end{aligned} \quad (13.90)$$

The structure is then moved to the new position, the time is incremented, and the process is repeated from stage 1.

## 13.10. Low Frequency Maneuvering Loads

The forces involved in the low frequency ship manoeuvring motion estimation normally consist of the structure inertia force, and low frequency hydrodynamic forces on the hull, propeller and rudder. In this section only the hydrodynamic force and moment on the hull due to low frequency motion are covered. The gyroscopic moment is included in [Equation 13.25 \(p. 193\)](#).

In the local structure axes (LSA), the hydrodynamic force and moment on the hull due to the low frequency ship motion in an unbounded ideal fluid are given by Newman (2017) [31],

$$\begin{aligned} F_j &= -\dot{U}_i m_{ji} - \varepsilon_{jkl} U_i \Omega_k m_{li} \\ M_j &= -\dot{U}_i m_{j+3,i} - \varepsilon_{jkl} U_i \Omega_k m_{l+3,i} - \varepsilon_{jkl} U_i U_k m_{li} \end{aligned} \quad (13.91)$$

where the indices  $j, k, l$  have the values 1,2,3 and  $i=1,2, \dots, 6$ ,  $\varepsilon_{jkl}$  is the alternative tensor,  $U_i$  is the translational term ( $i=1,3$ ) related to the current speed or rotational velocity ( $i=4,6$ ) in the LSA,  $\Omega_k = U_{k+3}$  and  $m_{li}$  is the low (or zero) frequency added mass in the LSA.

The term  $-\varepsilon_{jkl} U_i U_k m_{li}$  in the hydrodynamic moment  $M_j$  is named as the Munk moment. Note that the off-diagonal 6x6 submatrices of the added mass due to the hydrodynamic interaction of structures are not accounted for in [Equation 13.91 \(p. 211\)](#).

The inertia force and moment terms in [Equation 13.91 \(p. 211\)](#) could be expressed as the derivatives of the linear and angular momentums,

$$\begin{aligned} F_j &= -\frac{d}{dt}(m_{ji} U_i) - \varepsilon_{jkl} U_i \Omega_k m_{li} \\ M_j &= -\frac{d}{dt}(m_{j+3,i} U_i) - \varepsilon_{jkl} U_i \Omega_k m_{l+3,i} - \varepsilon_{jkl} U_i U_k m_{li} \end{aligned} \quad (13.92)$$

Denoting  $\theta_3$  as the yaw angle, the yaw motion Euler transformation matrix is given by

$$\mathbf{E}_{yaw} = \begin{bmatrix} \cos\theta_3 & -\sin\theta_3 & 0 \\ \sin\theta_3 & \cos\theta_3 & 0 \\ 0 & 0 & 1 \end{bmatrix} \quad (13.93)$$

The matrix form of the translational and rotational velocity in the LSA is

$$\mathbf{U}^L(t) = (U_1, U_2, U_3, U_4, U_5, U_6)^T = \begin{bmatrix} \mathbf{E}_{yaw} & 0 \\ 0 & \mathbf{E}_{yaw} \end{bmatrix}^T \mathbf{V}_g(t) \quad (13.94)$$

where  $\mathbf{V}_g(t)$  is the translational and rotational velocity related to the current speed in the fixed reference axes (FRA) at the time  $t$ .

Defining the rotational velocity and translational velocity matrices in the LSA as

$$\boldsymbol{\Omega}^L = \begin{bmatrix} 0 & U_6 & -U_5 \\ -U_6 & 0 & U_4 \\ U_5 & -U_4 & 0 \end{bmatrix}, \quad \mathbf{V}^L = \begin{bmatrix} 0 & U_3 & -U_2 \\ -U_3 & 0 & U_1 \\ U_2 & -U_1 & 0 \end{bmatrix} \quad (13.95)$$

the maneuvering force and moment in the FRA are written in the matrix form as

$$\begin{aligned}
\mathbf{F}_m(t) &= - \begin{bmatrix} \mathbf{E}_{yaw} & 0 \\ 0 & \mathbf{E}_{yaw} \end{bmatrix} \frac{d}{dt} \left\{ \mathbf{A}_{lf}^L \mathbf{U}^L(t) \right\} + \begin{bmatrix} \mathbf{E}_{yaw} & 0 \\ 0 & \mathbf{E}_{yaw} \end{bmatrix} \begin{bmatrix} \boldsymbol{\Omega}^L & 0 \\ \mathbf{V}^L & \boldsymbol{\Omega}^L \end{bmatrix} \mathbf{A}_{lf}^L \mathbf{U}^L(t) \\
&= - \begin{bmatrix} \mathbf{E}_{yaw} & 0 \\ 0 & \mathbf{E}_{yaw} \end{bmatrix} \frac{d}{dt} \left\{ \mathbf{A}_{lf}^L \begin{bmatrix} \mathbf{E}_{yaw} & 0 \\ 0 & \mathbf{E}_{yaw} \end{bmatrix}^T \mathbf{V}_g(t) \right\} + \begin{bmatrix} \mathbf{E}_{yaw} & 0 \\ 0 & \mathbf{E}_{yaw} \end{bmatrix} \begin{bmatrix} \boldsymbol{\Omega}^L & 0 \\ \mathbf{V}^L & \boldsymbol{\Omega}^L \end{bmatrix} \mathbf{A}_{lf}^L \mathbf{U}^L(t) \\
&= - \begin{bmatrix} \mathbf{E}_{yaw} & 0 \\ 0 & \mathbf{E}_{yaw} \end{bmatrix} \mathbf{A}_{lf}^L \begin{bmatrix} \mathbf{E}_{yaw} & 0 \\ 0 & \mathbf{E}_{yaw} \end{bmatrix}^T \dot{\mathbf{V}}_g(t) \\
&\quad - \begin{bmatrix} \mathbf{E}_{yaw} & 0 \\ 0 & \mathbf{E}_{yaw} \end{bmatrix} \mathbf{A}_{lf}^L \frac{d}{dt} \left\{ \begin{bmatrix} \mathbf{E}_{yaw} & 0 \\ 0 & \mathbf{E}_{yaw} \end{bmatrix}^T \right\} \mathbf{V}_g(t) \\
&\quad + \begin{bmatrix} \mathbf{E}_{yaw} & 0 \\ 0 & \mathbf{E}_{yaw} \end{bmatrix} \begin{bmatrix} \boldsymbol{\Omega}^L & 0 \\ \mathbf{V}^L & \boldsymbol{\Omega}^L \end{bmatrix} \mathbf{A}_{lf}^L \mathbf{U}^L(t)
\end{aligned} \tag{13.96}$$

in which  $\mathbf{A}_{lf}^L = [m_{ij}]$  ( $i=1,6, j=1,6$ ) is the low (or zero) frequency added mass matrix in the LSA.

Denoting

$$\mathbf{D}_{yaw} = \frac{d\mathbf{E}_{yaw}}{dt} = \Omega_3 \begin{bmatrix} -\sin\theta_3 & -\cos\theta_3 & 0 \\ \cos\theta_3 & -\sin\theta_3 & 0 \\ 0 & 0 & 0 \end{bmatrix} \tag{13.97}$$

Equation 13.96 (p. 212) is further expressed as

$$\begin{aligned}
\mathbf{F}_m(t) &= - \begin{bmatrix} \mathbf{E}_{yaw} & 0 \\ 0 & \mathbf{E}_{yaw} \end{bmatrix} \mathbf{A}_{lf}^L \begin{bmatrix} \mathbf{E}_{yaw} & 0 \\ 0 & \mathbf{E}_{yaw} \end{bmatrix}^T \dot{\mathbf{V}}_g(t) \\
&\quad - \begin{bmatrix} \mathbf{E}_{yaw} & 0 \\ 0 & \mathbf{E}_{yaw} \end{bmatrix} \mathbf{A}_{lf}^L \begin{bmatrix} \mathbf{D}_{yaw} & 0 \\ 0 & \mathbf{D}_{yaw} \end{bmatrix}^T \mathbf{V}_g(t) + \begin{bmatrix} \mathbf{E}_{yaw} & 0 \\ 0 & \mathbf{E}_{yaw} \end{bmatrix} \begin{bmatrix} \boldsymbol{\Omega}^L & 0 \\ \mathbf{V}^L & \boldsymbol{\Omega}^L \end{bmatrix} \mathbf{A}_{lf}^L \mathbf{U}^L(t)
\end{aligned} \tag{13.98}$$

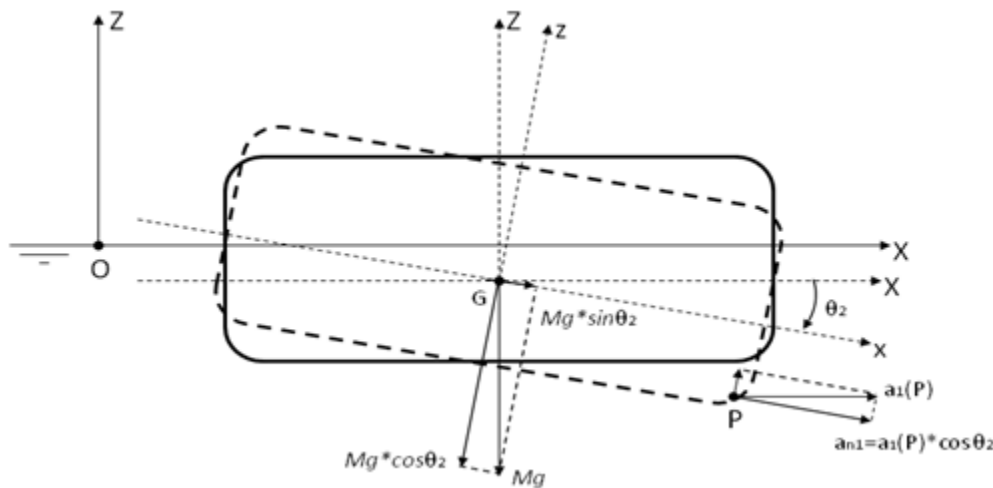
# Chapter 14: Extended Functionalities

Some extended functionalities of the Aqwa suite are presented in this chapter. Most of these extensions are currently available in the Aqwa Graphical Supervisor as post-processing functions.

## 14.1. Effective Nodal Acceleration RAOs

Effective nodal accelerations in the local structure axes (LSA) can be calculated in Aqwa. As shown in [Figure 14.1: Effective Surge Acceleration in LSA \(p. 213\)](#), the structure has a pitch motion RAO of  $\theta_2$  and a surge motion RAO of  $u_1$ , for a unit amplitude wave with frequency of  $\omega$ . The motion RAOs  $\theta_2$  and  $u_1$  are complex numbers.

**Figure 14.1: Effective Surge Acceleration in LSA**



Based on the assumption of small amplitude motion responses, the gravitational force in the local structure axes (LSA) can be approximated as

$$\begin{aligned}\vec{F}_g &= Mg(\sin\theta_2, 0, -\cos\theta_2) \\ &\approx Mg(\theta_2, 0, -1) + O(\varepsilon^2)\end{aligned}\tag{14.1}$$

Denoting  $P: \vec{x}=(x,y,z)$  as a nodal position in the local structure axes, the nodal acceleration in the local structure x-axis is

$$\begin{aligned}a_{n1} &= a_1(P)\cos\theta_2 \\ &= -\omega^2(u_1 + \theta_2 z)\cos\theta_2 \\ &\approx -\omega^2(u_1 + \theta_2 z) + O(\varepsilon^2)\end{aligned}\tag{14.2}$$

The inertia force due to the local acceleration in the x-direction is

$$-Ma_{n1} = M\omega^2(u_1 + \theta_2 z)\tag{14.3}$$

Summing the above inertia force with the gravitational force in the local structure x-axis, the effective nodal acceleration in this local axis is defined as

$$-Ma_{n1}^e = -Ma_{n1} + Mg\theta_2 \quad (14.4)$$

which can be simplified to:

$$a_{n1}^e = a_{n1} - g\theta_2 \quad (14.5)$$

Similarly, the effective nodal acceleration RAO in the local structure y-axis is

$$a_{n2}^e = a_{n2} + g\theta_1 \quad (14.6)$$

where  $a_{n2} \approx -\omega^2(u_2 - \theta_1 z) + O(\varepsilon^2)$ , in which the sway and roll motion RAOs  $u_2$  and  $\theta_1$  are complex numbers.

The effective roll acceleration is defined as

$$a_{n4}^e = -\omega^2 \left\{ \theta_1 + \tan^{-1} \left[ \frac{\text{Re}(a_{n2})}{g} \right] + i \times \tan^{-1} \left[ \frac{\text{Im}(a_{n2})}{g} \right] \right\} \quad (14.7)$$

where  $i$  is the imaginary unit.

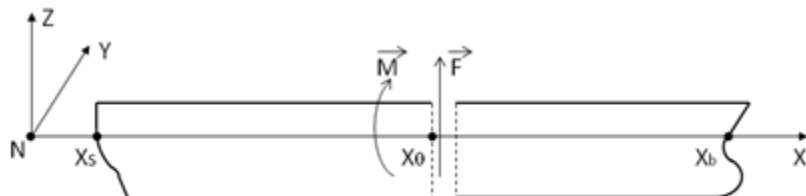
Based on the definitions in [Equation 14.5 \(p. 214\)](#) through [Equation 14.7 \(p. 214\)](#), the effective nodal x- (surge), y- (sway) and about x- (roll) velocity and motion RAOs in the local structure axes are defined as

$$\begin{aligned} v_{nj}^e &= \frac{i}{\omega} a_{nj}^e \\ u_{nj}^e &= -\frac{1}{\omega^2} a_{nj}^e \text{ where } j=1,2 \text{ or } 4 \end{aligned} \quad (14.8)$$

## 14.2. Shear Force and Bending Moment along Axes

Aqwa calculates the shear force and bending moment distribution of a free-floating structure along a specified neutral axis parallel to either the X-, Y-, or Z-axis of the fixed reference axes (FRA).

As an example, assume that the shear force and bending moment distribution along a neutral axis parallel to the fixed reference X-axis is required when the structure is at its equilibrium position. As shown in [Figure 14.2: Bending Moment and Shear Force Distribution Along a Neutral Axis \(p. 215\)](#), the axis system, NXYZ, is defined where the X-axis is the neutral axis, and the Y- and Z-axes are parallel to the fixed reference Y- and Z-axes respectively. The mass distribution is defined from stern  $X_s$  to bow  $X_b$ ; for a cross-section normal to the neutral axis, the intersection point between this cross-section and the neutral axis is located at  $\vec{X}_0 = (X_0, 0, 0)$  (where  $X_s \leq X_0 \leq X_b$ ) in the NXYZ frame.

**Figure 14.2: Bending Moment and Shear Force Distribution Along a Neutral Axis**

The external hydrodynamic force and moment with respect to the neutral axis are

$$\vec{F}_f(\omega, x_0) = \iint_{S_x} (-p\vec{n}) dS \quad (14.9)$$

$$\vec{M}_f(\omega, x_0) = \iint_{S_x} [(\vec{X} - \vec{X}_0) \times (-p\vec{n})] dS$$

where  $\omega$  is the wave frequency,  $S_x$  is the wetted surface partition from the stern to the cross-section,  $p$  is the summation of the hydrostatic and total hydrodynamic pressures (consisting of the incident wave, diffraction wave, radiation wave, and the hydrostatic varying pressures), and  $\vec{n}$  is the normal vector of the wetted hull surface pointing towards the fluid field. The bending moment acts about the intersection point  $\vec{X}_0$ .

If the linearized drag forces/moment with respect to the intersection point  $\vec{X}_0$  on tube and disc elements are included, the drag force/moment expression given by [Equation 6.20 \(p. 116\)](#) can be used. However, the relative location vector defined by [Equation 6.18 \(p. 116\)](#) should be changed to

$$\vec{r}_t = \vec{X}_t - \vec{X}_0 = (x_t, y_t, z_t) \quad (14.10)$$

The linearized drag force/moment contribution to the shear force and bending moment at the intersection point  $\vec{X}_0$  is the summation over all tube/disc elements in the range of  $[X_s, X_0]$ .

The gravitational force and moment with respect to the intersection point  $\vec{X}_0$  are represented as

$$\vec{F}_g(\omega, x) = \sum_{X=X_s}^x \left\{ (0, 0, -m_j g) - \vec{\theta} \times (0, 0, -m_j g) \right\} \quad (14.11)$$

$$\vec{M}_g(\omega, x) = \sum_{X=X_s}^x \left\{ (\vec{X}_j - \vec{X}_0) \times [(0, 0, -m_j g) - \vec{\theta} \times (0, 0, -m_j g)] \right\}$$

where  $\vec{\theta} = (\theta_1, \theta_2, \theta_3)$  is the rotational motion response and  $m_j, \vec{X}_j$  are the mass and geometric center of the  $j$ -th section between  $[X_s, X_0]$ , respectively.

The inertia force and moment with respect to the intersection point  $\vec{X}_0$  are

$$\begin{aligned}\vec{F}_m(\omega, x) &= \omega^2 \sum_{X=x_s}^{x_0} m_j(u_j, v_j, w_j) \\ \vec{M}_m(\omega, x) &= \omega^2 \sum_{X=x_s}^{x_0} \left\{ m_j(\vec{X}_j - \vec{X}_0) \times (u_j, v_j, w_j) + (\theta_1, \theta_2, \theta_3) [I_{xxj}] \right\}\end{aligned}\quad (14.12)$$

where  $(u_j, v_j, w_j)$  is the motion response at the center of mass of the  $j$ -th section and  $[I_{xx}]$  is the moment of inertia matrix of the  $j$ -th section.

The summations of the corresponding static components in [Equation 14.9 \(p. 215\)](#) and [Equation 14.11 \(p. 215\)](#), which consist of the hydrostatic and gravitational force/moment components only, are referred to as the hydrostatic shear force and bending moments. The summations of all other corresponding components in [Equation 14.9 \(p. 215\)](#) through [Equation 14.12 \(p. 216\)](#) are the dynamic shear force and bending moments.

The maximum value of the shear force/bending moment RAO amplitudes among all of the calculated wave frequency points at a specified section is named as the shear force/bending moment RAO envelope at that section.

If the shear force and bending moment distribution is required along a neutral axis parallel to either the fixed reference Y- or Z-axis, the integration and summation involved in [Equation 14.9 \(p. 215\)](#) through [Equation 14.12 \(p. 216\)](#) should simply be performed in the Y- or Z-direction.

## 14.3. Splitting Force and Moment

The splitting force and moment of the specified partition of a free-floating structure can be calculated in Aqwa, provided that a hydrodynamic diffraction and radiation analysis has already been carried out.

The mass distribution over the floating structure is required in this calculation. It should be noted that the total mass and the resolved center of gravity based on this mass distribution must be equal to that calculated by the hydrodynamic diffraction and radiation analysis. If this condition is not satisfied, non-zero residual forces may cause erroneous results in the splitting forces.

The specified structure partition is defined within a virtual rectangular box  $\Omega_B$  with the lowest vertex  $B_1:(X_{min}, Y_{min}, Z_{min})$  and the highest vertex  $B_2:(X_{max}, Y_{max}, Z_{max})$ , as shown in [Figure 14.3: Structure Partition and Reference Point for Splitting Force Calculation \(p. 217\)](#). The edges of this box are aligned with the fixed reference axes. The output splitting force and moment consist of the force and moment acting on the structure partition enclosed by this virtual box  $\Omega_B$ . The moment is determined about a reference point  $Q: \vec{X}_Q=(X_Q, Y_Q, Z_Q)$  defined in the fixed reference axes.

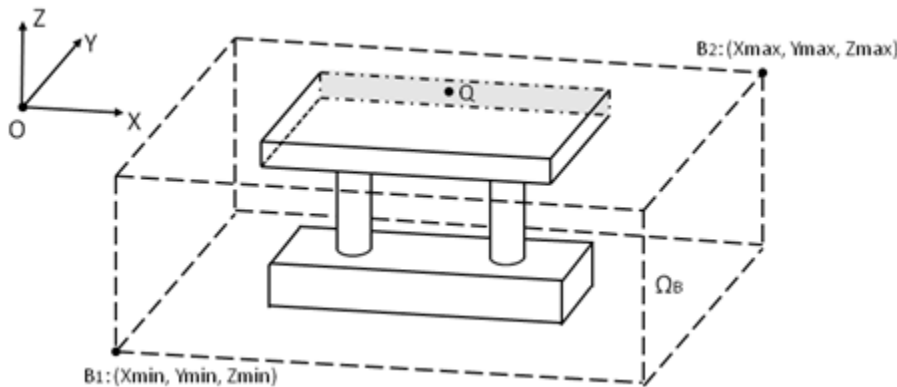
The external hydrodynamic force and moment with respect to the reference point  $\vec{X}_Q$  are

$$\begin{aligned}\vec{F}_f(\omega) &= \iint_{S_B} (-p\vec{n}) dS \\ \vec{M}_f(\omega) &= \iint_{S_B} [(\vec{X} - \vec{X}_Q) \times (-p\vec{n})] dS\end{aligned}\quad (14.13)$$

where  $\omega$  is the wave frequency,  $S_B$  is the wetted surface partition of the floating structure enclosed by the virtual box  $\Omega_B$ ,  $p$  is the summation of the hydrostatic and total hydrodynamic pressures (consisting

of the incident wave, diffraction wave, radiation wave, and the hydrostatic varying pressures), and  $\vec{n}$  is the normal vector of the wetted hull surface pointing towards the fluid field.

**Figure 14.3: Structure Partition and Reference Point for Splitting Force Calculation**



The gravitational force and moment with respect to the reference point  $\vec{X}_Q$  are represented as

$$\begin{aligned}\vec{F}_g(\omega) &= \sum \{(0, 0, -m_j g) - \vec{\theta} \times (0, 0, -m_j g)\} \\ \vec{M}_g(\omega) &= \sum \{(\vec{X}_j - \vec{X}_Q) \times [(0, 0, -m_j g) - \vec{\theta} \times (0, 0, -m_j g)]\}, \quad (\vec{X}_j \in \Omega_B)\end{aligned}\quad (14.14)$$

where  $\vec{\theta} = (\theta_1, \theta_2, \theta_3)$  is the rotational motion response, and  $m_j$  is the structure mass at the location  $\vec{X}_j \in \Omega_B$ .

The inertia force and moment with respect to the reference point  $\vec{X}_Q$  are

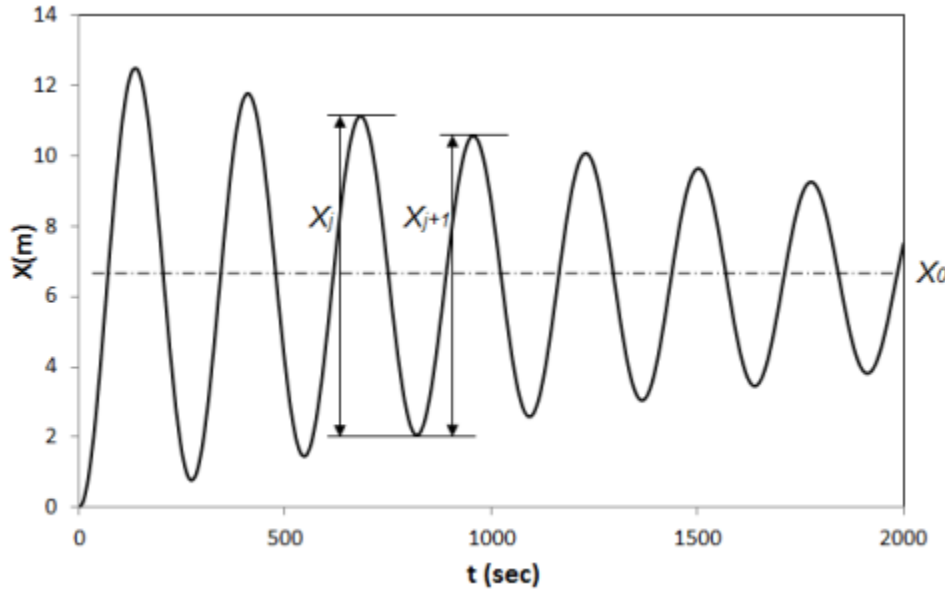
$$\begin{aligned}\vec{F}_m(\omega) &= \omega^2 \sum m_j (u_j, v_j, w_j) \\ \vec{M}_m(\omega) &= \omega^2 \sum \{m_j (\vec{X}_j - \vec{X}_Q) \times (u_j, v_j, w_j)\}\end{aligned}\quad (14.15)$$

where  $(u_j, v_j, w_j)$  is the motion response at the location  $\vec{X}_j \in \Omega_B$ .

The summations of all of the corresponding components in [Equation 14.13 \(p. 216\)](#) through [Equation 14.15 \(p. 217\)](#) are the splitting force and moment about the reference point  $\vec{X}_Q$  for the specified structure partition shown in [Figure 14.3: Structure Partition and Reference Point for Splitting Force Calculation \(p. 217\)](#).

## 14.4. Evaluation of Percentage of Critical Damping from Twang Test

The damping property for a specified degree of freedom of a floating structure can be estimated using a numerical twang test record. As shown in [Figure 14.4: Freely-Decaying Record \(p. 218\)](#), the structure center of gravity is shifted by a distance  $\Delta X$  along the specified degree of freedom from its equilibrium position  $X_0$  in still water at time  $t=0$ . A time history of its freely-decaying response can then be calculated by an Aqwa time domain analysis.

**Figure 14.4: Freely-Decaying Record**

Assuming that the motion in this degree of freedom has no interaction with other motions, and that there are no other external dynamic forces, the linear single degree of freedom dynamic system has an analytical response of the form:

$$X(t) = X_0 + \Delta X e^{-\zeta_c \omega_n t} \cos(\omega_d t) \quad (14.16)$$

where  $\omega_n$  is the natural frequency,  $\omega_d = \omega_n \sqrt{1 - \zeta_c^2}$  is the damped natural frequency, and  $\zeta_c$  is the required percentage of critical damping denoted in [Equation 11.22 \(p. 177\)](#).

The percentage of critical damping may be measured by the logarithmic decrement [7]

$$d_c = \ln \left( \frac{X_j^{\max} - X_0}{X_{j+1}^{\max} - X_0} \right) = \frac{2\pi\zeta_c}{\sqrt{1 - \zeta_c^2}} \quad (14.17)$$

where  $X_j^{\max}$  and  $X_{j+1}^{\max}$  are the heights of two successive maxima.

Based on the linear dynamic system assumption, the ratio of the heights of two successive maxima is approximately equal to the square of the ratio of the heights of a crest-trough and its adjacent trough-crest, such as  $X_j$  and  $X_{j+1}$  shown in [Figure 14.4: Freely-Decaying Record \(p. 218\)](#). The linear percentage of critical damping can therefore be estimated by

$$\zeta_{cj} = \frac{d_c}{\sqrt{d_c^2 + 4\pi^2}} \quad (14.18)$$

$$\text{where } d_c = \ln \left( \frac{X_j^{\max} - X_0}{X_{j+1}^{\max} - X_0} \right) = 2 \ln \left( \frac{X_j}{X_{j+1}} \right).$$

From [Equation 14.18 \(p. 218\)](#), it should be noted that the calculated percentage of critical damping may vary over time. To further investigate this time-dependent variation, a nonlinear representation of the damping property can be introduced as

$$\zeta_{Cj}^{(1)} + \zeta_{Cj}^{(2)} \frac{8}{3\pi} v_j = \zeta_{Cj} \quad (14.19)$$

where  $\frac{8}{3\pi} v_j = \frac{2}{3\pi} \omega_d (X_j + X_{j+1})$  is the equivalent velocity amplitude within one natural period, and the quadratic and linear terms are given by

$$\begin{aligned}\zeta_{Cj}^{(2)} &= \frac{\zeta_{Cj} - \zeta_{C(j+1)}}{\frac{8}{3\pi}(v_j - v_{j+1})} \\ \zeta_{Cj}^{(1)} &= \zeta_{Cj} - \frac{8}{3\pi} v_j \zeta_{Cj}^{(2)}\end{aligned}\quad (14.20)$$

Using the definition in [Equation 11.22 \(p. 177\)](#), the ratio of the nonlinear damping and mass can be derived from [Equation 14.19 \(p. 219\)](#),

$$\left(\frac{C}{M}\right)_j = \left(\frac{C}{M}\right)_j^{(1)} + \left(\frac{C}{M}\right)_j^{(2)} \frac{8}{3\pi} v_j \quad (14.21)$$

where  $\left(\frac{C}{M}\right)_j^{(k)} = 2\omega_n \zeta_{Cj}^{(k)}$  where  $k=1,2$ .

## 14.5. Aqwa Parallel Processing Calculation

Aqwa employs the OpenMP for multi-threaded parallelization on a symmetric-multiprocessing (SMP) machine (see Hermanns [16]) in hydrodynamic diffraction analysis (Aqwa-Line) and time domain dynamic cable and tether analysis.

The actual number of cores used by Aqwa during parallel processing,  $N_a$ , is defined as the smallest number between the user-defined number, the total number of cores in the node on which Aqwa is executed, and the total number of available parallel licenses + 4. This number is used when executing a hydrodynamic diffraction analysis.

In hydrodynamic diffraction analysis (Aqwa-Line), the parallel processing is carried out in the following calculations:

1. First-order hydrodynamic properties
2. Difference and sum frequency full QTF matrices
3. Directional coupling QTF matrices
4. Wave elevation database

The parallel scaling performance of hydrodynamic diffraction (Aqwa-Line) is generally good for medium to large-scaled problems (number of diffracting panel elements), and the parallelization will always deliver some degree of speed-up. An example of the parallel calculation efficiency on a 12-physical-core workstation for a single ship model is listed in [Table 14.1: Speed-Up of Hydrodynamic Diffraction Ana-](#)

lysis ( $S_N$ ) (p. 220), where 22,276 diffraction panels, 20 wave frequencies, and 13 wave directions are defined.

**Table 14.1: Speed-Up of Hydrodynamic Diffraction Analysis ( $S_N$ )**

| Calculation items                  | Number of Cores (N) |      |      |      |      | Percentage of elapsed Times on a Single Core |
|------------------------------------|---------------------|------|------|------|------|--|
|                                    | 2                   | 4    | 6    | 8    | 12   |  |
| 1 <sup>st</sup> order hydrodynamic | 1.52                | 2.43 | 3.13 | 3.49 | 4.00 | 85.0   |
| Difference/sum frequency QTF       | 1.62                | 2.10 | 2.33 | 2.48 | 2.54 | 0.7  |
| Directional coupling QTF           | 1.39                | 1.63 | 1.94 | 2.01 | 2.01 | 0.6  |
| Wave elevation                     | 1.49                | 2.37 | 3.08 | 3.50 | 3.81 | 13.7   |
| Total elapsed time of HD analysis  | 1.51                | 2.40 | 3.09 | 3.44 | 3.90 | 100.0  |

**Note:**

$S_N = T_1 / T_N$  is defined as the ratio of the elapsed time to execute the calculation item on a single core to the time (in seconds) on N cores.

In the hydrodynamic response analysis (Aqwa-Librium, Aqwa-Drift, Aqwa-Fer and Aqwa-Naut), the parallel processing is carried out in the following calculations:

1. Element pressure estimation in time domain (Aqwa-Naut)
2. Irregular wave database at each time step (Aqwa-Naut)
3. Database of static composite moorings on sloped seabed
4. Dynamic cable in time domain (Aqwa-Drift and Aqwa-Naut)
5. Tether in time domain (Aqwa-Drift and Aqwa-Naut)

To ensure efficiency while minimizing total memory use in time domain dynamic cable and/or tether analysis, the fewest number of required cores for dynamic cable and tether calculation are determined based on the total number of dynamic cables and tethers in each mooring configuration and the actual number of cores available to Aqwa.

In each time step, the number of OpenMP parallel loops for dynamic cable calculation is required:

$$L = \frac{M_{cd}}{N} + \min \left\{ \text{mod} \left( M_{cd}, N \right), 1 \right\} \quad (14.22)$$

where  $M_{cd}$  is the number of dynamic cables in a mooring configuration and  $N$  is the number of cores used for parallel dynamic cable calculation.

Aqwa assigns  $N$  memory blocks to copy the thread-private variables and common blocks for each thread.

If the actual number of cores for Aqwa,  $N_a$  was used for parallel dynamic cable calculation, the number of OpenMP parallel loops for a set of moorings would be:

$$L^{(0)} = \frac{M_{cd}}{N_a} + \min \left\{ \text{mod} \left( M_{cd}, N_a \right), 1 \right\} \quad (14.23)$$

The fewest number of required cores,  $N_c$ , is determined by:

$$N_c = \min \{N_a, N_a - 1, \dots, N_a - i\} \quad (14.24)$$

under the condition

$$L^{(i)} = \frac{M_{cd}}{N_a - i} + \min \left\{ \text{mod} \left( M_{cd}, N_a - i \right), 1 \right\} = L^{(0)} \text{ where } i < N_a \quad (14.25)$$

From [Equation 14.25 \(p. 221\)](#) it can be observed that employing the fewest number of cores requires the smallest number of memory blocks for parallel dynamic cable calculation while keeping the number of OpenMP parallel loops the same. In other words, using the fewest number of cores ensures the same simulation time as using the maximum available cores, while minimizing memory usage.

The same approach is employed to determine the fewest number of cores required for the parallel processing calculation of tethers in a time domain analysis.

The actual number of cores used in the Aqwa parallel calculation is listed in [Table 14.2: Summary of Cores Used in Parallel Calculation \(p. 221\)](#).

**Table 14.2: Summary of Cores Used in Parallel Calculation**

| Module  | Number of Cores Used            |
|---|---------------------------------|
| Aqwa-Line (Hydrodynamic Diffraction)  | Min(Num_Cores, Num_Proc, HPC+4) |
| Aqwa_Librium (Hydrodynamic Response: Stability) with composite mooring on sloped seabed   | Min(Num_Cores, Num_Proc, HPC+4) |
| Aqwa_Fer (Hydrodynamic Response: Stability) with composite mooring on sloped seabed   | Min(Num_Cores, Num_Proc, HPC+4) |
| Aqwa_Naut (Hydrodynamic Response: Regular Wave) (1) with time domain element pressure output                                    | Min(Num_Cores, Num_Proc, HPC+4) |
| Aqwa_Naut (Hydrodynamic Response: Regular Wave) (2) with composite mooring on sloped seabed                                     | Min(Num_Cores, Num_Proc, HPC+4) |
| Aqwa_Naut (Hydrodynamic Response: Regular Wave) (3) with dynamic cable and/or tether  | $N_c$                           |
| Aqwa_Naut (Hydrodynamic Response: Irregular Wave)   | Min(Num_Cores, Num_Proc, HPC+4) |
| Aqwa_Drift (Hydrodynamic Response: Slow Drift only, Irregular Wave with slow Drift) (1) with composite mooring on sloped seabed | Min(Num_Cores, Num_Proc, HPC+4) |

| Module   | Number of Cores Used |
|--|----------------------|
| Aqwa_Drift (Hydrodynamic Response: Slow Drift only, Irregular Wave with slow Drift) (2) with dynamic cable and/or tether | $N_c$                |

**Note:**

Num\_Cores: User required number of cores

Num\_Proc: Total number of cores in the node

HPC: Number of available HPC licenses

$N_c$ : The fewest number of cores defined by [Equation 14.24 \(p. 221\)](#) for dynamic cable or tethers

The speed-up values of the Aqwa-Drift time domain analyses of a tension-leg platform model with 16 tethers are listed in [Table 14.3: Speed-Up of Hydrodynamic Time Domain Analysis with Tethers \( \$S\_N\$ \) \(p. 222\)](#). In this model, each tether is modeled by 200 elements. The simulation in the 3-hour duration with the time step interval of 0.2 seconds is carried out on a 12- physical-core (24-logical-processors) workstation. The speed-up of 16 cores shows that using above the number of physical cores for parallel calculation may not achieve higher efficiency.

**Table 14.3: Speed-Up of Hydrodynamic Time Domain Analysis with Tethers ( $S_N$ )**

| Number of Cores (N) | 2    | 4    | 6    | 8    | 16   |
|---------------------|------|------|------|------|------|
| Speed-up            | 1.77 | 2.86 | 3.41 | 4.07 | 3.85 |

# Chapter 15: References

---

1. American Petroleum Institute (API) (2000), Planning, Designing and Constructing Fixed Offshore Platforms - Working Stress Design, API RP2A-WSD, 21st Edition.
2. American Petroleum Institute (API) (2005), Design and Analysis of Stationkeeping Systems for Floating Structures, API RP2SK, 3rd Edition.
3. Aranha, J.A.P. and Martins, M.R. (1997), 'Slender body approximation for yaw velocity terms in the wave drift damping matrix', Proceedings of 12th Int. Workshop on Water Waves and Floating Bodies, Marseilles, France.
4. Barltrop, N.D.P. (1998), Floating Structures: a guide for design and analysis, Vol. 1, CMPT and OPL.
5. Barltrop, N.D.P. and Adams, A.J. (1991), Dynamics of Fixed Marine Structures, 3rd Edition, Butterworth-Heinemann Ltd, ISBN: 0750610468
6. Borgman, L.E. (1967), 'Random hydrodynamic forces on objects', the Annals of Mathematical Statistics, Vol.38, No.1, pp37-51.
7. Cambridge University, Engineering Department (2000), Mechanics Data Book, 2000 Edition.
8. Chen, X.B. (2006), 'The set-down in the second-order Stokes' waves', Seventh International Conference on Hydrodynamics, 4–6 Oct. 2006. The Island of ISCHIA, Italy, ICHD 2006.
9. Cheetham, P., Du, S., May, R. and Smith, S. (2007), 'Hydrodynamic analysis of ships side by side in waves', International Aerospace CFD Conference, Paris, June 2007.
10. Cummins, W.E. (1962), 'The impulse response function and ship motions', Technical Report 1661, David Taylor Model Basin - DTNSRDC, 1962.
11. Det Norske Veritas (DNV) (2011), Modelling and Analysis of Marine Operations, DNV-RP-H103.
12. DNV Recommended Practice (2010), Environmental Conditions and Environmental Loads, DNV-RP-C205 Oct 2010.
13. Du, S.X., Hudson, D.A., Price, W.G. and Temarel, P. (2009), 'Implicit expressions of static and incident wave pressures over the instantaneous wetted surface of ships', Proceedings of the Institution of Mechanical Engineers Part M: Journal of Engineering for the Maritime Environment, Vol. 223, No. 3, pp. 239-256.
14. Du, S.X., Hudson, D.A., Price, W.G. and Temarel, P. (2011), 'The occurrence of irregular frequencies in forward speed ship seakeeping numerical calculations', Ocean Engineering, Vol. 32, pp. 235-247.
15. Faltinsen, O.M. (1990), Sea Loads on Ships and Offshore Structures, Cambridge University Press, ISBN: 0521458706.

16. Hermanns, M. (2002), *Parallel Programming in Fortran 95 Using OpenMP*, Universidad Politencia de Madrid, Spain.
17. Houmb, O.G. and Overvik, T. (1976), 'Parameterization of wave spectra', Proceeding of the first Conference on Behaviors of Offshore Structures (BOSS' 76), Trondheim, Norway, Vol. 1, pp.144-169.
18. International Standard Organization (ISO) (2005), Petroleum and Natural Gas Industries - Specific Requirements for Offshore Structures. Part 1: Metocean Design and Operating Conditions, BS EN ISO 19901 1:2005, ISBN: 0580475077
19. Inglis, R.B., Price, W.G. (1981), 'A three dimensional ship motion theory—comparison between theoretical predictions and experimental data of the hydrodynamic coefficients with forward speed', Trans. RINA, Vol. 124, pp.141–157.
20. ITTC (2002), 'The special committee on waves: final report and recommendations to the 23rd ITTC', Proceedings of the 23rd ITTC, Vol. 2, Venice, Italy.
21. ITTC (2011), 'ITTC Recommended Procedures 7.5-02-07-04.5 - Numerical estimation of roll damping'.
22. Kawahara, Y., Maekawa, K., Ikeda, Y. (2009), 'A simple prediction formula of roll damping of conventional cargo ships on the basis of Ikeda's method and its limitation', Proceedings of the 10th International Conference on Stability of Ships and Ocean Vessels (STAB2009), St. Petersburg, Russia.
23. Kim, Y. and Sclavounos, P.D. (1998), 'A finite-depth unified theory for linear and second-order problem of slender ships', Journal of Ship Research, Vol.2, No. 4, pp.297-309.
24. Kim, S., Sclavounos, P.D. and Nielsen, F.G. (1997), 'Slow-drift responses of moored platforms', the 8th BOSS Conference, Delft University of Technology, The Netherlands, 7-10 July 1997.
25. Lee, C.H. and Nielsen, F. G. (1996), '[Analysis of oscillating-water-column device using a panel method](#)', 11th International Workshop on Water Waves and Floating Bodies, Hamburg, Germany, March 1996.
26. Lee, C.H. and Newman, J.N. (2016), 'An extended boundary integral equation for structures with oscillatory free-surface pressure', International Journal of Offshore and Polar Engineering, Vol. 26, No. 1, March 2016, pp. 41-47.
27. Malenica, S., Zalar, M. and Chen, X.B. (2003), 'Dynamic coupling of seakeeping and sloshing', Proceedings of The Thirteenth (2003) International Offshore and Polar Engineering Conference, Honolulu, Hawaii, USA.
28. Newman, J.N. (1974), 'Second-order, slowly-varying forces on vessels in irregular waves', International Symposium on the Dynamics of Marine Vehicles on Structures in Waves, Bishop R. E. D. and Price W.G. (Editors), Mechanical Engineering Publications Ltd, London, UK, pp.193-197.
29. Newman, J.N. (1967), 'The drift force and moment on ships in waves', Journal of Ship Research, Vol.11, pp.51-60.
30. Newman, J.N. (1978), 'The theory of ship motions', Advances in Applied Mechanics, Vol.18, pp.221-283.
31. Newman, J.N. (2017), *Marine Hydrodynamics*, 40th Anniversary Edition, The MIT Press.
32. Newman, J.N. (2018), 'Resonant response of a moonpool with a recess', [Applied Ocean Research](#), Volume 76, July 2018, pp. 98-109.

- 
33. Ochi, M.K. and Hubble, E.N. (1976), 'Six parameter wave spectra', Proceedings of the 15th Coastal Engineering Conference, ASCE, Honolulu, USA.
  34. Ochi, M.K. and Shin, Y.S. (1988), 'Wind turbulent spectra for design consideration of offshore structures', Proceedings of Offshore Technology Conference, Houston, USA, Paper No. 5736, pp. 461-467.
  35. Ostergaard, N.H., Lyckegaard, A., and Andreasen, J.H. (2011), 'Simulation of frictional effects in models for calculation of the equilibrium state of flexible pipe armouring wires in compression and bending', Journal of Structural Mechanics, Vol. 44, No. 3, pp. 243-259.
  36. Pawłowski, M. (2016), 'The stability of a freely floating ship', Polski Rejestr Statków Technical Report No. 72, January 2016.
  37. Pinkster, J.A. (1980), 'Low frequency second order wave exciting forces on floating structures', PhD. Thesis, TU Delft.
  38. Rainey, R.C.T (1995), 'Slender-body expressions for the wave load on offshore structures', Proc. R. Soc. London A, 450, pp. 391-416
  39. Randall, R.E. (1997), Element of Ocean Engineering, Society of Naval Architects and Marine Engineers, ISBN: 0939773244.
  40. Rawson, K.J. and Tupper, E.C. (1984), Basic Ship Theory, Third edition, Longman Group Limited, ISBN: 0582305276.
  41. Robinson, R.W. and Stoddart, A.W. (1987), 'An engineering assessment of the role of non-linearities in transportation barge roll response', Transactions of Royal Institution of Naval Architects, pp. 65-79
  42. Wheeler, J.D. (1970), 'Method for calculating forces produced by irregular waves', Journal of Petroleum Technology, 249, pp. 359-367.
  43. Wichers, J.E.W. (1979), 'Slowly Oscillating Mooring Forces in Single Point Mooring Systems', BOSS 1979, London, August 1979.
  44. Zhao, H.J., Song, Z.Y., Li, L., Kong, J., Wang, L.Q., and Yang, J. (2016), 'On the fifth-order Stokes solution for steady water waves', China Ocean Engineering, Vol.30, No. 5, October 2016, pp. 794-810.

